# APPLIED COMPUTATIONAL FLUID DYNAMICS IN ELECTRONICS PACKAGING

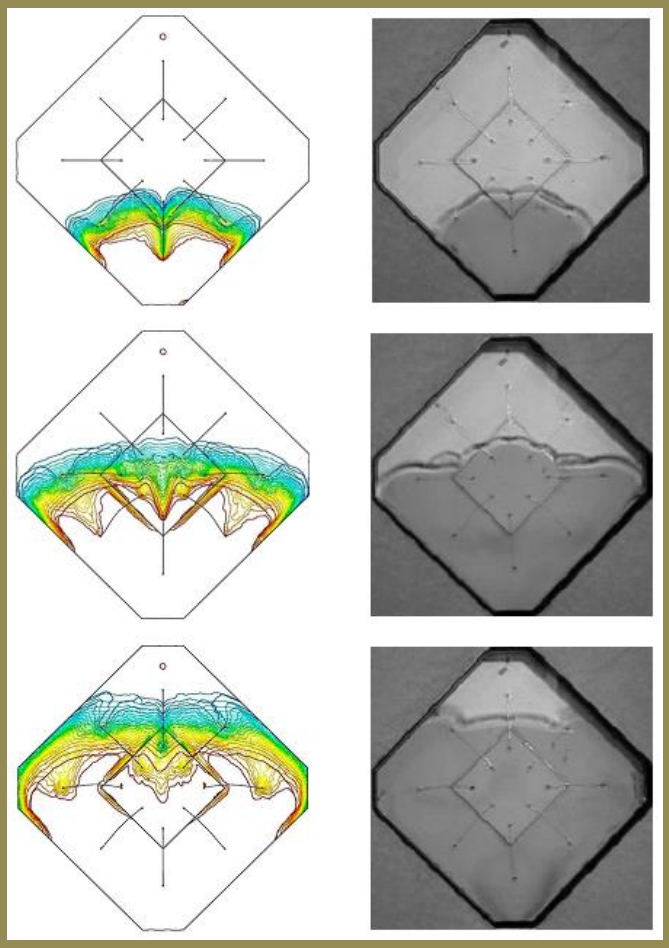

**By**

**Dadan Ramdan**

Medan Area University Press

**DADAN RAMDAN**

# APPLIED COMPUTATIONAL FLUID DYNAMICS IN ELECTRONICS PACKAGING

Medan Area Universty Press
Medan, 2015

# Applied Computational Fluid Dynamics in Electronics Packaging

Author:
**DADAN RAMDAN**

**Published by: Medan Area University Press**
Address: Jalan Kolam Nomor 1 Medan Estate, Medan
Telephone: 061-7366878
Mobile: +6181376699314
e-mail: Medanareuniversitypress@yahoo.co.id



**ISBN**: **978-602-1577-11-0**

First Edition, April 2015

The National Library: Cataloguing in Publication

Applied Computational Fluid Dynamics in Electronics Packaging:
Medan Area University Press, 2015,
187 page; 20 cm.

*Fill out the responsibility of printing*

# PREFACE

This is an introductory textbook for Applied Computational Fluid Dynamics in Electronics Packaging. The reduction of IC chip size has a significant impact to the modern electronic industry especially on the circuit design and IC assembly process. The increasing of I/O counts in a small scale IC chip result in severe wire deformation and deformation issues during transfer moulding process. In this book, visualization of wire sweep phenomenon during the encapsulation process of plastic ball grid array (PBGA) package is studied through a three-dimensional (3D) fluid structure interaction (FSI) technique; which FV- and FE-based software are connected by using mesh-based parallel code coupling interface (MpCCI). The effect of polymer rheology, inlet pressure, arrangement of inlet gate, number of stacked die, wire diameter and size of mould cavity vents, on the melt flow behaviour, wire sweep, filling time, cavity pressure and stress distributions, are mainly studied. A 3D model of mould and wires was created by using GAMBIT, and the fluid/structure interaction was simulated by using FLUENT and ABAQUS software integrated with MpCCI for the real-time calculations. The Castro-Macosko model and Kamal model are used to incorporate the polymer rheology and the Volume of Fluid (VOF) technique is applied for melt front tracking. User-defined functions (UDFs) were incorporated to allow the curing kinetics. However, in the experimental work, the effects of FSI phenomenon in the PBGA package was studied using a scaled-up package size to mimic the encapsulation process. The effects of stacked die, inlet gate arrangement, outlet vent, and inlet pressure of mould cavity on the melt flow behaviour and wire sweep were investigated. The constant viscosity of test fluid was utilized for experiment. The numerical results of melt front patterns and wire sweep were compared with the experimental results and it was found in good conformity. Three types of Epoxy Moulding Compound (EMC) were utilized for the study of fluid flow within the mould cavity. The melt front profiles and viscosity versus shear rate for all cases were analyzed and presented. The numerical results of melt front behaviour and wire sweep were compared with the previous experimental results and found in good agreement. In the present study, the lower viscosity shows the lower air trap, lower pressure distributions and lower wire deformation. Optimized design of the PBGA gives better PBGA encapsulation process and minimizes the wire sweep. The physical and process parameter (i.e., pressure inlet, wire diameter, vent height) were optimized via response surface methodology (RSM) using central composite design (CCD) to minimize the deformation of wire sweep, filling time and void in package during the PBGA encapsulation process. Fluid structure interaction (FSI) was considered in the optimization of the PBGA encapsulation process. The optimum empirical models were tested and well confirmed with the simulation results. The optimum design of the PBGA with 12 wires for both physical and process parameters ware characterized by 5.57 MPa inlet pressure, 0.05 mm wire diameter, and 0.36 mm vent height. Therefore, the strength of MpCCI code coupling in handling FSI problems is proven to be excellent. This present work is expected to be a reference and guideline for microelectronics industry.

Medan, November 2015
Writer,

Dadan Ramdan

# ACKNOWLEDGEMENTS

First of all, I express my gratitude to the almighty Allah who is the ultimate source of guidance in all our endeavors. Next, I am deeply obliged and thankful to my supervisor Prof. Dr. Mohamad Zulkifly Abdullah whose cordial support, motivation and timely advises made me highly comfortable throughout this research work and to write the textbook. The friendly and helpful attitude also his valuable guidance to the current research has helped to maintain full confidence on the research methodology and findings.

My special thanks to all my colleagues for whom I have great regard, especially Dr. Muhammad Khalil Abdullah @ Harun and Dr. Khor Chu Yee. I wish to extend my warmest thanks to all those who have helped me in the CFD laboratory, School of Mechanical and Aerospace Engineering, Engineering Campus, Universiti Sains Malaysia.

My special thanks are due to my colleague Mr. Liong, Mr. Mior, Mr. Tony, Mr. Najib and Mr. Syahrizal Abdul Aziz whose advices the technical software,without whose helps, this research would not have been successful.

I have to say thousands 'thank-you' to all my family, wherever they are, particularly my wife and family members and my siblings for their support and encouragement which has enabled me to complete this project. They have given me inspiration to work hard and motivated me during this research work. Last but not the least I express my gratitude to my Rector Universitas Medan Area and Head of Yayasan Pendidikan Haji Agus Salim and all those who helped me for the moral and material support of this work.

The authors are grateful to Intel Tech. (M) Sdn. Bhd. for the financial support for this research work, and Directorate General Strengtening Research and Development,Research, Technlogy, and Higher Education Ministery, Republic of Indonesia for research funding competition program Funding Year 2014 and 2015.

November 2015
Dadan Ramdan

# CONTENTS

**CHAPTER 4 – SIMULATIONS AND EXPERIMENTS ON PBGA ENCAPSULATION PROCESS**

## LIST OF SYMBOLS

| | |
|---|---|
| $A_1$, $A_2$ | Pre-exponential factors 1/s. |
| $B$ | Exponential-fitted constant Pa.s. |
| $C_1$, $C_2$ | Fitting constant. |
| $C_P$ | Specific heat J/kg.K. |
| $C_D$ | Drag coefficient |
| $D$ | Drag force per unit length of the wire |
| $D_N$ | Largent deformation normal to the wire |
| $d$ | Wire diameter |
| $E$ | Elastic modulus of wire |
| $E_1$, $E_2$ | Activation energies K. |
| $F$ | External body force. |
| $f$ | Front advancement parameter. |
| $f_B$ | Bending geometry factor for the bending moment. |
| $f_T$ | Twisting geometry factor for the bending moment. |
| $G$ | Shear modulus of wire |
| $g$ | Gravitational acceleration. |
| $H$ | Height of wire |
| $I$ | Momentum of inertia of the wire |
| $I_p$ | Polar moment of inertia of the wire |
| $k$ | Thermal conductivity W/m.K. |
| $k_1$, $k_2$ | Rate parameters described by an Arrhenius temperature dependency 1/s. |
| $L$ | Length of the wire span |
| $M$ | Linear viscous operators. |
| $m_1$, $m_2$ | Constants for the reaction order. |
| $N$ | Non-linear viscous operators. |
| $n$ | Power law index. |
| $P$ | Static pressure Pa. |
| $Re$ | Reynolds number |
| $S$ | Length of the wire |
| $T$ | Absolute temperature K. |
| $t$ | Time s. |
| $T_b$ | Temperature-fitted constant K. |
| $U$ | Undistributed upstream velocity of fluid |
| $u$ | Fluid velocity component in x-direction mm/s. |
| $\vec{u}$ | velocity of solid in $x$, $y$ and $z$ axis mm/s. |
| $v$ | Fluid velocity component in y-direction mm/s. |
| $w$ | Fluid velocity component in z-direction mm/s. |
| $x, y, z$ | Cartesian coordinates. |

***Greek letters***

| | |
|---|---|
| $\alpha$ | Conversion of reaction. |
| $\alpha_{gel}$ | Degree of cure at gel. |
| $\dot{\alpha}$ | Curing rate. |
| $\Delta H$ | Exothermic heat of polymerization J/kg. |
| $\eta$ | Viscosity Pa.s. |
| $\eta_0$ | Zero shear rate viscosity Pa.s. |
| $\rho$ | Density kg/m$^3$. |

| | |
|---|---|
| $\rho_s$ | Density of solid kg/m$^3$ |
| $\tau$ | Shear stress Pa. |
| $\dot{\gamma}$ | Shear rate 1/s. |
| $\tau^*$ | Parameter that describes the transition region between zero shear rates and the power law region of the viscosity curve Pa. |
| $\Phi$ | Energy source term J. |

## LIST OF ABBREVIATIONS

| | |
|---|---|
| **AMI** | Autodesk Mould-flow Insight |
| **CABGA** | Chip Array Ball Grid Array |
| **CAE** | Computer-aided Engineering |
| **CCD** | Central Composite Design |
| **CCD Camera** | Computer Capture Digital Camera |
| **CFD-ACE-U** | Computational Fluid Dynamics - Aides Computer Engineering-Unit |
| **CSP** | Chip Scale Package |
| **DOE** | Design of Experiment |
| **EMC** | Epoxy Moulding Compound |
| **FEA** | Finite Element Algorithm |
| **FE** | Finite Element |
| **FEM** | Finite Element Method |
| **FFT** | Flow Free Thin |
| **FSI** | Fluid-Structure Interaction |
| **FVM** | Finite Volume Method |
| **GNF** | Generalized Newtonian Fluid |
| **GUI** | Graphical User Interface |
| **IC** | Integrated Circuit |
| **I/O** | Input/output |
| **LQFP** | Low Plastic Quad Flat Pack |
| **MMAP** | Matrix Molded Array Package |
| **MpCCI** | Mesh-based parallel Code Coupling Interface |
| **MUF** | Moulded Underfill |
| **OA** | Orthogonal Array |
| **PBGA** | Plastic Ball Grid Array |
| **PDA** | Personal Data Access |
| **PGE** | Power Ground Embedded |
| **PLICE** | Plastic Integrated Circuit Encapsulation |
| **PWB** | Printed Wire Bonding |
| **RSM** | Response Surface Methodology |
| **S-CSP** | Stacked-Chip Scale Package |
| **SiP** | System in Package |
| **SOT** | Small Outline Transistor |
| **TBGA** | Thin Ball Grid Array |
| **TQFP** | Tape Quad Flip Chip Package |
| **UDF** | User-Defined Function |
| **USM** | Universiti Sains Malaysia |
| **UTM** | Universal Testing Machine |
| **VCR** | Video Camera Recorder |
| **VDCM** | Vacuum Dip Compression Molding |
| **VOF** | Volume of Fluid |

## CHAPTER 1: INTRODUCTION

The introductory background of the IC package encapsulation process is presented in this chapter. The technical challenges in wire deformation, encapsulation process simulation and Plastic Ball Grid Array (PBGA) package are also briefly discussed. In the later sub-chapters, the problem statement, the significance of the current study, research objectives and contribution, the scope of study and the thesis outline are presented.

### 1.1 Transfer Molding

Transfer moulding is an economical method for encapsulation process. During transfer moulding process, the epoxy moulding compound (EMC) is transferred from a reservoir into the cavities under the application of heat and pressure. The processes of transfer moulding are shown in Figure 1.1(a) and (b).

Transfer moulding is a two-step process. In the first step, the melt front of EMC flows and fills up the mould cavity. In the second step, it involves the processes of curing, packing, cooling, and solidification. After the EMC fills up the mould cavity, there is a series of chemical reactions taking place in the mould cavity. As a result, the viscosity of EMC increases before it starts to gel and solidify.

If the plunger pressure is high, it might cause defects within the IC package. In the package, wire bonding is still the dominant microelectronic packaging technology (Kung et al., 2012). The more typical examples of process defects include wire sweep, misaligned leads, paddle shift, warpage, voids, incomplete curing, non-uniform encapsulation and etc. An illustration of defect sites and types, which occur during transfer moulding process, is shown in Figure 1.2. These defects can be eliminated by the stringent design of mould cavity and optimized parameter settings to minimize shear rate and flow stresses during transfer moulding process.

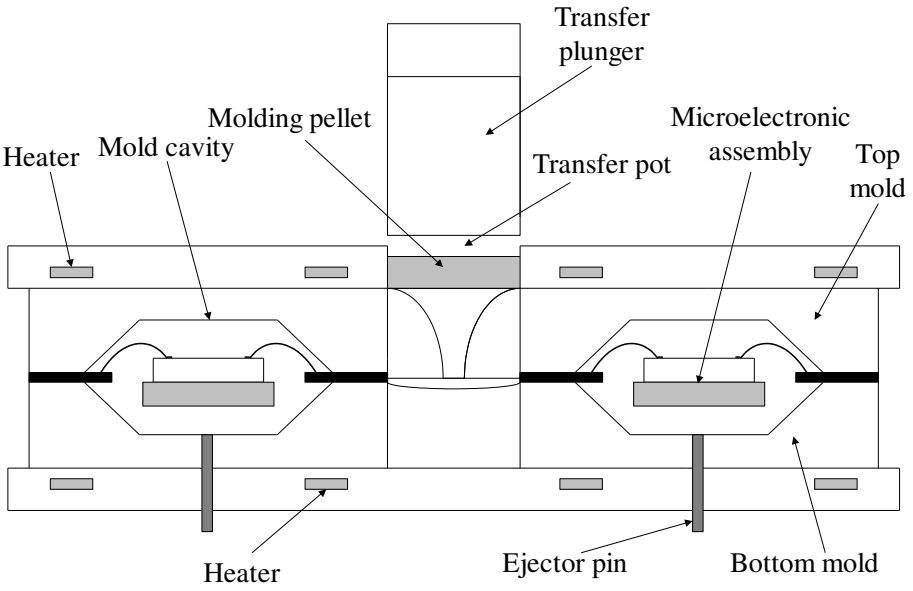


(a) Before moulding.

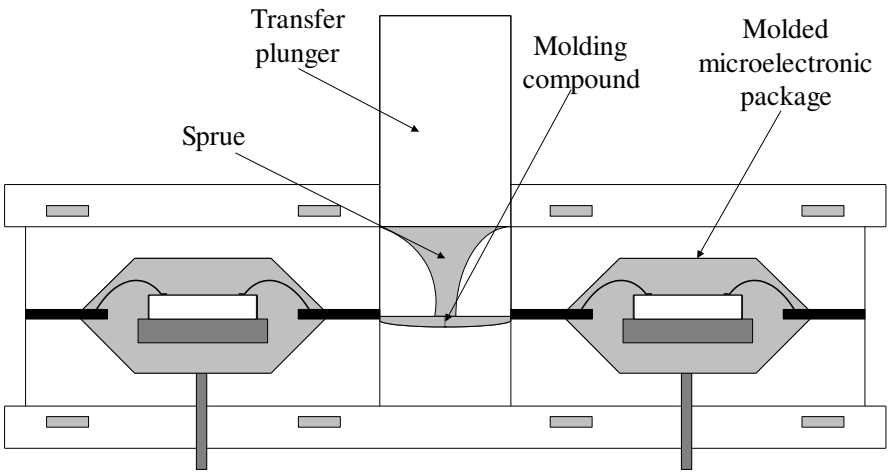


(b) After moulding.

Figure 1.1 Transfer moulding of encapsulation process (Ardebiri and Pecht, 2009): (a) Before moulding and (b) After moulding.

In the continuous miniaturization of IC package, there are rising technical challenges in circuit design and assembly processes of IC packages.

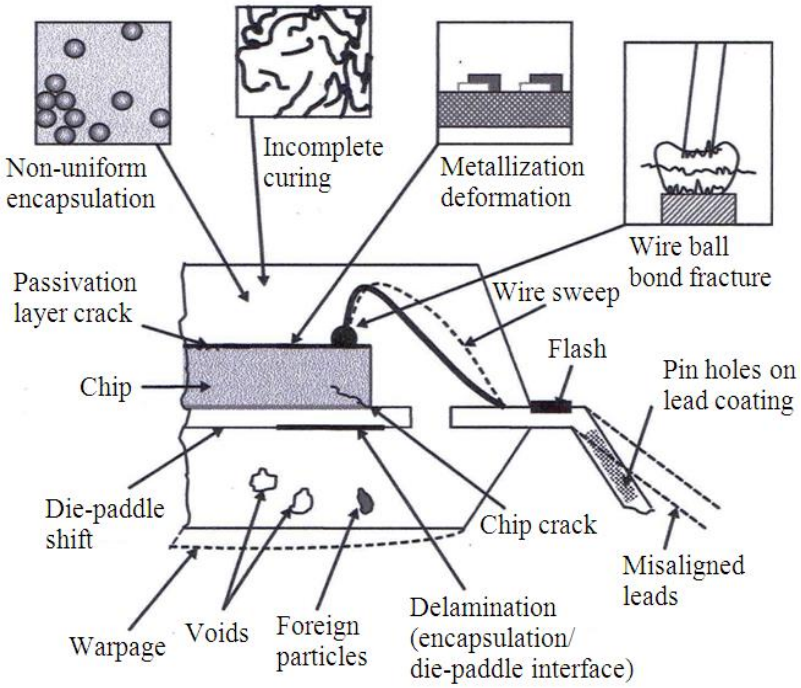


Figure 1.2 Defects produced during the encapsulation process (Ardebiri and Pecht, 2009).

However, the miniaturization of IC package with increasing number of input/output (I/O) counts has resulted in serious wire sweep during transfer moulding

process. An illustration of epoxy moulding compound (EMC) behaviour during the encapsulation process is shown in Figure 1.3. Large wire deformation may initiate several problems such as open circuit and short circuit (Su et al., 2003). Therefore, wire deformation has been classified as the vital issue in the IC encapsulation process (Jong et al., 2005). Many researchers have attempted to solve this problem by using the computer-aided engineering (CAE) to predict the wire sweep problems.

Wire sweep is most often caused by the EMC that flows transversely across the bond wires during encapsulation process, which usually occurs around the mid-span of a wire.

The wire sweep in the encapsulation process involves an interactions between fluid flow and structural deformation, which making it a typical fluid-structure interaction (FSI) problem. Numerous researchers have focused on this issue using various simulation tools such as CFD and CAE techniques.

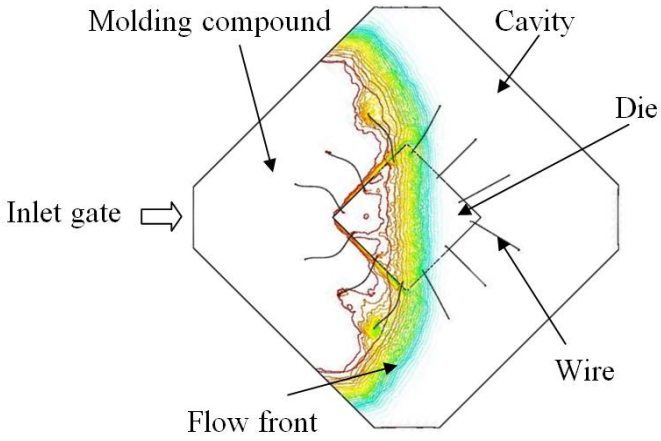


Figure 1.3 Epoxy moulding compound flows into the cavity.

Currently, EMC is widely used as the encapsulant material in plastic encapsulated IC packages (Lu et al., 2009). EMC has the advantage in terms of manufacturability, availability, and low cost. The rheological properties of EMC also play an important role that may influence the final quality in the encapsulation process. This is because the encapsulation process and final physical appearance of IC packages are much dependent on it. The most common rheokinetic model used is the Castro-Macosko model. It is especially useful in predicting the viscosity of thermoset polymers (Abdullah et al., 2009). The EMC rheological effects on wire deformation and melt front behaviour will also be discussed in this research work.

## 1.2 Plastic Ball Grid Array (PBGA)

PBGA is classified as a high-density IC packaging technology that could accelerate the advancement of microelectronic industry. This is determined by a broad adoption of PBGA in convenient multimedia products. Since then, the market opportunities for PBGAs have extended more than 30% per year (Ardebiri and Pecht, 2009). This technology has enabled more dies stacking design in a single package for

higher performance. Besides that, this will also provide outstanding performance and manufacturing cost reduction to the end users.

Many advantages of using PBGA over similar lead count leaded devices include (Mawer, 1996) several aspects:

a. Reduce board space due to the compact package design.
b. Provide better thermal and electrical performance.
c. Excellent surface mount yields when compared to fine pitch leaded devices.
d. Design of package with lower profile characteristics (i.e., overall thickness).
e. Handling and assembly compatibility with existing surface mount technology, test and equipment.
f. Diminish the total cost compared to leaded devices due to reduced scrap, rework and lack of need for fine-pitch assembly equipment.

Figure 1.4 and Figure 1.5 depict the schematic of cross-section and a typical plastic ball grid array (PBGA) package. In the PBGA technology, substrate and solders balls have been applied to replace the traditional lead-frame, which offers many advantages over fine-pitch technology such as providing a high-density of interconnector. Moreover, these include other advantages on better assembly process and electrical performance.

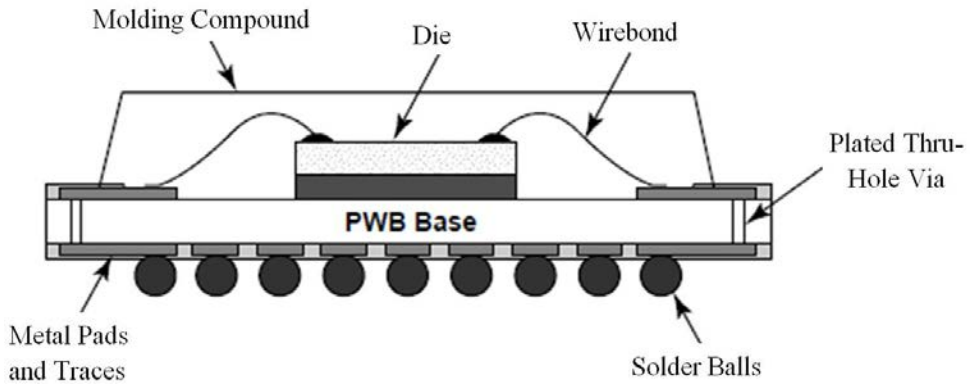


Figure 1.4 Schematic cross-section of a typical PBGA package (Zhang et al., 2000)

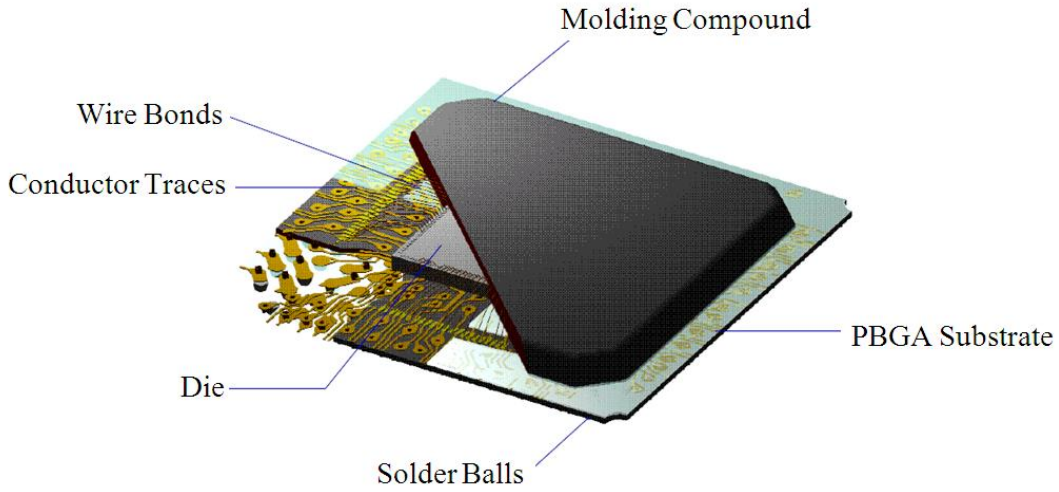


Figure 1.5 Package of Plastic Ball Grid Array (PBGA) Configuration (Texas Instrument, 2009).

## 1.3 IC Packaging

Recent advances in IC packaging, for example, moulded array package technology of PBGA encapsulation process by the transfer moulding process, subjected to the flow induced stress of EMC. This flow stress can cause the lead-frame and the wire bonds to deform permanently from their original geometry. A phenomenon of wire sweep is shown in Figure 1.6. Large deformation of a bonding wire can cause package failure; either short circuit or open circuit due to the contact between adjacent wire and a broken wire. Even if the deformation is not severe, it will deteriorate electrical and mechanical performance of the device and shorten its lifetime. Therefore, it is important to minimise or avoid the wire sweep deformation during encapsulation process based on the proper control of package design and operating process.

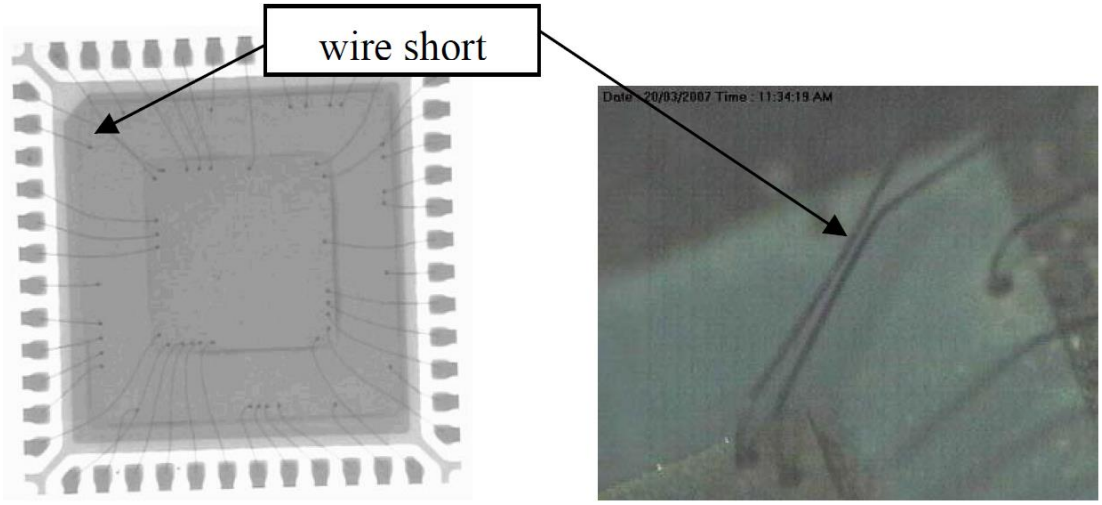


(a) Actual image. (b) Enlarge image.

Figure 1.6 Example of wire sweep in a package (Abdullah, 2008): (a) Actual image and (b) Enlarge image.

The wire sweep during encapsulation is considered as a fluid-structure interaction (FSI) problem, which always involved the interaction of EMC flow and package structures. The resulting drag force from the EMC flow causes wire deformation, this phenomenon is known as the wire sweep. However, the report of the FSI application for the wire sweep is still lacking in the simulation of two-ways analysis and also in the experimental work. The FSI phenomenon in encapsulation process should be addressed to solve the FSI-related defects.

In the actual PBGA encapsulation process, the visualisation of FSI phenomenon is difficult and constrained by small IC package size, limitation of visualization equipment, and the costlier experimental setup. Besides that, the non-transparent packaging mould used in the PBGA encapsulation process also causes difficulties in visualising the FSI phenomenon. Typically, the deformation of wire bonds is observed from the top view of the package using X-ray. It is the best method for observing FSI phenomenon through vertical and top views of the mould for better understanding. Moreover, investigations of the wire sweep phenomenon can also be conducted by using simulation tools.

Optimal design of PBGA provides the optimum encapsulation process and minimizes the wire sweep. The physical and process parameter (i.e., pressure inlet, wire diameter, vent height) should be optimised to minimise the deformation of wire sweep, filling time and voids in package during the PBGA encapsulation process. However, FSI should be considered in the optimisation of the PBGA encapsulation process.

## 1.4 Simulation

By considering the problem statement, the numerical study of encapsulation process is important in improving the quality of IC package and reducing the production cost. This will further decrease the development cost needed in producing electronic gadgets such as mobile phones, PC tablets, laptops and etc.

The quality of IC package is a major concern. In the ongoing trend, most of the PBGA package is produced in a thin and wide pattern, which could possibly trigger even more serious process defects during encapsulation process. The more common process defects such as wire sweep, warpage and voids could decrease the overall production yield. These critical defects have to be considered during the initial stage of package development (Sze and Papageorge, 1998). It is reported that the industry is attempting to produce thin IC packages with more stacking dies and high density of wire.

In the current research, both simulation and experimental results are important, which can provide useful guidelines in understanding the FSI phenomenon that occurs during encapsulation process. Moreover, the knowledge acquired from the research can be a good reference in the industry.

## 1.5 Objectives of the Book

The general objective of this book is to investigate the fluid structure interaction during PBGA encapsulation process. The understandings of encapsulation process are significant for PBGA designers and engineers to obtain the optimal PBGA package design and process control. In order to achieve these aims, six main objectives were set out as mentioned below:

1. To validate the predictions of modelling tools, CFD and CAE in the fluid flow and structural analyses of PBGA encapsulation process.
2. To predict and comprehend the effect of inlet gate and outlet vent arrangements on the fluid melt front profile and wire deformation during the encapsulation process.
3. To investigate the effect of stacked dies and gate orientation on wire sweep during encapsulation process of scale-up PBGA.
4. To perform the effect of inlet pressure to the Von Mises stress and shear stress of wire on the mould filling process of scale-up PBGA.
5. To carry out the effect of EMC rheological properties on wire sweep by applying the Castro-Macosko viscosity model and the Kamal curing models in the encapsulation process of actual size PBGA.
6. To optimise the physical and process parameters, those are found to be having a dominant effect on wire deformation, mould filling time and voids in the actual size PBGA encapsulation process.

## 1.6 Aims of the Study

This study contributes to the knowledge development in microelectronics packaging in the following aspects:

a. Introducing a new method to solve the FSI of wire sweep in the encapsulation process by using two-ways and real time MpCCI coupling method.
b. The numerical analysis uses User-defined functions (UDFs) to account for curing kinetics. The Castro−Macosko viscosity model with curing effect was written into C language using Microsoft VISUAL Studio 2005 and compiled as UDF in FLUENT.
c. Scaled-up PBGA encapsulation process contributes the clear visualisation of the FSI phenomenon, fluid flow and wire sweep mechanism through the top view of transparent mould.
d. The parametric studies and optimisation of PBGA encapsulation process contribute better understanding, clear visualisation on fluid and structure of wire sweep phenomena for engineers in microelectronic industry.

## 1.7 Scope of the Book

In this book, 3D computer analysis is applied via MpCCI in understanding FSI phenomenon during encapsulation of PBGA package. The effect of EMC rheological properties, stacked dies, inlet gate arrangements, and size of outlet vents on the overall wire sweep, EMC melt front, and pressure and shear stress distributions is studied.

In the simulation, EMC is considered as a generalised Newtonian fluid (GNF). In the encapsulation process, the EMC flow behaviour is modelled by the Castro-Macosko viscosity and Kamal curing models. These models are written in C language and compiled by using user-defined functions into the FLUENT analysis. Volume of fluid (VOF) technique is applied for melt-front tracking. The subsequent structural deformation of wire sweep is computed in ABAQUS. The present work discusses the effect of inlet pressure on wire deformation, stacked dies and inlet gate arrangements on fluid flow during the encapsulation process on scale-up PBGA by experimentally and simulation. This research also discusses the optimisation of physical and process parameters of the PBGA package for the analysis of wire sweep, void and filling time during the encapsulation process. Besides, the flow effect due to different inlet pressure is also considered in this study. The fluid flow during encapsulation process is viewed from the top, and comparisons are made between the numerical and experimental results.

In the present study, the computational fluid dynamic code FLUENT 6.3 is used to analyse the effect of outlet vent and inlet gate arrangements on flow behaviour during encapsulation of scale-up four wires PBGA. A 3D model is developed and analyzed using the finite volume method. Three different arrangements of mould, namely, 2-vents, 4 vents and 6 vents, and 1 inlet gate, 2 inlet gates and 3 inlet gates are applied in the analysis. Two different die height and inlet gate arrangement are studied numerically and experimentally in scale-up eight wires PBGA. The Castro–Macosko model is used to consider polymer rheology with curing effect in the viscosity behaviour of the EMC. Three different EMC properties, designated as Cases A, B and C, were studied for analyzing of fluid flow and wire sweep inside the mould cavity. Optimization of package design and process parameters is also studied. A program written in C language is employed in the User-Defined Function (UDF) to calculate the curing kinetics of EMC. The VOF technique is also applied to track the flow front of the

EMC. The numerical results of the flow patterns and the filling time of the three arrangements of EMC properties are compared.

Wire sweep profiles and pressure field are analyzed and presented. The simulation results are compared with the previous experimental result that available in the literature and it is found in good agreement. In the simulation, the Castro–Macosko viscosity model with considering curing kinetics was applied to describe the EMC behaviour. However, volume of fluid (VOF) technique was applied for to track the EMC flow front. Void problems or incomplete filling around packages and the multi-inlet gate are also discussed in the present paper. The results of the simulation and previous experimental results are found to be in good agreement.

## 1.8 Books Outline

In this book, there are five chapters. In Chapter 1, a brief presentation on encapsulation process, background of the study, encapsulation process simulation, PBGA, problem statement, significance of the study, objectives and scope of book. In Chapter 2, literature studies of mould flow and wire deformation in the PBGA encapsulation process are introduced. The numerical and experimental approaches are discussed in Chapter 3. In Chapter 4, model validation as well as results and discussions are presented in details. The discussion of wire sweep defect has also been extended to several case studies, which include the effect of inlet gate arrangement, stacked dies, inlet pressure, rheological properties, physical and process parameters. The process optimization is also being presented in the chapter. In the final chapter, the conclusion and recommendations for future works are discussed.

## CHAPTER 2: MOULDING PROCESS

### 2.1 Introduction

Smaller, faster and cheaper characteristics of complex microelectronic devices are the demands in current electronic trend, the modern packages such as, mobile phone, Personal Data Access (PDA), other portable and handheld electrical products are necessary to increase I/O numbers, reduce die and package sizes and manufacturing costs. Nowadays, microelectronic devices have many types of modern package, e.g. flip chip; wafer level packaging and tape automated bonding technologies (Schueller et al., 1997). In the IC packaging, wire bonding technique is still the dominant microelectronic packaging technology (Kung et al., 2012) such as PBGA and its prospectus market has been gradually increase to 2020 (Prior, 2010). Low cost of IC package trend and small form factor packaging is shown in Figure 2.1.

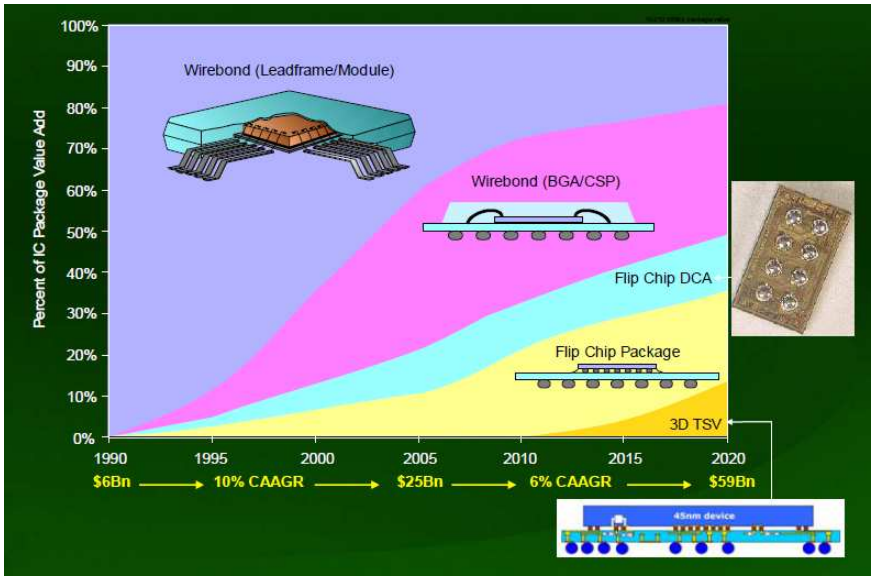


Figure 2.1 IC Package value trend of low cost and small form factor packaging (Prior, 2010).

Integrated Circuit (IC) devices have a great constraint in these products. To keep these IC devices working appropriately, it needs to protect the IC from physical break and contamination. The major objectives of IC encapsulation process are given as followed (Chen, 1990).

a. Protection of the device from mechanical and chemical hazards.
b. Thermal path for heat dissipation.

Due to the cause of cost and efficiency, modern electronic package uses plastic as the body material for packaging. Moulded plastic is then used to protect the chip and leadframe from physical damage and contamination.

In this chapter, the various issues that related to the problems arising from the encapsulation process and how to overcome these problems are solved and described base on previous papers. The paper review begins from moulding process experimentally and numerically analysis of encapsulation, the influence moulding process parameter and design packages of the wire bonding profile and fluid flow behaviour, and papers discussed optimization of the parameters.

## 2.2 Moulding Process

Transfer moulding is the most popular and well establish microelectronics encapsulation technique for electronics packaging. Typically, several moulding defects in this process are wire sweep, paddle shift, short shot, air trap, as well as other stress-induced problems (Abdullah et al., 2010). These defects may attribute by various factors such as improper selection of processing conditions, moulding material, lead frame layout, or mould design. Furthermore, trends to produce faster, smaller, and cheaper electronic products are driving packaging technology toward a higher packaging density with thinner and smaller profiles. This condition has made the process of encapsulation much more complicated and unpredictable (Chang et al., 2004). The samples of some packages are shown in Figure 2.2 which is the die stacking technology that applicable for memory devices or memory-logic devices.

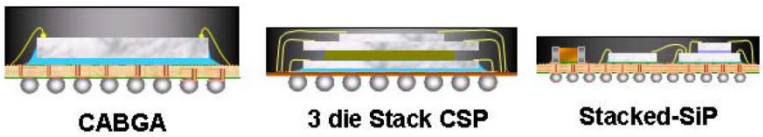


Figure 2.2 Conventional CABGA and thin multi-die stacking or stacked SiP (Lee et al., 2006)

In recent years, there has been a significant demand for stacked die technology due to it characteristics. The stacking of chips in leaded and substrate package can efficiently minimize package size and cost (Abdullah et al., 2008, 2010). Stacked-chip packages can be packed using die attach, wire bonding, and moulding methods. However, some challenges in stacked die development were thin wafer back grinding and handling, thermal issues due to the low thermal conductivity of the nonconductive die attach paste between die to die, and delamination issues due to package material mismatch, among others (Abdullah et al., 2009, Yao et al., 2003). Many researchers have studied this mould-filling process. However, only an amount of substantial works that related to the present study are reviewed in the current chapter.

The numerical analysis that considers the time-dependent behaviour of EMC and the presence of inserts in the mould cavities during encapsulation process is complicated and difficult. However, once a good quantitative model of the encapsulation process has been verified, considerable time and cost can be saved. Long and costly experimental runs are no longer needed to be carried out by trial and error to restore a mould or qualify a new compound.

3-D FEM model of PBGA package was simulated by Tay and Lee (2002) considering different gate positions. Teng and Hwang (2008) studied the behaviour of EMC melt fronts during the LQFP mould filing process, which modelled by using Castro-Macosko and Kinetic's models.

Recently, Khor et al. (2011) investigated the effect of different inlet gate arrangements in TQFP encapsulation process. GAMBIT was utilized to build a 3D model of plastic TQFP package and fluid flow analysis was solved by FLUENT software. Su et al. (2003) introduced “In-Pack” for wire sweep analysis that combined global flow analysis (C-MOULD) and structure analysis (ANSYS).

CFD code (CFD-ACE-U) and a structural dynamics code (FEM-STRESS) was used by Yang et al. (2001) through a two-way coupling technique. They used CFD and

structural dynamics codes to compute the transient flow field in encapsulation process and the transient deformations and stresses in wires.

Lim and Lee (2000) performed numerical simulations of three-dimensional (3D) mould filling during resin transfer moulding. They used the finite element method to predict the flow front while the epoxy moulding compound (EMC) is injected into a mould cavity preloaded with a porous fibrous pre-form. To check the 3D EMC front location as a function of time inside the pre-form, an optical fibber is used as sensing element. The experimental data were found to agree well with the numerical results.

Sato and Yokoi (2000) had developed a transparent mould with a glass-inserted structure, which enables observation of the dynamic melt behaviour inside the cavity along the thickness direction. The melt flow profile and the behaviour of the flow front surface were recorded using a high-speed video system and the data was analyzed with an image processor. Several experiments revealed that the melt advanced slipping on the cavity surface or lead frame. The melt flow is suggested to be affected by the melt in the opposite cavity beyond the lead frame.

Teng and Hwang (2008) studied the prediction of EMC flow front in the mould filing process of LQFP package. The EMC flow was modelled using Kinetics model and Castro-Macosko viscosity model. However, they did not include the degree of conversion of the moulding compound in their study.

Nguyen et al. (2000) studied transfer moulding numerically. They presented, discussed, and compared the results from experimental and computational studies on plastic encapsulation for a 144-lead TQFP package. The experimental results were obtained using an instrumented moulding press system. The computational predictions were carried out by using newly developed software for the modelling of transfer moulding process. Their predicted results were compared with the corresponding experimental measurements in terms of pressure, temperature, and flow front advancement in the cavities and runners. The experimental and computational results were demonstrated a good conformity, especially for the flow-front shapes and locations.

Shojaeia et al. (2002) presented numerical simulations of a 3D isothermal mould filling process based on the concept of the control volume by using finite element method. Quasi-steady state and partial saturation formulations were employed to track the flow front advancement in numerical analysis. Pre-form permeability may be a function of fluid velocity. Hence, the proposed numerical schemes accounted for the velocity dependency of permeability. The correlation between pre-form permeability and fluid velocity during mould filling had made the numerical schemes complex. The two schemes were evaluated by a comparison with analytical solutions for simple geometries and it was found in excellent agreement.

Gokce and Advani (2004) investigated the moulding process, where the resin is injected into the mould cavity containing preplaced reinforcement fabrics, through openings known as gates. During the process, the displaced air leaves the mould through openings (vents). Gate and vent locations were found significantly affect process output, such as fill time, pressure requirements, and whether or not the fabrics will be saturated entirely. In their study, a cascaded optimization algorithm was proposed for simultaneous gate and vent locations optimization in the presence of race tracking during mould filling. This algorithm is created by integrating branch and bound search with map-based exhaustive search.

Abdullah et al. (2007) numerically examined the encapsulation of the stacked-Chip Scale Package (S-CSP). They presented a study of flow visualization during encapsulation in S-CSP. The Navier–Stokes equation was solved by using the finite

difference method. The prediction of numerical model was verified by the experimental results, the flow front profile was found in good agreement. The predictions also showed that the short shot problem that occurred for the die top clearance lower than 0.25 mm.

Recently, Khor et al. (2011) studied the effect of inlet gate arrangement on the filling time during TQFP encapsulation. A 3D model of plastic TQFP packages was built using GAMBIT and simulated by FLUENT software.

Ishiko et al. (2006) presented a thermoelectric simulation for optimizing the wire-bonding position in insulated gate bipolar transistor modules, using the SOLIDIS 3-D simulator. They demonstrated that wire-bonding optimization by thermoelectric simulation could contribute not only to the realization of more compact power modules but also to improvements in the module reliability.

The rheological properties of the EMC play a crucial role in the encapsulation process, where the rheology is defined as the science of flow and deformation of matter (Abdullah et al., 2009). The final physical properties of IC package and processing rely on its characteristics. The most common and excellent rheology model for EMC material is Castro–Macosko model, especially for thermoset polymer rheology (Abdullah et al., 2009). The effect of gaps between the die top and mould cap surface and between adjacent dies on EMC rheology during stacked-chip-scale packages encapsulated was reported by Abdullah et al. (2009). Rheokinetic simulation of the mould-filling behaviour, mould void, and wire sweep dependences of gate size was analyzed by Lee et al. (2006). Three dies stack CSP 294LD of 4 × 4 mould array selected in this study with four different mould gate types. The simulation performed full 3 dimensional rheokinetic of mould filling behaviour by applying Castro-Macosko model. Experimental validations used for checking melt front advancements, mould voids and wire sweeping dependencies for each gate type.

Chen et al. (2007a) had successfully integrated the mould filling simulation and structural analysis software to predict the lead-shift phenomenon in an IC package. Their simulated results were verified with experiments. In this simulation, only unbalanced flow caused pressure difference was considered as loadings for the simulation.

## 2.3 Experimental Apparatus of Transfer Moulding Process

To enhance the understanding on the effects of the process parameter and design of IC package on the filling process, wire sweep or wire displacements. There is a need of experimental apparatus for the visualization during the transfer moulding process. The experimental set up had been introduced by Yang et al. (2000), Reddy et al. (1998), Yoshihara et al. (1999b), Chai and Zohar (1999), and Han and Wang, (1995a, 1995b).

Yang et al. (2000) introduced PBGA encapsulation process numerically and experimentally. In this study, the encapsulation mould was covered with a transparent top plate and the cavity filling process during transfer moulding was recorded by using a CCD camera. The wire sweep in the filling of cavities using original plane package and ribbed packages were evaluated and compared. Experiment facilities for flow visualization in the encapsulation process are schematically shown in Figure 2.3, and the detailed construction of mould is shown in Figure 2.4.

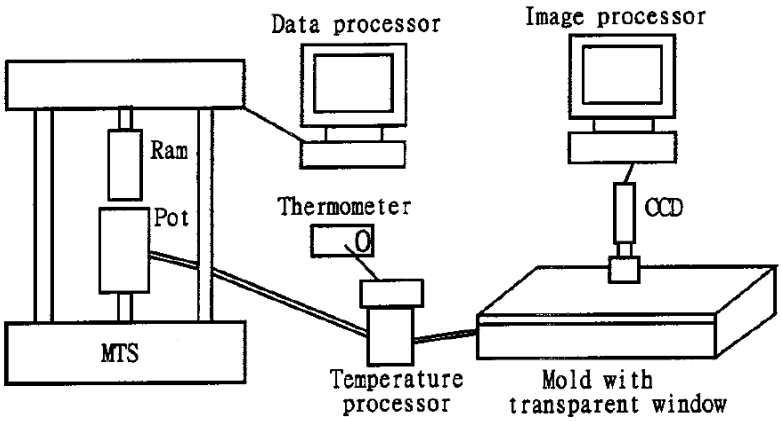


Figure 2.3 Schematic of facilities for flow visualization experiment (Yang et al., 2000).

The geometry of the cavity and typical wire bond geometry used in the experiment are shown in Figure 2.5. The effects of ribbed geometry on the thermal warpage and wire sweep of PBGA encapsulation were investigated in their study. Three rib geometries namely border, diagonal, and cross with a variation of rib widths and thicknesses were compared with the original plane geometry. Finite element analyses of thermal warpage during the reflow process of PBGA moulding with and without ribbed geometry were also carried out. They concluded that the cavities with ribs were significantly reduced the wire sweep compared with non-ribbed cavities.

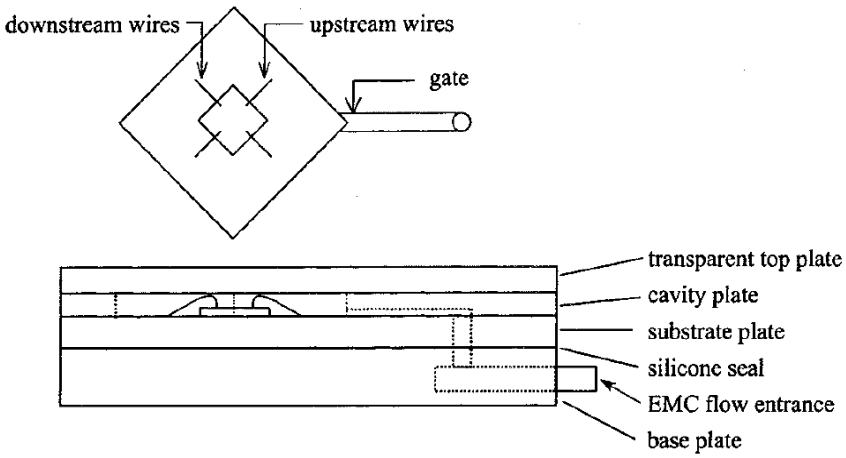


Figure 2.4 Sketch showing the detailed construction of mould (Yang et al., 2000).

Reddy et al. (1998) verified the numerical predictions of the fluid-front advancement and pressure variation within the cavity by conducting experiments with mould cavities in the microchip encapsulation process. The experimental setup as illustrated in Figure 2.6, which consists of an Instron Universal Testing Machine (UTM) that was utilized to obtain a constant velocity of the piston in a hydraulic piston-cylinder. A steel pipe was connected from the cylinder to the mould.

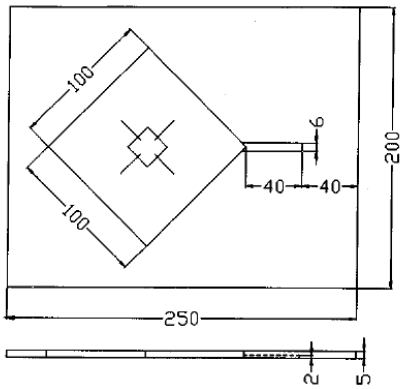


(a) Geometry of the cavity

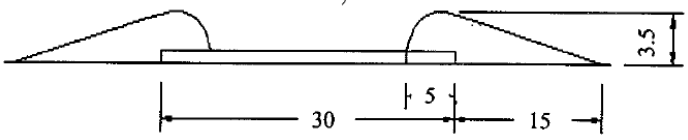


(b) Typical wirebond geometry

Figure 2.5 Sketch showing (a) geometry of the cavity and (b) typical wirebond geometry (Yang et al., 2000).

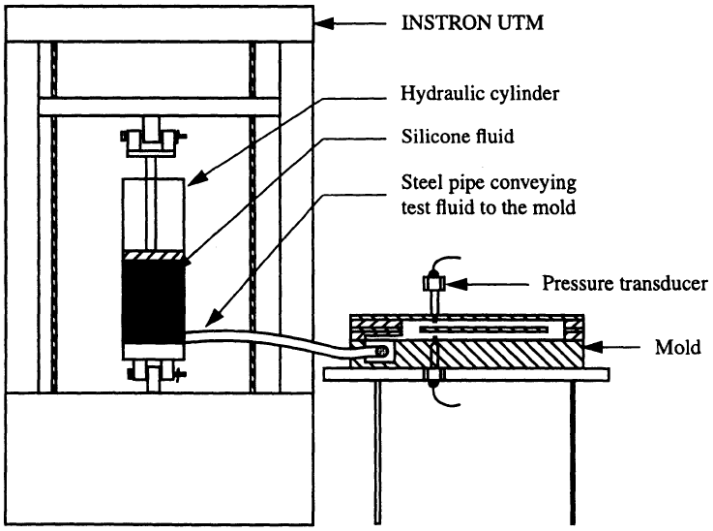


Figure 2.6 Schematic of experimental set up (Reddy et al., 1998)

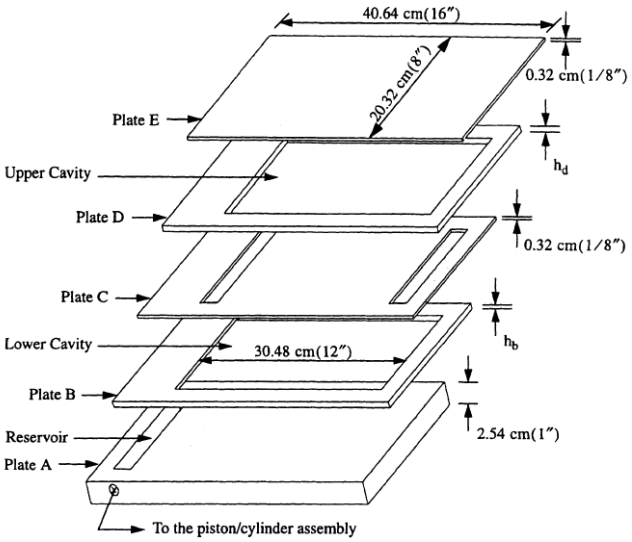


Figure 2.7 Geometry and dimension of the experimental mould plates (Reddy et al., 1998)

The experimental mould plates used by Reddy et al. (1998) are shown in Figure 2.7. The mould consists of five rectangular plates of various thicknesses, which were held together by eighteen screws that positioned along the outer edge. To enable a video recording of the fluid-front advancement during mould filling, the transparent Plexiglas was used as one of the mould plates.

Yoshihara et al. (1999a) investigated wire sweep by carried out an experiment considering the loop shape of the wire during the plastic IC packages encapsulation through the transfer moulding technique. The experimental investigation of the wire sweep was performed and its governing factors were studied. The wire bonding conditions of the bonder were varied, producing various loop shapes as shown in Figure 2.8. The specimen was a wire loop on the island of the lead frame (Figure 2. 9). Their experimental setup is shown in Figure 2.10. The specimen was positioned in the cavity, in which the wire loop was perpendicular to the direction of liquid flow (Figure 2. 11).

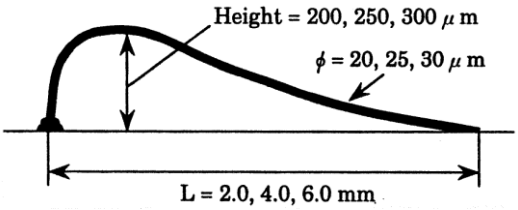


Figure 2.8 Wirebond geometry used in the experiments by Yoshihara et al. (1999a).

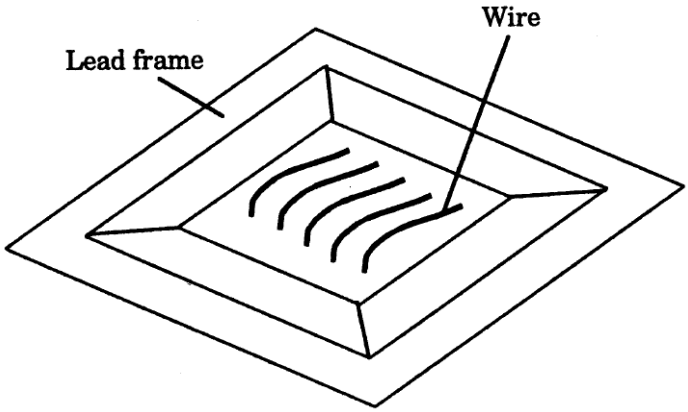


Figure 2.9 Specimen that fabricated by Yoshihara et al. (1999a).

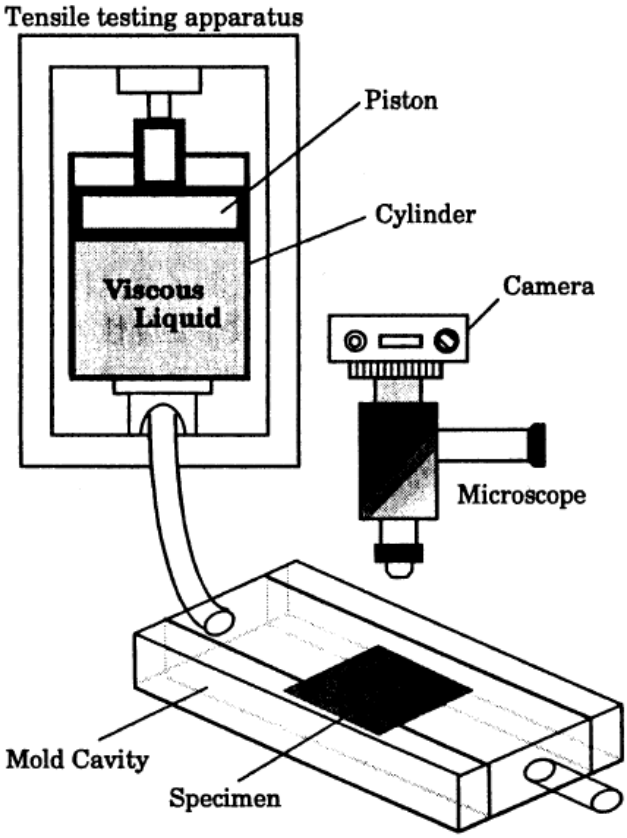


Figure 2.10 Schematic of the experimental setup (Yoshihara et al., 1999a).

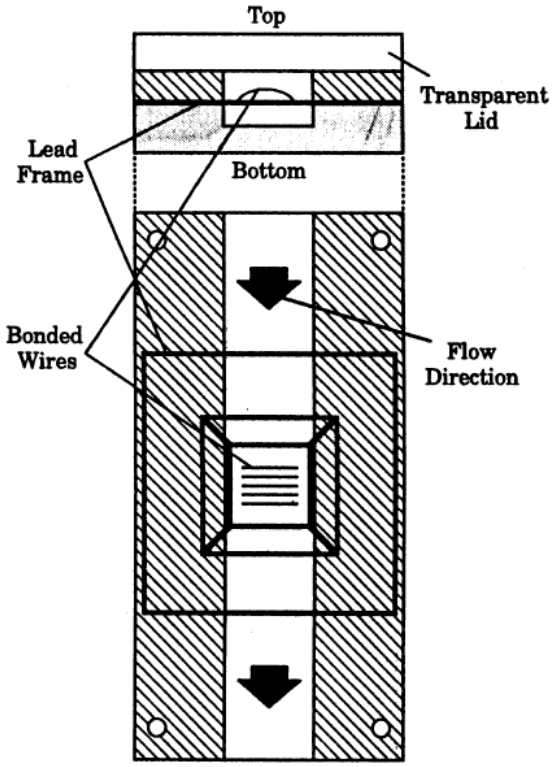


Figure 2.11 Spectrum setup in the mould cavity (Yoshihara et al., 1999a).

The effects of some parameters including fluid-flow velocity, wire-bond density or number of wire, mould cavity height, and mould vent size are the important factors of wire sweep of a 160L QFP package. These factors were investigated and analyzed experimentally by Chai and Zohar (1999). The displacement of the wires under different conditions was recorded on the video system. The displacement values are measured from the recorded images. A schematic experimental setup as shown in Figure 2.12, had been developed to allow in-situ monitoring and recording of the wire sweep phenomenon. The location of wires that coincided with the sparse configuration is depicted in Figure 2.13.

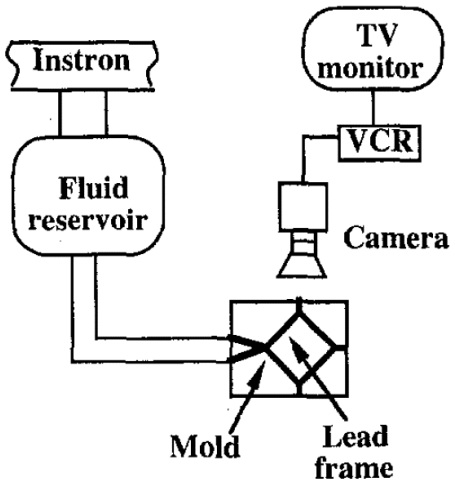


Figure 2.12 Schematic of the experimental setup (Chai and Zohar, 1999).

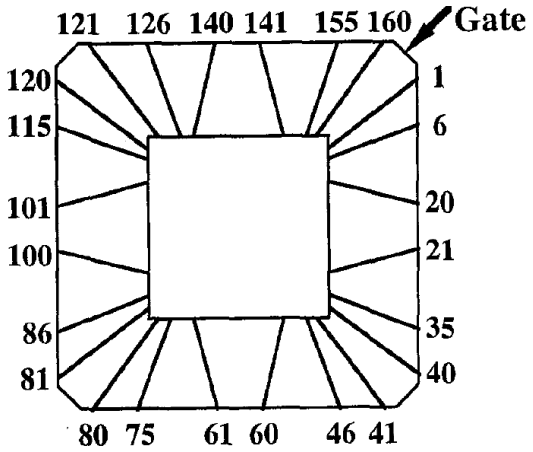


Figure 2.13 The position of the 24 wire bonds in the sparse arrangement of a 160L QFP lead-frame (Chai and Zohar, 1999).

Wire sweep phenomenon during the encapsulation process of the semiconductor chips had been studied experimentally by Han and Wang, (1995a, 1995b). A transfer-moulding machine was used to deliver the fluid to flow through a runner to the cavity. A wire that located in the mid-plane of a rectangular cavity was deformed when the fluid fills through the cavity. Clear silicone oil (Dow-Corning 200) and a transparent mould (made of polycarbonate) were used in their experiment. Wire deformation under different fluid velocities was recorded on the video system and the deformation value was measured on the screen from the recorded image. Figure 2.14 shows the schematic of experiment for the measurement of wire deformation and wire attached in the middle of a rectangular cavity.

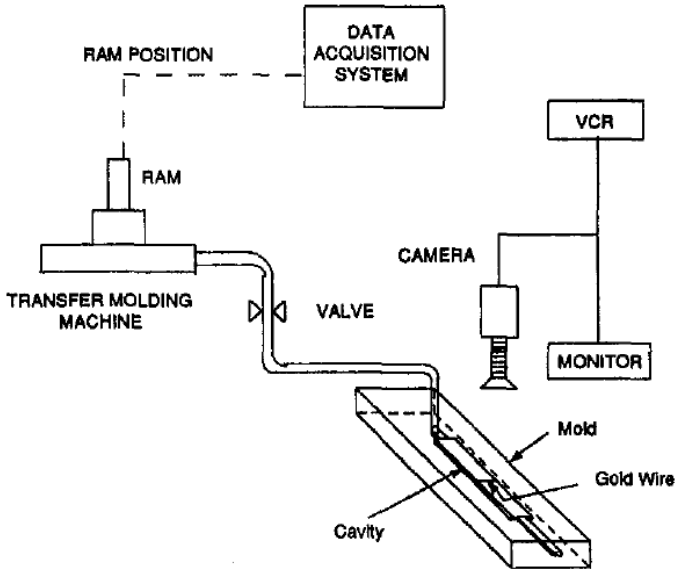


(a) Schematic of experiment

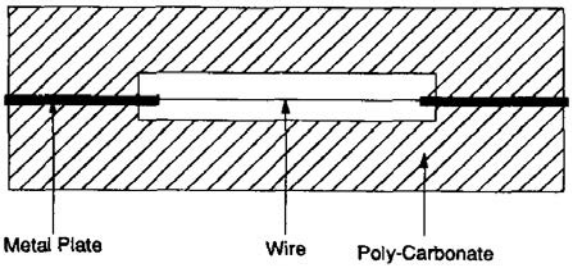


(b) Wire attached

Figure 2.14 (a) Schematic of experiment for measurement of wire deformation due to flow. (b) Wire attached in the middle of a rectangular cavity (Han and Wang, 1995b).

## 2.4 PBGA Encapsulation Process

Plastic ball grid array (PBGA) packages are typically used in many electronic applications (Qin, et al., 2012). Tay and Lee (2002) had simulated a PBGA package considering different gate positions using a 3-D finite element model (FEM). The effects of packaging materials and structure on interfacial delamination under the temperature excursions in the presence of moisture for two-dies stack with fine-pitch BGA were analyzed in detail by Kapoor et al. (2004).

Nguyen et al. (1999) carried out an experiment to capture the flow front during the plastic IC encapsulation process. A 24 mm × 24 mm of PBGA mould was equipped with a window and video camera to record the encapsulation process. Computational simulations of the cavity filling process were also performed by using CFDRC's PLICE (Plastic Integrated Circuit Encapsulation) CAD (from CFDRC, Huntsville, AL) and flow simulation software suites. Their simulation results showed only partial agreement with the moulding results; it was attributed from the model simplifications in order to reduce the computing time.

Cohn et al. (1995) described the experience and knowledge gained in designing and developing the 225 - 388 BGA's package. Design guidelines, thermal/electrical characterization and qualification data were reported in their study.

## 2.5 Wire Sweep Analysis

During the encapsulation of microelectronic chips by the transfer moulding process, the gold wire bonds, which allow electrical connection from the chip to the lead-frame or to the bond finger, are subjected to flow stress from the moulding compound. This flow stress can cause the lead-frame and the wire bonds to deform permanently from their original geometry or position; this phenomenon known as wire sweep and paddle shift in the industry. If the displacement of a bonding wire is too large, it can cause a package failure; for example, short circuit due to contact between adjacent wires or open circuit due to a broken wire breakage (Su et al., 2003). Even if the displacement is not so severe, wire sweep can initiate deterioration of the electrical and mechanical performance of the device, which will shorten its lifetime. Hence, it is imperative to reduce the wire sweep deformation during encapsulation. Wire sweep has been recognized as one of the major defects in the encapsulation of microelectronic chips by the transfer moulding process (Jong et al., 2005). The package used in their

study was a fine-pitch BGA with 492 lead counts (Figure 2.15). The comparison between simulation and experimental results of wire sweep is shown in Figure 2.16.

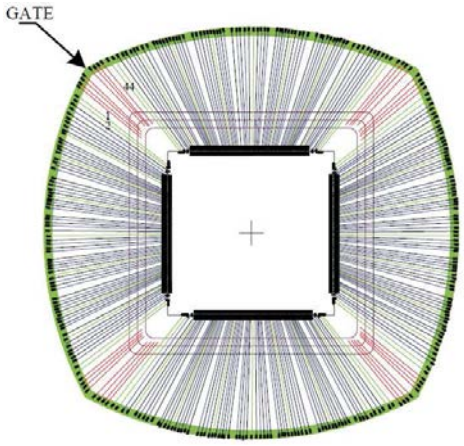


Figure 2.15 The 44 reference wires (marked green line) (Jong et al., 2005)

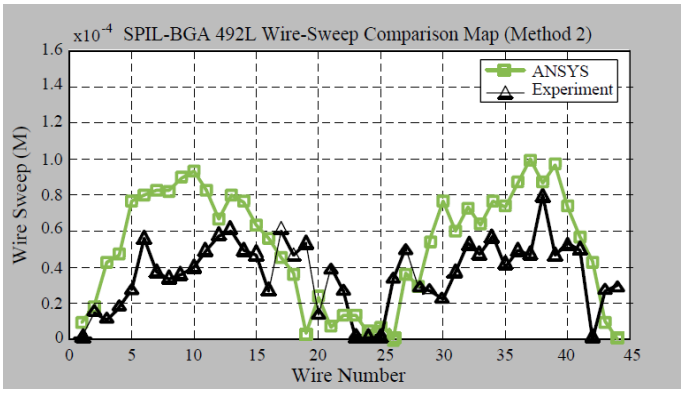


Figure 2.16 The wire-sweep comparison of BGA 492L (Jong et al., 2005).

Kung et al. (2006a) proposed the prediction of sweep deformation of wire bond model based on the bending moment and the twisting moment that imposed on the wire bond. They analyzed the numerical and experimental results of sweep deformation. Most wire sweep and deformation were caused by the twisting moment instead of the bending moment in semiconductor packaging applications. According to Kung et al. (2006a), the sweep deformation percentages from the twisting moment and the bending moment highly depend on the ratio of bond height and bond span. The decrease of bond height and bond span cause increase of twisting moment induced sweep deformation. They had performed a set of wire sweep experiments and compared with the predictions of the model. Since the interconnection distance of the multi-chip modules is usually longer than a single-chip system. Thus, wire sweep and wire sag issues had been mentioned in their studies for the applications of 3-dimensional packaging technology in the multi-chip module systems.

Wire sweep is a major defect in plastic IC packages and it has becomes more critical in the packages with high-density of wire (Jong et al., 2005, Pei and Hwang, 2005a, Muniandy et al., 2006). It can be happen due to any causes such as high resin viscosity, high inlet velocity, and unbalanced flows in the cavity, void transport, late packing, and filler collision (Han and Hwang, 1995b). In the microelectronic industry, the minimization of wire sweep always involves modifications in physical design such

as lead-frame design, mould design, device layout, moulding compound and process parameters based on experience and trial-and-error method. These steps are costlier and time-consuming. Thus, CAE tool could be an efficient method to resolve the problem of wire sweep through the simulation modelling.

The continuous reduction of chip size in the modern electronics industry has a significant impact on the circuit design and assembly process of integrated circuit (IC) packages. Reduced chip size with increased I/O counts results in serious wire deformation during the transfer moulding process. If the deformation of the wire is too large, it can cause a short circuit by touching the adjacent wires or an open circuit due to wire breakage (Su et al., 2003). Wire sweep has been recognized as one of the major defects in the encapsulation of microelectronic chips by the transfer moulding process (Jong et al., 2005). The package used in their study was a fine-pitch BGA with 492 lead counts (Figure 2.15). The comparison between simulation and experimental results of wire sweep is shown in Figure 2.16.

Recently, computer-aided engineering (CAE) has been applied by many researchers due to its excellent calculations and predictions on wire sweep problems. The prediction of wire sweep during the encapsulation may involve coupling technique on the moulding flow and structural deformation of wires, which is fluid/structure interaction (FSI) analysis. Many researchers had attempted this analysis by using various computational computer-aided engineering (CAE) techniques.

Yang et al. (2001) developed two-way coupling computational technique consisting of a CFD code (CFD-ACE-U) that computed the transient flow field during moulding process, and a structural dynamics code (FEM-STRESS) that computed the transient deformations and stresses of wires. The proposed technique could describe how wire sweep evolved with time throughout a package. Su et al. (2003) introduced a wire sweep investigation package "In-Pack," which joint global flow analysis (C-MOULD) and structure analysis (ANSYS), and the results showed better trend and accuracy than the C-MOULD microchip encapsulation. In the integrated CAE of wire sweep proposed by Yang et al. (2004), a true 3-D thermal flow solver based on a highly flexible prismatic element generation technique calculated the resin flow, the flow analysis was linked with structure analysis to provide the total solution for wire sweep assessment. Jong et al. (2005) implemented the modified C-MOULD reactive moulding solution to study the effect of wire density during encapsulation, by controlling the shape factor. They found a better solution for melt-front advancement and wire-sweep, and the predictions were validated by experiment results on a typical high-pin-count package (BGA 492L). Pie and Hwang (2005a) studied the effect of wire density by including wires in the mesh model for 3-D mould filling analysis, the solid mesh models were generated by the stacking method. A thin small outline package with 53 wires was used as the demonstration example. A three-dimensional mould filling analysis tool, MOULDEX3D-RIM, was used to simulate the flow of EMC during the moulding process and ANSYS was used as the structural analysis tool. The methodology of computational modelling and predictions of paddle shift during moulding process were studied by Pie and Hwang, (2005b). The methodology was described the flow modelling of the polymer melt around the lead-frame and paddle during the filling process. The pressure loading induced by the flow was extracted to the paddle. The effect on the overall model performance of different element types for the mould-filling and the structural analyses was also investigated in their study. The Kamal curing kinetics relation was applied to model the conversion of EMC in the flow region and the Castro-Macosko's viscosity model was used for the viscosity calculation of the EMC.

The mould-filling simulation was performed by Mouldex3D-RIM, commercial 3D mould filling software and ANSYS was used for the structural analysis.

Yao et al. (2005) conducted experiments to find out the threshold of a wire span of 23-$\mu$m diameter wire. 3-D finite element analysis was applied to further explain the wire sweep under the action of melt flow. It was found that the wire diameter had a significant role in wire sweep when the loop height and wire span were fixed. A non-sweep encapsulation technology that combined glob top and conventional transfer moulding processes was presented for long wire span and resulted in little wire sweep.

Kung et al. (2006a) proposed a sweep deformation model based on the evaluation of bending and twisting moments using ANSYS, and they verified the model by experiments. They revealed that the ratio of the bond height and the bond span crucially affect the percentages of sweep deformation from the twisting moment and the bending moment. Later, Kung et al. (2008) derived a method for evaluating the sweep resistance of wire bonds to obtain load versus transverse displacement curves.

Brand et al. (2008) studied a single die package using MOULDFLOW software, and experiment by considering different stacking configurations. The effects of varying loop height, stack height, and the type of moulding compound were quantified in terms of the maximum wire sweep. The wire sweep could be reduced by reducing the loop height; however, higher stacking of dies had increased the wire sweep.

Kung et al. (2006b) studied sweep characteristics of wire bond during the transfer moulding process for semiconductor packages through elevated-temperature. The various temperatures were done experimentally for obtaining the material properties of gold wire. A methodology was proposed to predict the elevated temperature behaviour of wire bond sweep. The increase of the sweep deformations is more related to bond span than bond height was obtained from the proposed methodology.

Chou et al. (2009) developed integration of CAE technology of pre-process connection, filling and structure analysis and post-process, which gives a comprehensive solution for microchip encapsulation. With this technology, wire sweep and paddle shift phenomenon in the package can be examined easily. ANSYS was adopted in the numerical analysis of their study. The simulation results were compared with the experiment and the wire sweep of each wire was also calculated.

Chylak et al. (2006) studied loop wire bonds design of stacked die BGA to reduce wire sweep due to mould flow. The sample of shape laterally and vertically with variants such as the “J” loop, the “M” (Multi-Bend) loop, and “Spider” loop. The illustration of “J” loop and “M” loop is shown in Figure 2.17.

Kung et al. (2006a) investigated the effects of the bending moment and the twisting moment on the sweep deformation model for different wire bond geometry. Besides, they also analyzed both experimentally and analytically for the bending geometry factor versus the ratio of bond height and bond span (*H*/*L*) in the range of 0.375–0.09375 as illustrated in Figure 2.19. The values of the bending geometry factor decrease drastically with the increasing of *H*/*L* ratio. They also calculated analytically the characteristics of the twisting geometry factor versus the ratio of *H*/*L* as depicted in Figure 2.20. As displayed in Figure 2.20, the values of the twisting geometry factor change linearly with the *H*/*L* ratio. Moreover, the geometry factors of the bending moment and the twisting moment were also obtained in their study (Kung et al. 2006a).

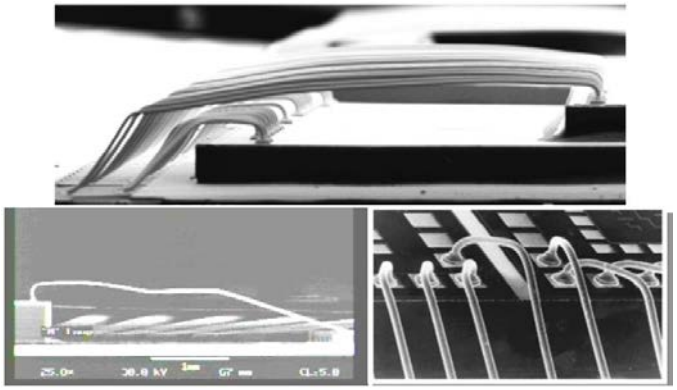

Figure 2.17 BGA wire looping (Chylak et al., 2006).

The geometry of a wire bond with the chip thickness (t), the bond spans (*L*) and the bond height (*H*) described by Kung et al. (2006a) is shown in Figure 2.18.

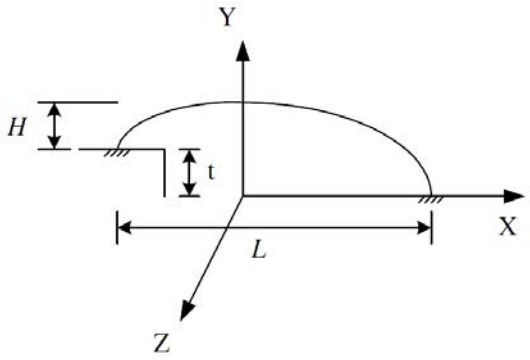


Figure 2.18 Geometry and notations of wire bond (Kung et al., 2006a).

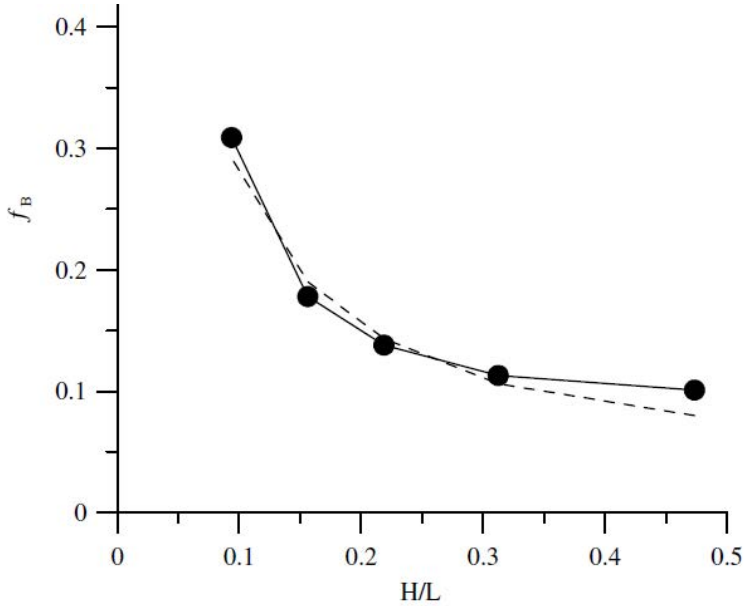


Figure 2.19 The bending geometry factor versus the ratio of bond height and bond span (Kung et al., 2006a).

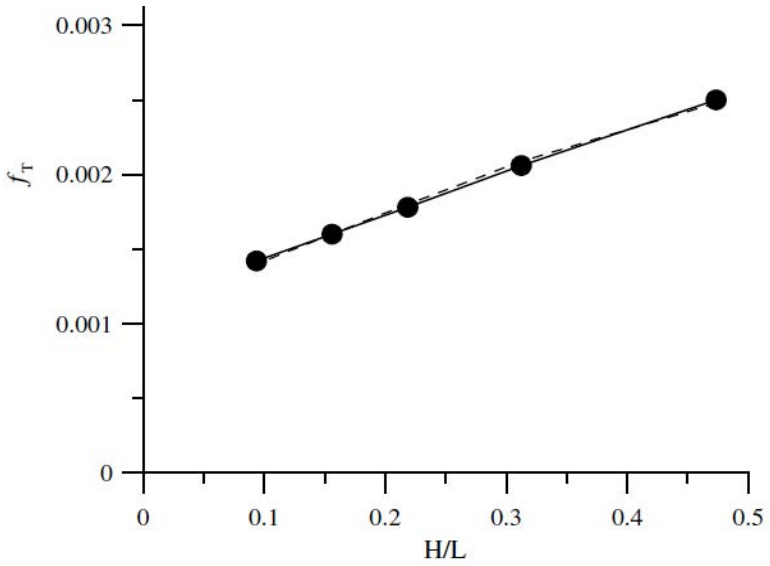


Figure 2.20 The twisting geometry factor versus the ratio of bond height and bond span (Kung et al., 2006a).

In most of the semiconductor packaging applications, the bond height is relatively small as compared with the bond span in most geometry of wire bond (Kung et al. 2006a). The ratio of *H*/*L* is approximate to be 0.1 was considered. Kung et al. (2006a) proposed the maximum sweep deformation ($\delta_{max}$) of the wire bond with bond height $H$, and bond span $L$, to be

$$\delta_{max} = S * D\left(f_B\left(\frac{H}{L}\right)\frac{H^3}{EI} + f_T\left(\frac{H}{L}\right)\frac{L^3}{GI_p}\right) \quad (2.1)$$

$$I = \frac{\pi d^4}{64} \quad (2.2)$$

$$I_p = \frac{\pi d^4}{32} \quad (2.3)$$

$$G = \frac{E}{2(1+\upsilon)} \quad (2.4)$$

where $S$ is the bond length, $D$ is the drag force per unit length of wire bond, $f_B$ is the bending geometry factor for the bending moment, $f_T$ is the twisting geometry factor for the twisting moment, $I$ is the moment of inertia, $I_p$ is the polar moment of inertia, $d$ is the diameter of wire, E is the modulus Young's and $\upsilon$ is the Poisson's ratio.

Kung et al. (2012) studied more in depth regarding to the wire sag problem for long wire bonds, which applied in 3-dimensional and/or in multi-chip module packaging. A sag stiffness of a wire bond was used to represent sag resistance of specific profiles of wire bond. Their study also considered wire sag in the experiments of wire bonds and verified numerical analysis by using a 3-D model of ANSYS, commercial FEA software.

Chai and Zohar (1999) had reported that most of the wire sweep was approximately proportional to the volume flow rate. The numbers of the wire bonds seriously affected the sweep level. The denser the wire bonds, the less susceptible to flow-induced loading due to rough interaction. The mould cavity height increases, the

wire sweep decreases exponentially to an asymptotic value. The vent size influenced the flow field in a non-uniform style and leads to different trend of the sweep levels. The sweep of the four wires that closer to the gate increases, while the sweep of the respite of the wires decreases.

Yoshihara et al. (1999a) reported the result of the wire deformation within the elastic region. It was found that wire sweep decreased very rapidly when the wire diameter increased. It was noted that wire sweep increased as the loop height increased. As packages become thinner, the loop height becomes lower in current design tendencies. Therefore, wire sweep should decrease relative to this parameter. Although low loop wires can improve the problem of contact between adjacent wires, however, there was an increased possibility of contact with the chip. Therefore, the problem of wire sweeps still important even for low loops. That wire sweep increases with the span.

Brand et al. (2008) attempted to fill the gap on qualifying the consequences of various wire bonds and mould process parameters by carried out the experiment using diverse test vehicles with different stacking arrangements. Particularly, the effects of varying loop height, stack height, and mould compound type were considered in terms of maximum wire sweep. They found that the loop height had a significant effect on wire sweep and the maximum wire sweep had been reduced from 6% until less than 3% by reducing the loop height. Additionally, their study found that higher number of die stacks caused the inclination to increase the wire sweep.

Figure 2.21 shows a numerical simulation of MOULDFLOW without pre-view of wire sweep, which displays fluid flow phenomenon. The higher flow velocities were identified around the no die regions and the presence of die caused slower flow velocity. Besides, stacked die also acted as the obstruction to the flow and backfilling are evidently found around the intermediate space of 2 stacked dies.

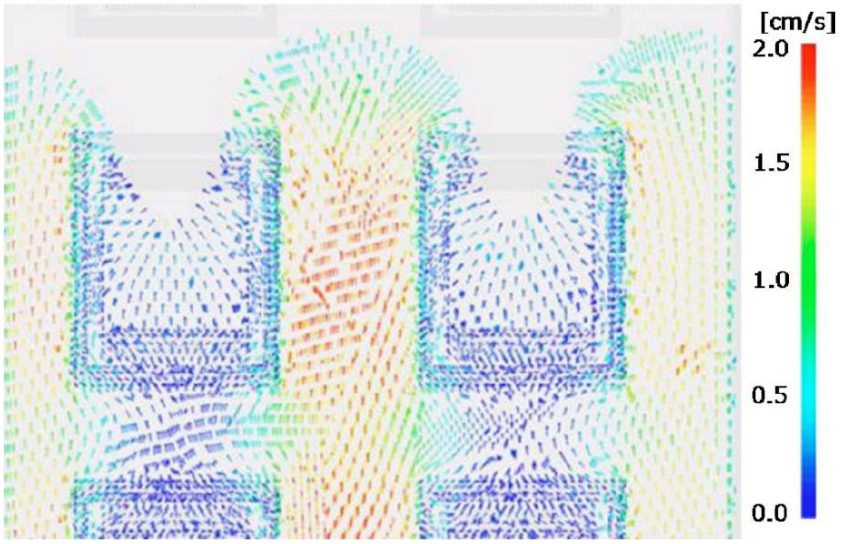


Figure 2.21 Flow velocity profile for stacked dies package that simulated by MOULDFLOW without wires sweep (top view) (Brand et al., 2008).

Nguyen et al. (1990) investigated the effects of material properties and the mould cavity/leadframe aspect ratio, the wire modulus, and the wire bond configurations (e.g., diameter, length, and orientation.) on wire sweep experimentally. A 14-lead bipolar device attached to a recessed bonded with gold wires and copper leadframe was the test vehicle.

## 2.6 Fluid Structural Interaction (FSI)

The interaction between the fluid flow and wire bonding may cause wire deformation. Therefore, it is important to understand the wire sweep behaviour in the design of wire bonds as well as in the IC encapsulation and process control. Wu et al. (1998) had carried out 3-D modelling of the wire sweep in the encapsulation process of rectangular packages. They observed that wire sweep was influenced by several factors such as the orientation, angle of the wire bond in the cavity, curing time, Reynolds number of fluid flow, moulding temperature and gate position. Similarly, Yoshihara et al. (1999a) reported that the wire bonding design such as the wire height, span, and diameter also affected the wire sweep in the IC encapsulation. They also carried out the experiments to investigate the elastic and plastic deformation regions of wire bonding.

Bailey et al. (2006) evaluated the performance of a custom VernaFlo® device using the fully coupled fluid/structure interaction solution provided by the ABAQUS co-simulation capability. During the analysis, a constant fluid topology was required in FLUENT. The effects of cavitations on the flow were considered. The computation results were compared to available experimental data.

Wintergerste (2002) had investigated the deformation of the mixer that caused by the fluid flow by using the coupling of commercial CFD (STAR-CD) and FEA (PERMAS) codes through a communications library called MpCCI.

In fact, wire sweep during encapsulation is a typical fluid–structure interaction (FSI) problem, which is normally handled by a coupled analysis of fluid flow and structural deformation. The use of a finite-volume flow solver and a finite-element structural solver, coupled through a mesh-based parallel code-coupling interface (MpCCI) has been reported for a variety of engineering problems (Yigit et al., 2008, Thirifay and Geuzaine, 2011, Gatzhammer et al., 2010).

Various studies have reported on the implementation of finite volume method (FVM) and finite-element method (FEM), which integrated with mesh-based parallel code coupling interface (MpCCI) for flow analysis and structural analysis (Yigit et al. 2008, Thirifay and Geuzaine 2011, Gatzhammer et al. 2010).

Khor, et al. (2012a) carried out an experiment and simulation of FSI by using FLUENT and ABAQUS code through coupling by using MpCCI software to investigate the phenomenon in moulded underfill (MUF) packaging. They fabricated a scaled-up IC package and studied the effects of FSI phenomenon in the moulded packaging. Their investigation using virtual modelling technique was proven to be excellent in handling FSI problem and the simulation was substantiated by experiment result. Besides, Khor et al. (2012a) also extended the study in actual-size IC packaging using the FSI modelling.

In the MpCCI coupling analysis, the program functions as a data library to transfer fluid induced forces to structural analysis. MpCCI program arrange the coupling data on different structured or unstructured meshes, see Figure 2.22. The meshes in most cases are distributed on several parallel processes. Therefore, MpCCI search and determine the neighborhood meshes and fit it accordingly. Then, MpCCI performs the interpolation on the coupling data. During the simulations, the neighborhood meshes search is usually performed only once during the initialization stage. The remeshing is only requires on a rapidly changing mesh, which initiates the neighborhood search at every coupling step.

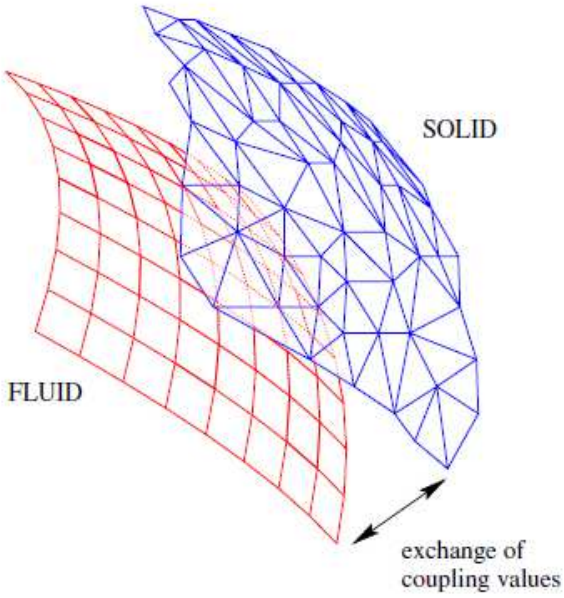


Figure 2.22. Data exchange between two non-matching grids (distance exaggerated) (Joppich et al. 2006).

## 2.7 Encapsulation Process Optimization

Wire sweep had been analyzed by using a design of experiment with considering three factors, i.e. transfer time, transfer force, and two types of EMC (Abdullah I., et al., 2007).

The wire sweep of SOT package in array matrix arrangement was analyzed by Han et al. (2011a) through the experimental and simulation works. They used two different simulation methods, which are 3D analysis and Dual Domain analysis. These methods were employed to predict the flow pattern and wire sweep during the transfer moulding process with a hybrid finite element/finite-difference method using commercial software Autodesk MOULDFLOW Insight (AMI). They reported that the sharply increased velocity was the key reason for the wire sweep when the vent located at the side of the mould and due to the flow front concentration. In order to address the issue, they carried out an optimization of transfer moulding process with transfer profile. Their simulation results revealed that the optimization of transfer moulding process is an effective way to solve this problem.

Liu et al. (2007) studied the optimization by using PGE (Power Ground Embedded) design to improve wire sweep for 44um fine pitch device and wire sweep could be controlled below 5%. FFT (Flow Free Thin) mould with optimized parameter had provided excellent wire sweep performance and wire sweep was controlled within 1.5%.

Ganesh and Sivakumar (2002) develop ultra low loop reverse wire bonding method on capped Copper bond pad metallization. To achieve desired second bond pull and minimum loop height ensuring enough die edge to wire clearance during wire bonding, bond parameters and looping parameters were optimized.

Liu et al. (2004b) evaluated the curing behaviour of two epoxy moulding compounds experimentally from different sources. Kissinger and Ozawa methods were used to estimate the activation energies for curing reactions. These two EMCs were also

considered in their study through transfer moulding process. The warpage of the encapsulated substrates with a dummy die were measured and the moulded parts were inspected using an acoustic microscope. The processing conditions of these two EMCs were optimized using design of experiments (DOE) method. Through the two-level DOE, they determined and evaluated the factors for warpage control and void formation. Liu et al. (2004b) had considered six process parameters for their DOE study to establish the relationship between the package quality and the processing parameters and to find the dominant process parameters. Those parameters included mould temperature; preheat time, transfer time, curing time, holding pressure and switchover pressure.

Muniandy et al. (2006) had implemented a top gate moulding for TBGA package to offer significant improvement in package performance and reduction in manufacturing cost. They investigated through experiment and Finite Element Analysis. The material and process characterization could be carried out efficiently by optimized the substrate design and improvement in component material properties through several designs of experiment's (DOE) . Key attractions to this relatively new moulding concept were its improvement in wire sweep performance for ultra fine pitch wire bonding and the ability to capitalize desirable mechanical properties of mould compound over liquid encapsulation material. The evaluation of the TBGA package on the mechanical aspects was performed via ANSYS commercial finite element software.

Khor and Abdullah (2012b) had investigated the optimization of moulded underfill (MUF) encapsulation process considering FSI using response surface methodology (RSM) to minimize the stress concentration and deformation of the IC structures. Pressure inlet, solder bump standoff height, chip thickness, gap-wise between chips, and mould and filled time were chosen as the physical and process parameters. Central composite design (CCD) was applied to optimize the IC encapsulation via response surface methodology. They noted that optimized parameters yielded minimum stress concentration of chip and solder bump, chip deformation, and void in package during the IC encapsulation process.

## 2.7 Summary

The major trend for electronic products is towards lower weight, smaller size, lower cost, higher performance and lower power consumption. In order to make the trend and target possible, several encapsulation process investigation have been reported. Numerous efforts have been done by previous workers on experiments and simulations of encapsulation process. The trial-and-error method in the investigation is neither efficient nor economic. Various parameters have been considered in the investigation to identify the problems and the solutions in wire sweep of PBGA packages encapsulation process.

Small scale and compact characteristic of PBGA package has constrained the real time visualization of the wire sweep phenomenon during encapsulation process in microelectronic industry. Therefore, the scaled-up IC package using transparent mould is advantageous to provide better visualization during the process. Several scholars have attempted to carry out the experiment without compared the wire sweep result with simulation result. Scaled-up IC packages had been fabricated with simplified wire region (e.g. single wire) and package size (e.g. simple rectangular cavity). In this study, the scaled-up PBGA encapsulation has been fabricated by referring to the IC chip and wire bond of actual package. Different inlet positions of the mould, stacking die effect, inlet pressure effect have been considered in the current experimental work. The

experimental results (flow profile and wire sweep) will be compared with the FSI simulation predictions for the validation purpose.

However, computer aided engineering (CAE) software have facilitated the improvement of encapsulation process on the flow and structure visualization studies. Thus, CAE commercial software analysis provides a significant contribution for finding those solutions in the electronics packaging industry by avoiding trial-and-error method and reduces the time of investigation. From the literature, the simulation works had been started with 2-D model using Hele-Shaw approximation followed by 3-D model. FEM is a familiar method used by previous researchers. However, this method requires large memory and it is time consuming; this made it impractical in the microelectronic industry. Therefore, the researchers tried to look for an appropriate method to overcome those problems. Accordingly, they switched over to finite volume method (FVM) with VOF technique to track and solve them. FLUENT 6.3 are designed based on FVM formulation for fluid flow phenomena's. Thus, CFD software, FLUENT 6.3.26 is utilized in the present study to investigate and solve the problem in electronics packaging technology. Accordingly, a novel 3D computational technique using the MpCCI method is introduced on the PBGA encapsulation process for the prediction of wire sweep and flow front analysis. This method utilizes the finite-volume flow solver FLUENT and the finite-element structural solver ABAQUS, interfaced by MpCCI.

## CHAPTER 3: EXPERIMENTAL AND SIMULATION

This book consisted of experimental and simulation studies in plastic ball grid array (PBGA) encapsulation process. The experiment was carried out by using a simple transfer moulding system on a scaled-up eight wires PBGA encapsulation process. In the simulation, the flow-front profile of EMC and wire sweep behaviours within the mould cavity were predicted through the simulation tools, FLUENT and ABAQUS, which were connected through MpCCI coupling interface to handle a two-way and real time encapsulation process under the effect of FSI.

### 3.1 Introduction

It is important to understand the physics that govern the flow characteristics of EMC. The flow characteristics of EMC are complicated, given the complex properties of EMC that change under the effect of temperature, shear rate and curing rate as described in the rheokinetic models. To solve the complex flow, specific physical laws must be satisfied and expressed in mathematical terms. The basic mathematics for a comprehensive general-purpose model is derived from the conservation of mass, momentum and energy. These basic principles lead to the derivation of the continuity, Navier-Stokes and energy equations for solving the model. However, for material, there are also one or more constitutive equations that specifically describe the material properties such as shear thinning behaviour or shear rate of material. These equations may also become more complex when there are combinations of equations to calculate the temperature-dependent viscosity. Although there is complexity in the equations, the target of the model is to apply these mathematical equations and to solve them to perform the prediction of EMC flow characteristics in the simulation.

The PBGA encapsulation process involves the interaction between fluid and structure, which could cause wire sweep. In fact, wire sweep during encapsulation is a typical FSI problem, which can be solved by using a coupling technique between fluid flow and structural deformation. During the simulation, finite-volume and finite-element structural solvers are coupled through a mesh-based parallel code coupling interface (MpCCI). MpCCI functions as a library data, which enables the exchange of simulation data between the solvers in real time, and the deformation of wire, is calculated simultaneously.

### 3.2 Governing Equations

In the present study, the simulation model is governed by several fundamental equations. The continuity and momentum equations were applied to model the fluid flow characteristics. The energy equation, which is dependent on the temperature of process condition, was also considered. Besides, the Castro−Makosco viscosity model is incorporated with the Newtonian fluid model and namely as generalized Newtonian fluid (GNF). Castro-Macosko model was developed by Castro and Macosko (1980). It is to describe the polymerization and to predict the viscosity of moulding material. The Castro−Makosco viscosity model was utilised for the polymer rheology model, which manages the change of viscosity due to the temperature effect and it shows the linear relationship for shear stress and shear rate of the fluid. However, the volume of fluid (VOF) model was applied for melt front tracking in the analysis. By considering Cross

model and Castro-Macosko models, molten EMC material behaves more or less as Newtonian fluid with the change in viscosity being the non-Newtonian aspect in the encapsulation process. Besides, Lee et al. (2008) reported another reason for the assumption of EMC as a generalized Newtonian fluid; it was because of the negligible of fluid elasticity when the degree of cure in the filling stage was low during encapsulation process. Therefore, the behaviour of the EMC in the simulation is usually assumed as generalized Newtonian fluid as described by both viscosity models. The operational shear rate during the EMC transfer moulding process is varied from 10 to 1000 1/s (Hassan et al., 2008).

### 3.2.1 Fluid Analysis

In the simulation model, the EMC and air were assumed to be incompressible. The governing equations that describe the fluid flow are the conservations of mass, momentum and energy, as listed below:

The conservation of mass or the continuity equation is:

$$\frac{\partial u}{\partial x}+\frac{\partial v}{\partial y}+\frac{\partial w}{\partial z}=0 \tag{3.1}$$

Eq. (3.1) is the form of the mass conservation equation and is valid for incompressible flows. The mass conservation equations in x, y and z directions for describing the incompressible flows are as follow:

x-direction

$$\frac{\partial u}{\partial t}+u\frac{\partial u}{\partial x}+v\frac{\partial u}{\partial y}+w\frac{\partial u}{\partial z}=-\frac{1}{\rho}\frac{\partial p}{\partial x}+\left[\frac{\partial}{\partial x}\left(\eta\frac{\partial u}{\partial x}\right)+\frac{\partial}{\partial y}\left(\eta\frac{\partial u}{\partial y}\right)+\frac{\partial}{\partial z}\left(\eta\frac{\partial u}{\partial z}\right)\right]+\rho g_x \tag{3.2}$$

y-direction

$$\frac{\partial v}{\partial t}+u\frac{\partial v}{\partial x}+v\frac{\partial v}{\partial y}+w\frac{\partial v}{\partial z}=-\frac{1}{\rho}\frac{\partial p}{\partial y}+\left[\frac{\partial}{\partial x}\left(\eta\frac{\partial v}{\partial x}\right)+\frac{\partial}{\partial y}\left(\eta\frac{\partial v}{\partial y}\right)+\frac{\partial}{\partial z}\left(\eta\frac{\partial v}{\partial z}\right)\right]+\rho g_y \tag{3.3}$$

z-direction

$$\frac{\partial w}{\partial t}+u\frac{\partial w}{\partial x}+v\frac{\partial w}{\partial y}+w\frac{\partial w}{\partial z}=-\frac{1}{\rho}\frac{\partial p}{\partial w}+\left[\frac{\partial}{\partial x}\left(\eta\frac{\partial w}{\partial x}\right)+\frac{\partial}{\partial y}\left(\eta\frac{\partial w}{\partial y}\right)+\frac{\partial}{\partial z}\left(\eta\frac{\partial w}{\partial z}\right)\right]+\rho g_z \tag{3.4}$$

where, $\rho$ is the density, $u$ is the velocity vector, $P$ is the static pressure, and $g_i$ are the gravitational acceleration in the $i$ direction, respectively.

The energy equation in terms of $h$ (static enthalpy) can be written as,

$$\rho C_p\left(u\frac{\partial T}{\partial x}+v\frac{\partial T}{\partial y}+w\frac{\partial T}{\partial z}\right)=k\left(\frac{\partial^2 T}{\partial x^2}+\frac{\partial^2 T}{\partial y^2}+\frac{\partial^2 T}{\partial z^2}\right)+\Phi \tag{3.5}$$

where $k$ is the thermal conductivity, $T$ is the absolute temperature and $\Phi$ is the energy source term and it contains two contributions of polymer properties:

$$\Phi=\eta\dot{\gamma}^2+\dot{\alpha}\Delta H \tag{3.6}$$

$$\dot{\gamma} = \sqrt{\left(\frac{\partial u}{\partial x}\right)^2 + \left(\frac{\partial v}{\partial y}\right)^2 + \left(\frac{\partial w}{\partial z}\right)^2} \tag{3.7}$$

where $\eta$ is the viscosity and $\dot{\gamma}$ is the shear rate, $\dot{\alpha}$ is the curing rate and $\Delta H$ is the reaction heat. The moulding compound was assumed to be a generalised Newtonian fluid (GNF).

Several models have been used to predict the relationship between viscosity ($\eta$) and the degree of polymerization. The Castro–Macosko model, as expressed in Eq. (3.6) and (3.7), has been applied by Jong et al. (2005), Nguyen et al. (2000), and Khor et al. (2011) and it is used in this simulation. It is described as follows:

$$\eta(T, \dot{\gamma}) = \frac{\eta_0(T)}{1+\left(\frac{\eta_0(T)\dot{\gamma}}{\tau^*}\right)^{1-n}} \left(\frac{\alpha_g}{\alpha_g - \alpha}\right)^{C_1 + C_2\alpha} \tag{3.8}$$

where $T$ is the absolute temperature, $n$ is the power law index, $\eta_o$ the zero shear rate viscosity, $\tau^*$ is the parameter that describes the transition region between zero shear rates and the power law region of the viscosity curve, $\alpha$ is the conversion of reaction, $\alpha_g$ is the conversion at the gel point, and $C_1$ and $C_2$ are fitting constants.

$$\eta_o(T) = Bexp\left(\frac{T_b}{T}\right) \tag{3.9}$$

$B$ is an exponential-fitted constant and $T_b$ is a temperature fitted-constant. In addition, the Kamal curing kinetics is coupled together with the Castro–Macosko model. This model predicts the rate of chemical conversion of the compound as follows:

$$\frac{d\alpha}{dt} = (k_1 + k_2\alpha^{m_1})(1-\alpha)^{m_2} \tag{3.10}$$

$$k_1 = A_1 exp\left(-\frac{E_1}{T}\right) \tag{3.11}$$

And

$$k_2 = A_2 exp\left(-\frac{E_2}{T}\right) \tag{3.12}$$

where $A_1$ and $A_2$ are the Arrhenius pre-exponential factors, $E_1$ and $E_2$ are the activation energies, and $m_1$ and $m_2$ are the reaction orders. The curing degree ($\alpha$) of the EMC can be defined as a ratio of the heat released to the total heat released at complete conversion (Nguyen et al. 2000, Wang et al. 2010).

$$\alpha(t) = \frac{\Delta H(t)}{\Delta H_{total}} \tag{3.13}$$

The Newtonian fluid equation is as follow:

$$\eta = \frac{\tau}{\dot{\gamma}} \tag{3.14}$$

where, $\tau$ is the shear stress and $\dot{\gamma}$ is the strain rate.

The basic idea of VOF scheme is to locate and evolve the distribution of, say, the liquid phase by assigning each cell in the computational grid a scalar $f$, which specifies the resin proportion in each particular cell. Thus, $f$ takes the value of 1 ($f = 1$) in cell which contains only resin, the value 0 ($f = 0$) in cells which are void of resin, and a value between 0 and 1 ($0 < f < 1$) in "interface" cells or can be referred as the resin melt front. The equation of melt front over time is governed by the following transport equation:

$$\frac{dF}{dt} = \frac{\partial F}{\partial t} + u\frac{\partial F}{\partial t} + v\frac{\partial F}{\partial t} + w\frac{\partial F}{\partial t} - \left(\frac{\partial^2 F}{\partial x^2} + \frac{\partial^2 F}{\partial y^2} + \frac{\partial^2 F}{\partial z^2}\right) = 0 \quad (3.15)$$

### 3.2.2 Wire Sweep Analysis

To calculate the drag force exerted on the wires by the resin flow, the value of velocities and viscosities have to be determined from the mould filling simulation. Then, the Lamb's model is utilized to calculate the drag force as follows (Su et al., 2003, Pei and Hwang, 2005a, and Han and Huh, 2000):

$$D = \frac{C_D \rho U^2 d}{2} \quad (3.16)$$

where $D$ is the drag force per unit length, $\rho$ is the fluid density, $U$ is the undistributed upstream velocity, $d$ is the wire diameter and $C_D$ is the drag coefficient which can be written as (Su et al., 2003, Pei and Hwang, 2005a, and Han and Huh, 2000):

$$C_D = \frac{8\pi}{Re[2.002 - \ln(Re)]} \quad (3.17)$$

where Re is the Reynold number.

In order to assist the designer of a wire profile to obtain a reasonable allowed sweep, a sweep deformation model based on the contribution of the bending moment and the twisting moment has been proposed by Kung et al. (2006a). According to the model, the sweep deformation of the wire δ can be written as:

$$\delta_{max} = S \times D\left(f_B\left(\frac{H}{L}\right)\frac{H^3}{EI} + f_T\left(\frac{H}{L}\right)\frac{L^3}{GI_p}\right) \quad (3.18)$$

where $D$ is the drag force per unit length of the wire and $S$ is the length of the wire, $f_B$ is the bending geometry factor for the bending moment, $f_T$ is the twisting geometry factor for the twisting moment, $H$ is the height of wire, $L$ is the length of wire span (See Figure 2.18), $G$ is the shear modulus of wire, $E$ is the elastic modulus of wire, $I$ is the moment of inertia of the wire, $I_p$ is the polar moment of inertia of the wire.

In order to make a comparison between the results of simulation and experiment, a dimensionless parameter, wire sweep index (See Figure 3.1), is used. The wire sweep index is calculated from making the largest deformation normal to the wire divided by the projected length of the wire (Nguyen et al., 1997, Pei, 2004, Onodera et al., 2007).

Wire Sweep Index (%) = $D_N/L$ (3.19)

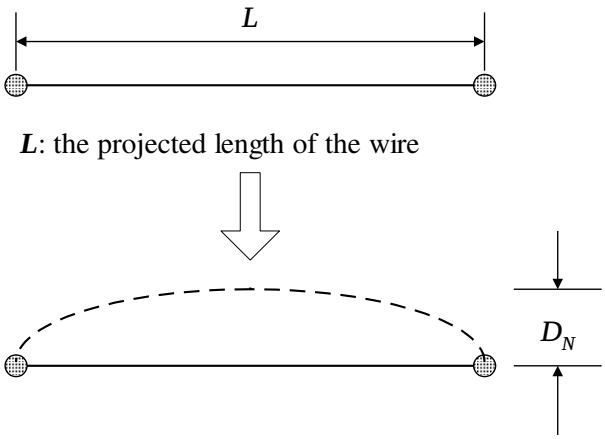


Figure 3.1 Definition of wire sweep

### 3.2.3 Code Coupling with MpCCI

In the present study, the FSI activity during the encapsulation process is visualized by using the virtual model that is created and simulated in FLUENT and ABAQUS. During the simulation analysis, the two-way coupling method is implemented in parallel for FSI as shown in Figure 3.2. The pressure data generated from the flow (FLUENT) is transferred to ABAQUS for structural analysis by MpCCI. The deformation of the structure in ABAQUS will give the feedback to the flow analysis in the FLUENT in the real time calculations. The deformed wire bonds may cause instability on the flow front profile. The extreme deformation of wire bond during the encapsulation process could cause failure for the package during the process due to short circuit problem. Therefore, the deformation of wire bonds during the encapsulation process is also crucial for the packaging design.

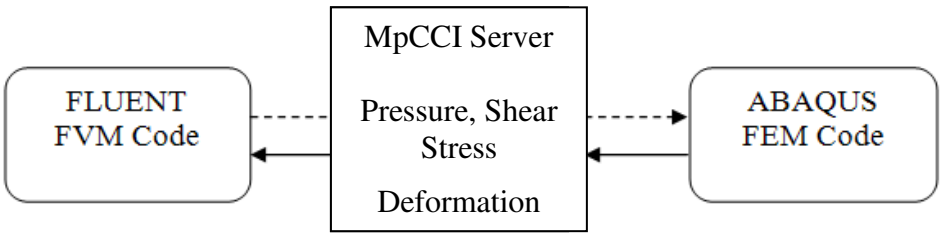


Figure 3.2 Data exchange from FLUENT and ABAQUS by MpCCI.

MpCCI nowadays is the most widely used software for the coupling of several codes. It works quite well for a fixed pair of codes (Wolf, 2007, Yigit et al. 2008). MpCCI is a software library that enables the exchange of data defined on meshes of two or more simulation codes in the coupling region. Since the meshes need not match point by point, MpCCI performs an interpolation and, in the case of parallel codes, keeps track of the distribution of the domains onto different processes (Thirifay and Geuzaine, 2008). In this way, the intricate details of the data exchange are hidden behind the concise interface of MpCCI. Consequently, the simulation codes themselves are changed only moderately when they are prepared for coupling via MpCCI.

For the communication between the involved codes, the message-passing interface is used (Schreiber et al., 2005). At the interface between fluid and structure, there is some mapping of data between two, in general a non matching grid. In the MpCCI concept, this mapping is done directly from one solver to the other with the help of either given library routines. This implies that each solver has to know the grid of the other solver and, thus, inhibits the exchange of one solver without changing the code of the other one.

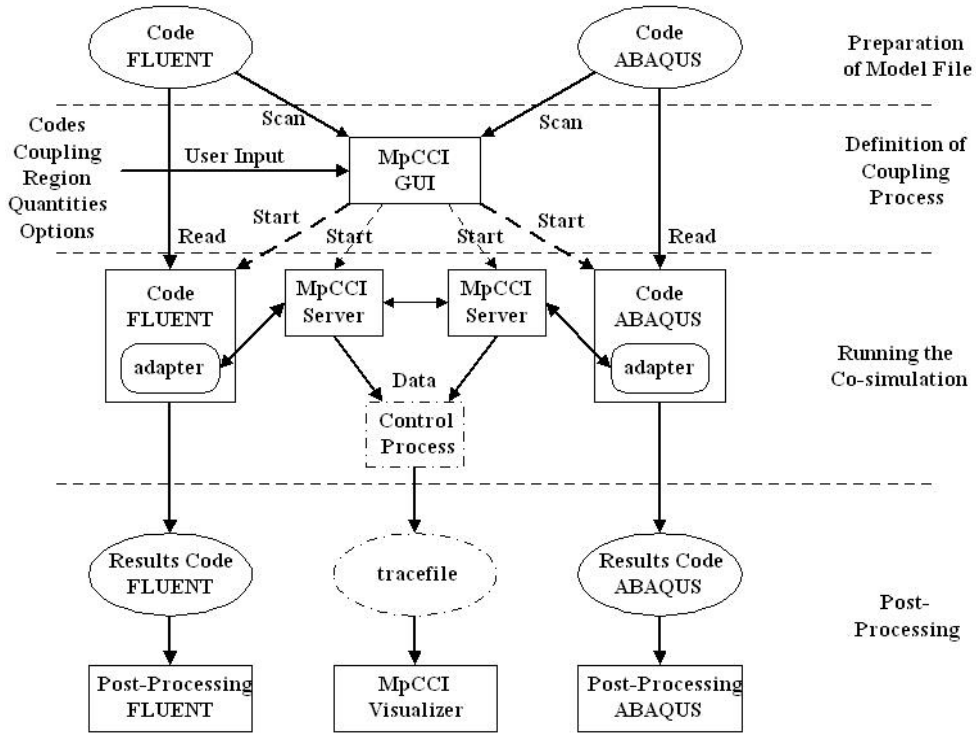


Figure 3.3 FLUENT and ABAQUS coupling simulation process (MpCCI 3.1.0-1 Doc., 2009).

Running a co-simulation with MpCCI require the process given in Figure 3.3. There are four steps of the complete co-simulation with MpCCI: 1) preparation of model files, 2) definition of the coupling process, 3) running the co-simulation; and 4) post processing (MpCCI, 2009). First, each domain is modelled separately and created for each simulation code. The models contain a definition of the coupling region. The interface between solid and fluid depends on the coupling regions, which are the surfaces (wires in the PBGA package) that have been defined in both codes. During the simulation the MpCCI software distributes the data on the surface of wires. Simulation codes, the corresponding model files and the coupled region, quantities, and a coupling algorithm must be selected in the second step. This step is completely supported by the MpCCI GUI. Next, starting with the MpCCI server, both coupled codes are started. Each code computes its part of the problem while MpCCI controls the quantity exchange. Lastly, the results can be analysed with the post-processing tools of each simulation code, with the FLUENT and ABAQUS visualizer. The sample of coupling process is shown in Appendix A.

For the fluid structure coupling, an implicit portioned approach is employed (Thirifay and Geuzaine, 2008). Figure 3.4 a schematic view of an iteration process, which is performed for each time step, is given. After the initializations the flow field is determined in the actual flow geometry. From this, the friction and pressure forces on

the interacting walls are computed, which are then passed to the structural solver as boundary conditions. The structural solver computes the deformations with which the fluid mesh is modified, before the flow solver is started again.

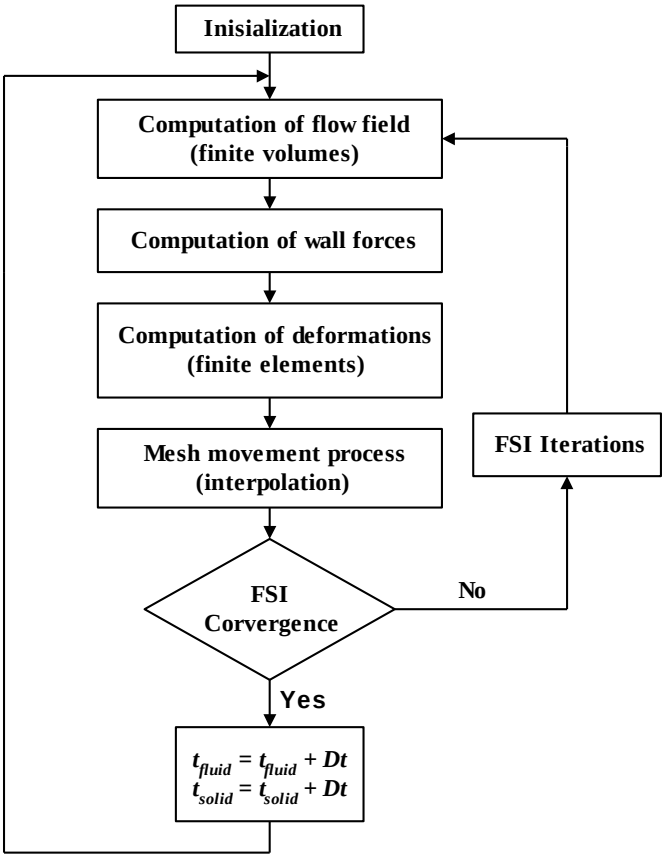


Figure 3.4 Flowchart of couple solution procedure (Michael, 2005, Yigit et al. 2008).

## 3.3 Influence of Number of Mould Cavity Vents and Inlet Gate on Wire Sweep in Scale-up Four-wire PBGA Encapsulation Process

### 3.3.1 Problem Description

In all the previous works on wire sweep prediction, the fluid and structural solvers were run separately and coupled manually. As a promising breakthrough in the FSI analysis, MpCCI technique has recently been introduced for the simultaneous real time coupling of fluid and structural solvers. The use of a finite volume flow solver and a finite element structural solver, coupled through MpCCI was reported for variety of engineering problems (Yigit et al., 2008, Thirifay and Geuzaine, 2008, Gatzhammer et al., 2010). However, as far as the authors are aware, the use of MpCCI for wire sweep analysis and the study on the effect of number of vents on wire deformation during the encapsulation of PBGA package have not been reported so far. To address this problem, the finite-volume flow solver FLUENT and the finite-element structural solver ABAQUS are interfaced by MpCCI. Polymer rheology model with curing effect (the Castro−Macosko model) is used in the fluid flow model and the VOF technique is applied for melt front tracking of the EMC. The numerical analysis uses User-defined

functions (UDFs) to account for curing kinetics. Keeping one gate, three configurations of mould cavity with 2, 4 and 6 vents are simulated. Melt front profiles, wire sweep, pressure field, and stress distribution on wires, are analysed for each case. The proposed model is well validated by the published experimental results of Yang et al. (2000). Table 3.1 summarises the material properties of the EMC considered in the current simulation.

Table 3.1 Material properties of EMC used in the mould filling analysis (Nguyen et al., 2000).

| | Parameter | Value | Unit |
|---|---|---|---|
| Castro−Macosko Model | $\alpha_g$ | 0.17 | - |
| | $B$ | 0.000381 | Kg/m/s |
| | $T_b$ | 5230 | K |
| | $n$ | 0.7773 | - |
| | $\tau$ | 0.0001 | $N/m^2$ |
| | $C_1$ | 1.03 | - |
| | $C_2$ | 1.50 | - |
| Curing Kinetics | $m_1$ | 1.21 | - |
| | $m_2$ | 1.57 | - |
| | $A_1$ | 33530 | 1/s |
| | $A_2$ | 30540000 | 1/s |
| | $E_1$ | 7161 | K |
| | $E_2$ | 8589 | K |
| | $\alpha$ | 0.05 | - |
| Density | $\rho$ | 2000 | Kg/m3 |
| Specific Heat | $Cp$ | 1079 | J/Kg-K |
| Thermal Conductivity | - | 0.97 | W/m-K |
| Reference Temperature | $T$ | 298 | K |

### 3.3.2 FSI Simulation Model and Boundary Condition

#### 3.3.2.1 Fluid Model in FLUENT

The VOF model in FLUENT 6.3.26 is utilized to simulate the process (Khor et al., 2010a,). In the VOF model, a single set of momentum equations is shared by the fluids, and the volume fraction of each of the fluids in each computational cell is tracked throughout the domain (Khor et al., 2010b). Air and EMC are defined as the phases in the analysis. Implicit solution and time dependent formulation are applied for the volume fraction in every time step. The volume fraction of the encapsulation material is defined as one and zero value for air phase.

The Castro−Macosko viscosity model with curing effect was written into C language using Microsoft VISUAL Studio 2005 and compiled as UDF in FLUENT. The sample of UDF list code of Castro−Macosko viscosity model that refer to Table 3.1 is shown in Appendix B. The mould cavity package models with different number of vents and different inlet gates, and its boundary conditions are shown in Figures 3.5a, 3.5b, 3.6a and 3.6b respectively. The dimension of mould cavity is 10 cm × 10 cm × 0.5 cm, die is 3 cm × 3 cm × 0.1cm and inlet gate is 0.8 cm × 0.8 cm (Han and Huh, 2000). The flow direction is diagonal of x and z direction to the un-deformed wire axis and the properties are approximately the same as those used in ref. (Han and Huh, 2000). In the

current study, the model is created by using GAMBIT software and average 395000 tetrahedral elements are generated for simulation (Figure 3.7) in terms of accuracy and computational cost. Besides, time step size is also tested and 0.001 s (Khor et al., 2010a) is found to be the optimum. The governing equations are discretized by the first order upwind scheme, and solved by SIMPLE algorithm.

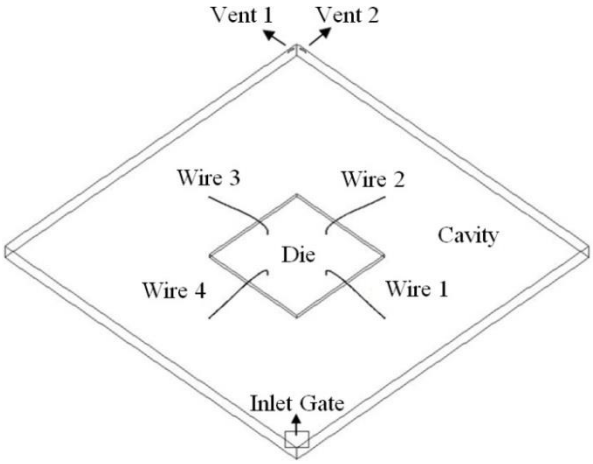


(a) 2 vents

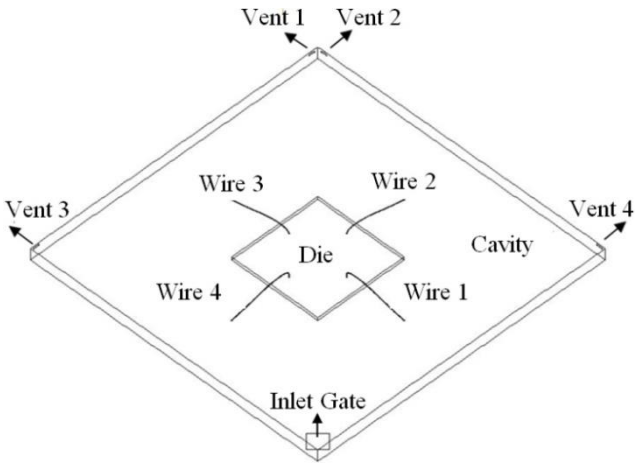


(b) 4 vents

Figure 3.5a Mould cavity models of scale-up four-wire PBGA with different outlet vent: (a) 2 vents, (b) 4 vents

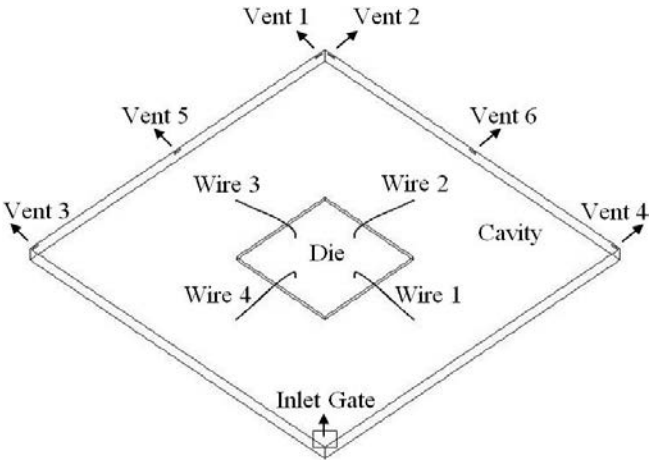


(c) 6 vents

Figure 3.5b Mould cavity models of scale-up four-wire PBGA with different outlet vent: (c) 6 vents (continued).

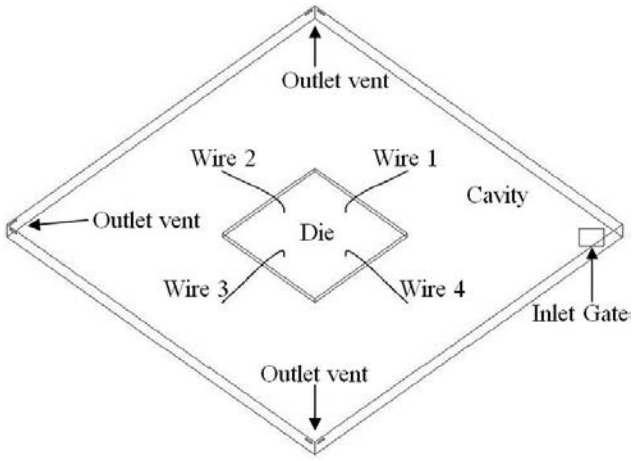


(a) One inlet gate

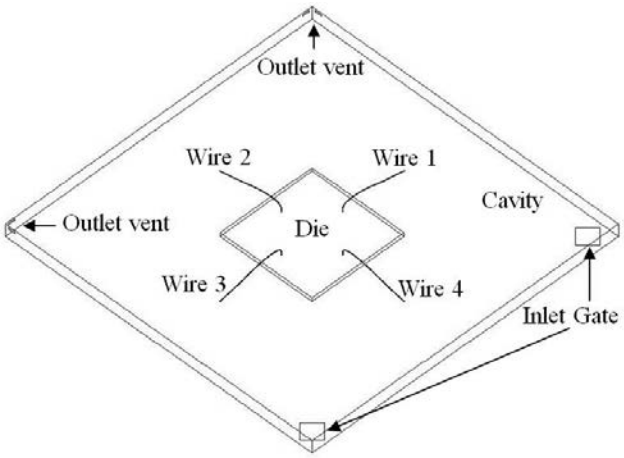


(b) Two inlet gates

Figure 3.6a Mould cavity models of scale-up four-wire PBGA with different inlet gate: (a) One inlet gate and (b) Two inlet gates.

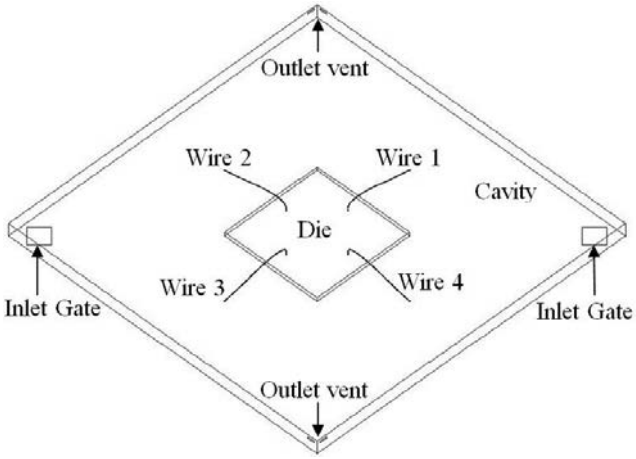


(c) Two inlet gates diagonal

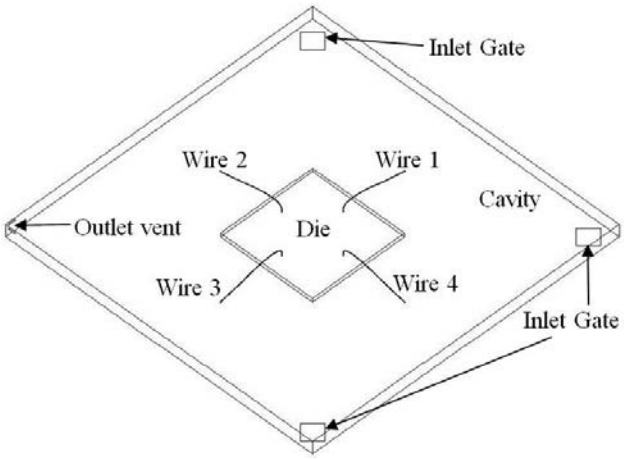


(d) Three inlet gates

Figure 3.6b Mould cavity models of scale-up four-wire PBGA with different inlet gate: (c) Two inlet gates diagonal and (d) Three inlet gates (continued).

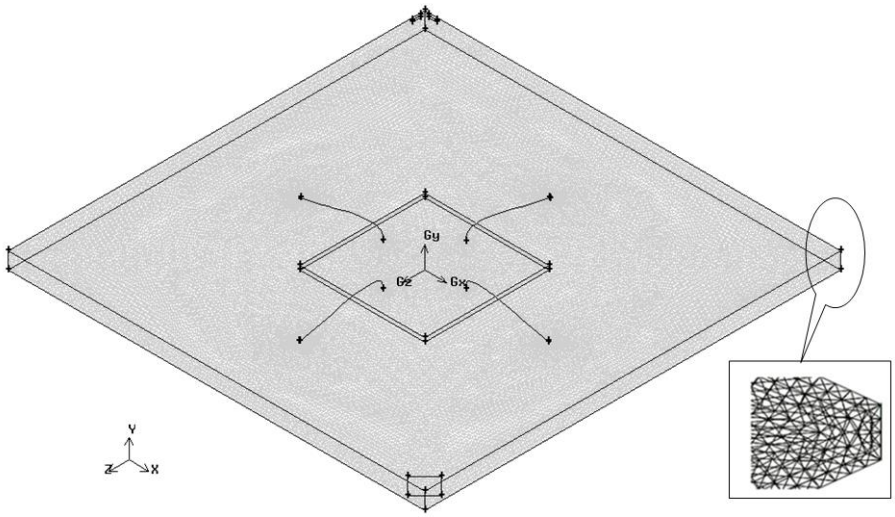


Figure 3.7 Meshed models of scale-up four-wire PBGA with 2 vents for FLUENT analysis.

The boundary and initial conditions used in the calculation are as follows (Khor et al., 2010b):

(a) On the wall: $u_i = 0$; $T = T_w$, $\frac{\partial p}{\partial n} = 0$

(b) On the melt front: $p = 0$ (Gauge pressure)

(c) At the inlet: $u = u_{in}(x,y,z)$; $T = T_{in}$

The mould temperature was considered as 175 $^{o}$C and the package inlet velocity was 0.6 m/s. The simulation is performed on an Intel Core 2 Duo processor E7500, 2.93 GHz with 2 GB of RAM; it took around 74 hours for each case to complete 15000 iterations in time steps of 0.001s.

### 3.3.2.2 Wire Model in ABAQUS

Commercial FEM based software; ABAQUS has been used in this study to calculate the wire deformation. The structures of the wires are imported from GAMBIT in ACIS '.sat' format. The dimensions of the gold wire used in this study are chosen according to the model of Yang et al. (2000). The wire (Figure 3.8) has a span, $L$ = 20 mm, height $H$ = 3.5 mm and diameter $d$ = 0.14 mm. The wire is divided into 10191 tetrahedral elements (The element is defined by four nodes having three degrees of freedom at each node) as shown in Figure 3.9. The shape of the wire is also classified as typical Q-auto loop wire (Brand et al., 2008). The ball bond boundary conditions of wire were set as fixed in ABAQUS and shown in Figure 3.10. The wire mechanical properties are as follows: elastic modulus, $E$ = 50 GPa (Yang et al., 2004), density, $\rho$ = 19330 kg/m$^3$, Poisson's ratio, $v$ = 0.42.

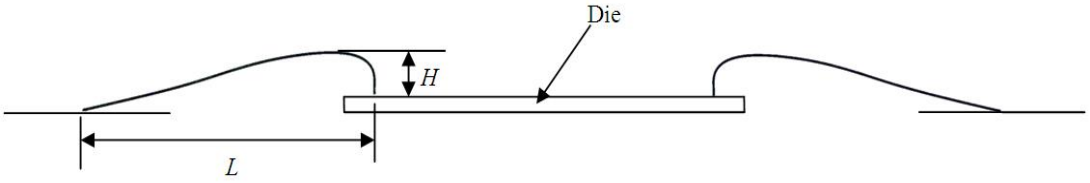


Figure 3.8 Wire specifications of scale-up four-wire PBGA.

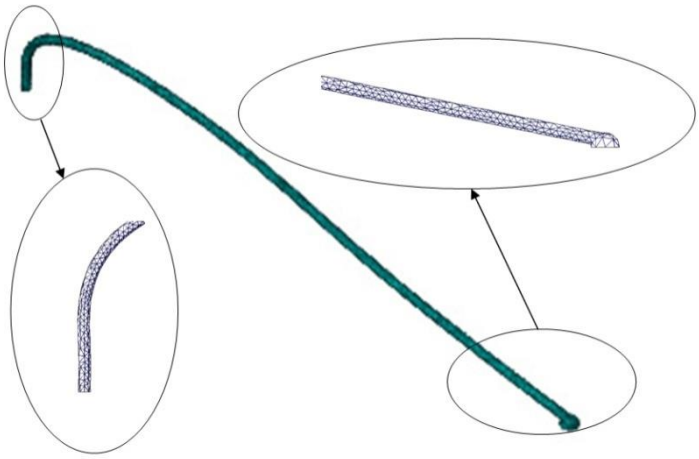

Figure 3.9 Meshed wires of scale-up four-wire PBGA for ABAQUS analysis.

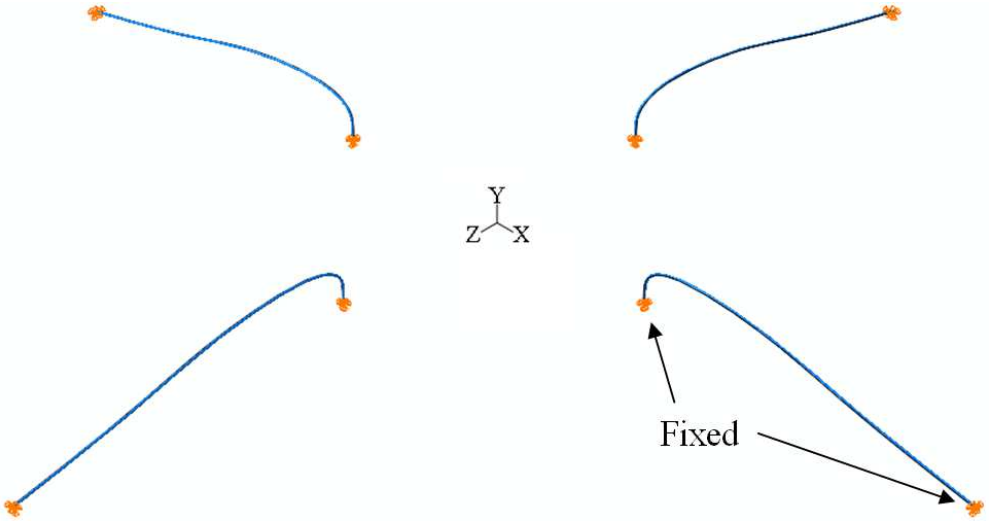


Figure 3.10 Boundary conditions of wires of scale-up four-wire PBGA in ABAQUS.

## 3.4 Wire Sweep Analysis Considering Stacked Die Effect and Arrangement of Inlet Gate of Scale-up Eight-wire PBGA Encapsulation Process

### 3.4.1 Problem Description

The small PBGA and non-transparent packaging mould used in the actual encapsulation process causes difficulties in visualisation of the FSI phenomenon. The deformation of the wire bond is normally observed from the top view of the package using x-ray. It is the best method for visualising FSI through vertical and top views of the mould for better understanding of FSI. Investigation can also be conducted using simulation tools. However, the visualisation of FSI during the encapsulation of PBGA is complicated. Therefore, a transparent and scaled-up mould was fabricated to emulate the package with single and stacked die with copper wires for the encapsulation process, as illustrated in Figure 3.11 and 3.12 for PBGA with centre inlet and corner inlet respectively. Two different packages (single die and stacked die) were considered to provide the better visualisation of FSI on the interaction phenomenon between fluid and wires in the experimental work. The virtual modelling technique using finite volume (FV) and finite element (FE) codes was applied for the FSI analysis.

The inlet gates in the moulding equipment are located as depicted in Figure 3.11, which can be easily removed and polished if necessary. Properly designed inlet gates should allow proper flow of material as it enters the mould cavity. Inlet gates should be located at points away from the functioning parts of the moulded component.

Outlet vents are provided in all transfer moulds to facilitate the escape of trapped air. The locations of these outlet vents depend on the part design, and locations of pins and inserts. The outlet vent is sufficiently small so that it allows the air but not the moulding compound to pass through. Outlet vents are often placed at the far corners of the cavity, near inserts where a knit line will be formed, or at the point where the cavity fills last.

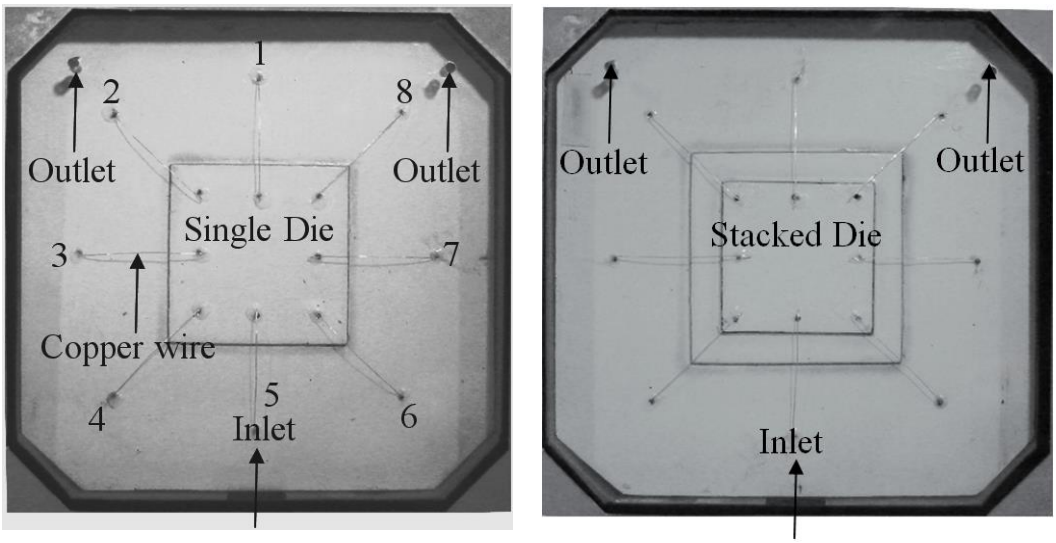


(a) Single die. (b) Stacked die.

Figure 3.11 Scale-up of eight-wire PBGA model with centre inlet: (a) Single die and (b) Stacked die.

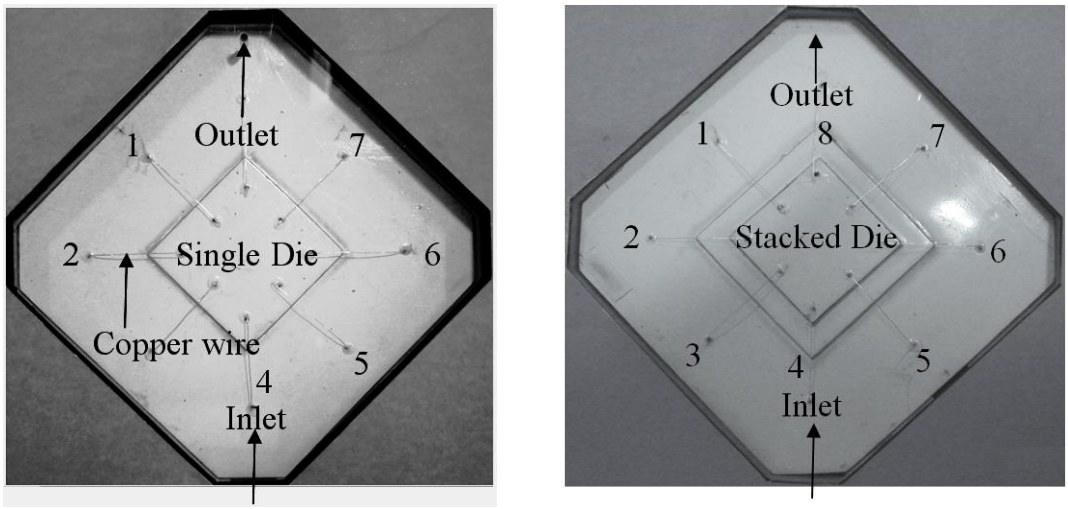


(a) Single die. (b) Stacked die.

Figure 3.12 Scale-up of eight-wire PBGA model with corner inlet: (a) Single die and (b) Stacked die.

### 3.4.2 Experimental Setup

In the present study, the experiment of scaled-up PBGA encapsulation process was carried out using the system depicted in Figures 3.13 and 3.14. The actual diagram and the schematic of experimental setup are illustrated in Figures 3.13 and 3.14 respectively. The dimension of the wire was built as presented in Figure 3.15. The wire bond span has a length $L$ = 2 cm, height of wire $H$ = 0.15 cm, and diameter of wire $d$ =

0.01 cm. The elastic modulus ($E$) of copper wire is 47.296 GPa that measure by using tensile test. The graph of tensile test result is presented in Appendix C.

A test fluid with a constant viscosity of 4 Pa·s that measured by using viscometer (Appendix D) and a density of 1067 kg/m$^3$ was utilised as the fluid medium. The servomotor illustrated in Figure 3.13 controlled the system delivery of the test fluid into the mould.

The system was tested to obtain a constant voltage for the experiment. The FSI process during encapsulation was recorded using a camera and processed by computer. The detailed and exploded views of the mould of scale-up eight-wire PBGA with centre and corner inlet are presented in Figure 3.16 − 3.19 respectively. The mould was fabricated from transparent perspex for better visualization. The material used for the imitated die was a thin layer of acrylic. Scale-up eight-wire models of the PBGA package with different heights of die and inlet arrangement were built and sized, as shown in Figure 3.20 and 3.21 respectively. The dimensions of the cavity were 8 cm × 8 cm × 0.5 cm. The total thickness of the imitated dies was 0.11 cm for a single die package and 0.22 cm for a stacked die package. The dimensions of the imitated die were 3 cm × 3 cm × 0.11 cm for the single die and 2.5 cm × 2.5 cm × 0.11 cm (top die) and 3.5 cm × 3.5 cm × 0.11 cm (bottom die) for the stacked die. The experiment presented here is focused on the interaction between the test fluid and the wire. Therefore, the effect of temperature is not considered in this experiment.

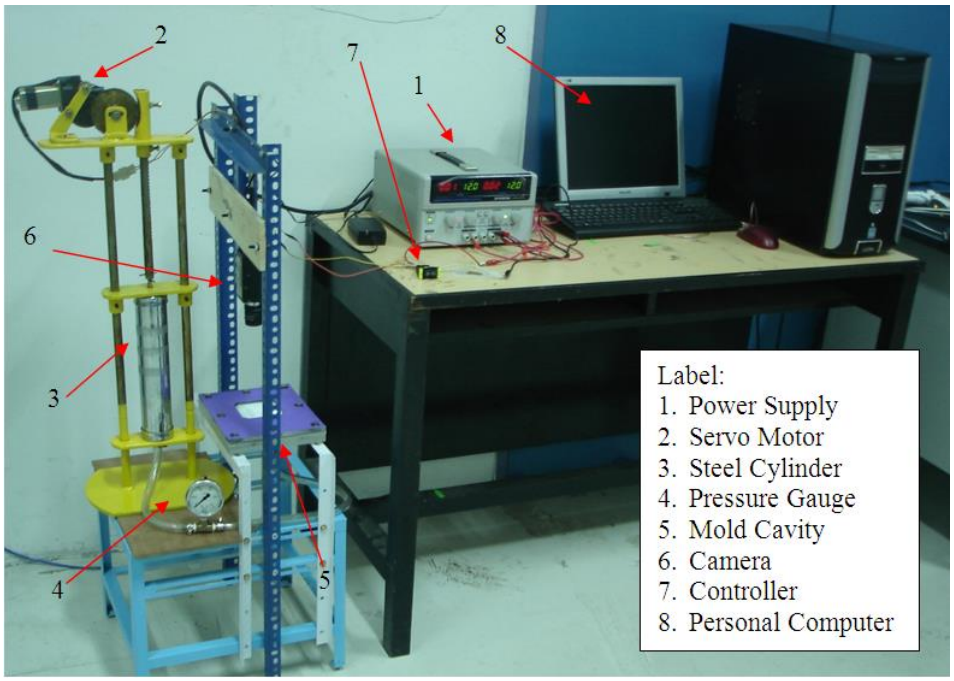


Figure 3.13 Actual diagram of the experimental setup.

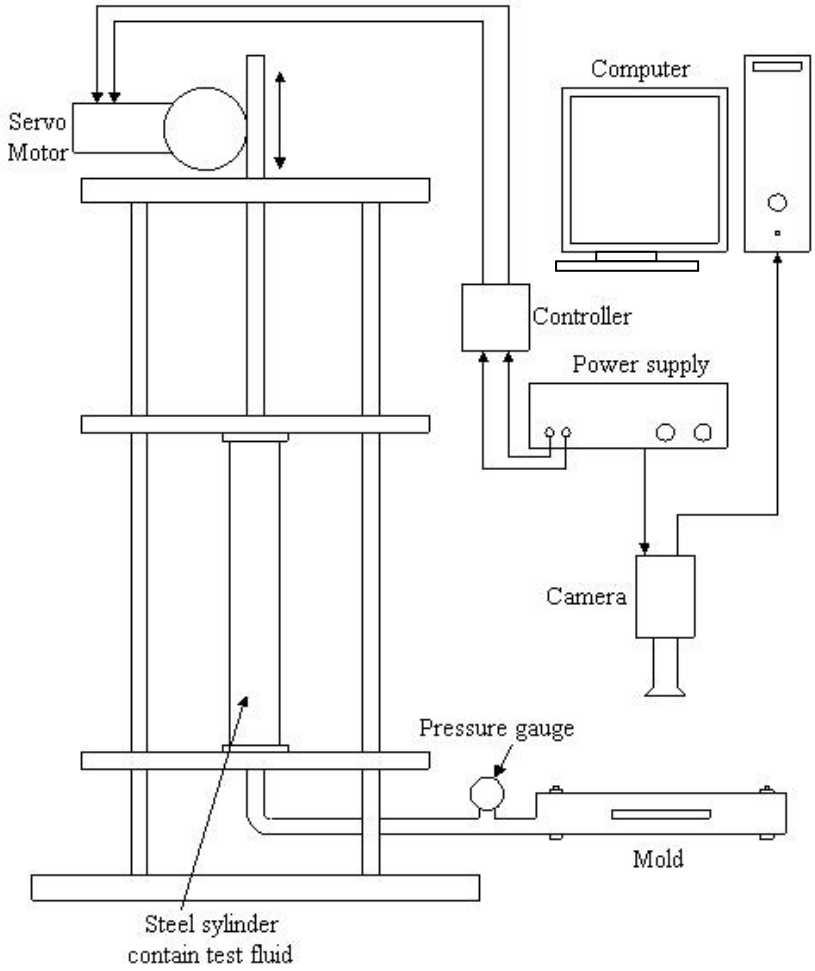


Figure 3.14 Schematics diagram of the experimental setup.

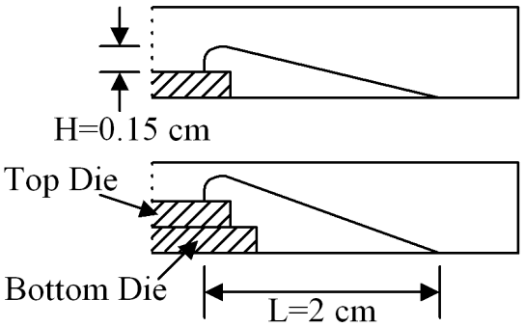


Figure 3.15 Dimension of the wire of scale-up eight-wire PBGA model.

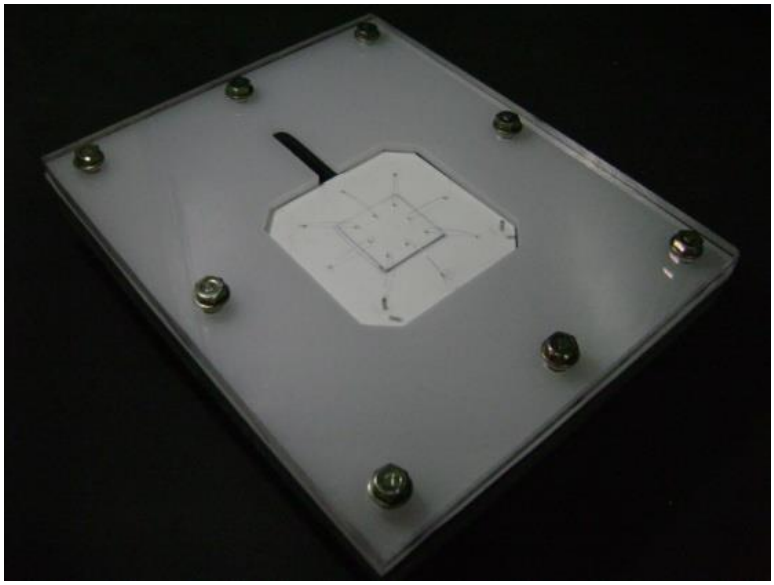

Figure 3.16 Detailed construction of mould of scale-up eight-wire PBGA model with centre inlet.

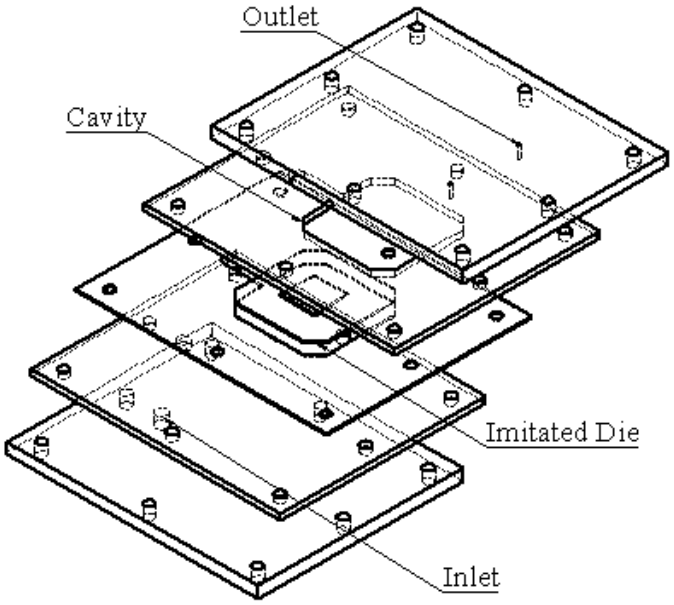


Figure 3.17 Exploded views of the mould of scale-up eight-wire PBGA model with centre inlet (Layer 1: top plate, Layer 2: cavity plate, Layer 3 - 5 base plates with inlet).

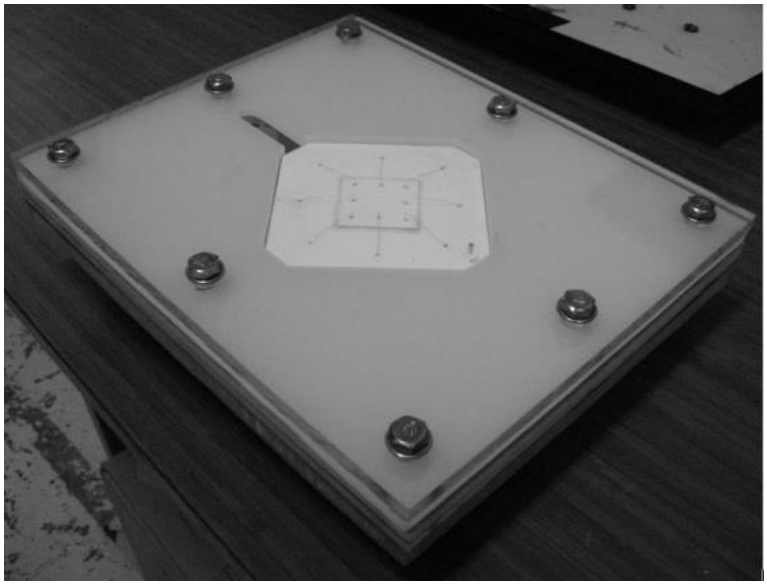

Figure 3.18 Detailed construction of mould of scale-up eight-wire PBGA model with corner inlet.

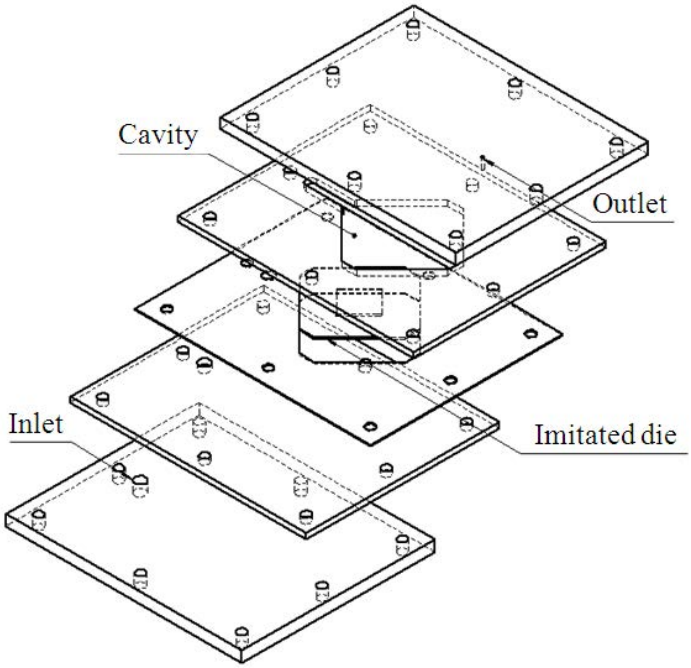


Figure 3.19 Exploded views of the mould of scale-up eight-wire PBGA model with corner inlet. (Layer 1: top plate, Layer 2: cavity plate, Layer 3 - 5 base plates with inlet).

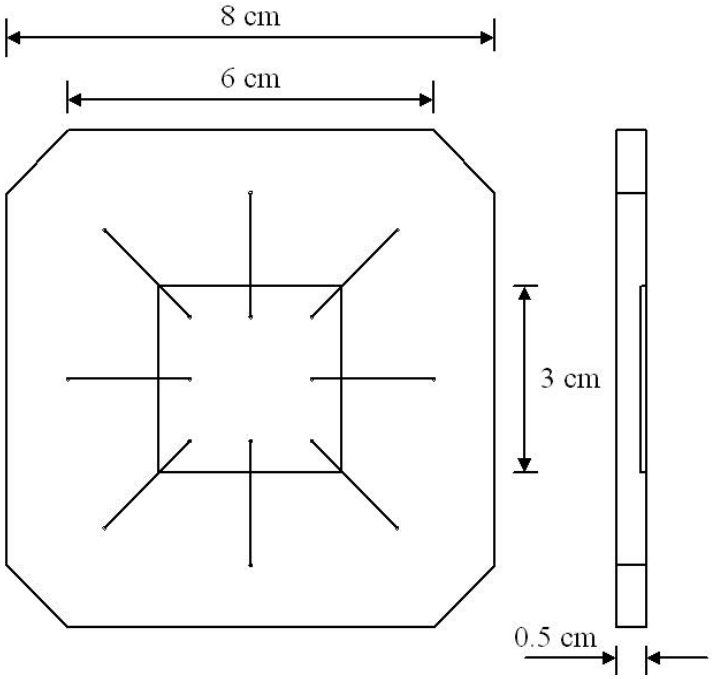


Figure 3.20 Dimension of scale-up eight-wire PBGA model of single die.

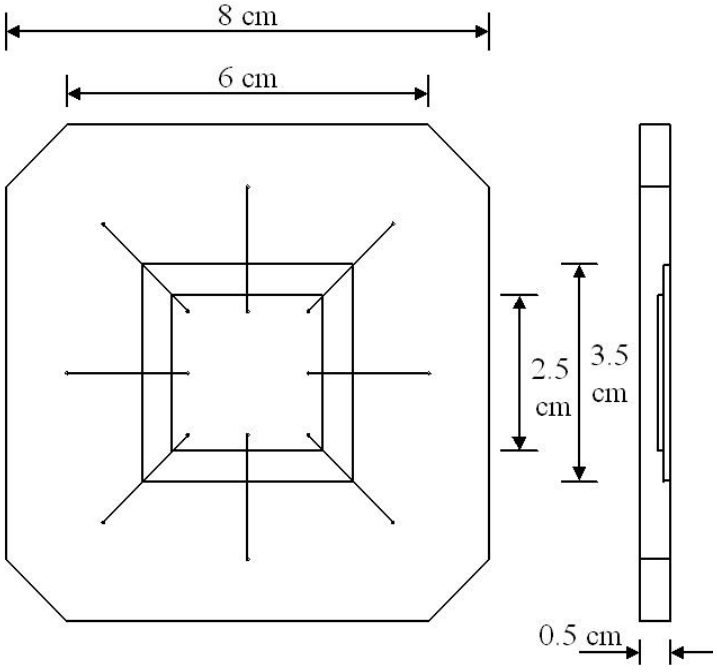


Figure 3.21 Dimension of scale-up eight-wire PBGA model of stacked die.

### 3.4.3 FSI Simulation Model and Boundary Condition

The concept of the FSI modelling is the coupling of FVM- and FEM-based software in conducting fluid and structural analysis. During FSI analysis, the transformation of analysis generated from the FLUENT 6.3.26 to ABAQUS 6.9 was performed using MpCCI (Khor et al., 2012a). Real-time data were transferred from one

program to another. During the interaction, the forces induced from the fluid acting on the wires were directly solved by ABAQUS. Thus, the deformations of the wires were calculated simultaneously. The wires were defined as the coupled regions in FSI simulation. FLUENT was used to analyse the fluid flow modelling by simulating the physic of the flow front that fed into the cavity. ABAQUS was used to calculate the displacement, von Mises stress, and shear stress of wires during the encapsulation process.

### 3.4.3.1 Fluid Model in FLUENT

In the FLUENT analysis, the 3-D model was built according to the dimensions of the package that was fabricated in the experimental work. The model was meshed with a total of 457424 and 481919 tetrahedral elements for scale-up eight-wire PBGA with centre inlet of single and stacked die respectively. The total meshes for scaled-up eight-wire PBGA with corner inlet of single and stacked die are 459889 and 497986 tetrahedral elements. Figure 3.22 illustrates the boundary conditions for single and stacked die and Figure 3.23 illustrates the meshed model of the imitated scale-up eight-wire PBGA package for single and stacked die. The surfaces of the mould, die, and wire were defined as wall boundaries with no-slip condition. Temperature effects were not considered in the experiment. Therefore, this process was assumed to be isothermal during the simulation and was set at room temperature. The FSI phenomenon focused on the fluid feeding into the cavity until the "final" stage, which is before the plunger is retracted from the fluid cylinder.

Air and test fluid are defined as the phases in the analysis. The implicit solution and the time-dependent formulation are applied for the volume fraction in every time step. The volume fraction of the encapsulation material is defined as 1 and 0 value for the air phase. The boundary and initial conditions that are used in the calculation are as follows (Khor et al., 2012a):

(a) On the wall: $u = v = w = 0$; $T=T_w$, $\frac{\partial p}{\partial n} = 0$.
(b) On the melt front: $p = 0$. (Gauge pressure)
(c) At the inlet: $p = p_{in}(x,y,z)$; $T= T_{in}$.

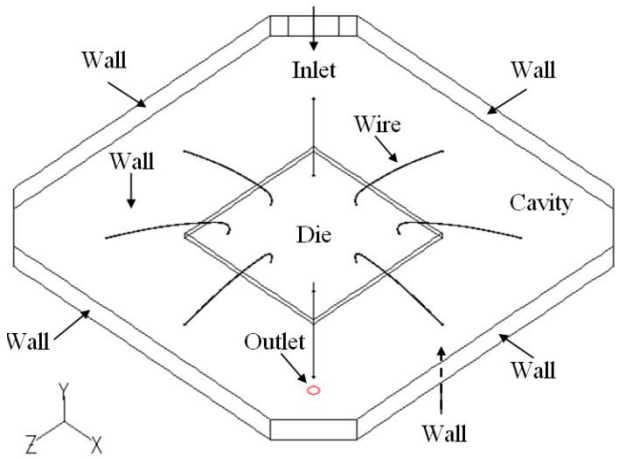


(a) Single die.

Figure 3.22 Boundary conditions of scale-up eight-wire PBGA model: (a) Single die

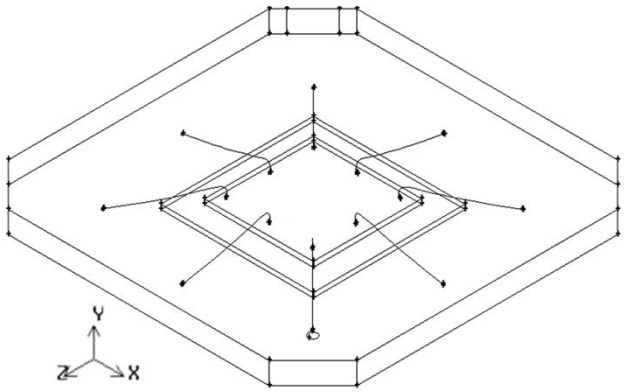


(b) Stacked die.

Figure 3.22b Boundary conditions of scale-up eight-wire PBGA model: (b) Stacked die.

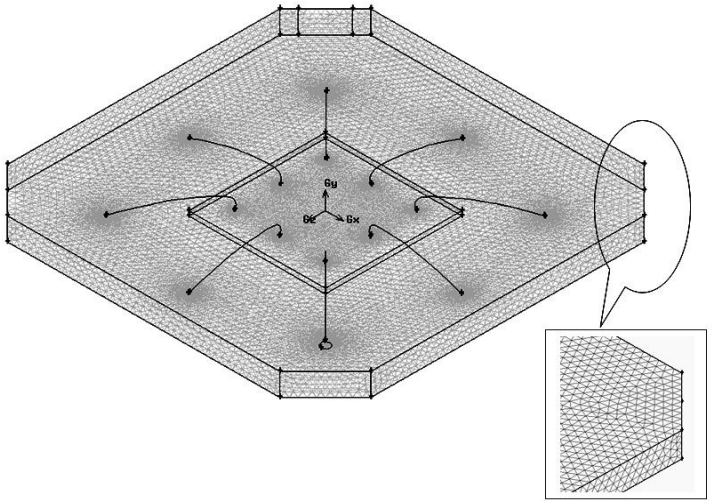


(a) Single die.

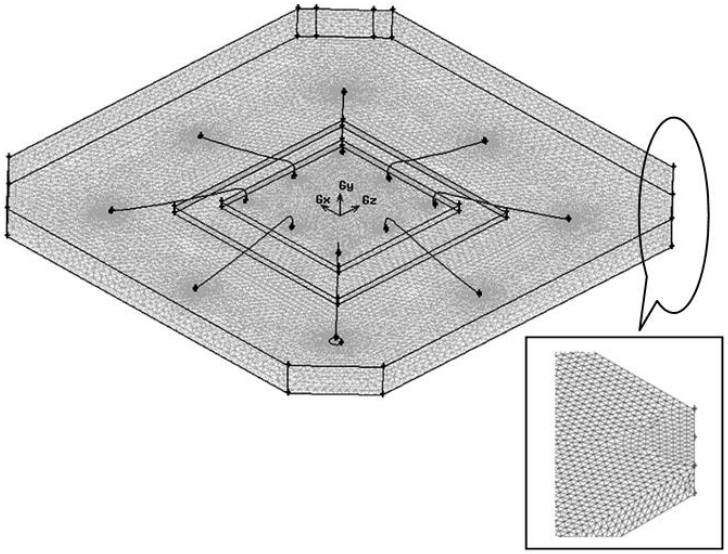


(b) Stacked die.

Figure 3.23 Meshed model of scale-up eight-wire PBGA package: (a) Single die and (b) Stacked die.

In the present study, the geometry of the scaled-up eight-wire PBGA is modelled using 3-D finite volume grid. The dimensions of the mould model were 8 cm × 8 cm × 0.5 cm and the analysis was performed on two different types of package (Single dies and stacked die). The outlet vent position of the mould cavity is opposite to the inlet gate, as shown in Figure 3.22, and considered the boundary conditions in the present investigation. Only eight wires were considered in the wire region of the package in the simulation and experiment.

In the encapsulation process, test fluid was used as the moulding compound. The test fluid density and viscosity were 1067 kg/m$^3$ and 4 Pa.s respectively. The voltage was set as 6 Volt (70.7 kPa) as Case 1, 9 Volt (113.3 kPa) as Case 2, and 12 Volt (161.4 k.Pa) as Case 3 during the process. The inlet pressure was measured by fluid Pressure Gauge. The simulation was performed on an Intel Core 2 Duo processor E7500, 2.93 GHz with 2 GB of RAM; it took around 4 hours for each case to complete 4000 iterations for optimum time steps of 0.001 s (Khor et al., 2010a).

### 3.4.3.2 Simulation Model and Boundary Conditions in ABAQUS

Figure 3.15 shows the model of wire dimension for structural analysis. The 3-D meshed model was generated using tetrahedral elements with the sweep method by ABAQUS 6.9 (Khor et al., 2012a). The mechanical aspects were considered. Thus, the structures of the coupled regions were defined as deformable in the analysis.

The commercial FEM-based software ABAQUS is employed in this study to calculate the wire deformation. The structures of the wires are imported from GAMBIT in ACIS '.sat' format in order to get the identical coordinate. The wire bond span has a length $L$ = 2 cm, height of wire $H$ = 0.15 cm, and diameter of wire $d$ = 0.01 cm. The wire bond is divided into 3087 (single die) and 3675 (stacked die) tetrahedral elements as shown in Figure 3.24. The shape of the wire is classified as typical Q-auto loop wire bond (Brand et al., 2008). The ball bond boundary conditions of the wire were set as fixed in ABAQUS and shown in Figure 3.25. The mechanical properties of wire are as follows: elastic modulus $E$ = 47.296 GPa, density $\rho$ = 8960 kg/m$^3$, and Poisson's ratio $v$ = 0.355.

In the experiment, the structures of wires were properly positioned on the die in the cavity. In addition, some basic assumptions were considered in the FEM analyses for simplification purpose. The elastic behaviour was taken as homogeneous and isotropic in the structures of wire (Khor et al., 2012a). The solder bond was neglected where the solder pad was not considered in the scaled-up PBGA model. The temperature effect on the structures was not considered in the experimental work. Therefore, no thermal effect on the creep and fracture behaviour was considered in the present modelling. In reality there are some residual stresses in the wirebond due to the wire looping process, especially at the neck of the wirebond adjacent to the ball bond. However, in the finite element simulation of the structural deformation of the wirebonds, the wirebonds were assumed to have no initial stress before the action of the flow-induced forces (Tay and Lee, 2002).

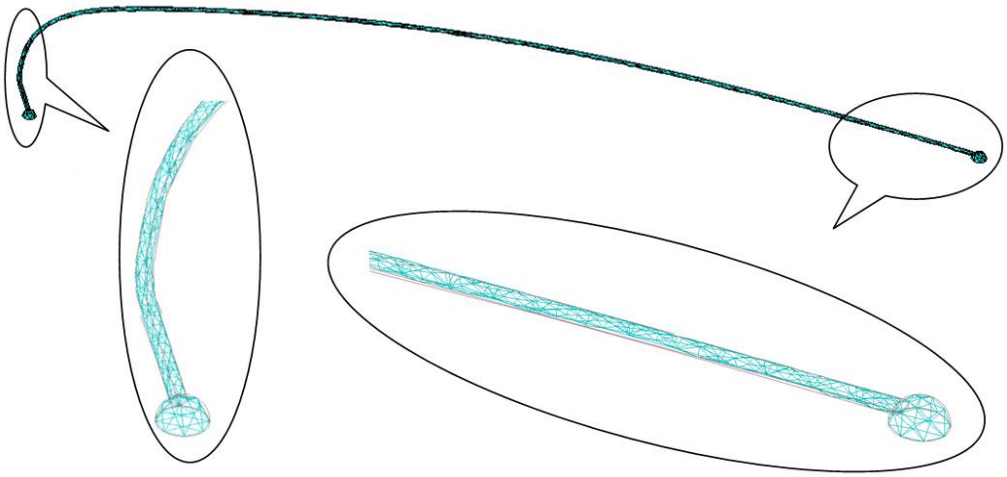

Figure 3.24 Meshed wire for ABAQUS analysis for Single Die of scale-up eight-wire PBGA model.

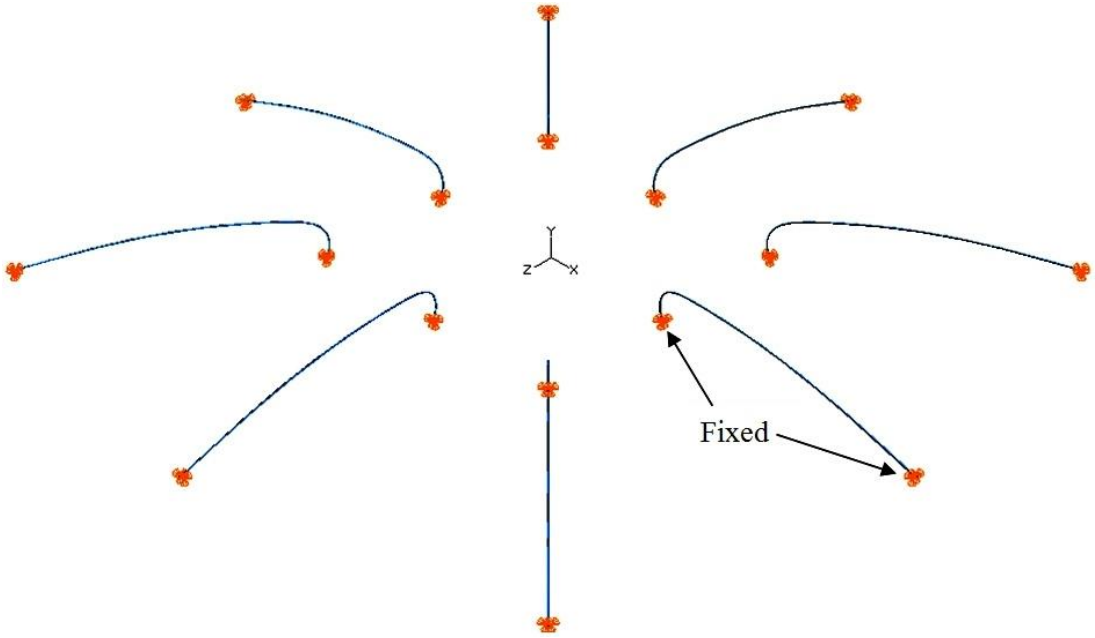


Figure 3.25 Boundary conditions of wires in ABAQUS for Single Die of scale-up eight-wire PBGA model.

## 3.5 Wire Sweep Analysis Considering Rheology Effect of actual size PBGA Encapsulation Process

### 3.5.1 Problem Description

In fact, wire sweep during encapsulation is a typical FSI problem, which is normally handled by a coupled analysis of fluid flow and structural deformation. The use of a finite-volume flow solver and a finite-element structural solver, coupled through MpCCI has been reported for a variety of engineering problems (Yigit et al., 2008; Thirifay and Geuzaine, 2011; Gatzhammer, 2010). However, the use of MpCCI has not been reported so far for wire sweep analysis. Accordingly, a novel 3-D computational technique using the MpCCI method is introduced on the PBGA encapsulation process for the prediction of wire sweep. This method utilizes the finite-

volume flow solver FLUENT and the finite-element structural solver ABAQUS, interfaced by MpCCI. Polymer rheology model with curing effect (the Castro−Macosko model) is used in the fluid flow model, and the volume of fluid (VOF) technique is applied for melt-front tracking of the EMC. The numerical analysis uses UDFs to account for the curing kinetics. In the present study, the computational fluid dynamic code FLUENT 6.3 (Khor et al., 2010a) is used to analyze the effect of rheology on the flow behaviour and wire sweep of the encapsulation process of PBGAs. The 3-D models are developed and analyzed by using finite volume method. Three different EMC properties, designated as Case A, Case B, and Case C, were studied for analyzing of fluid flow and wire sweep inside the mould cavity. Numerical results of flow patterns and percentage of the void of the three arrangements of EMC properties are compared. Wire sweep profiles and pressure field are analyzed and presented. The simulation results are compared with the previous experimental result available in literature.

### 3.5.2 FSI Simulation Model and Boundary Condition

#### 3.5.2.1 Fluid Model in FLUENT

The VOF model in FLUENT 6.3.26 is utilised to simulate the process (Khor et al., 2010b). EMC types are set at different parameters, as shown in Table 3.2.Table 3.2 summarizes the material properties of the EMC considered in the current simulation (Jong et al., 2005; Nguyen et al., 2000; Wu at al., 1998). Air and EMC are defined as the phases in the analysis. Implicit solution and time dependent formulation are applied for the volume fraction in each time step. The volume fraction of the encapsulation material is defined as 1 and that of the air phase as 0. Besides, the viscosity Castro−Macosko model and VOF techniques are applied to track the melt front. The PBGA chip package model used in the present study and its dimensions and boundary condition are shown in Figure 3.26 and 3.27 respectively. The boundary and initial conditions used in the calculation are as follows (Khor et al. 2011a):

(a) On the wall: $u = v = w = 0$; $T = T_w$, $\frac{\partial p}{\partial n} = 0$.
(b) On the melt front: $p = 0$. (Pressure gauge)
(c) At the inlet: $u = u_{in}(x,y,z)$; $T = T_{in}$.

Table 3.2 EMC material properties used in rheology effect.

| | | | Value | | |
|---|---|---|---|---|---|
| | | Unit | Case A (Jong et al., 2005) | Case B (Nguyen et al., 2000) | Case C (Wu et al., 1998) |
| Density | $\rho$ | kg/m$^3$ | 1578 | 2000 | 1820 |
| Tabulated Thermal Conductivity | $T$ | $^o$C | 66.95 | 175 | 75 |
| | $k$ | W/m.K | 0.74 | 0.97 | 0.669 |
| Tabulated Specific Heat | $T$ | $^o$C | 169.95 | 175 | 169.95 |
| | $C_p$ | J/kg.K | 1078 | 1079 | 1205 |
| Reactive I Viscosity | $N$ | - | 0.7773 | 0.7773 | 0.28 |
| | $\tau^*$ | Pa | 0.0001 | 0.0001 | 2361 |
| | $B$ | Pa.s | 0.04219 | 3.81E-04 | 0.416 |
| | $Tb$ | K | 4810 | 5.230E+03 | 2.091E+03 |
| | $C_1$ | - | 10.96 | 1.03 | 3.496 |
| | $C_2$ | - | 0.00626 | 1.50 | 8.503 |
| | $\alpha_g$ | - | 0.6946 | 0.17 | 0.17 |
| Reaction Kinetics | $H$ | J/kg | 3.91E+04 | 4.01 E+04 | 4.585E+04 |
| | $m_1$ | - | 0.4766 | 1.21 | 0.7241 |
| | $m_2$ | - | 1.08 | 1.57 | 1.234 |
| | $A_1$ | 1/s | 0.1 | 33.53E+03 | 8475 |
| | $A_2$ | 1/s | 5.926E+05 | 30.54E+06 | 9.715E+06 |
| | $E_1$ | K | 2E+004 | 7161 | 7216 |
| | $E_2$ | K | 7501 | 8589 | 8585 |

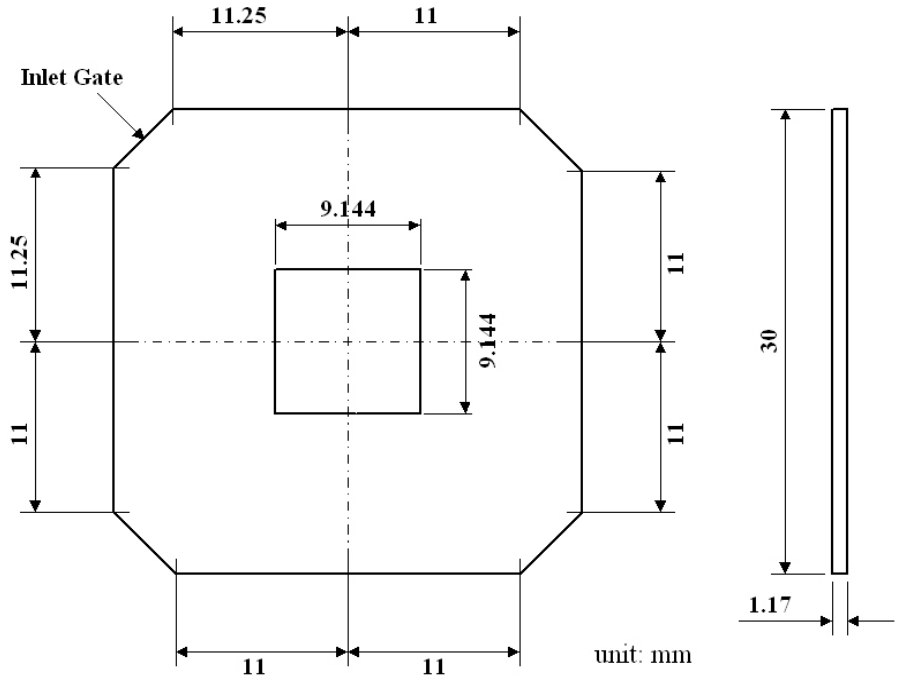


Figure 3.26 Dimension of actual size PBGA model package (Chen, 1990).

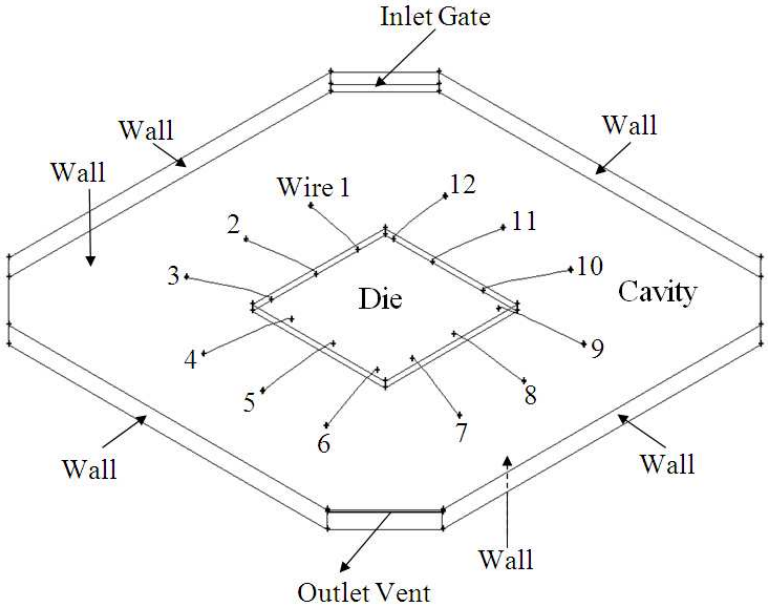


Figure 3.27 Boundary conditions of actual size PBGA model.

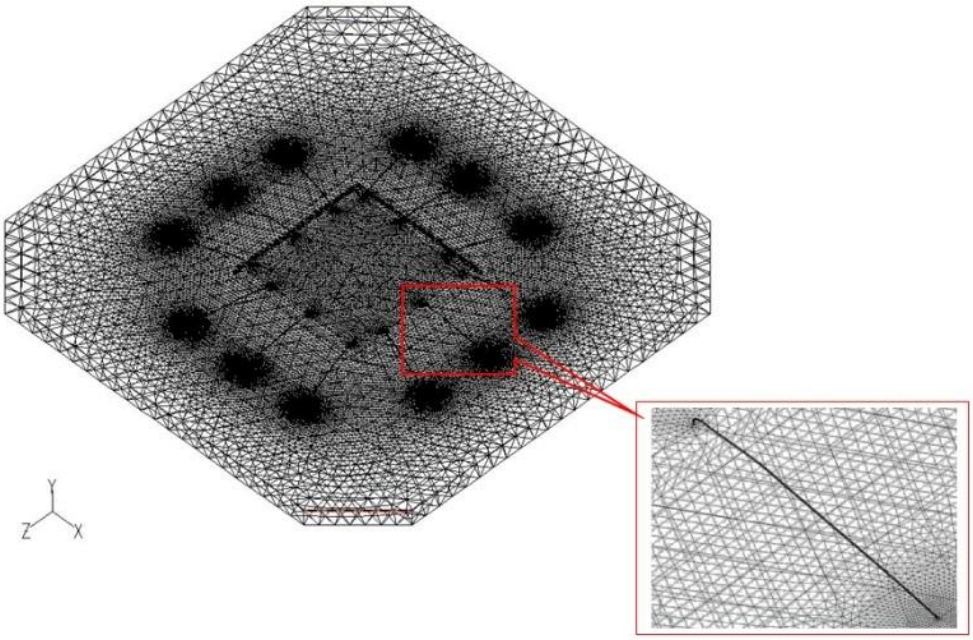

Figure 3.28 Meshed model of actual size PBGA package.

In the present study, geometry of the PBGA is modelled as a 3-D finite volume grid. The dimension of the mould model is 30 mm × 30 mm × 1.17 mm and the mould entrance is oppositely located to the outlet vent of the mould cavity as shown in Figure 3.27, and is considered the boundary conditions in the present investigation, and only 12 wires bonding are considered as the reference wires in the wire region of the package in the simulation refer to Chen (1990). In the present modelling, the walls boundaries are as shown in Figure 3.27 are defined as non-slip wall in the FLUENT. The meshed model is created by using the GAMBIT software, and an average 480000 tetrahedral

elements of the package volume are generated for simulation (Figure 3.28). The wire consists of surfaces of the ball bond and wire body. The total meshing of wire surface is 1626 triangles and for ball bond 40 triangles.

In the encapsulation process, EMC is used as the moulding compound. The mould temperature is set as 175 °C, and 0.3 m/s of inlet velocity is applied during the process. The simulation is performed on an Intel Core 2 Duo processor E7500, 2.93 GHz with 2 GB of RAM; it took around 12 hours for each case to complete the 14000 iterations in time steps of 0.001 s (Khor, 2010a).

### 3.5.2.2 Wire Model and Boundary Conditions in ABAQUS

The commercial FEM based software ABAQUS is used in this study to calculate the wire deformation. The structures of the wires are imported from GAMBIT in ACIS ".sat" format. The dimension of the wire is built according to Chen (1990) model. The wire bond span length $L$ = 4.875 mm, height of wire $H$ = 1.75 mm and diameter of wire $d$ = 0.032 mm. The wire bond is divided into 6240 tetrahedral elements as shown in Figure 3.29. The shape of the wire as also classified as typical Q-auto loop wire bond (Brand, 2008). The ball bond boundary conditions of wire are set as fixed in ABAQUS and shown in Figure 3.30. The wire mechanical properties are as follows: elastic modulus, $E$ = 34 GPa (Chen, 1990), density, $\rho$ = 19330 kg/m$^3$, Poisson's ratio, $v$ = 0.42 and reference temperature, $T$ = 175 °C.

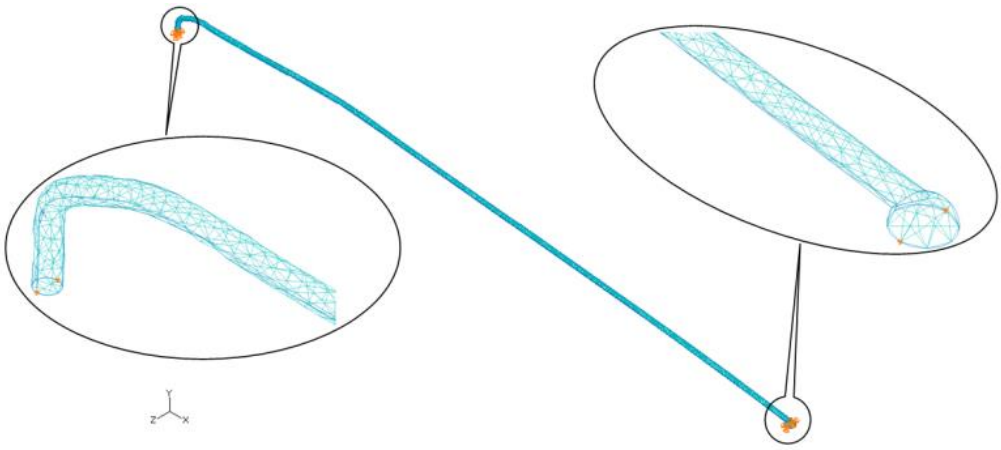

Figure 3.29 Meshed wire for ABAQUS analysis of actual size PBGA.

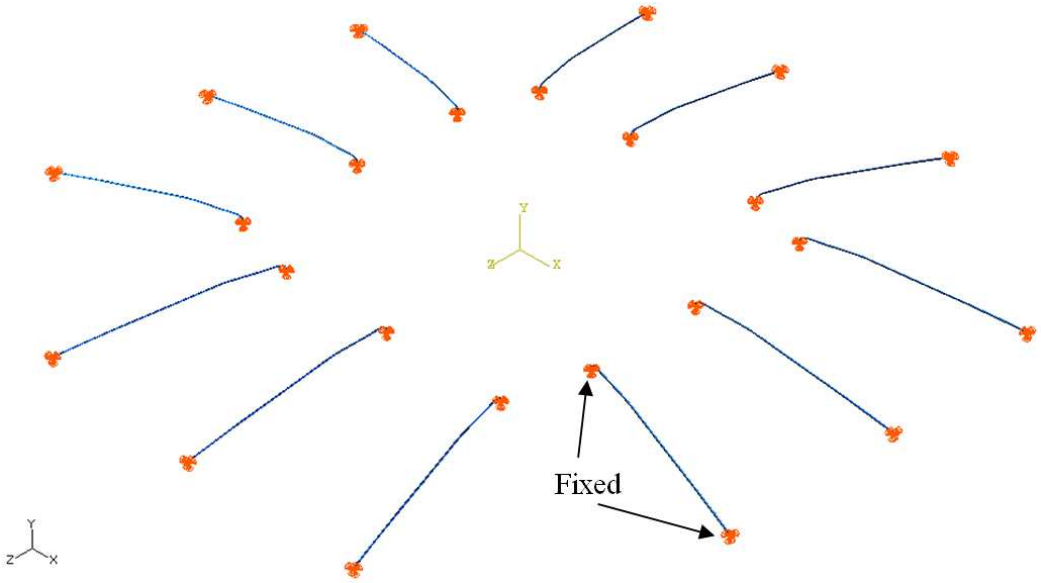


Figure 3.30 Boundary condition of wire in ABAQUS of actual size PBGA.

## 3.6 Optimization Using RSM of PBGA Encapsulation Process

### 3.6.1 Design Optimization

The design, mathematical modelling and optimization of this study were performed using Design Expert 6.0.6 software. Central composite design (CCD) was used to model the response surface methodology (RSM) in the design. The former is the most widely used numerical design for fitting a second order response surface (Kapoor et al., 2004). The independent variables (factor) used in this numerical study were inlet pressure, wire diameter, and vent height and coded as $A$, $B$ and $C$ respectively (Table 3.3). The independent variables were varied over three levels, between −1, 0 and +1, and the range was determined based on literature review. In the literature review the ranges of inlet pressure from 5 MPa (Teng and Hwang, 2008) to 10 MPa (Wang et al., 2010). Another factor that was concern in this study is the wire diameter. The maximum value for the wire diameter was set at 0.05 mm in order to reduce the wire deformation in encapsulation process. The wire diameter was varied from 0.03 mm to 0.05 mm. The wire diameter was designed based on the research work conducted by Kung et al. (2006a). Effect of mould vent size was introduced by Chai and Zohar (1999). The mould vent size may influence the filling time of the encapsulation process.

Generally, the CCD consists of a $2^k$ full factorial design with $2k$ axial or star runs, a total of 20 simulations were performed to assess the three factors, according to the equation CCD = $2^k + 2k + 6$, where $k$ is the number of factors. Fourteen simulations were improved with six replications at the design centre to evaluate the pure error, (Montgomery, 2009). Eq. (3.23) shows the quadratic model used to estimate the optimal point (Adlan et al., 2011, Khor and Abdullah, 2012b):

$$Y = \beta_o + \sum_{i=1}^{k} \beta_i X_i + \sum_{i=1}^{k} \beta_{ii} X_i^2 + \sum_{i_{i \le j}}^{k} \sum_{j}^{k} \beta_{ij} X_i X_j + \cdots + e \qquad (3.23)$$

where $Y$ is the response; $X_i$ and $X_j$ are the variables; $\beta_0$ is a constant coefficient; $\beta_i$, $\beta_{ii}$, and $\beta_{ij}$ are the interaction coefficients of linear, quadratic and second-order terms, respectively; $k$ is the number of studied factors; and $e$ is the random error.

The coefficient of determination ($R^2$) was used to identify the quality of the fit of polynomial model and the P-value associated with the 95% confidence level was used to evaluate the variables and the interactions between them. The significance and adequacy of the model was assessed according to the calculated F-value (Fisher variation ratio), probability value (Prob > F), and Adequate Precision.

Table 3.3 Actual and coded value for the independent variable of the CCD design.

| Factor (Symbol) | Coded value | | |
|---|---|---|---|
| | -1 | 0 | 1 |
| | Actual value | | |
| A. Inlet Pressure (MPa) | 5 | 7.5 | 10 |
| B. Wire Diameter (mm) | 0.03 | 0.04 | 0.05 |
| C. Vent height (mm) | 0.04 | 0.22 | 0.40 |

The regression analysis was performed using Design Expert 6.0.6 software to fit the simulation data into the second-order polynomial equation, and evaluate the variable and interaction between them. The statistical significance of the equation developed was also estimated through the software.

### 3.6.2 Modelling

The FSI simulation modelling consists of the fluid flow and structural analysis. Finite volume-based (FLUENT) and finite element-based (ABAQUS) software were used to perform the analysis of the PBGA encapsulation process. The basic idea of the current FSI is the real-time coupling (Khor et al., 2012a) between both analysis codes through the Mesh-based parallel Code Coupling Interface (MpCCI) method. During the simulation, the forces induced from the fluid flow (FLUENT) are transferred to the ABAQUS for simultaneous structural analysis. The deformation, stress concentration on the structures (wires), and EMC fluid flow were analyzed in the FSI analysis. The FSI phenomenon in the cavity focused on the fluid feeding until the final stage, before the plunger is retracted from the fluid cylinder. Figure 3.27 depicts the boundary conditions of the PBGA in fluid analysis. The meshed model of the PBGA was a mould cavity as illustrated in Figure 3.28, which provides a fluid domain for FLUENT analysis, and was created and meshed using GAMBIT software. The 3D model with different variables was meshed with 350000–500000 tetrahedral elements. A 75 $^{o}$C pre-heated temperature was set at inlet gate for EMC, and 175 $^{o}$C was set as the mould temperature. The Optimisation material properties of EMC are summarized in Table 3.1 (Case B in Table 3.2). The EMC material was selected based on Case B of previous study (in Section 3.5.1). The EMC more stable in flow front profile and can reduce the wire sweep in PBGA encapsulation process.

In the FEM modelling, the wires were meshed using hexahedral elements with sweep method, as illustrated in Figure 3.29. Similarly, several assumptions have been made for the present structural analysis included the fixed boundary of the model is shown in Figure 3.30. Homogeneous and isotropic in the elastic behaviour of structures were considered in the finite element (FE) analysis. The mechanical properties of wire are summarized in Table 3.4.

Table 3.4 Mechanical properties of wires (Chen, 1990).

| Parameter | Wire |
|---|---|
| Elastic modulus, $E$ (GPa) | 34 |
| Poisson ratio, $v$ | 0.42 |
| Solid density, $\rho_s$ (kg/m$^3$) | 19330 |

## 3.7 Summary

A 3-D computational analysis was used to predict the wire sweep in the imitation of scaled-up and the actual size PBGA encapsulation process. The FVM- and FEM-based software coupled with MpCCI were used to perform the study of FSI in virtual modelling of the encapsulation process. Moreover, the VOF technique was applied to track the flow front of EMC.

This research also discussed the optimisation of physical and process parameters of the actual size PBGA package by using RSM model in the analysis of wire sweep, filling time and void occurrence during the encapsulation process.

# CHAPTER 4: SIMULATIONS AND EXPERIMENTS ON PBGA ENCAPSULATION PROCESS

This chapter presents the simulations and experiments on PBGA encapsulation process and a detailed discussion with the observation. The results obtained from experimental results of a scaled-up eight-wire PBGA prototype encapsulation process with different stacked dies and inlet gates orientation and the simulation of melt front behaviour, pressure distribution within cavity, wire sweep profile and wire stress, also comparison between simulation, experiment, and previous experimental results of melt-front profile and wire sweep. The wire sweep considering rheological effect and optimization of an encapsulation process on actual size of PBGA through the simulations is discussed in this chapter.

## 4.1 Grid Independence Test

Grid independence test was performed to obtain the optimum mesh size. Five different mesh sizes were tested, and the corresponding filling percentage was estimated for a PBGA package that consisted of a single die and scaled-up four wires PBGA with stacked die and scaled-up eight-wire and also included an actual size PBGA. The simulations were performed by using a PC with an Intel Core 2 Duo processor E7500, 2.93 GHz with 2 GB of RAM; it took around seventy-four hours for each case to complete 15000 iterations for a case with 2 vents of scaled-up four wires PBGA. Then, for Case 3 (single and stacked die of scale-up eight-wire PBGA), it took around four hours for each case to complete 4000 iterations, and took around twelve hours for each case to complete 12000 iteration for Case B of actual size PBGA in optimum time steps of 0.001 s (Khor et al., 2011b).

The encapsulation process took about 13 s, 4 s and 12 s to fill completely for a scaled-up four-wire PBGA, a scale-up eight-wire PBGA and an actual size PBGA, respectively. Concerning the finest mesh size of 459697, 586617, 634341 (Test 4) and experimental results for scaled-up four-wire PBGA, single and stacked die of scaled-up eight-wire PBGA and actual size PBGA respectively, the discrepancies in the filling volume of tests 1, 2, 3 and 4 at 13 s, 4 s and 12 s are calculated. As summarized in Table 4.1- 4.4 and Figure 4.1, the deviations of Test 2 and 3 from 4 are found to be the same and nominal (0.29 % (scale-up four-wire PBGA), 0.30 % (single die of scale-up eight-wire PBGA), 0.25 % (stacked die of scale-up eight-wire PBGA) and 0.13 % (actual size PBGA)). Hence, for the present study, Test 2 with 395498, 446143, 564465 and 478822 elements are chosen as the optimum and closely with the experiment results of fluid volume, in terms of accuracy and computational cost.

Table 4.1 Summary of grid independency test of single die of a scale-up four-wire PBGA for 2 vents Case

| Test | 1 | 2 | 3 | 4 | Exp. |
|---|---|---|---|---|---|
| Element | 357,844 | 395,498 | 398,900 | 459,697 | - |
| % filling volume at 13 s | 83.46 | 84.13 | 84.13 | 84.42 | 84.00 |
| Deviation from size 5 | 0.96 | 0.29 | 0.29 | - | - |

Table 4.2 Summary of grid independency test of single die of a scale-up eight-wire PBGA for Case 3

| Test | 1 | 2 | 3 | 4 | Exp. |
|---|---|---|---|---|---|
| Element | 406,852 | 446,143 | 493,407 | 586,617 | - |
| % filling volume at 4 s | 97.83 | 98.02 | 98.02 | 98.32 | 99.00 |
| Deviation from size 5 | 0.49 | 0.30 | 0.30 | - | - |

Table 4.3 Summary of grid independency test of stacked die of a scale-up eight-wire PBGA for Case 3

| Test | 1 | 2 | 3 | 4 | Exp. |
|---|---|---|---|---|---|
| Element | 498,072 | 564,465 | 598,483 | 634,341 | - |
| % filling volume at 4 s | 93.16 | 97.00 | 97.00 | 97.25 | 98.5 |
| Deviation from size 5 | 4.24 | 0.25 | 0.25 | - | - |

Table 4.4 Summary of grid independency test of an actual size PBGA for Case B

| Test | 1 | 2 | 3 | 4 | Exp. |
|---|---|---|---|---|---|
| Element | 467,092 | 478,822 | 499,614 | 537,192 | - |
| % filling volume at 12 s | 78.95 | 83.66 | 83.50 | 82.52 | 87.13 |
| Deviation from size 5 | 8.18 | 3.47 | 3.63 | 4.61 | - |

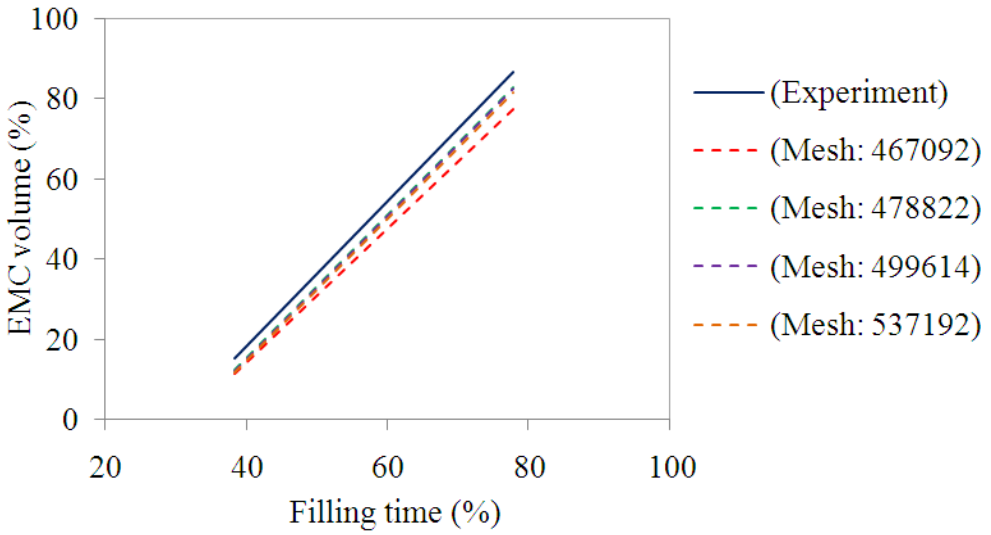


Figure 4.1 Grid independent test of an actual size PBGA for Case B.

## 4.2 Experiment and Model Validation

### 4.2.1 Scaled-up Four-wire PBGA Encapsulation Process

#### 4.2.1.1 Fluid Flow

The present simulation results of fluid flow (package with 2 vents) were validated with the experimental results of Yang et al. (2000) who investigated the flow behaviour of epoxy resin (D.E.R.331, Dow Chemical). Figure 4.2 shows the comparison of predicted and experimental flow profiles of the scaled-up four-wire PBGA encapsulation process from 33 % to 84 % of filling. The simulation results

showed separate profiles for wire sweep and EMC filling, at various stages of filling. The predicted EMC flow profiles showed a good agreement with the experimental results, at all percentage volume steps. Wire displacement phenomenon was observed when the EMC flow around the wire region. The percentage of EMC volume versus filling time for the simulation and the experiment was also plotted and compared as depicted in Figure 4.3; 6.7 % of maximum discrepancy was found for both results.

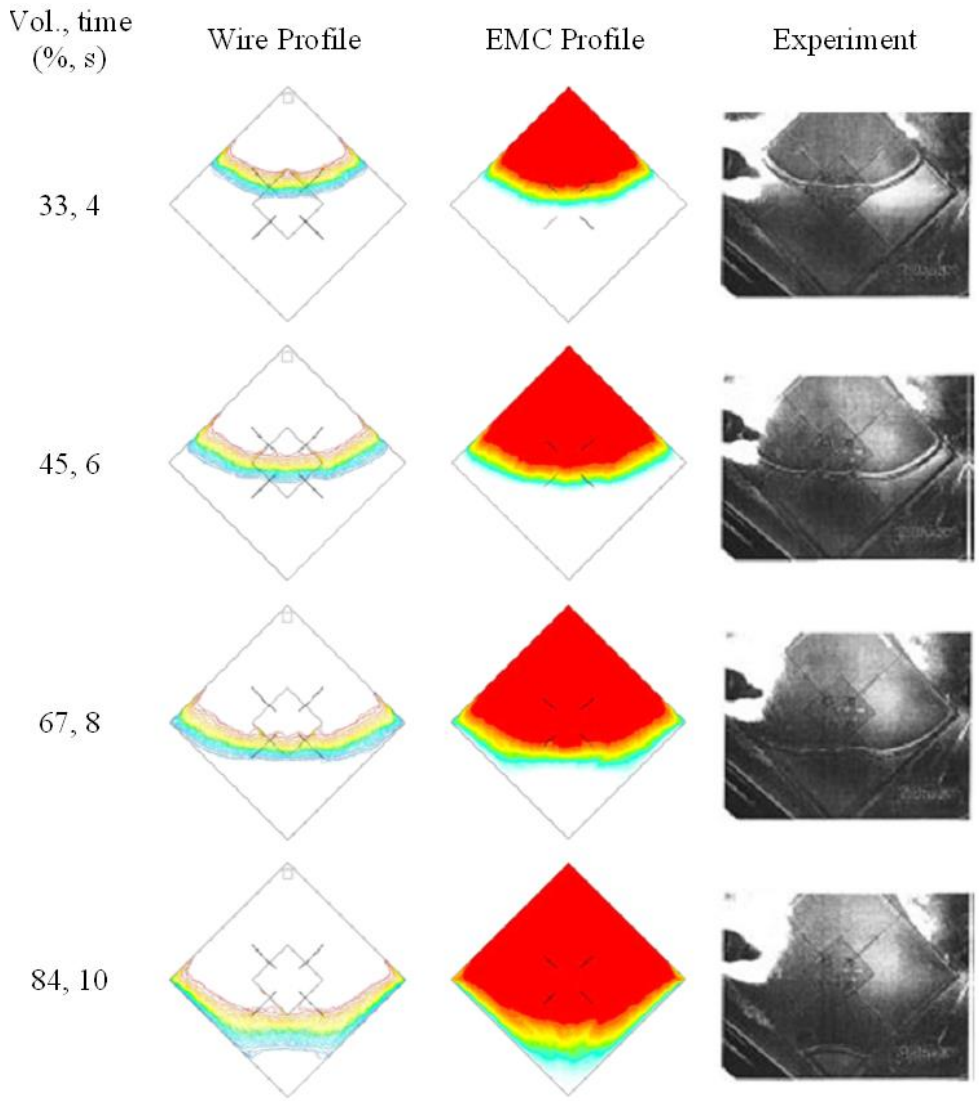


Figure 4.2 Comparison of simulation and experiment of scale-up four-wire PBGA (Yang et al., 2000) for wire deformation and EMC flow profiles (2 vents case).

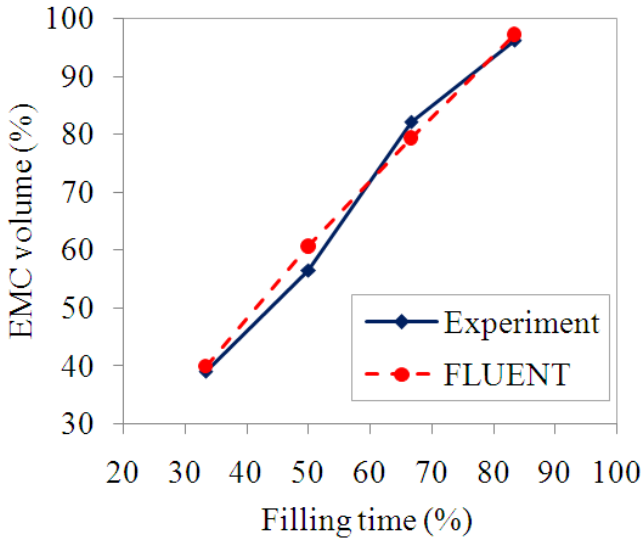


Figure 4.3 Comparison of EMC filled volume for experiment (Yang et al., 2000) and simulation (2 vents case) of scale-up four-wire PBGA.

#### 4.2.1.2 Wire Deformation

Furthermore, the wire deformation was validated by using analytical method that proposed by Kung et al. (2006a). The comparison between simulation and their analytical results of wire sweep deformation for wire 4, which presented in x-direction, is shown in Figure 4.4. The analytical calculation was referred to Eq. 3.18 with $f_B$ = 0.165, $f_T$ = 0.00165 and $H/L$ = 0.175. The average deviation at maximum displacement (after 60 % filling time) is found to be 6.5 %. The result had demonstrated a good quantitative agreement.

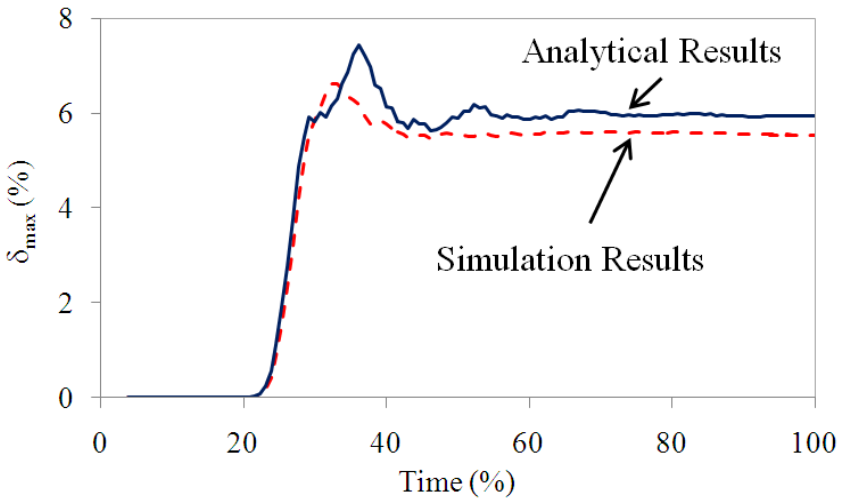


Figure 4.4 Comparison simulation and analytical results (Kung et al., 2006a) of wire sweep deformation for wire 4 in x-direction (2 vents case) of scale-up four-wire PBGA.

### 4.2.2 Scaled-up Eight-wire PBGA Encapsulation Process - Centre Inlet

#### 4.2.2.1 Fluid Flow of Single Die and Stacked Die

The experiment was conducted for a scaled-up eight-wire PBGA prototype with a centre inlet. This experiment focuses on the FSI phenomenon and flow mechanism. Therefore temperature effect was not considered in experiment. The temperature of inlet boundary was similar to room temperature. The filling process of the viscous fluid into the cavity was recorded on top of the transparent mould. FSI simulation was also performed on the imitated package with a single die and a stacked die, as presented in Figure 3.11 of Chapter 3. The flow front advancement of the simulation results were compared with the experimental results. The results showed that flow front predictions from the simulation code have nearly identical profile with the experimental results at different filling volumes of the test fluid. Figure 4.5 and Figure 4.6 show the comparison of FSI predicted and experimental flow profiles of the scaled-up eight-wire PBGA with centre inlet encapsulation process from 27 % to 75 % and 25 % to 78 % of the filling stages, which included the wire sweep for a single die and a stacked die of scale-up eight-wire PBGA with centre inlet, respectively. The simulation result is substantiated by the experimental results by using similar scaled-up eight-wire PBGA with centre inlet size, operating condition and material properties as used in the present numerical study. The predictions of flow front profiles and percentage of mould filling were well matched with the experimental results at all filling stages. The percentage of filled volume at various stages versus percentage filling time for Case 3 is compared in Figure 4.7, the maximum discrepancy is found at 2.86 % and 3.09 % for single die and stacked die of scale-up eight-wire PBGA with centre inlet, respectively. The predicted fluid flow profiles showed a good agreement with the experimental results at all percentage of filling stages.

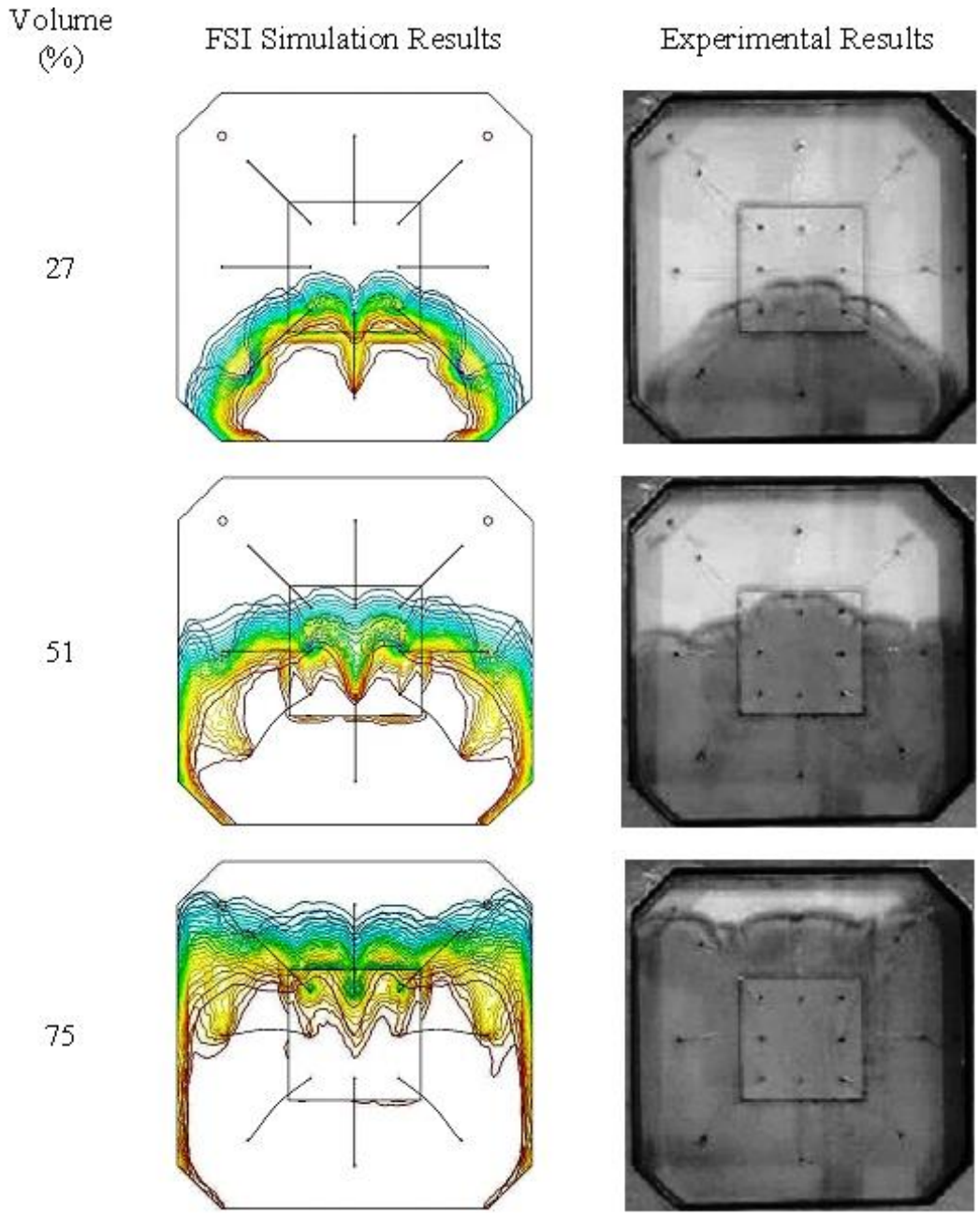


Figure 4.5 Comparison of FSI and experimental result of fluid flow front of single die of a scale-up eight-wire PBGA with centre inlet for Case 3.

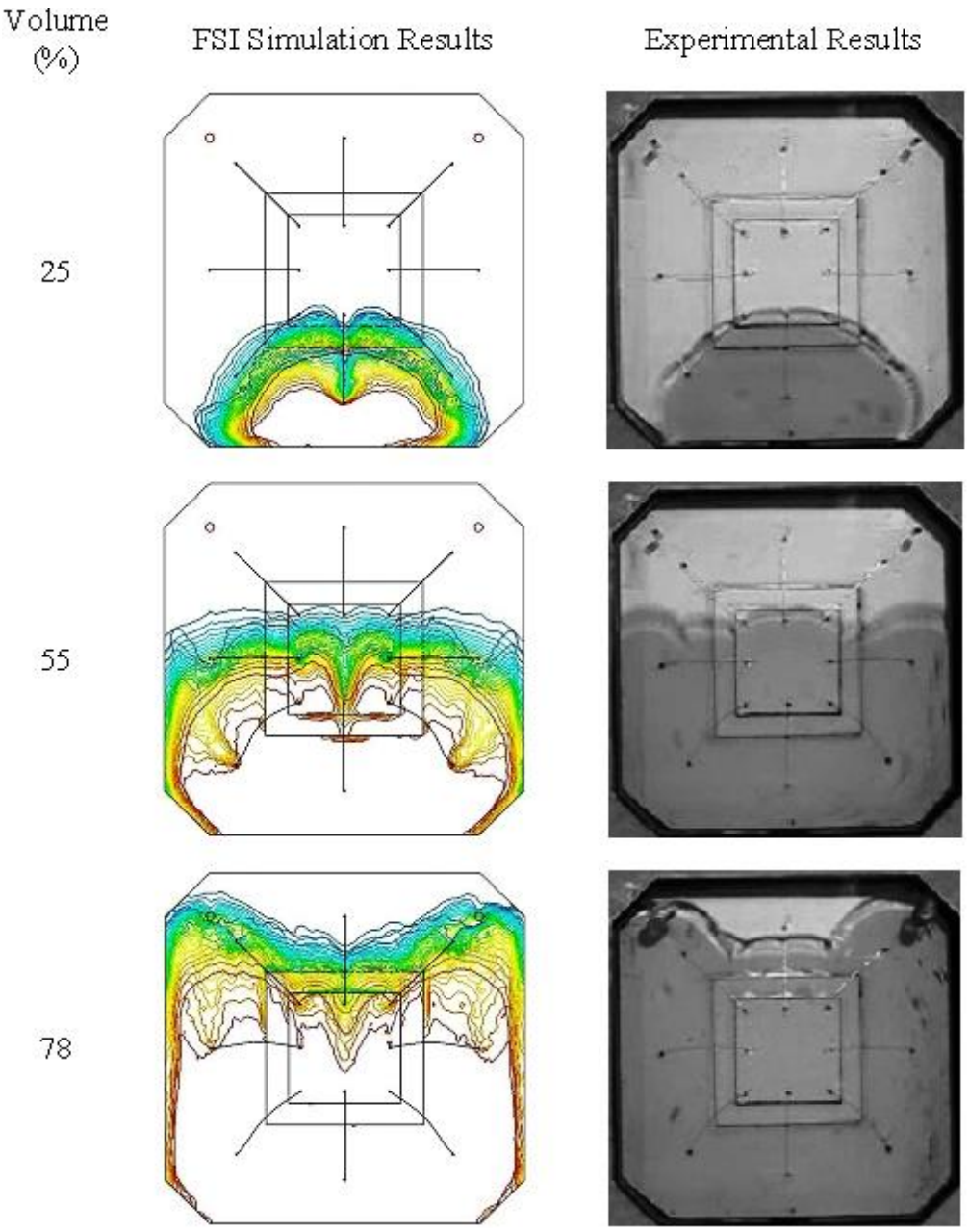


Figure 4.6 Comparison of FSI and experimental result of fluid flow front of stacked die of a scale-up eight-wire PBGA with centre inlet for Case 3.

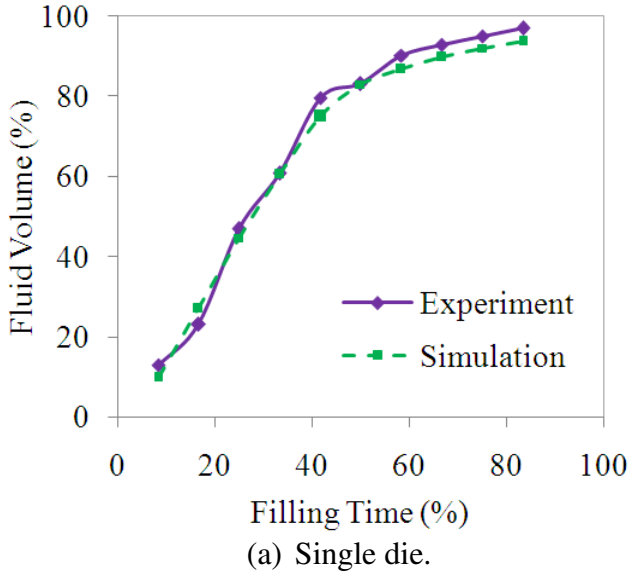


(a) Single die.

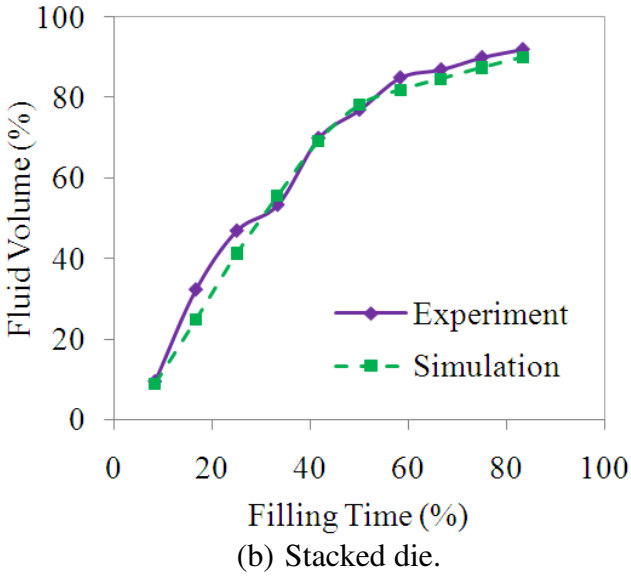


(b) Stacked die.

Figure 4.7 Percentage of filled volume versus percentage filling time of a scale-up eight-wire PBGA with centre inlet for Case 3: (a) Single die and (b) Stacked die.

#### 4.2.2.2 Wire Sweep of Single Die and Stacked Die

Wire displacement phenomenon was observed when the test fluid flows around the wire region. Figure 4.8 shows the FSI simulation and the experimental results of the wire deformation, which has approximately the similar trends. In the FSI simulation the PBGA encapsulation was carried out in ideal condition. However, there may be an unexpected uncertainty in the scaled-up experiment. Thus, this situation causes FSI result slight over-predict the wire sweep. The average discrepancy of maximum wire deformation was only 7.74 % for single die and 6.92 % for stacked die of a scale-up eight-wire PBGA with centre inlet. Therefore, the present modelling techniques yielded reliable predictions in handling the moulded packaging problem.

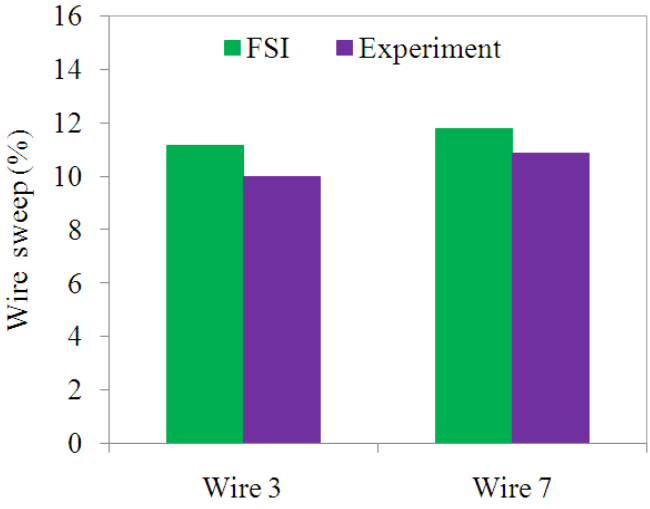


(a) Single die.

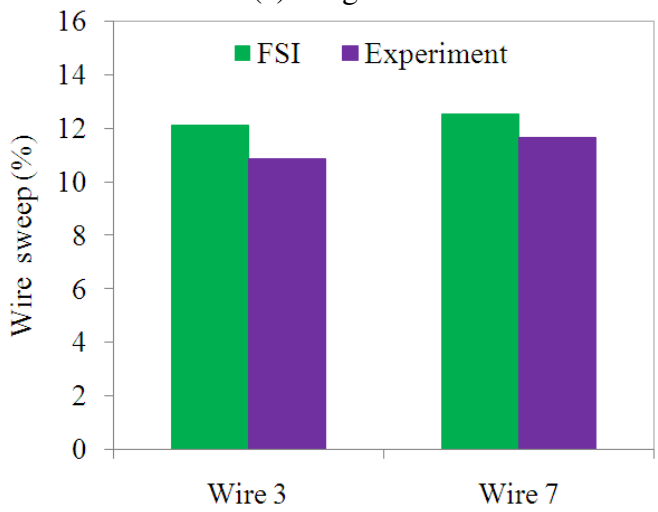


(b) Stacked die.

Figure 4.8 Percentage of wire sweep of wires 3 and 7of a scale-up eight-wire PBGA with centre inlet for Case 3: (a) Single die and (b) Stacked die.

In the last stage of filling process, as depicted in Figures 4.5 and 4.6, the dominant direction of deformation was found corresponds to the fluid flow, as clearly observed for wires 3 and wire 7 (Tay and Lee, 2002). Therefore, only these wires were focused in term of maximum displacement and stress distribution. Comparison of the wire deformation for a single and a stacked die of wires 3 and 7 in Case 3 are shown in Figure 4.9.

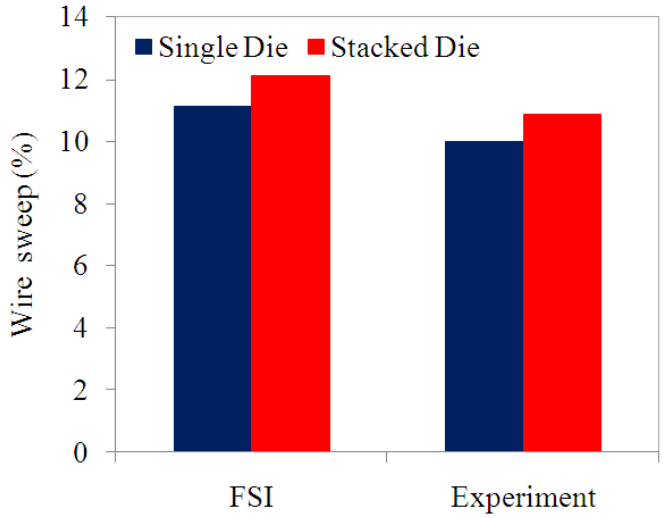


(a) Wire 3.

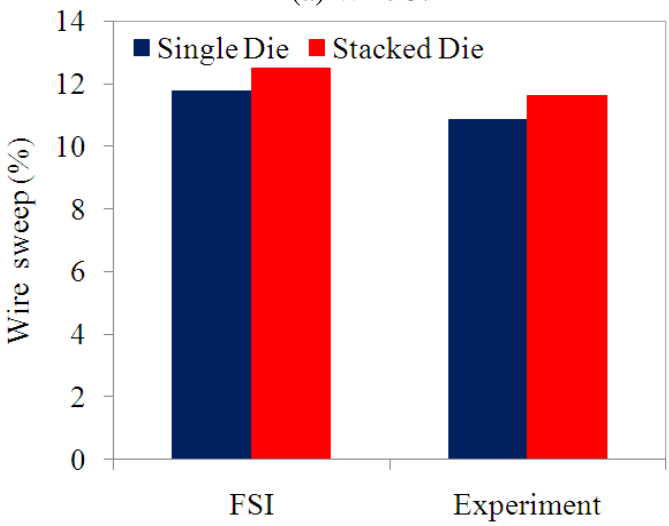


(b) Wire 7.

Figure 4.9 Comparison of wire sweep of single and stacked die of a scale-up eight-wire PBGA with centre inlet for Case 3: (a) Wire 3 and (b) Wire 7.

### 4.2.3 Scaled-up Eight-wire PBGA Encapsulation Process – Corner Inlet

#### 4.2.3.1 Fluid Flow of Single Die and Stacked Die

Similarly, the experiments of encapsulation process were also conducted for a scaled-up eight-wire PBGA prototype with corner inlet. The filling process of the viscous fluid into the cavity was recorded on top of the transparent mould. FSI simulation was also performed on the imitated package with single die and stacked die, as presented in Figure 3.12 of Chapter 3. The flow front advancement of the simulation results was compared with the experimental results. The results showed that flow front predictions from the simulation code had nearly the same profile with the experimental results at different filling volumes. Figure 4.10 and Figure 4.11 shows the comparison of predicted FSI and experimental flow profiles for the scale-up eight-wire PBGA with corner-inlet encapsulation process from 21 % to 78 % and 19 % to 80 % of filling, which includes wire sweep for single die and stacked die respectively. The simulation

result was substantiated by the experimental results by using the similar scaled-up eight-wire PBGA with corner inlet size, operating condition and material properties in the present numerical study. The predictions of flow front profiles and percentage of mould filling were well matching with the experimental results at all stage of filling. The percentage of filled volume at various stages versus percentage filling time for Case 3 was compared in Figure 4.12; the maximum discrepancy was found about 6.0 % and 4.97 % for single die and stacked die respectively of a scale-up eight-wire PBGA with corner inlet. The predicted test fluid flow profiles showed a good agreement with the experimental results, at all percentage of filling stages.

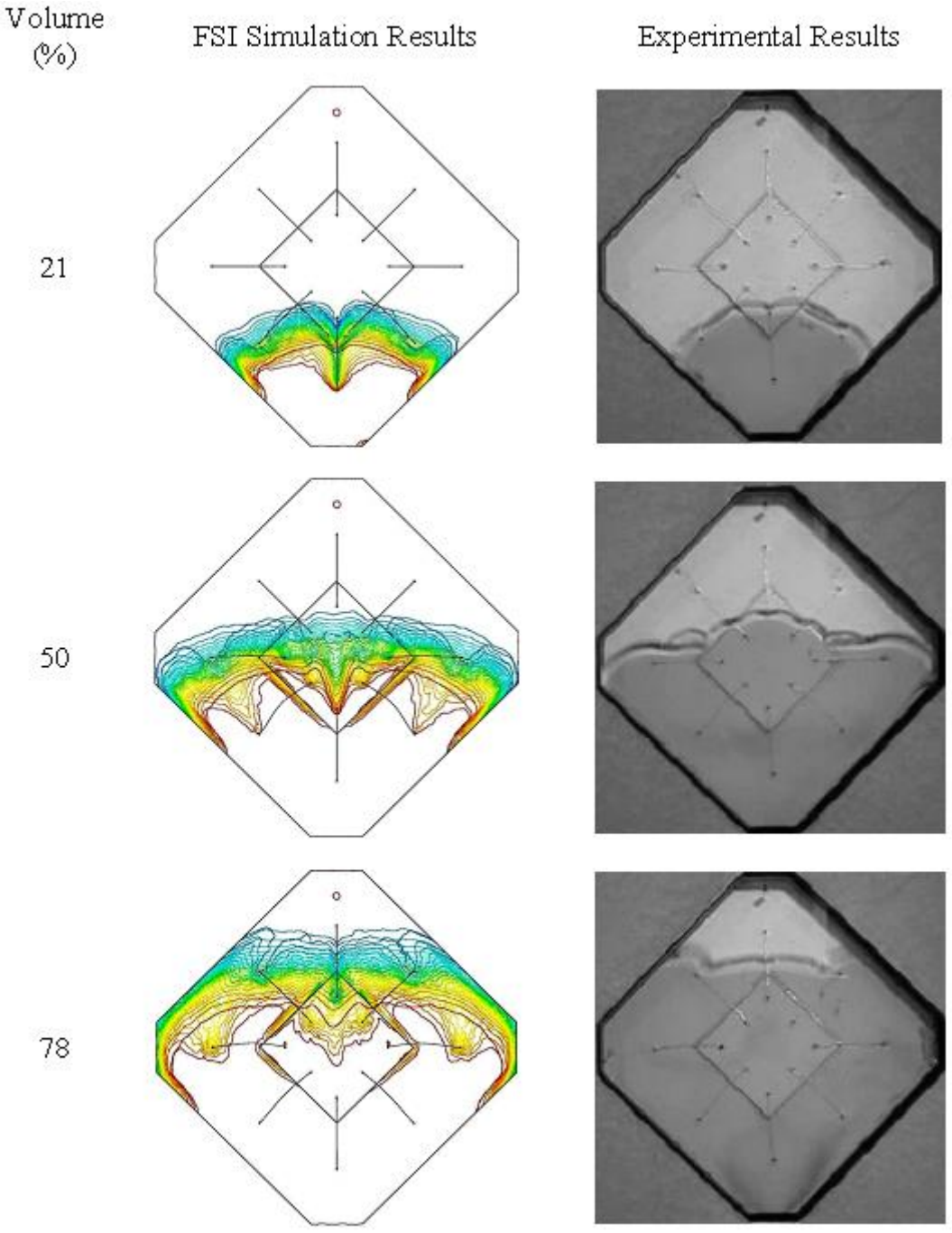


Figure 4.10 Comparison of FSI and experimental result of fluid flow front of single die of a scale-up eight-wire PBGA with corner inlet for Case 3.

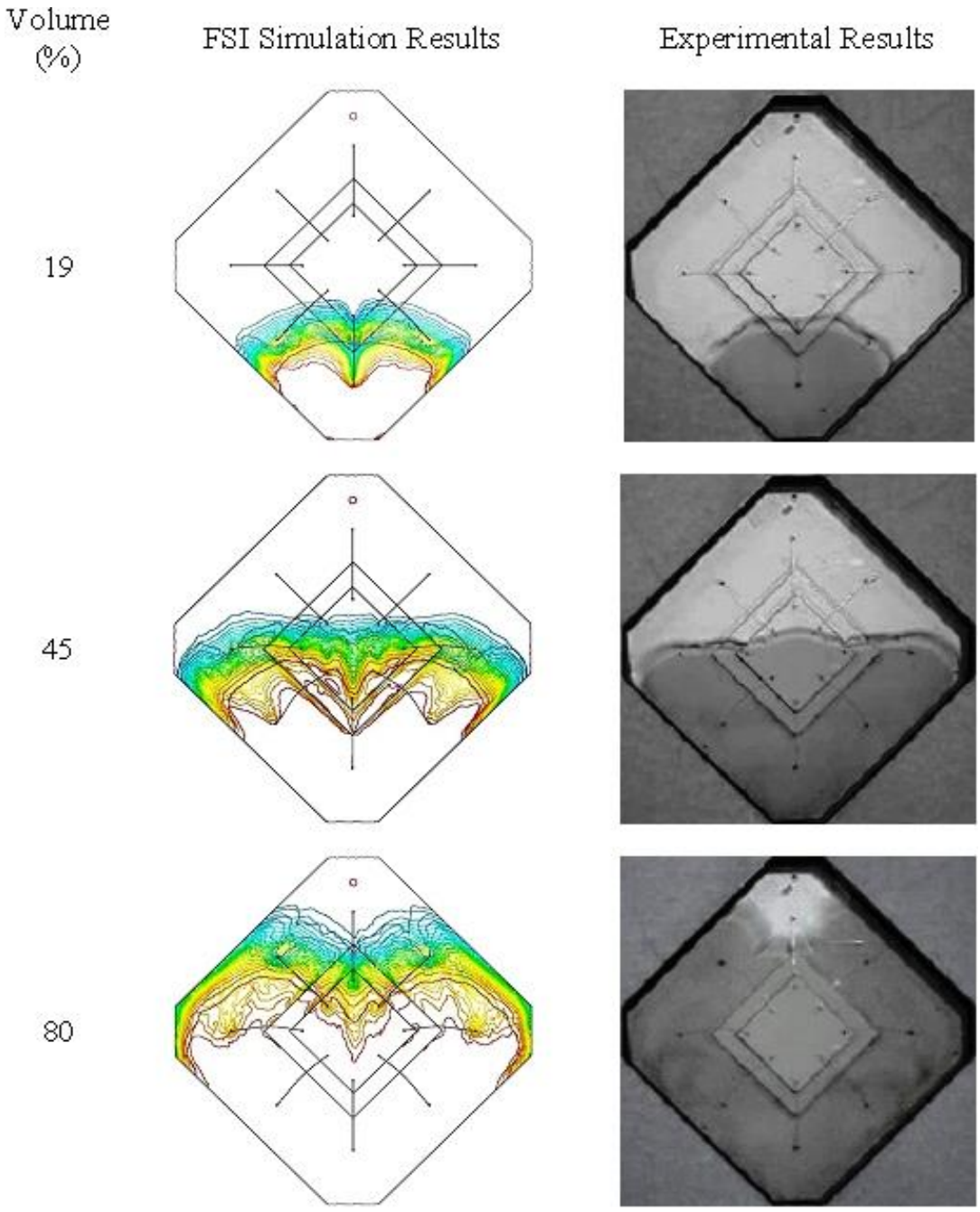


Figure 4.11 Comparison of FSI and experimental result of fluid flow front of stacked die of a scale-up eight-wire PBGA with corner inlet for Case 3.

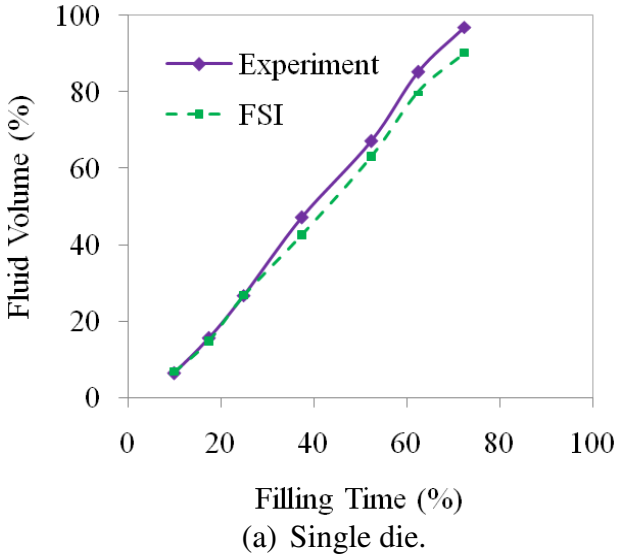

(a) Single die.

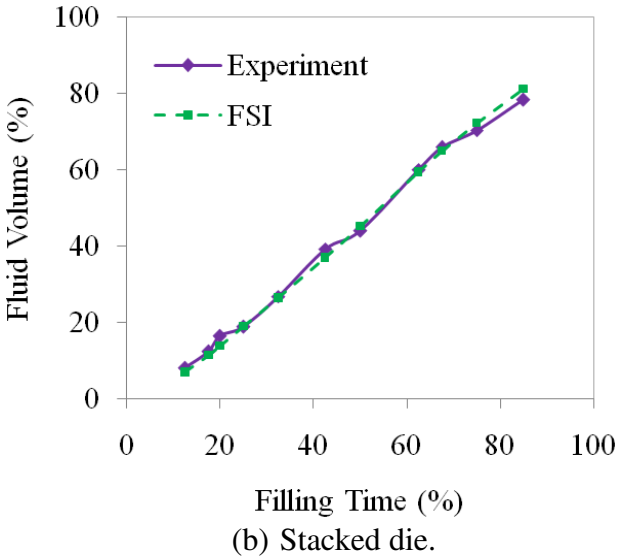

(b) Stacked die.

Figure 4.12 Percentage of filled volume versus filling time of a scale-up eight-wire PBGA with corner inlet for Case 3: (a) Single Die and (b) Stacked Die.

### 4.2.3.2 Wire Sweep of Single Die and Stacked Die

Wire displacement phenomenon was also observed when the test fluid flow around the wire region. Figure 4.13 shows FSI simulation and experimental results of wire deformation of a scale-up eight-wire PBGA with corner inlet, which was found approximately in identical trend. The average discrepancy of maximum wire deformation was only 4.95 % for single die and 8.45 % for stacked die of a scaled-up eight-wire PBGA with corner inlet. Therefore, the present modelling techniques yielded reliable predictions in handling moulded packaging problem.

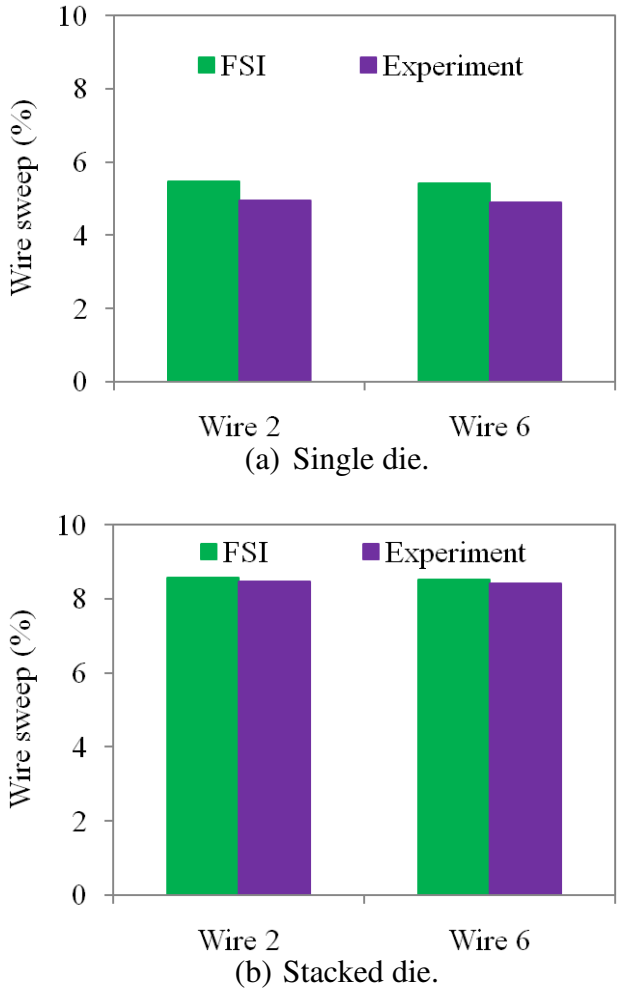


Figure 4.13 Percentage of wire sweep of wires 2 and 6 of a scale-up eight-wire PBGA with corner inlet for Case 3: (a) Single Die and (b) Stacked Die.

In the last stage of filling process as depicted Figure 4.10 and 4.11, the dominant direction of deformation was found corresponded to the fluid flow as clearly observed for wire 2 and wire 6 (Tay and Lee, 2002). Therefore, only these wires for a scale-up eight-wire PBGA with corner inlet were focused in term of maximum displacement and stress distribution. Comparison of wire deformation for single and stacked die of wire 2 and 6 in Case 3 is shown in Figure 4.14 of a scale-up eight-wire PBGA with corner inlet respectively.

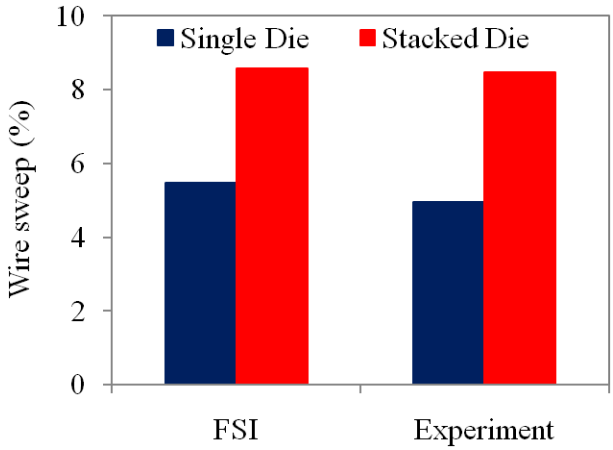


(a) Wire 2.

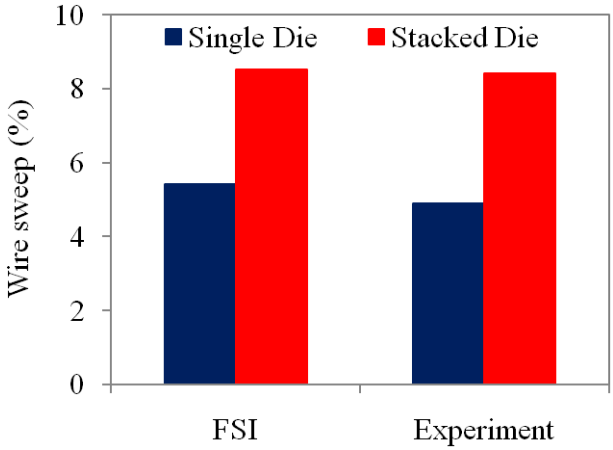


(b) Wire 6.

Figure 4.14 Comparison of wire sweep of single and stacked die of a scale-up eight-wire PBGA with corner inlet for Case 3: (a) Wire 2 and (b) Wire 6.

Based on the previous FSI simulations and experiment, it seemed that both the centre and corner inlet the die height could affect the sweep of the wires (Han et al., 2011b). Thus, the ratio of die height was introduced as an index to estimate the ratio effect on wire sweep behaviour. Figure 4.9 and Figure 4.14 demonstrated the wire sweep results in detail.

#### 4.2.3.3 Measurement and Validation of Inlet Pressure

The pressure in the mould cavity and inlet gate was measured by using pressure sensor and pressure gauge, respectively. The pressure gauge was installed between a steel cylinder (barrel) and the inlet gate. The pressure in cavity was measured by using pressure sensor that was placed on the top centre and corner of the cavity. The position of both sensors is displayed in Figures 4.15 and 4.16, respectively.


Figure 4.15 Pressure Validation on top corner position of pressure sensor at full filled.

Figure 4.15 shows the result when the mould cavity was fully filled. The pressure gauge displayed inlet pressure of 0.5 kg.f/cm$^2$. Then, the pressure value was used in the simulation. The simulation result of the maximum pressure inside cavity on the top corner was 34.7 kPa. However, the pressure sensor displayed 34.405 kPa as maximum pressure in the same position and the deviation for both results is only 0.85 %.

At different positions of pressure sensor, the increase of inlet pressure is shown in Figure 4.16. In this experiment, the inlet pressure was measured by using a pressure gauge and it showed pressure of 1.3 kg.f/cm$^2$. Similarly, this value was used as an inlet pressure parameter in the simulation. The maximum pressure value on top centre of the cavity of simulation result is 114.3 kPa, and the pressure sensor displayed of the maximum pressure in the same position was obtained at 113.8 kPa, and the deviation for both results is only 0.45 %. Detailed of fluid flow pressure gauge calibration graphically is shown in Appendix F.


Figure 4.16 Pressure Validation on top centre position of pressure sensor at full filled.

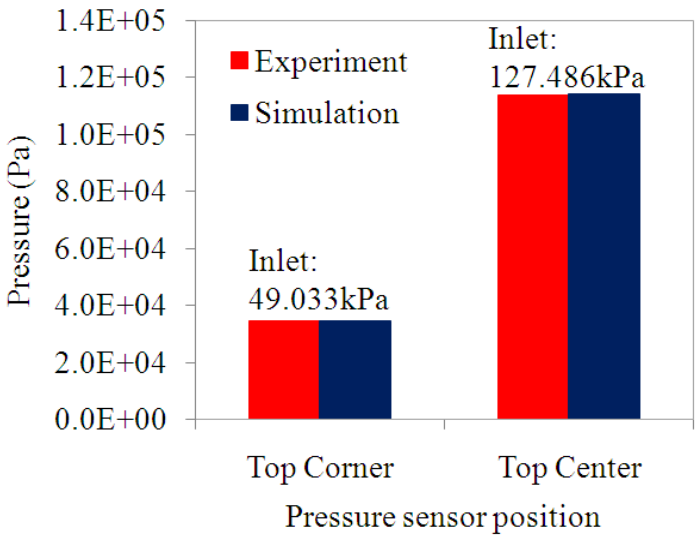


Figure 4.17 Comparison of pressure on top cavity for different pressure sensor position and inlet pressure.

The comparison of simulation and experimental results for the pressure at top of cavity for different positions and inlet pressure is described in Figure 4.17. The comparison shows a good agreement; therefore, this has demonstrated that the measurement of inlet pressure was reasonable in the experimental and simulation studies of the current research.

### 4.2.4 Actual Size of PBGA Encapsulation Process

#### 4.2.4.1 Fluid Flow Profiles

This simulation result was substantiated by the experimental results of Chen (1990) by using similar size of PBGA, operating condition, and material properties in the present study. The comparison of Case B simulation and experimental results for the melt-front profiles is shown in Figure 4.18. The predictions of flow-front profiles and percentage of mould filling matched well with the experimental results in all stages of mould filling. The percentage of the filled volume at various stages versus percentage of time of Case B is compared in Figure 4.19.

UDFs allow the user to customize FLUENT, and it can significantly enhance its capabilities. Based on the observation (Figure 4.18), the experiment and simulation of the melt-front closely match each other except on a number of voids observed in the experiment. The shape of the melt-front begins to diverge as it contacts the leading edge of the die. One melt-front is located directly above the dies, and the other on either side of the dies. The effect of dies is clearly shown in the melt fronts. The flow is retarded in this region due to flow resistance, causing the flows in other regions to advance. These results indicate that the simulation results are in good agreement with those of the experiments.

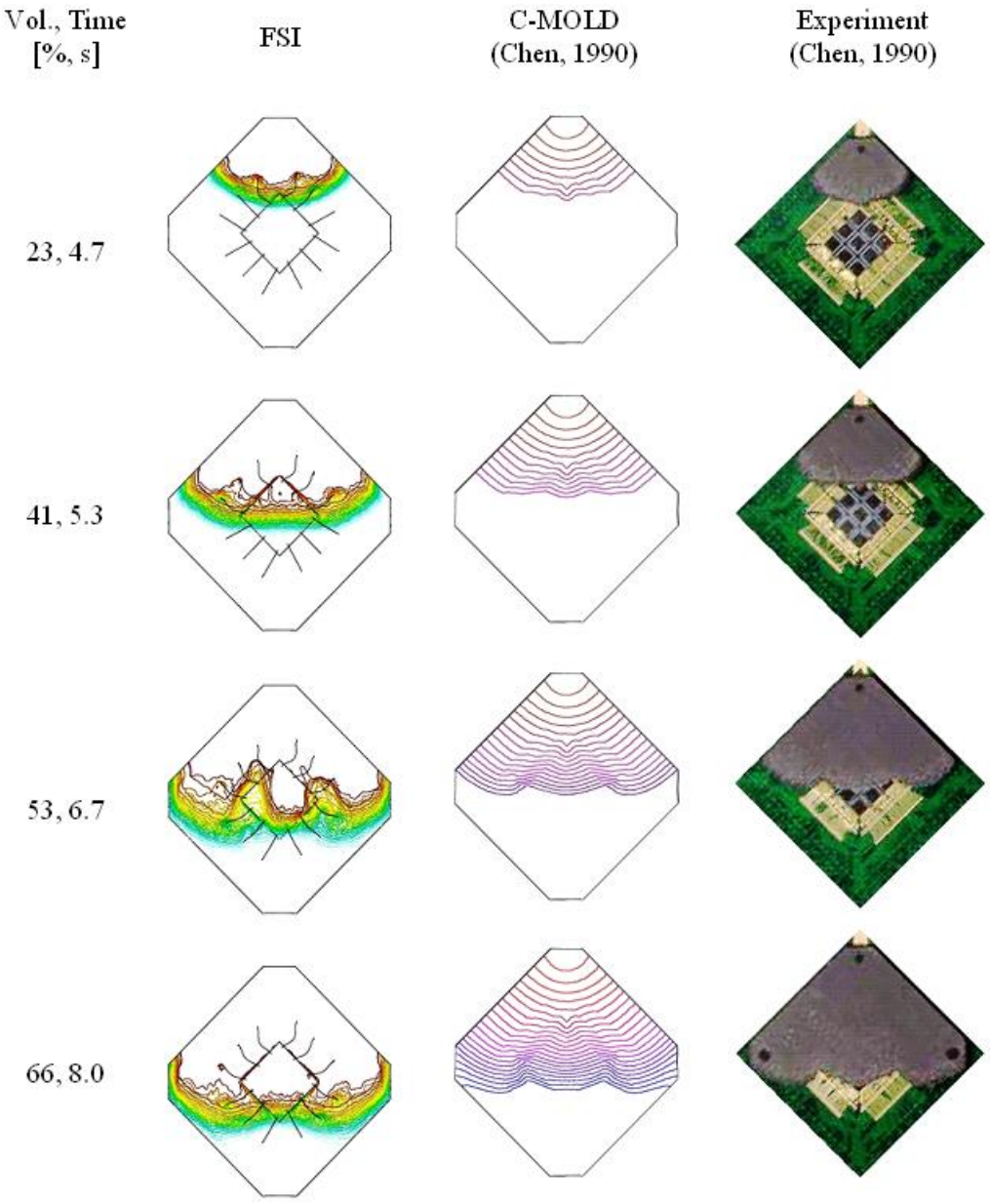


Figure 4.18 Comparison between experimental (Chen, 1990), C-MOLD simulation (Chen, 1990) and simulation results of EMC Flow of Case B of actual size PBGA.

The experimental results of short shot at the different percentage of filled volume are compared with the simulation results. Figure 4.18 demonstrates the melt-front advancement of actual size PBGA for both experimental and simulation results from 23, 41, 53 and 66 percentage of EMC filled volume. The experimental results were obtained by from previous work (Chen, 1990). At the initial stage, 23 % of EMC filled the volume; a top view of the current simulation result shows an almost similar flow-front profile as in the experiment. This is obviously shown in 41 % of the EMC filled volumes, the simulation results is well matched with the experimental result. For 53 and 66 % of EMC filled volume, the flow-front on top of the die was concave, while the flow-front around was convex. The simulation results show that the flow-front on top of the die dropped behind the experimental results except in the middle of the die. The difference with the experimental result might be attributed to the geometric model. The results show the faster flow-front at the free region which has no silicon die presence.

However, at 66 % of filling stage, good agreement of the flow profile is found for both results. Overall, the FLUENT prediction gives the better agreement to experimental results.

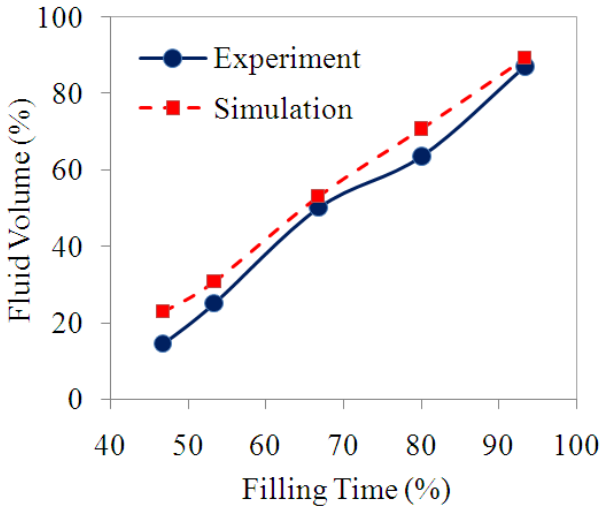


Figure 4.19 Comparison between experimental (Chen, 1990) and simulation results of percentage EMC Volume of Case B of actual size PBGA.

Figure 4.19 shows the percentage volume of the melt-fronts during the filling process. The approximate volume of the melt fronts is calculated from the experimental work (Chen, 1990) by taking the area of the melt-front. The results also show the comparison between experimental measurement and numerical simulation, which shows the good conformity.

### 4.2.4.2 Wires Sweep

Figure 4.20 shows the comparison between experimental (Chen, 1990) and FSI simulation of the maximum and minimum wire sweep of Case B. From the comparison, the average discrepancy of the maximum and minimum of wire sweeps between the present FSI predictions and experimental results (Chen, 1990) is approximately 8 %. This demonstrates the realistic predictions of present FSI in solving the wire sweep during the encapsulation process.

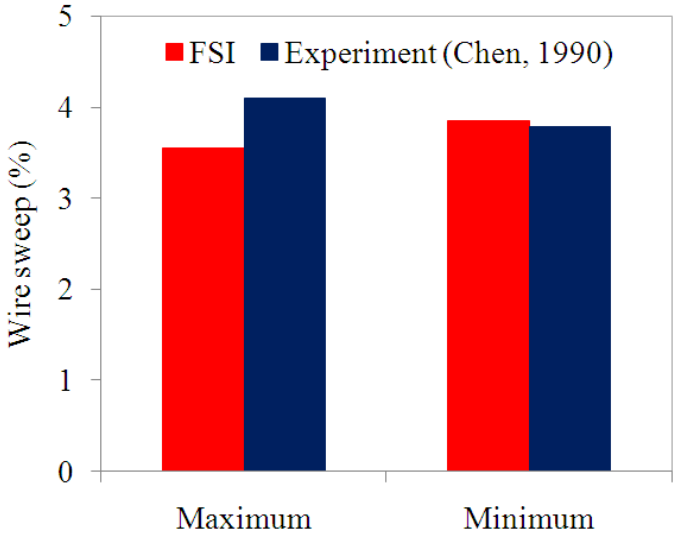

Figure 4.20 Comparison between experimental (Chen, 1990) and FSI simulation of wire sweep of Case B of actual size PBGA.

## 4.3 Influence of Number of Mould Cavity Vents and Inlet Gate on Wire Sweep in Scale-up Four-wire PBGA Encapsulation

### 4.3.1 Melt Front Profile

First of all, the effect of number of vents on the melt front profile is visualized for various stages of filling, as presented in Figure 4.21. It is observed that the melt flow pattern exhibits almost similar trend in all the cases; this indicates that the melt front advancement is not significantly influenced by the number of vents.

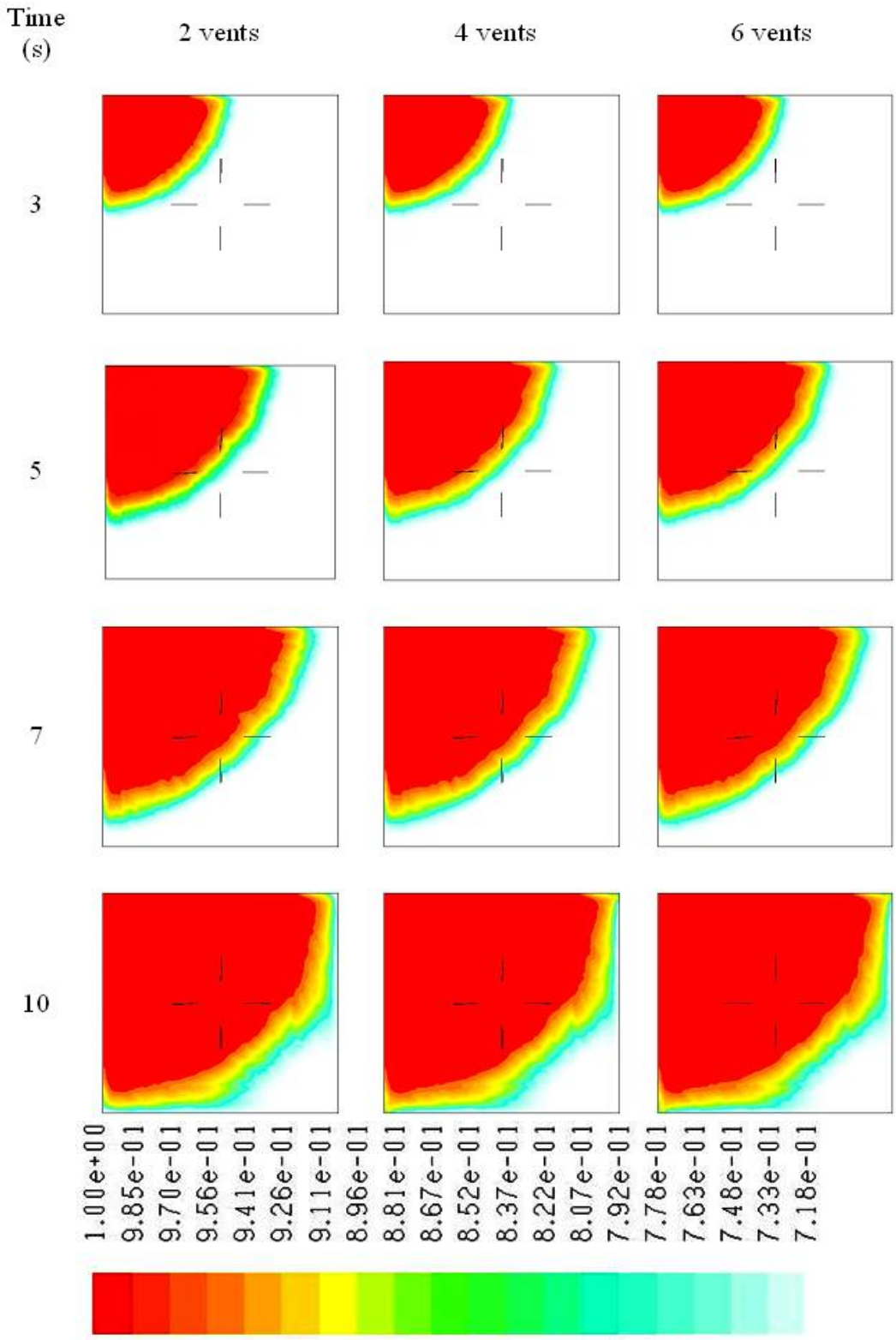


Figure 4.21 Melt front profiles of scale-up four-wire PBGA of three cases at various filling stages.

### 4.3.2 Wire Sweep

Figure 4.22 illustrates the phenomenon of wire deformation, predicted by ABAQUS. The deformation has been calculated at Point A (Figure 4.23). The wire sweep of wire 1 and wire 4 for all cases are shown in Table 4.5. Figure 4.24 shows the wire deformation in x, y and z directions for all wires of two-outlet vent arrangement. It can be clearly understood that the wires deformed to the horizontal (x) and vertical (y) axes (Yao, et al., 2005). For the wire 1, the deformation is the tendency in the z-direction and wire 2 in the x-direction respectively. The comparison of deformation magnitudes of wires 1 to 4 are shown in Figure 4.25. It is found that wire 4 has the highest deformation in the x-direction (Figure 4.23(a)). However, wire 1 has larger deformation in y and z directions as shown Figures 4.23(b-c). These deformations are due to the positioning of wire and the directions of wire bond span. In Figure 4.25, wires 1 and 4 show, higher deformation compared to wires 2 and 3. This is due to their orientation and the direction of EMC flow during the encapsulation process. The magnitude of wire deformation for each wire is also estimated and plotted as shown in Figure 4.26. It is clear that the wires 1 and 4 are significantly deformed compared to wires 2 and 3, in all cases. At the same time, it is worth noting that, as the number of vents increases, the sweep tendency decreases, presumably due the reduced pressure force inside the cavity.

Table 4.5 Wire deformation predicted by ABAQUS of different outlet vent

| Number of vents/No. of wire | Wire sweep (mm) | |
|---|---|---|
| | Wire 1 | Wire 4 |
| 2 vents | 0.65 | 0.60 |
| 4 vents | 0.49 | 0.57 |
| 6 vents | 0.37 | 0.55 |
| Uncertainty deformation on real wire sweep in industry (Jong et al., 2005) | 0.80 | |

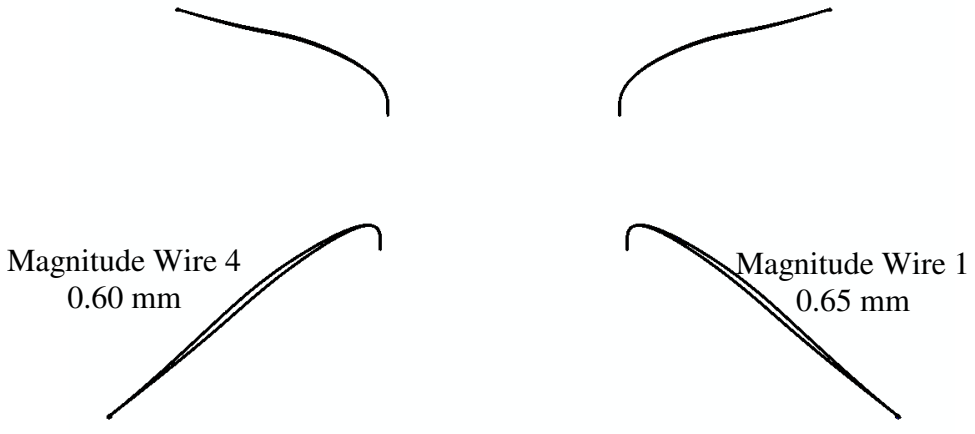


a) 2 vents

Figure 4.22 Illustration of wire sweep predicted by ABAQUS of scale-up four-wire PBGA: (a) 2 vents

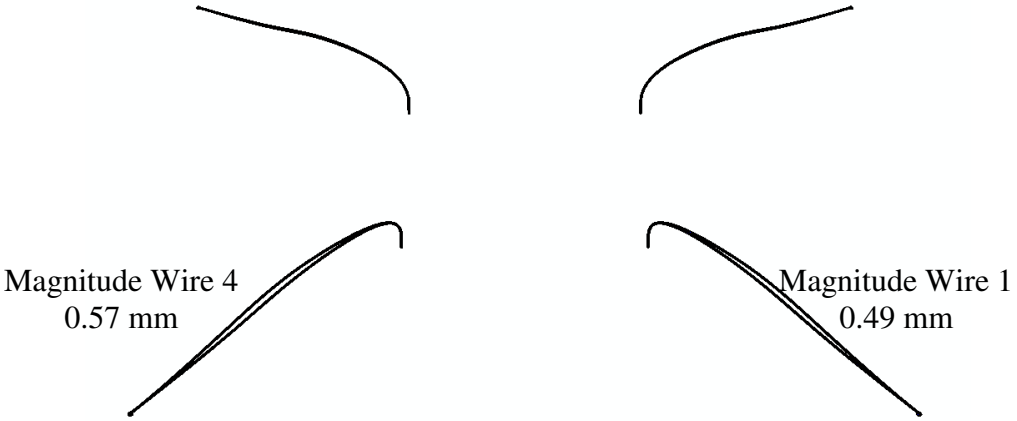


b) 4 vents

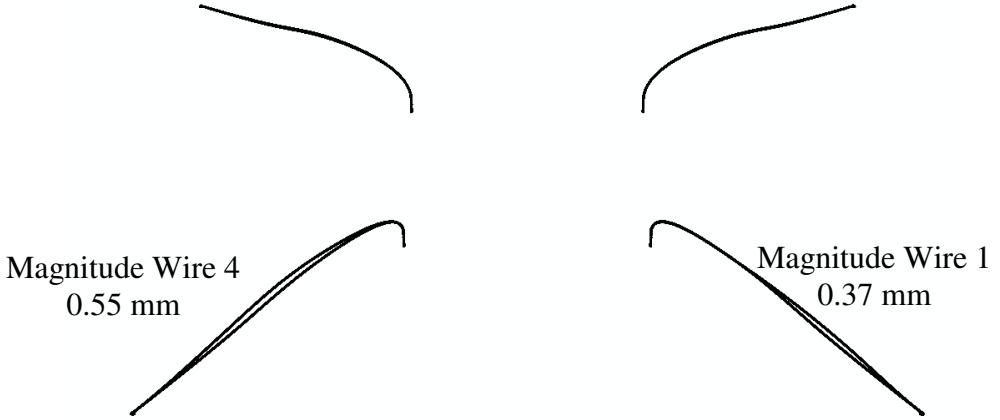


c) 6 vents

Figure 4.22 Illustration of wire sweep predicted by ABAQUS of scale-up four-wire PBGA: (b) 4 vents and (c) 6 vents.

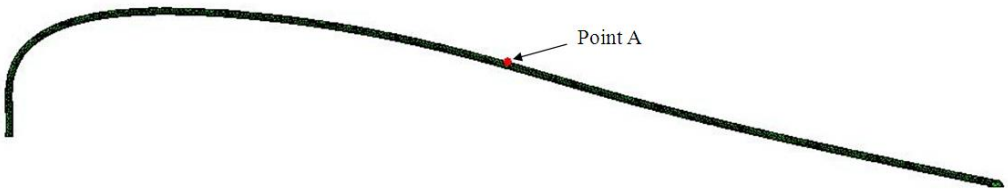


Figure 4.23 Measurement of wire deformation at Point A.

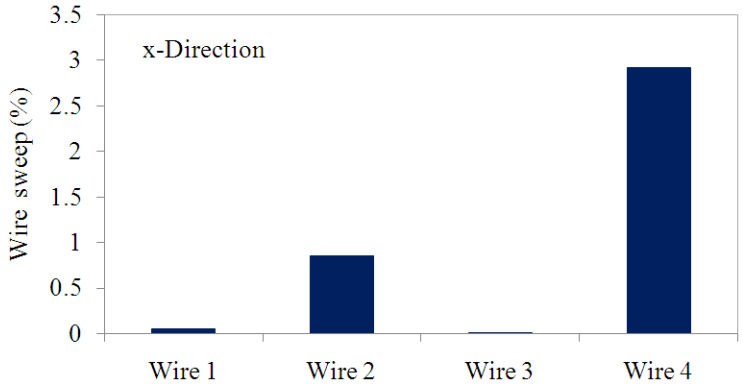


(a) x-direction.

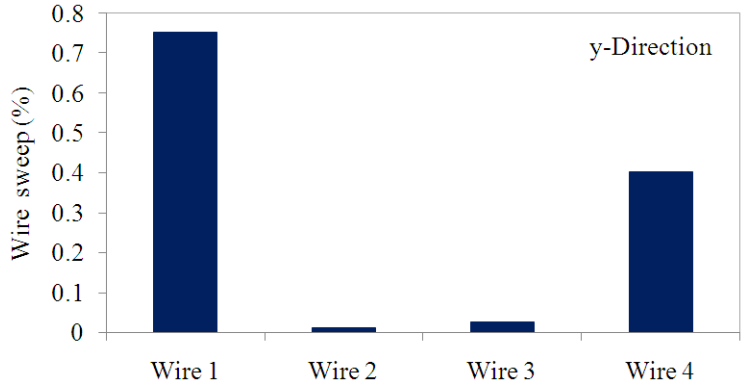


(b) y-direction.

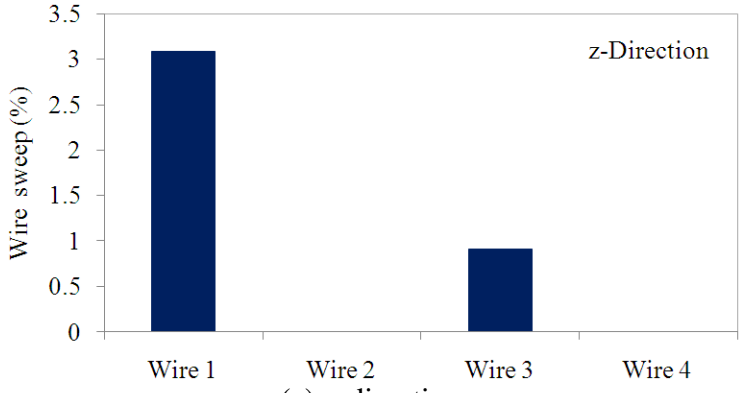


(c) z-direction.

Figure 4.24 Comparison of four wire deformation of two outlet vents arrangement at Point A: (a) x-direction, (b) y-direction and (c) z-direction.

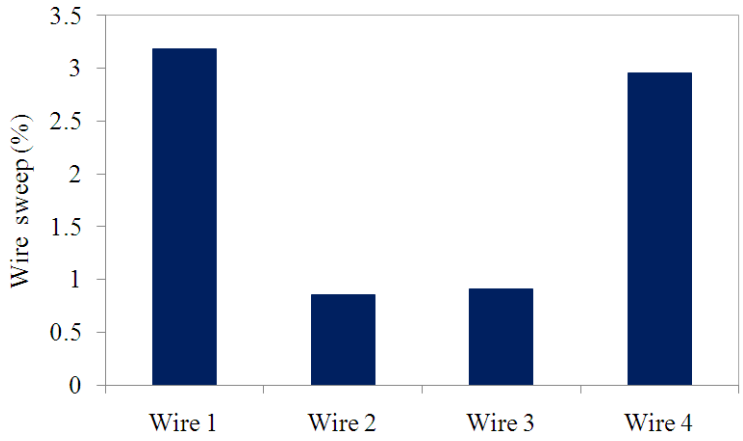


Figure 4.25 Comparison of wire sweep for all wires of two outlet vents arrangement at Point A.

Figure 4.26 shows the effect of the number of outlet vents on the wire deformation. The results show that the deformation of all wires is lower for six outlet vents compared to two outlet vents arrangements. The results illustrated the drag force induced by the EMC flow is lower for the case of six outlet vents arrangement. The lower the drag force will provide less stress concentration on the wire and will reduce the tension on the wire. Thus, number of outlet vents does influence on the wire deformation during the encapsulation process.

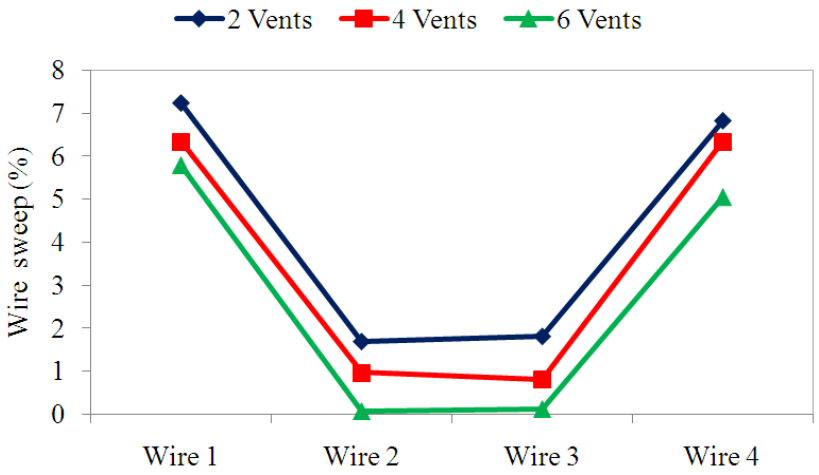


Figure 4.26 Comparison of deformation of wires 1-4 for all the cases of scale-up four-wire PBGA.

The results also shown that the wires 2 and 3 have lower deformation compared to wires 1 and 2 since the locations of wires 2 and 3 are behind the silicon die. The wires 1 and 4 are located near to the inlet gate have experienced higher induced drag force, thus, both wire has higher stress concentration. The phenomena will help the engineers to decide the appropriate location for the wire in order to avoid the wire overlap that might cause a short circuit or failure during the encapsulation process.

### 4.3.3 Pressure Distribution

Figure 4.27 shows the locations of pressure measurement of each wire during the encapsulation process, and Figure 4.28 shows the corresponding plots as a function of position point. The increase of pressure is due to the presence of EMC. As can be seen, pressure at Point 1 is the maximum due to the impact of incoming flow, gradually reduces with flow advancement as evident from the medium pressures at the identical locations Point 2 and Point 4, and the location Point 3 (near the exit) which shows the minimum pressure. The pressure directly influences the wire displacement and drag force acting on the wire structure, during the filling process. Thus, wires situated at high pressure location are expected to deform more compared to those at the low pressure region, as is clear from the increased sweep of wires 1 and 4 located near to Point 1. It is also worth noting from Figure 4.28 that, as the number of vents increases, the pressure decreases, leading to possible reduction in wire sweep.

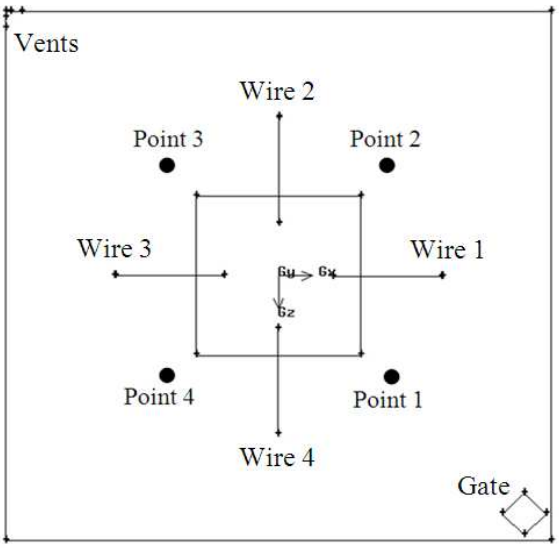


Figure 4.27 Locations of pressure measurement of scale-up four-wire PBGA.

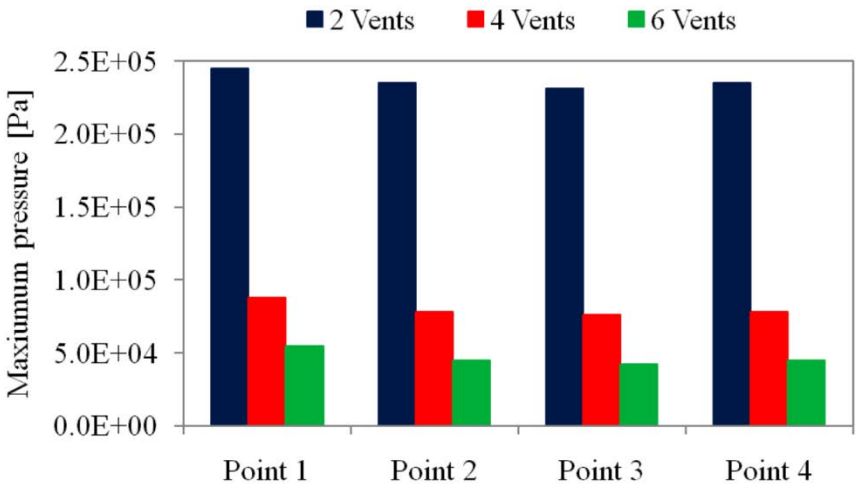


Figure 4.28 Comparison of maximum pressure at locations 1-4 for the three cases of scale-up four-wire PBGA.

### 4.3.4 Von-Mises Stress Distribution

The consolidated data of maximum Von-Mises stress developed in each wire for the three cases is given in Table 4.5. It is clear that wires 1 and 4 are subjected to maximum stress, owing to the influence of higher pressure force on them. However, the stress decreases significantly with the increase in the number of vents. Detailed view of stress distribution for wires 1 and 4, in maximum displacement is shown in Figure 4.29a, 4.29b, 4.30a and 4.30b respectively, which demonstrates that the highest stress is around un-deformed fixed boundary, especially near to the wire bonds. This means the sweep displacement of wire is dominated by the twisting moment instead of the bending moment (Kung et al., 2006). For clarity, only the two bond regions where stress is significant, are shown, that too only for the highly deformed wires (1 and 4). From Table 4.5, it is also worth noting that the maximum stresses in the case of 2 vents are alarmingly above the ultimate stress of the wire material (gold), which is $2.2 \times 10^8$ Pa (Liu et al., (2004b), and this failure threat is significantly eliminated by increasing the number of vents. Increase in number of vent reduces the pressure within the package (Figure 4.28), which also decrease the fluid induced forces on the wire. Thus the von-Mises stress subjected to the wire also decreases.

Table 4.6 Maximum Von-Mises stress in each wire for different cases during encapsulation process of scale-up four-wire PBGA.

| Wire | Maximum Von-Mises stress (Pa) | | |
|---|---|---|---|
| | 2 vents | 4 vents | 6 vents |
| 1 | $3.748 \times 10^8$ | $1.522 \times 10^8$ | $1.289 \times 10^8$ |
| 2 | $3.091 \times 10^8$ | $3.988 \times 10^7$ | $2.696 \times 10^7$ |
| 3 | $2.696 \times 10^8$ | $4.495 \times 10^7$ | $2.463 \times 10^7$ |
| 4 | $3.499 \times 10^8$ | $1.678 \times 10^8$ | $1.518 \times 10^8$ |

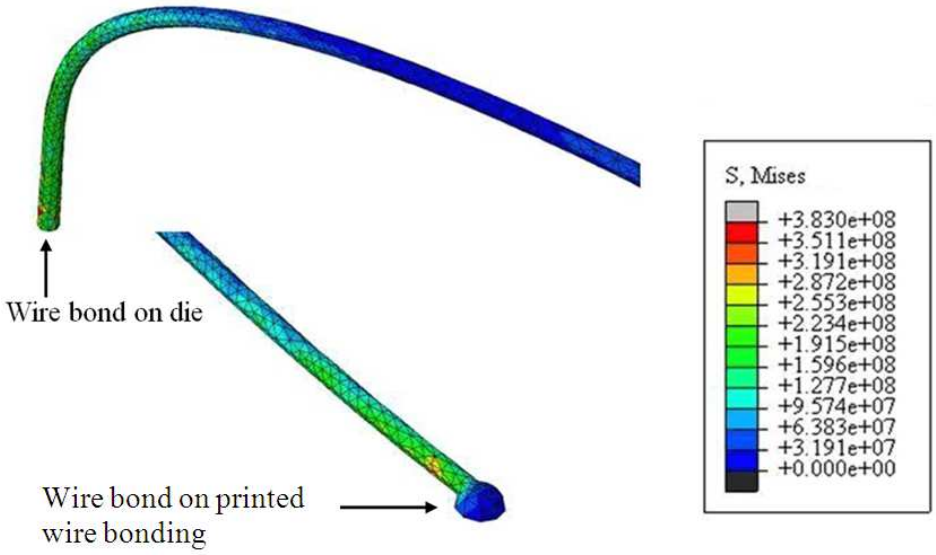


(a) Wire 1-2 vents.

Figure 4.29a Detailed view of von-Mises stress distribution for wire 1 for various numbers of vents of scale-up four-wire PBGA: (a) Wire 1-2 vents

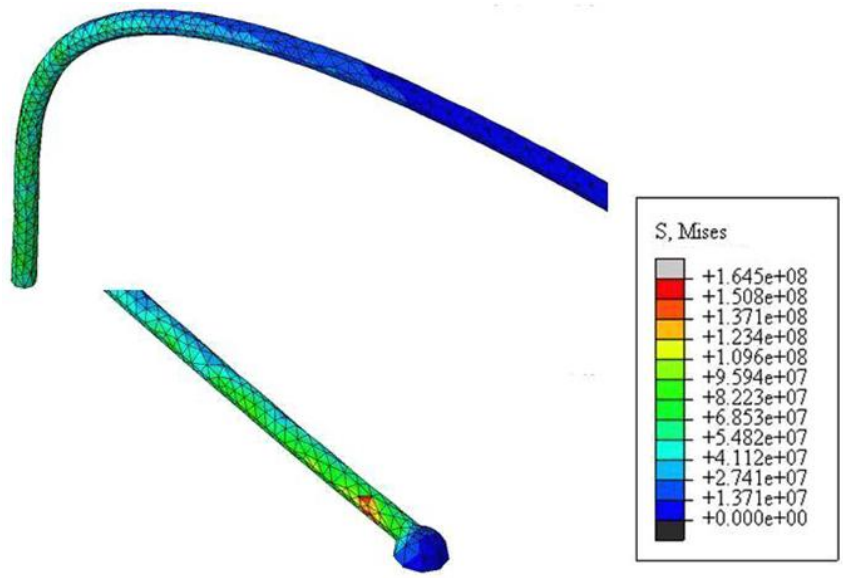


(b) Wire 1-4 vents.

Figure 4.29a Detailed view of von-Mises stress distribution for wire 1 for various numbers of vents of scale-up four-wire PBGA: (b) Wire 1-4 vents.

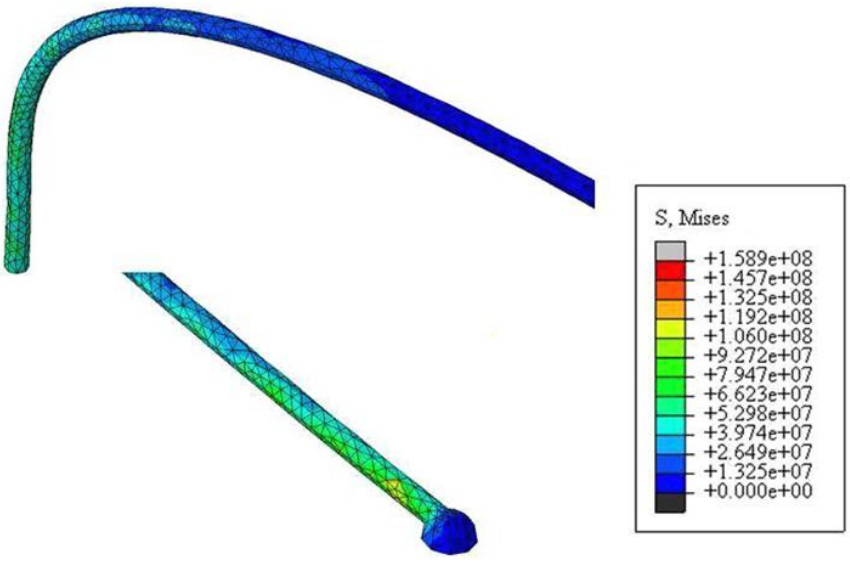


(c) Wire 1-6 vents.

Figure 4.29b Detailed view of von-Mises stress distribution for wire 1 for various numbers of vents of scale-up four-wire PBGA: (c) Wire 1-6 vents (continued).

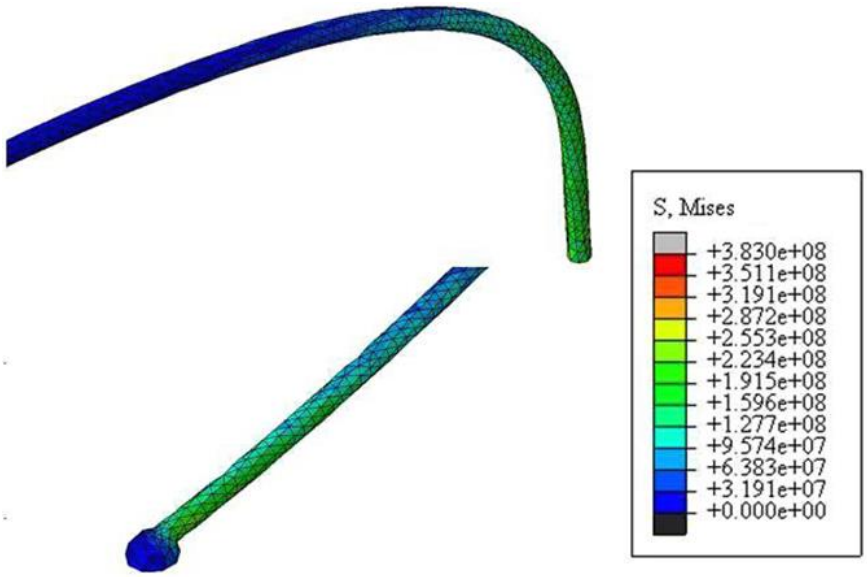


(a) Wire 4-2 vents.

Figure 4.30a Detailed view of von-Mises stress distribution for wire 4 for various numbers of vents of scale-up four-wire PBGA: (a) Wire 4-2 vents

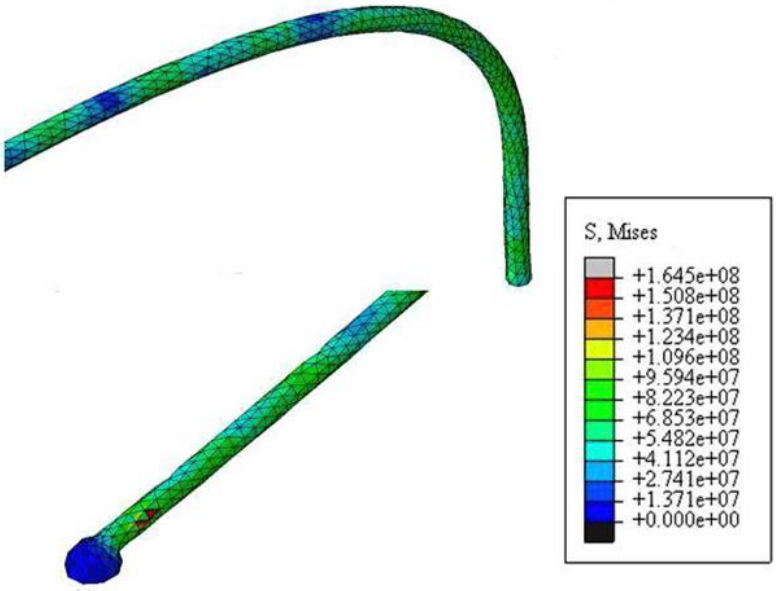


(b) Wire 4-4 vents.

Figure 4.30b Detailed view of von-Mises stress distribution for wire 4 for various numbers of vents of scale-up four-wire PBGA: (b) Wire 4-4 vents

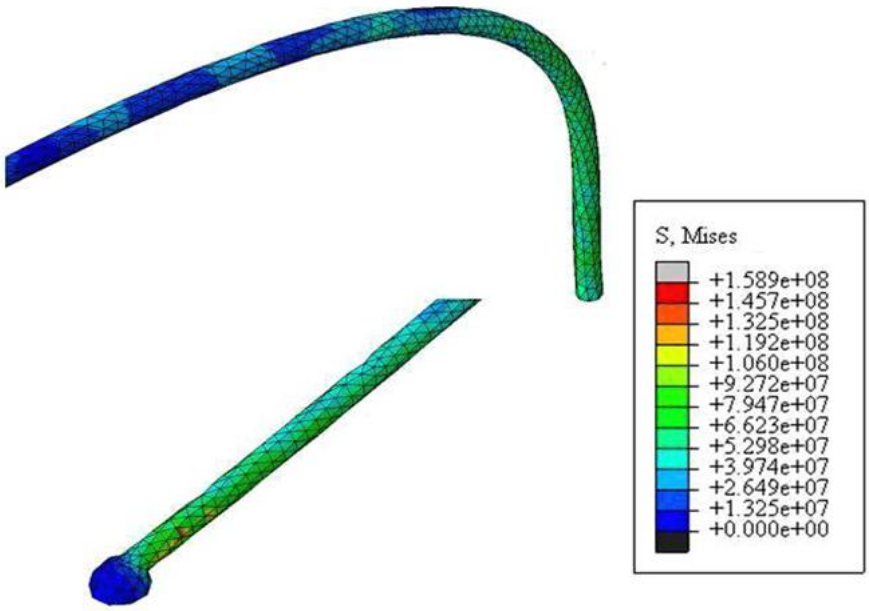


(c) Wire 4-6 vents.

Figure 4.30b Detailed view of von-Mises stress distribution for wire 4 for various numbers of vents of scale-up four-wire PBGA: (c) Wire 4-6 vents (continued).

### 4.3.5 Void Occurrence

It has been shown in the previous sections that the increasing in number of vents could reduce the wire sweep. However, it would be interesting to study the limiting factors of increasing the vents for a given mould cavity and number of gate. Thus in the present study, an attempt is also made to observe how the number of vents influence the development of voids during the encapsulation process. Figure 4.31 shows the melt front profiles showing the void locations for various cases, and Figure 4.32 shows the graphical comparison of the respective percentages of voids. It is observed that, as the number of vents increases, the void formation increases significantly; this apparently imposes restriction on the number of vents. However, as is clear from Figure 4.31, since the voids are situated near the walls, and the wire zone is not affected, the increased number of vents does not presumably pose significant threat on the quality of mould filling.

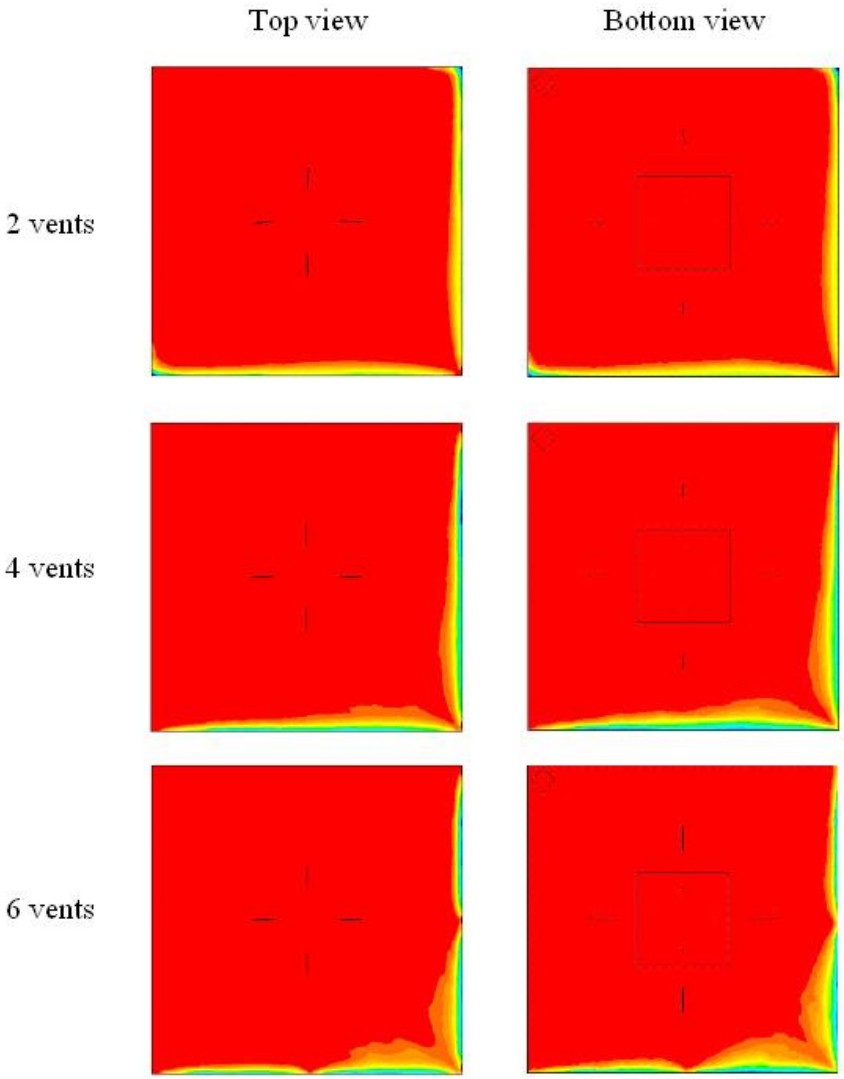


Figure 4.31 Mould filling contours for various cases after 15 s, showing voids of scale-up four-wire PBGA.

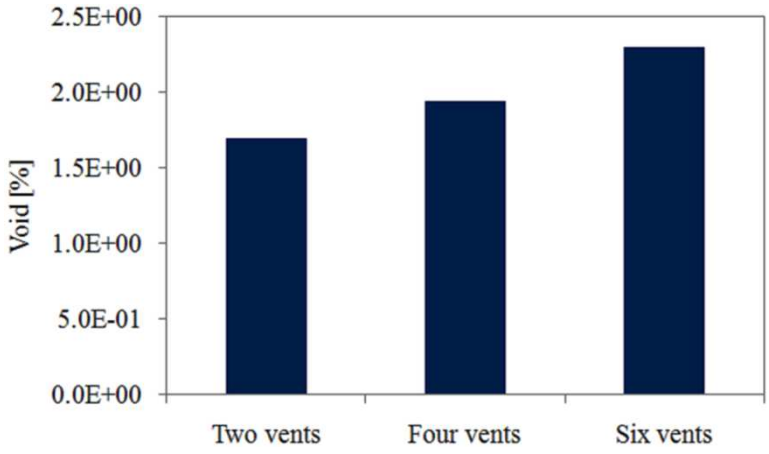


Figure 4.32 Voids percentage in various cases after 15 s of scale-up four-wire PBGA.

### 4.3.6 Conversion of the compound

Degree of conversion reflects the cure development of the moulding compound with time and it can be quite straight forward to follow if the cure process occurred in static mode. However, during dynamic mould filling process, other factors such filling pressure, temperature change due to non-Newtonian flow behaviour of the moulding

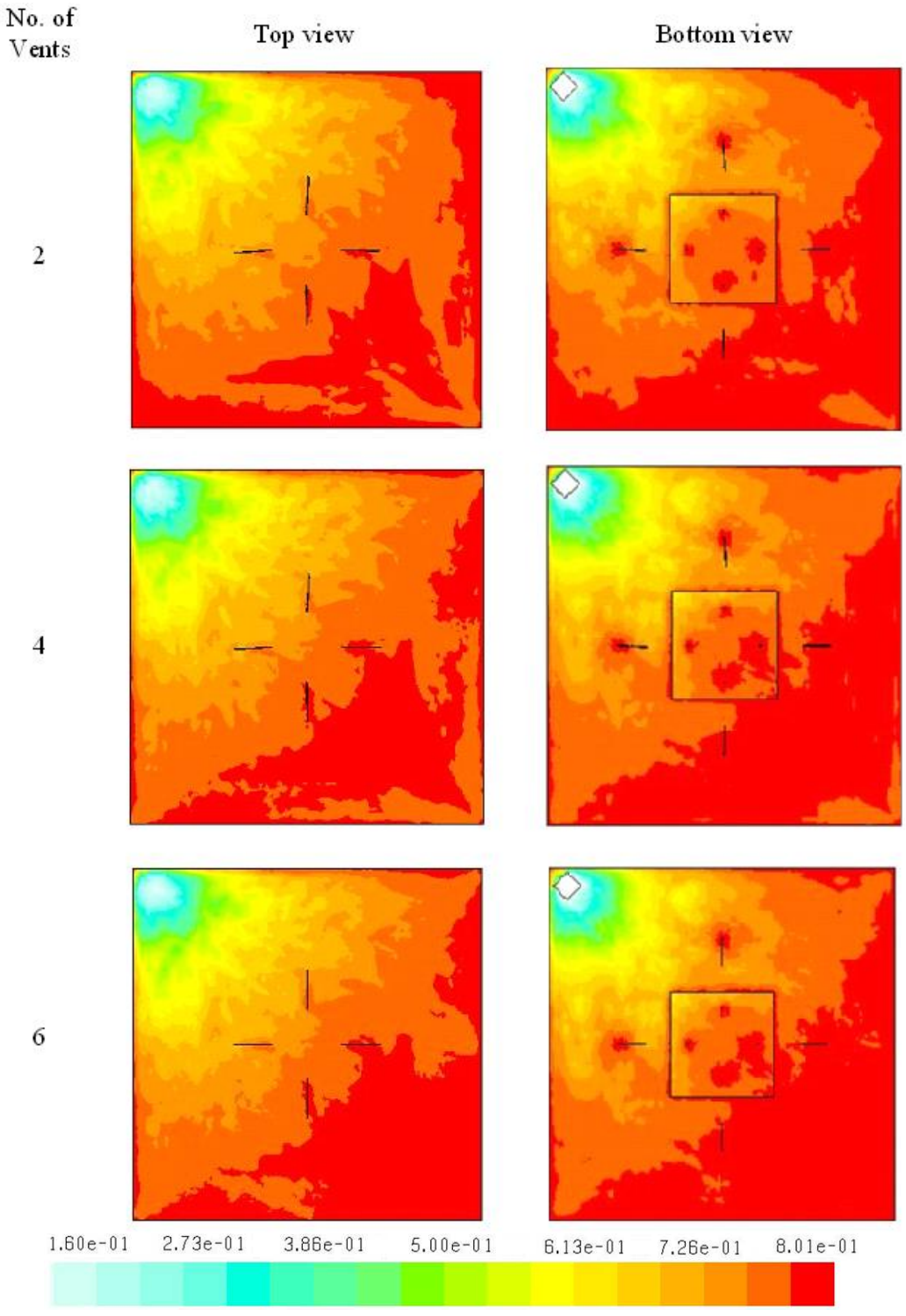


Figure 4.33 Predicted conversion of the mould compound at top and bottom view of the packages for different number of vents of scale-up four-wire PBGA.

compound and shear rate variation within the mould cavity make the prediction of conversion level to be quite difficult. The top and bottom view of conversion distribution of the packages is presented in Figure 4.33 for different number of outlet vents. It is observed that the conversion level is quite low at the cavity inlet gate and outlet vents, but higher around the package region. The predicted conversion of the mould compound at 15 s is 8.01e-01 for 2, 4, and 6 vents. This phenomenon is reasonable with the vents number variation. This is predictable since the combination of the Castro-Macosko viscosity model and the Kamal cure kinetics model have taken into account of two important factors, i.e. the dependence viscosity toward shear rate and dependence of conversion level (which also affects the viscosity of the moulding compound) toward temperature.

Mould filling of thermoset polymers consists of two competing events which usually occur simultaneously during the process. These events are: a) reduction of viscosity with shear rate due to non-Newtonian behaviour of the polymer fluid and b) increase in viscosity as the results of chemical reaction that occur during thermoset curing (Ardebiri and Pecht, 2009). The success of the mould filling process for thermoset polymer relies greatly on the compromise of both events and their dependence on process temperature. The filling must be as fast as possible to take full advantage of the first event; but when it comes to intricate and restricted moulding process such as IC packages encapsulations, the filling process would not be as smooth as anticipated, due to the second event. This is quite true in the vicinity of the package region where it is estimated that the melt front velocity is slower enough to cause initiation of the second event. In addition, the slower the fluid flows in these regions; more contact time is available for the compound to absorb heat from the mould surfaces which enhances the degree of conversion as observed in the simulation results.

### 4.3.7 Melt Front Profile and Wire Sweep Behaviour of Different inlet Gate of Scale-up four-wire PBGA

Increasing of the number of inlet gates resulted in the reducing of the wire sweep and minimizing the filling time. Figure 4.34a and 4.34b shows the melt front profile of different inlet gates to the wire sweep in the cavity. Wire sweep of each cases are presented in Figure 4.35a and 4.35b. As reported by Khor et al. (2011), increased of inlet gate had raised the pressure distribution within the cavity during encapsulation process. However, they only focused on the fluid flow analysis. As the extension from their work, the multi-inlet gate was considered in the current study by focusing on the wire sweep phenomenon.

As a result, from the simulation analysis, it was found that the increased in number of inlet gates raised the wire sweep during the encapsulation process. The wire that normal to the flow direction was found has higher deformation. This is because the wire experienced higher drag force when interaction occurs. Besides, the knit lines were form because of the interaction between two separating flows, which may increase the tendency of void formation in the package. More inlet gates yielded shorter filling time, but caused higher wire deformation. Therefore, the design of the IC package is significant to eliminate void and wire sweep during the encapsulation process.

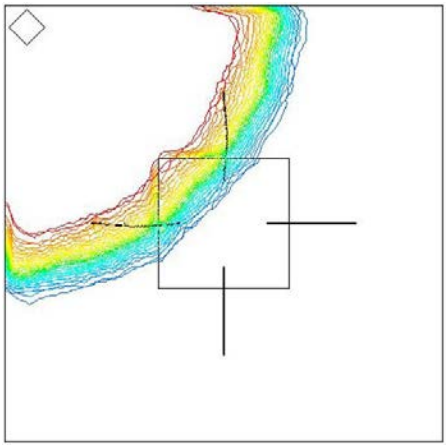

(a) 1 inlet gate.

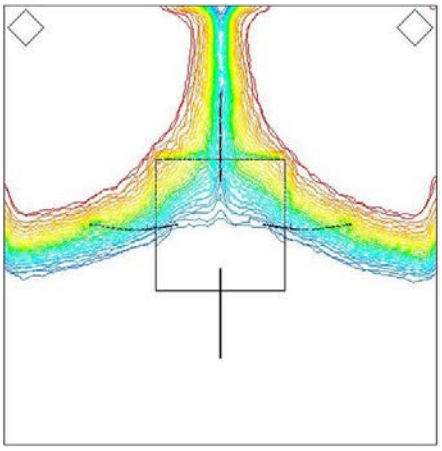

(c) 2 inlet gates.

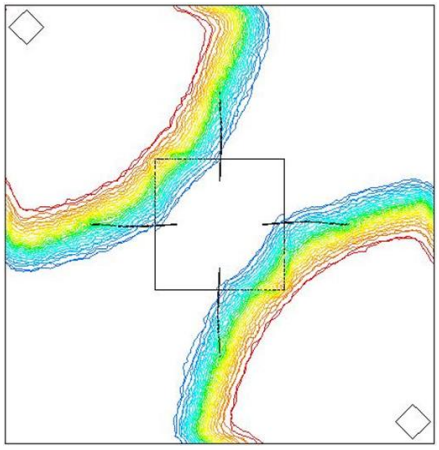

(c) 2 inlet gates diagonal.

Figure 4.34a Melt front and wire sweep profile of scale-up four-wire PBGA: (a) 1 inlet gate, (b) 2 inlet gates and (c) 2 inlet gates diagonal.

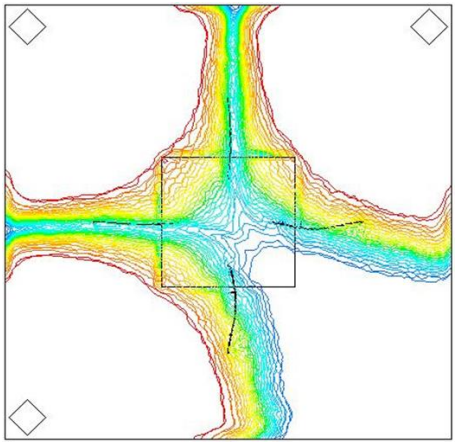

(d) 3 inlet gates.

Figure 4.34b Melt front and wire sweep profile of scale-up four-wire PBGA: (d) 3 inlet gates (continued).

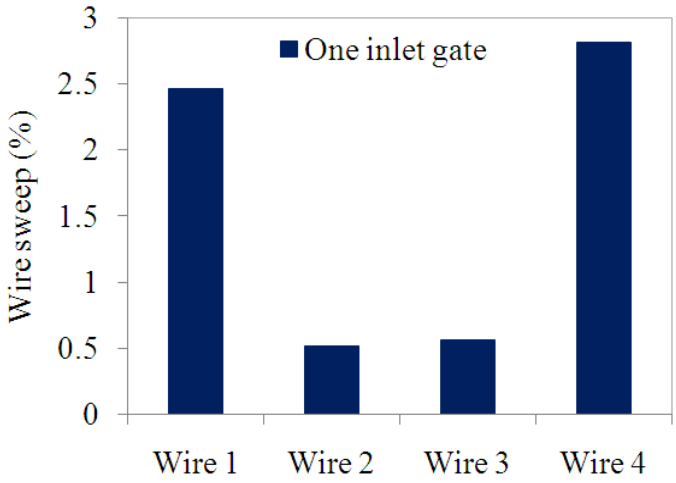


(a) 1 inlet gate.

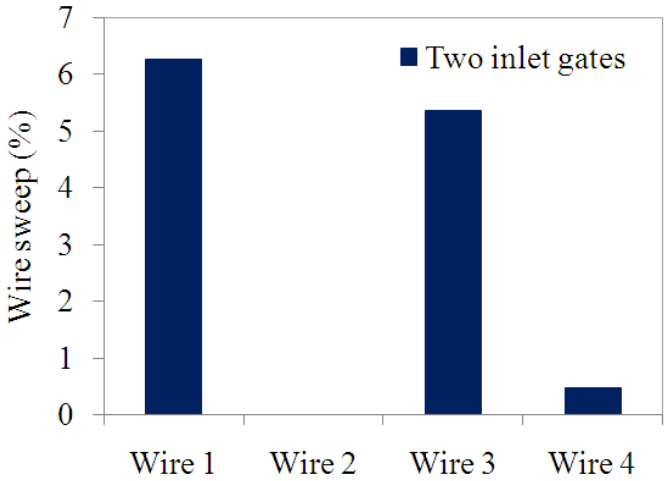


(b) 2 inlet gates.

Figure 4.35a Magnitude of deformation each wire of scale-up four-wire PBGA: (a) 1 inlet gate and (b) 2 inlet gates.

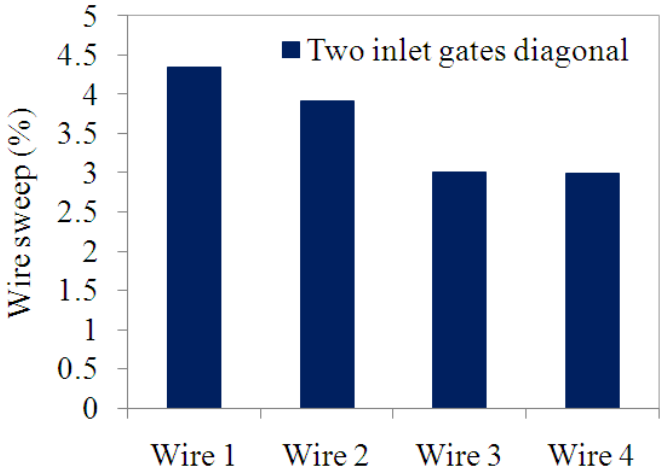


(c) 2 inlet gates diagonal.

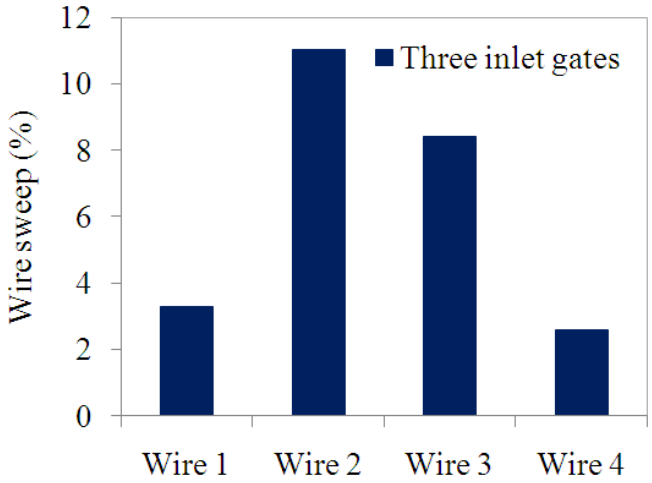


(d) 3 inlet gates

Figure 4.35b Magnitude of deformation each wire of scale-up four-wire PBGA: (c) 2 inlet gates diagonal and (d) 3 inlet gates (continued).

## 4.4 Wire Sweep Considering Stacked Die Effect of Scale-up eight-wire PBGA Encapsulation Process - Centre Inlet

### 4.4.1 Analysis of Inlet Pressure Effect in Packaging of Single and Stacked Die

During the wire deformation, largest wire sweep occurred at the middle of the silicon die (Wu et al. 1998). This was because of wire bonds (at the middle region) that positioned normal to the flow direction of the moulding compound. During the encapsulation process, wire at this region experienced higher lateral flow load, which resulted in large deformation of about 14.5 % of wire sweep during 27s of filling time (Wu et al. 1998). In a typical scaled-up eight-wire PBGA with inlet centre, tension on the excess wire resulted from sweep, because it offered small resistance to the traverse forces imposed by the moulding compound. However, with the lateral looping approach, the excess wire present in the lateral direction provided the required tension

(Brunner et al. 2004). Lower deformation was found on lateral loop of wire shape (3.3 %) when compared to the standard loop (6 %) using moulding compound EME-G760. Kung et al. (2006) had demonstrated that deformation of wire was dominated by the twisting moment instead of the bending moment. The wire loop shape has significant effect on the deformation in IC encapsulation. Yao et al. (2003) found that the normal shape of the wire loop possessed weak bend resistance at the middle region of wires, which resulted in more deformations when compared to M shape.

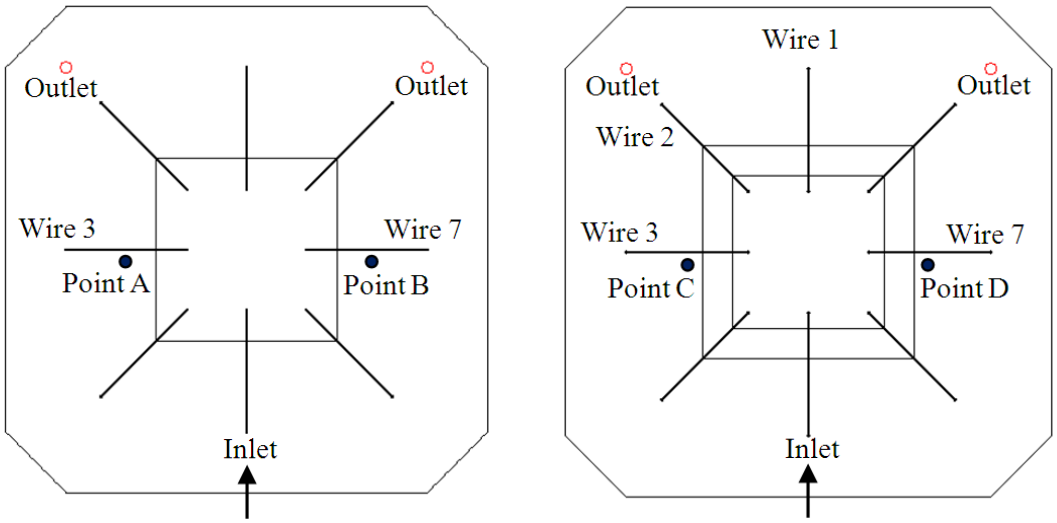


(a) Single die. (b) Stacked die.

Figure 4.36 Points position of pressure measurement on maximum wire deformation of scale-up eight-wire PBGA with centre inlet: (a) Single die and (b) Stacked die.

As mentioned in Section 4.2.2.2, the wires 3 and 7, which positioned at middle region of package, experienced the dominant deformations in the encapsulation process. Therefore, only the pressure around wire 3 and wire 7 are evaluated for the comparison. Figure 4.36 shows the locations of pressure measurement at Point A and Point B for single die package and Point C and Point D for stacked die package during the encapsulation process. Figure 4.37a and 4.37b shows the corresponding bar chart of pressure acting of each point for all cases for single and stacked die packages. The different inlet pressures of single and stacked die packages for all cases of wires 3 and 7 were shown in Figure 4.38a and 4.38b and percentage of filled volume versus filling time at different cases were plotted in Figure 4.39. The increase of inlet pressure is due to the presence of test fluid. As can be seen, pressure at Point A and Pont B (single die package) and Point C and Point D (stacked die package) is high due to the impact of continuous incoming flow.

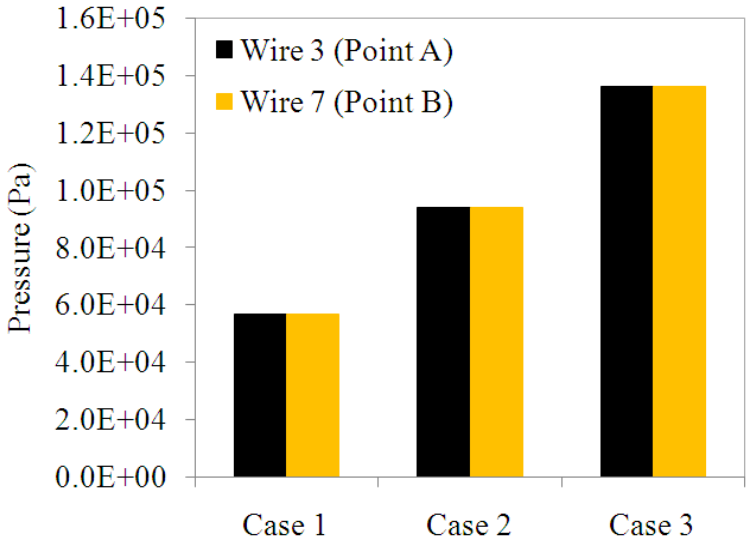


(a) Single die.

Figure 4.37a Pressure acting on wires 3 and 7 for all cases in single and stacked die packages of scale-up eight-wire PBGA with centre inlet: (a) Single die.

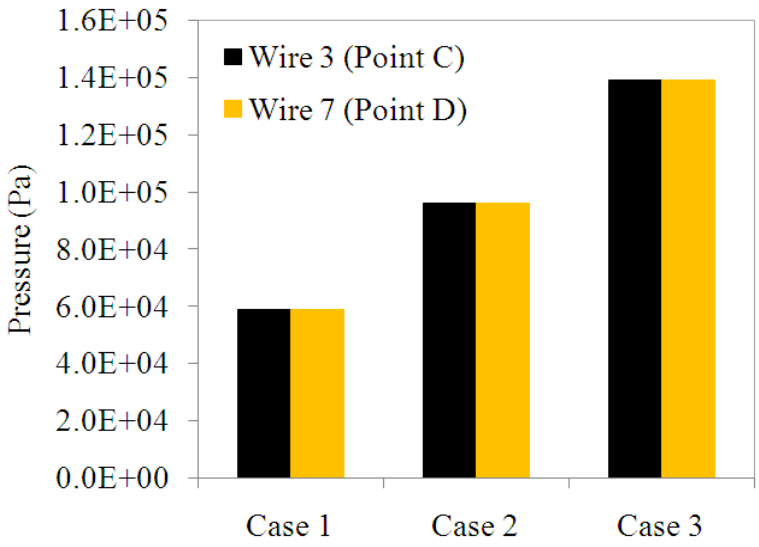


(b) Stacked die.

Figure 4.37b Pressure acting on wires 3 and 7 for all cases in single and stacked die packages of scale-up eight-wire PBGA with centre inlet: (b) Stacked die (continued).

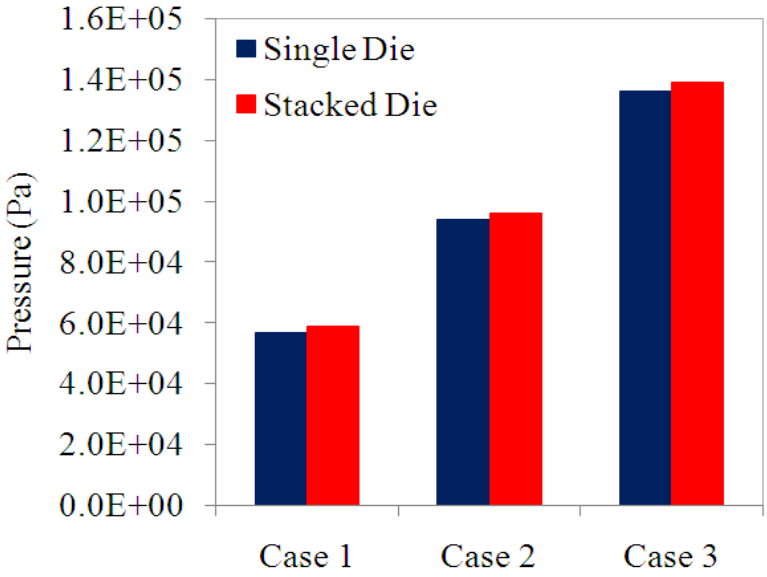


(a) Wire 3.

Figure 4.38a Different pressures at single and stacked die packages for all cases of wires 3 and 7 of scale-up eight-wire PBGA with centre inlet: (a) Wire 3.

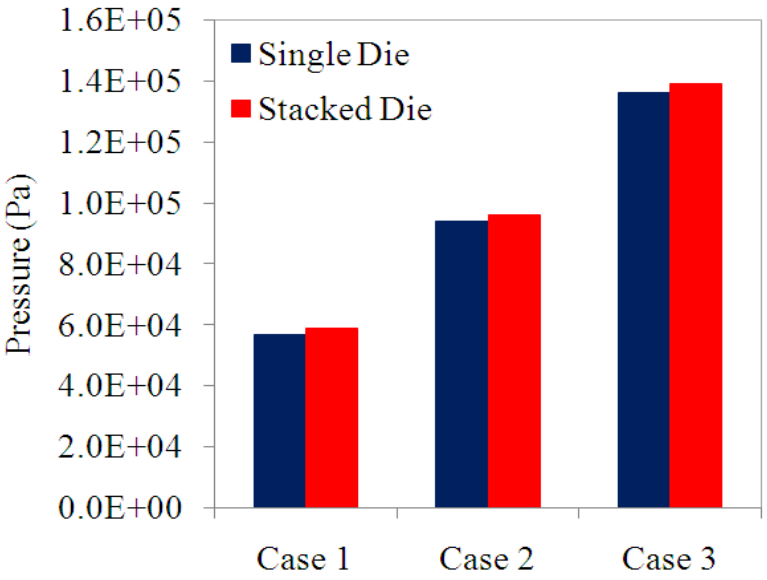


(b) Wire 7.

Figure 4.38b Different pressures at single and stacked die packages for all cases of wires 3 and 7 of scale-up eight-wire PBGA with centre inlet: (b) Wire 7 (continued).

The pressure directly influences the wire displacement and the drag force that acting on the wire structure, during the filling process (Figure 4.40). Thus, the wires which experienced higher pressure are expected to cause higher deformation compared to those at the low pressure. At the same time, it is worth noting that, as the inlet pressure increased, the wire sweep tendency increased, presumably due the increase of pressure force inside the cavity.

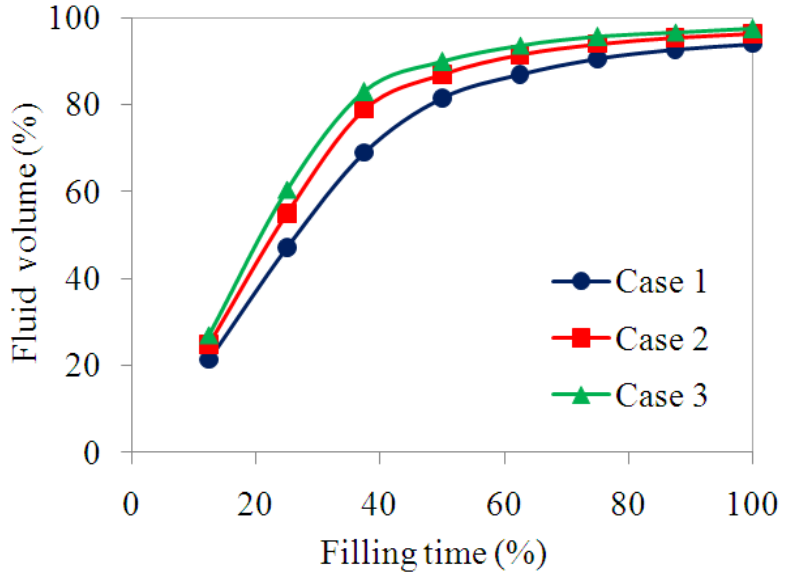


(a) Single die.

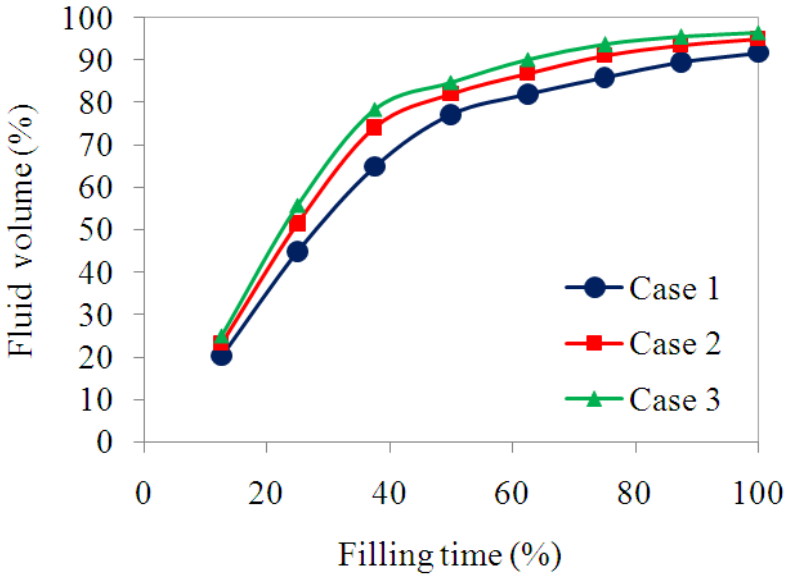


(b) Stacked die.

Figure 4.39 Percentage of filled volume versus filling time for different cases of scale-up eight-wire PBGA with centre inlet: (a) Single die and (b) Stacked die.

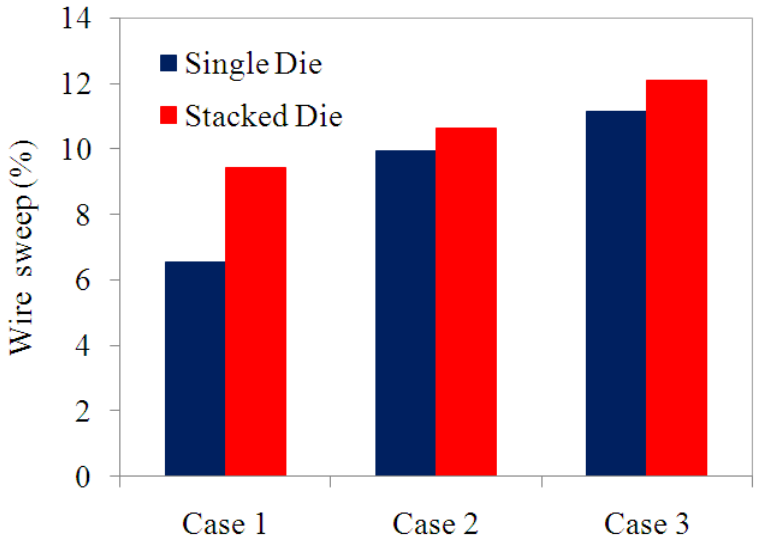


(a) Wire 3.

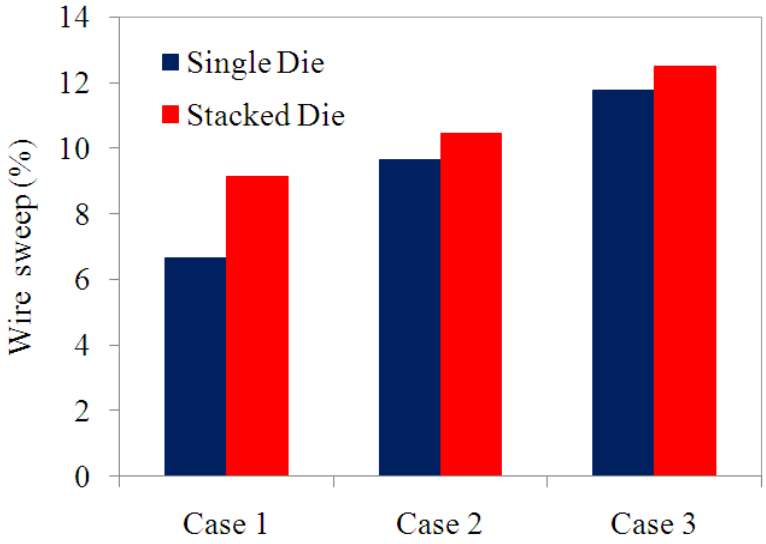


(b) Wire 7.

Figure 4.40 Deformations of wires 3 and 7 of scale-up eight-wire PBGA with centre inlet for all cases: (a) Wire 5 and (b) Wire 7.

### 4.4.2 Stress Analysis (Shear Stress)

The FSI modelling technique is capable to handle the prediction and simulation of complicated geometry in the structural analysis. In the actual experiment and in the industry, the stress of the structures during FSI is difficult to determine and costly, especially for miniaturised IC packaging. Therefore, this technique is essential for the continuous improvement and the investigation of microelectronic reliability.

Figure 4.41a - 4.46 illustrate the phenomenon of wire deformation, which predicted by ABAQUS. Detailed view of maximum stress distribution of all cases of

wire 7, at maximum displacement is shown in Figure 4.41a, 4.41b, 4.42a and 4.42b that demonstrates the highest stress around un-deformed fixed boundary, especially near to the wire bonds for single and stacked die respectively. According to the simulation, stress distribution varied according to the fluid force. At 2.0 s, maximum stress was concentrated at the joint between the die and the bumps (bending region). This means the sweep displacement of wire is dominated by the bending moment instead of the twisting moment (Kung et al., 2006). For clarity, only the two bond regions are shown where the stress was concentrated for the higher deformation of wires (3 and 7).The consolidated data of maximum Von-Mises stress in wire 3 and wire 7 for the three cases is given in Figure 4.43a and 4.43b. It is clearly shown that wires 3 and 7 were subjected to maximum stress, owing to the influence of higher pressure force. It is noting that the stress increased significantly with the increased in the inlet pressure.

Figure 4.44a, 4.44b, 4.45a and 4.45b shows the shear stress of the structures during the filling process for single and stacked die respectively. The fluid flow into the cavity subjected force upon the structure and induced stress in x and z direction as shown in Figure 3.22 of Chapter 3. The maximum shear stress distribution was concentrated at the twisting region. The consolidated data of maximum shear stress in wire 3 and wire 7 for the three cases is given in Figure 4.46. Comparison of von Mises and Shear stress of Wire 3 and Wire 7 of scale-up eight-wire PBGA with centre inlet is shown in Appendix G.

In the actual IC packaging, improper process control may lead the unintended occurrences on the wire such as overstress and serious deformation. These may cause failures or short circuit in the packaging. High shear stress can cause the reduction of reliability; the wire may degrade or fail, due to the overstress. Therefore, the FSI phenomenon during encapsulation for the actual-size of PBGA, and 3D packaging and integration should be considered in the process.

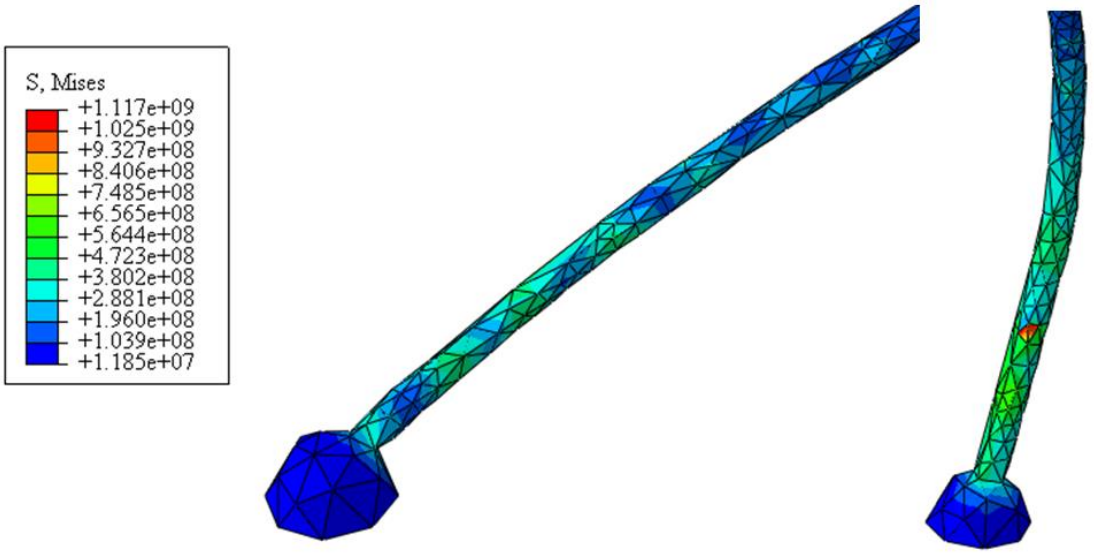


(a) Case 1.

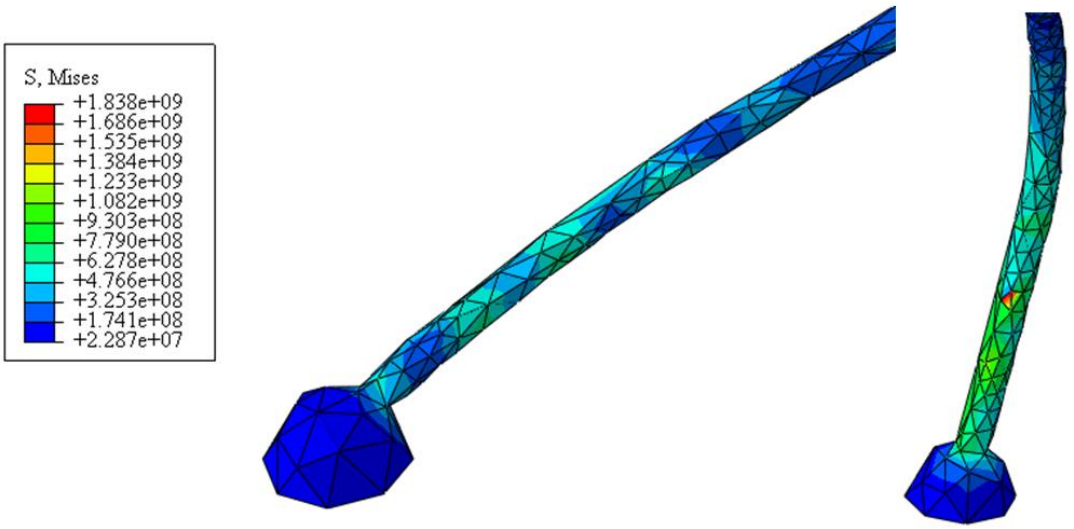


(b) Case 2.

Figure 4.41a Detailed view of maximum von Mises stress distribution for all cases of single die of scale-up eight-wire PBGA with centre inlet for wire 7: (a) Case 1 and (b) Case 2.

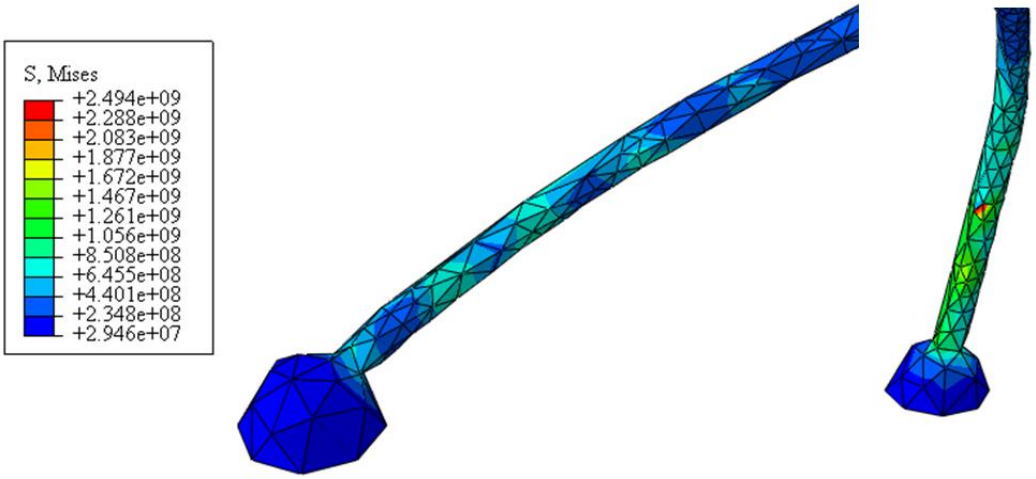


(c) Case 3.

Figure 4.41b Detailed view of maximum von Mises stress distribution for all cases of single die of scale-up eight-wire PBGA with centre inlet for wire 7: (c) Case 3 (continued).

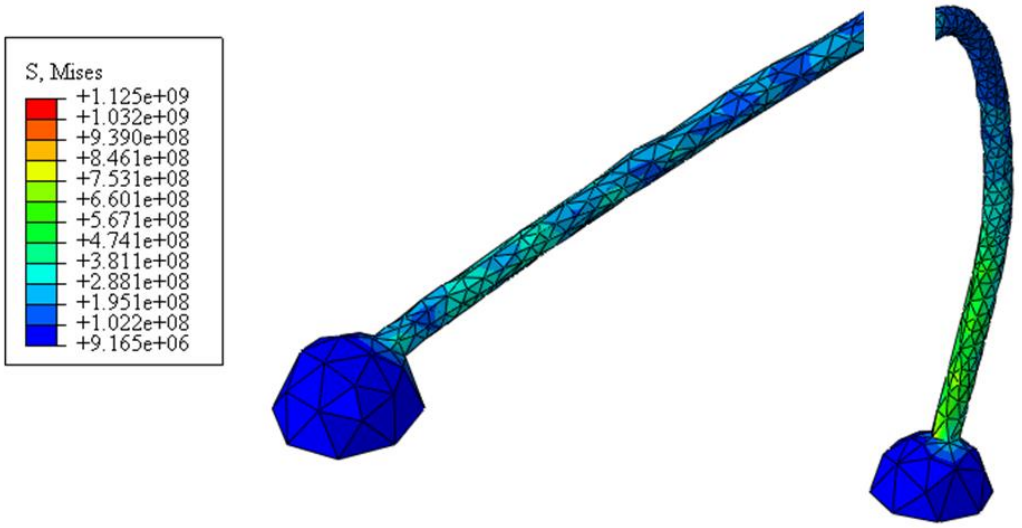


(a) Case 1.

Figure 4.42a Detailed view of maximum von Mises stress distribution for all cases of stacked die of scale-up eight-wire PBGA with centre inlet for wire 7: (a) Case 1.

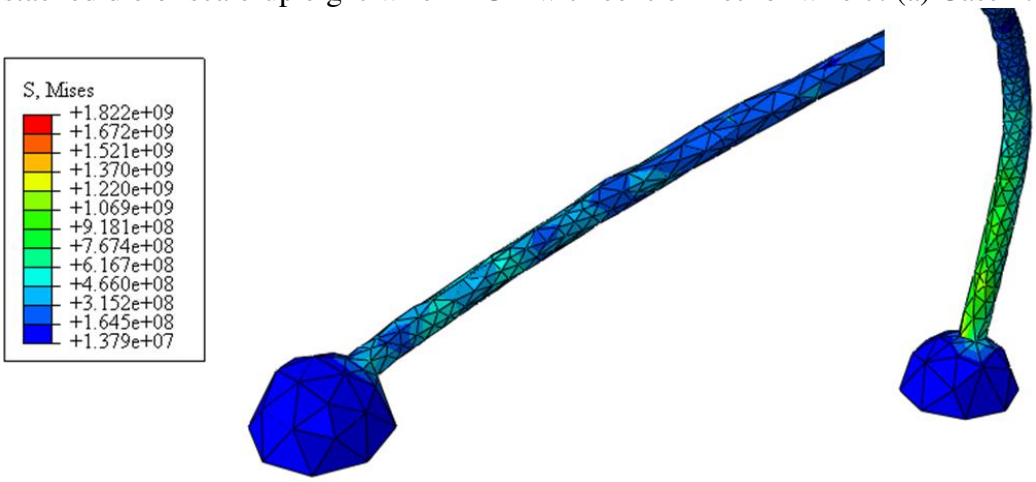


(b) Case 2.

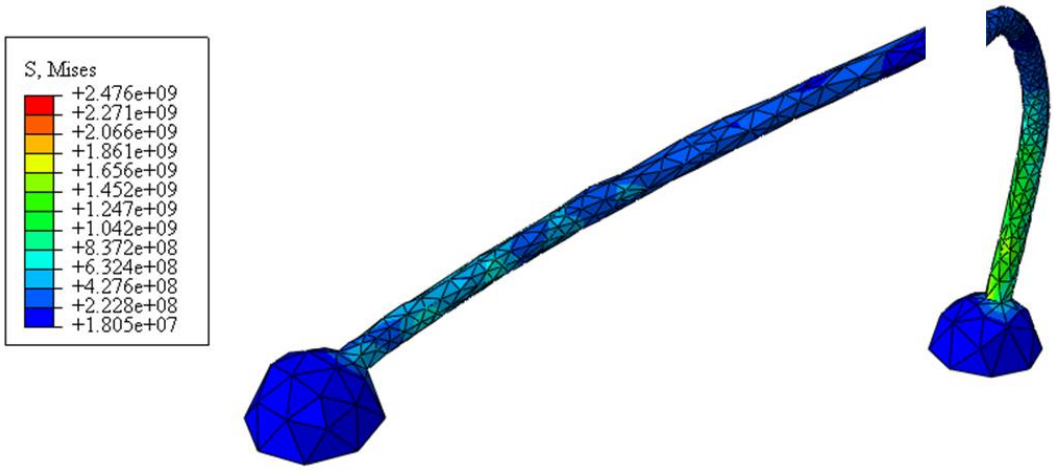


(c) Case 3.

Figure 4.42b Detailed view of maximum von Mises stress distribution for all cases of stacked die of scale-up eight-wire PBGA with centre inlet for wire 7: (b) Case 2 and (c) Case 3 (continued).

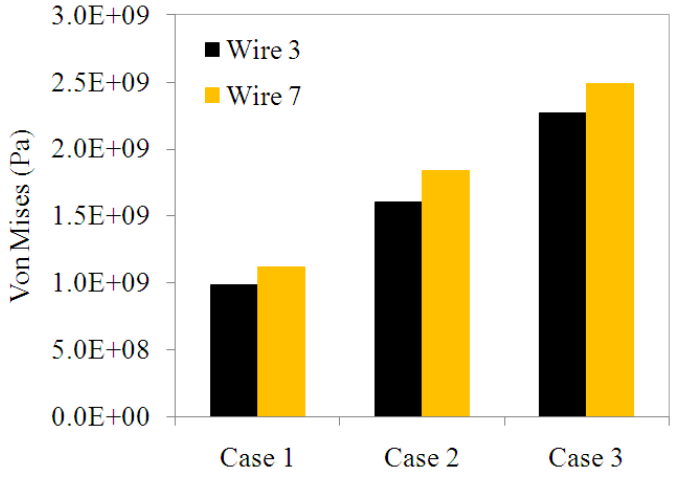


(a) Single die.

Figure 4.43a Maximum von Mises for all cases of scale-up eight-wire PBGA with centre inlet: (a) Single die.

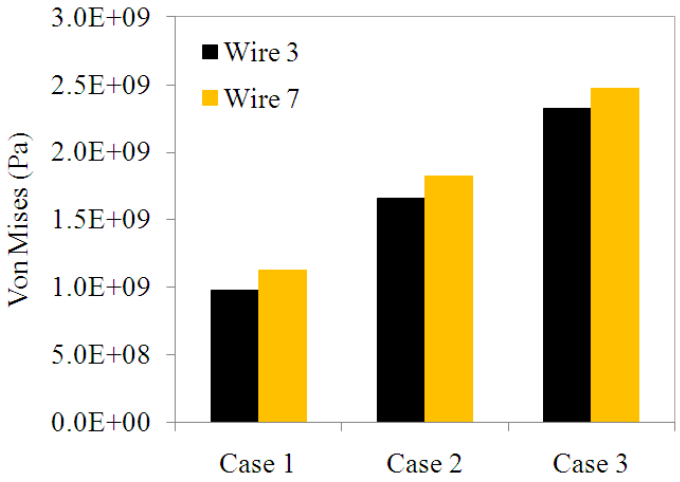


(b) Stacked Die.

Figure 4.43b Maximum von Mises for all cases of scale-up eight-wire PBGA with centre inlet: (b) Stacked die (continued).

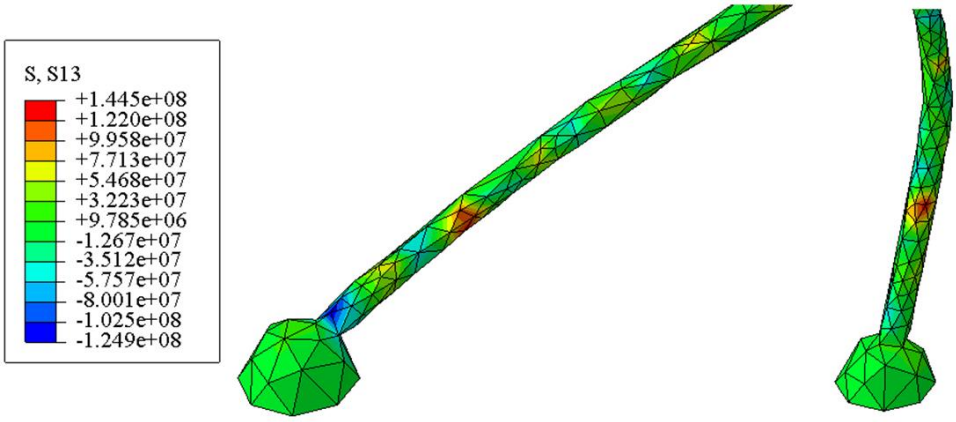


(a) Case 1.

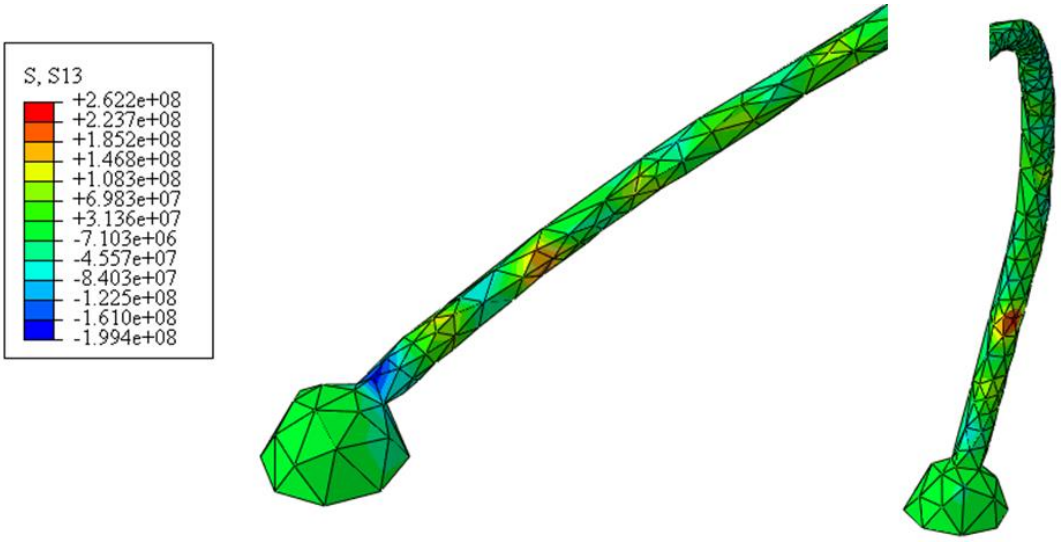


(b) Case 2.

Figure 4.44a Detailed view of maximum shear stress distributions for all cases of single die of scale-up eight-wire PBGA with centre inlet for wire 7: (a) Case 1 and (b) Case 2.

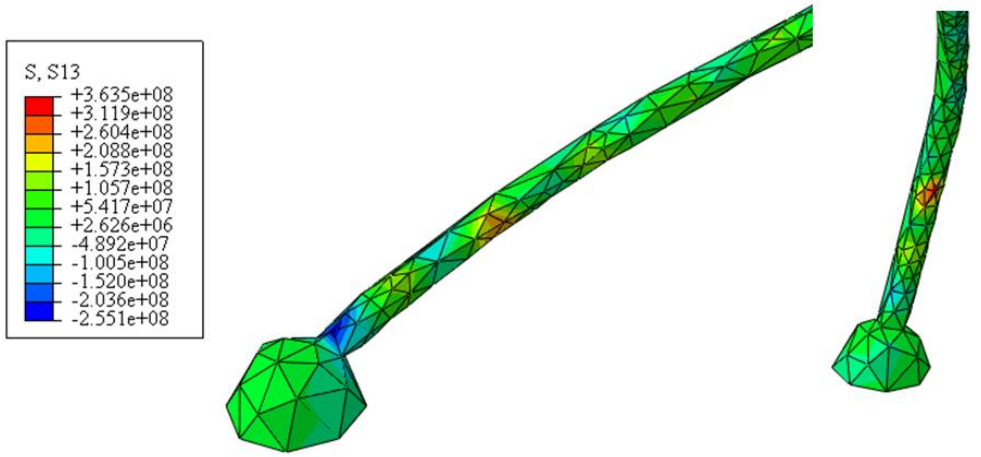


(c) Case 3.

Figure 4.44b Detailed view of maximum shear stress distributions for all cases of single die of scale-up eight-wire PBGA with centre inlet for wire 7: (c) Case 3 (continued).

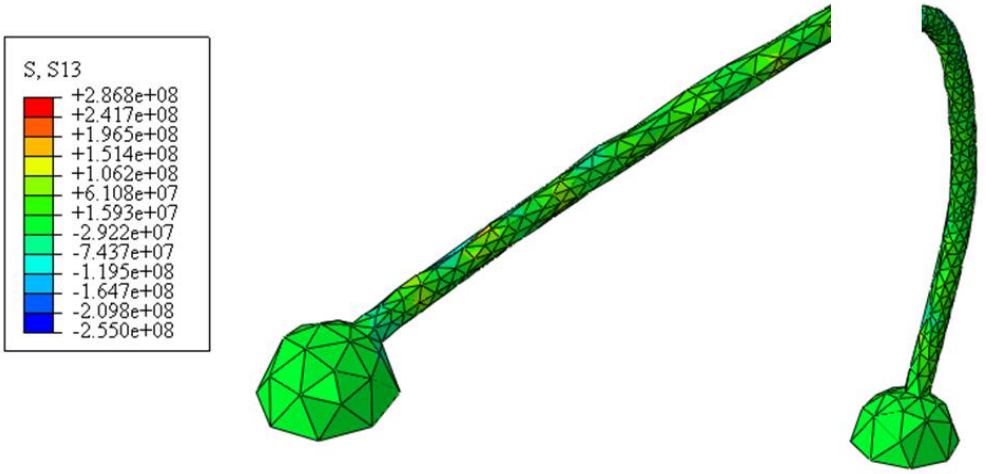


(a) Case 1.

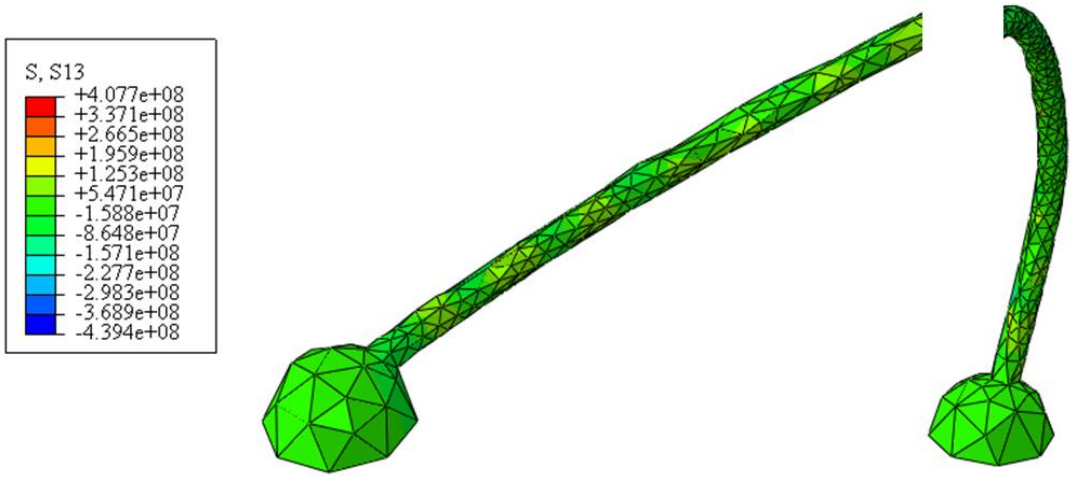


(b) Case 2.

Figure 4.45a Detailed view of maximum shear stress distributions for all cases of stacked die of scale-up eight-wire PBGA with centre inlet for wire 7: (a) Case 1 and (b) Case 2.

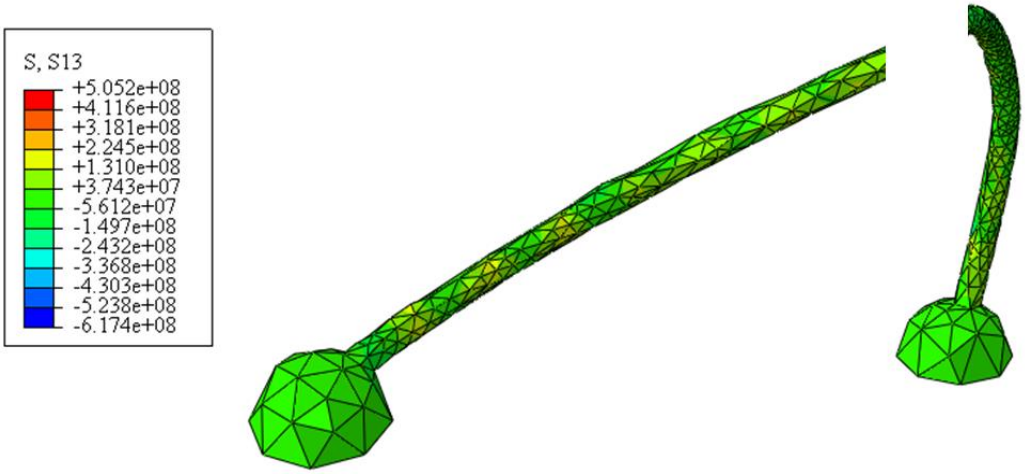


(c) Case 3.

Figure 4.45b Detailed view of maximum shear stress distributions for all cases of stacked die of scale-up eight-wire PBGA with centre inlet for wire 7: (c) Case 3 (continued).

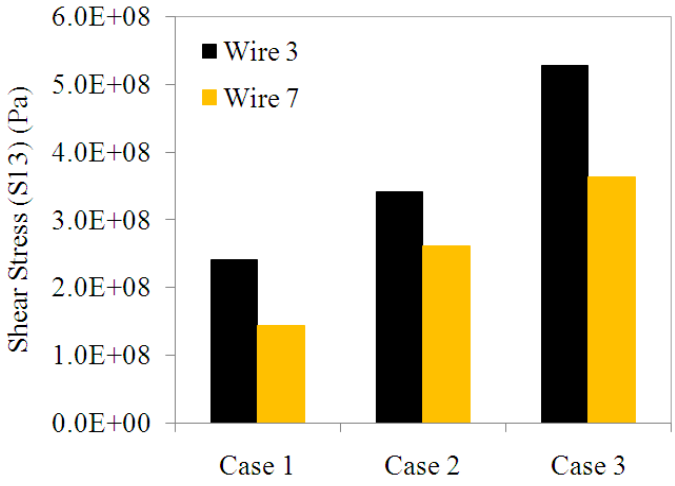


(a) Single die.

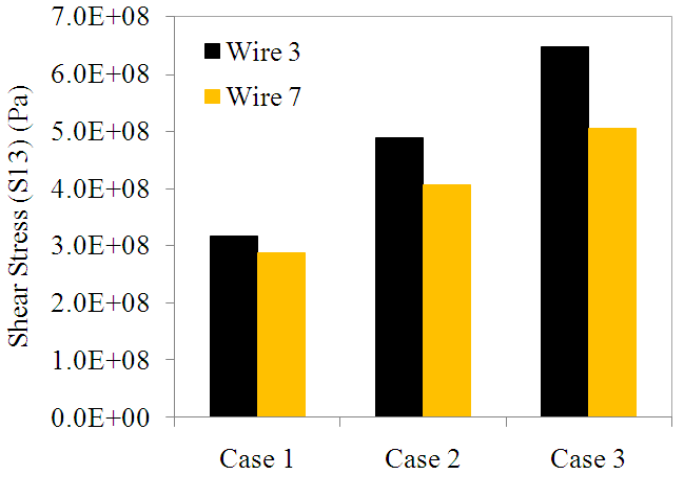


(b) Stacked Die.

Figure 4.46 Maximum shear stress for all cases of scale-up eight-wire PBGA with centre inlet: (a) Single die and (b) Stacked die.

## 4.5 Wire Sweep Considering Stacked Die Effect of Scale-up eight-wire PBGA Encapsulation Process – Corner Inlet

### 4.5.1 Analysis of Pressure Effect in Packaging of Single and Stacked Die

During the wire deformation, largest wire sweep occurred at the middle of the silicon die (Wu et al., 1998). This was due to the fact that wire bonds (at the middle region) were positioned normal to the flow direction of the moulding compound. During the encapsulation process, wire at this region experienced higher lateral flow load, which resulted in large deformation of about 14.5 % of wire sweep during 27 s of filling time (Wu et al., 1998). In a typical PBGA, tension on the excess wire resulted from sweep, because it offered small resistance to the traverse forces imposed by the moulding compound. However, with the lateral looping approach, the excess wire present in the lateral direction provided the required tension (Brunner et al., 2004). Lower deformation was found on lateral loop of wire shape (3.3 %) when compared to the standard loop (6 %) using moulding compound EME-G760. Kung et al., (2006a) had demonstrated the deformation of wire was dominated by the twisting moment instead of the bending moment. The wire loop shape has significant effect on the deformation in IC encapsulation. Yao et al., (2003) found that the normal shape of the wire loop possessed weak bend resistance at the middle region of wires, which resulted in more deformations when compared to M shape.

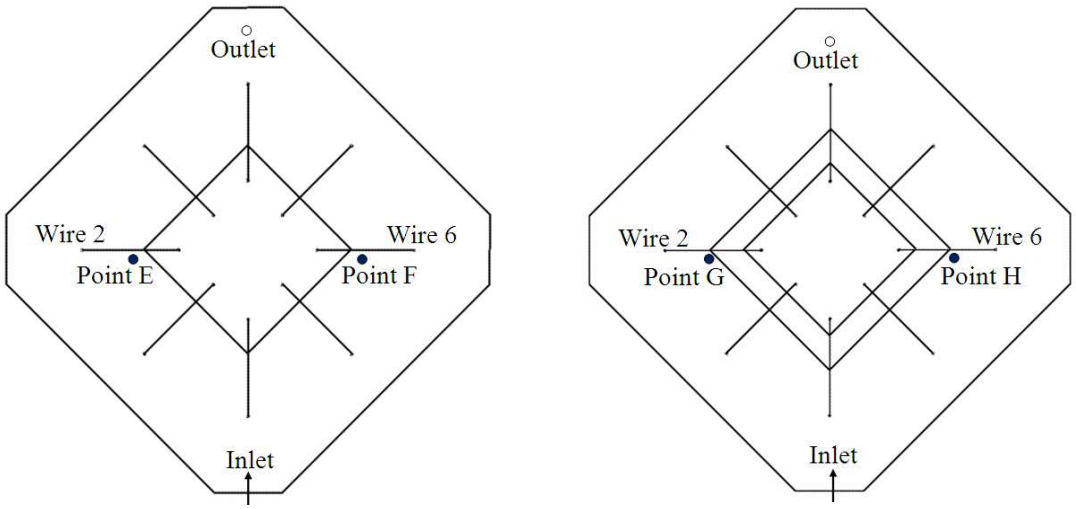


(a) Single die. (b) Stacked die.

Figure 4.47 Points position of pressure measurement on maximum wire deformation of PBGA with corner inlet: (a) Single die and (b) Stacked die.

As mentioned in Section 4.2.4.2 in above, the wires 2 and 6, which positioned at middle region of package experienced the dominant deformations in the encapsulation process. Therefore, only the pressure around wire 2 and wire 6 are evaluated for the comparison. Figure 4.47 shows the locations of pressure measurement at Point E and Point F for single die package and Point G and Point H for stacked die package during the encapsulation process. Figure 4.48 shows the corresponding bar chart of pressure acting of each point for all cases for single and stacked die packages. The different inlet pressures of single and stacked die packages for all cases of wires 2 and 6 were shown in Figure 4.49 and percentage of filled volume versus filling time at different cases were plotted in Figure 4.50. The increase of inlet pressure is due to the presence of test fluid. As can be seen, pressure at Point E and Pont F (single die package) and Point G and Point H (stacked die package) is high due to the impact of continuous incoming flow. The pressure directly influences the wire displacement and the drag force that acting on the wire structure, during the filling process (Figure 4.51). Thus, the wires which experienced higher pressure are expected to cause higher deformation compared to those at the low pressure. At the same time, it is worth noting that, as the inlet pressure increased, the wire sweep tendency increased, presumably due the increase of pressure force inside the cavity.

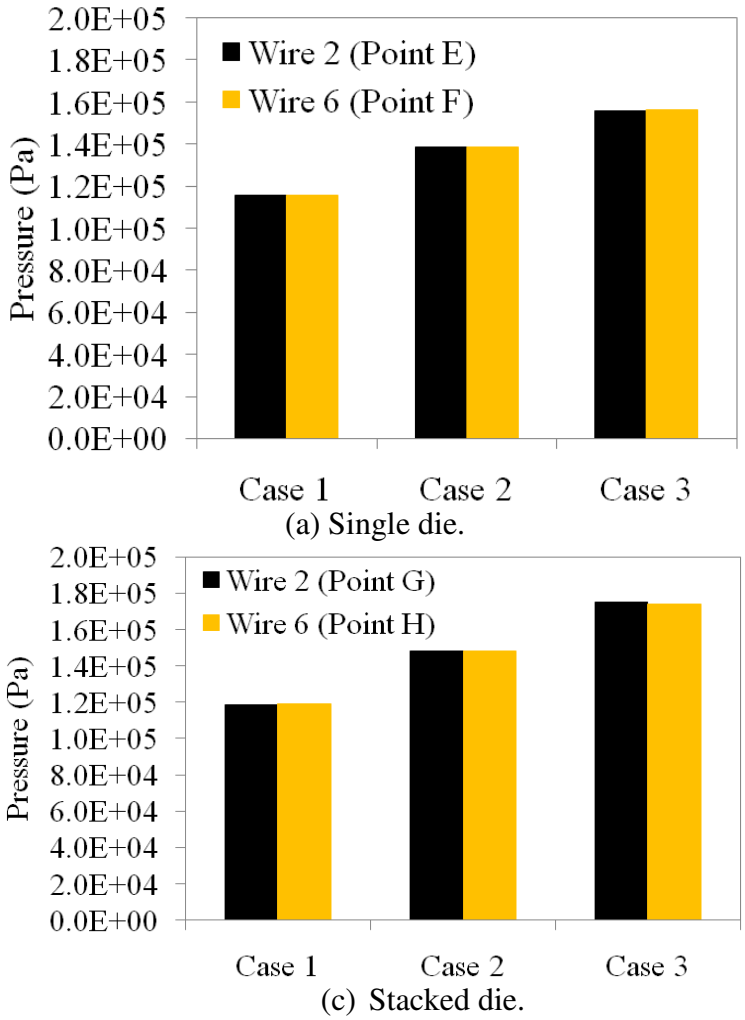


Figure 4.48 Pressure acting on wires 2 and 6 for all cases in single and stacked die packages of scale-up eight-wire PBGA with corner inlet: (a) Single die and (b) Stacked die.

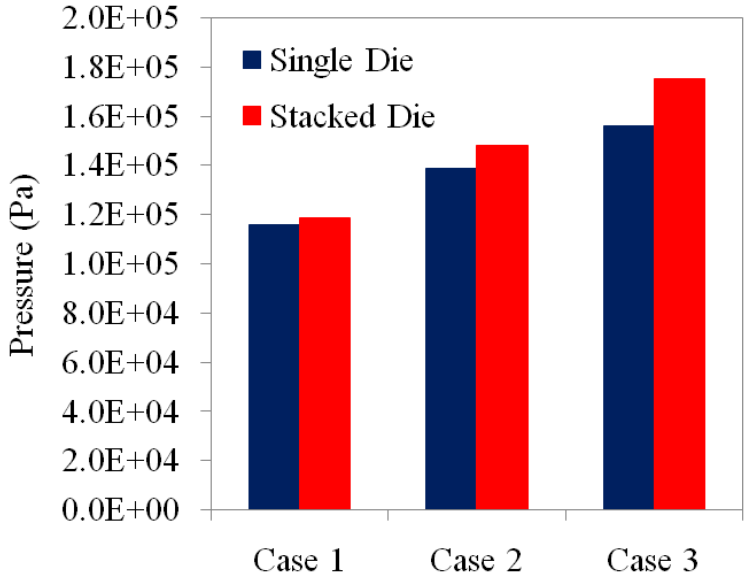


(a) Wire 2.

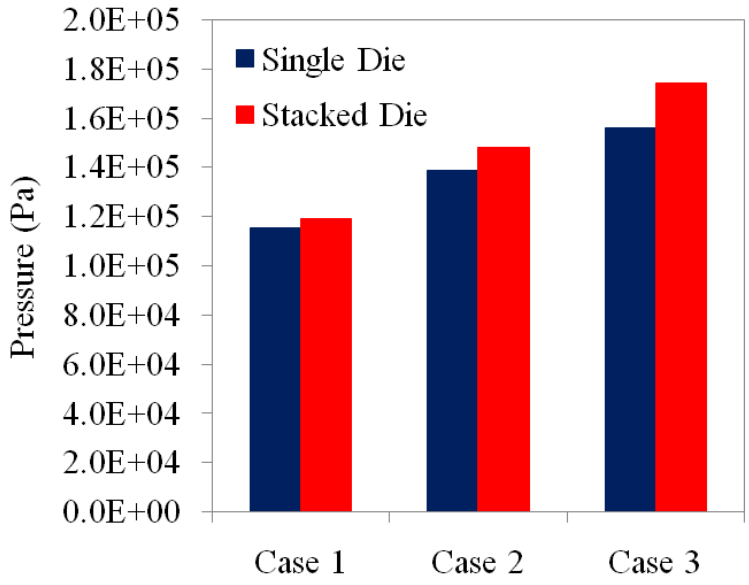


(b) Wire 6.

Figure 4.49 Different pressures at single and stacked die packages for all cases of wires 2 and 6 of scale-up eight-wire PBGA with corner inlet: (a) Wire 2 and (b) Wire 6.

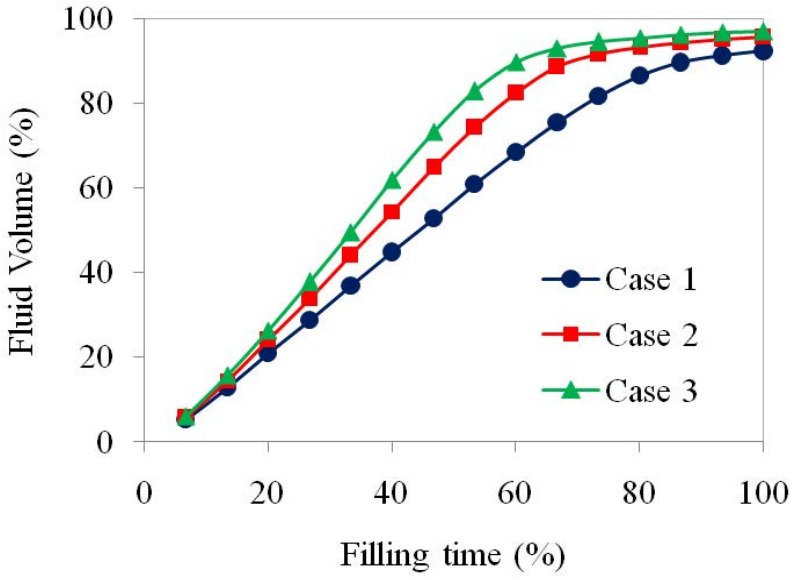


(a) Single die.

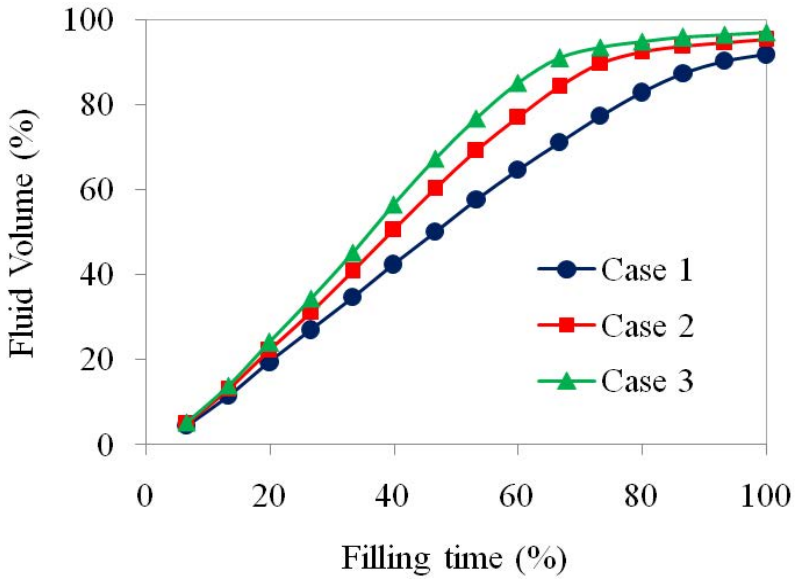


(b) Stacked die.

Figure 4.50 Percentage of filled volume versus filling time for different cases of scale-up eight-wire PBGA with corner inlet: (a) Single die and (b) Stacked die.

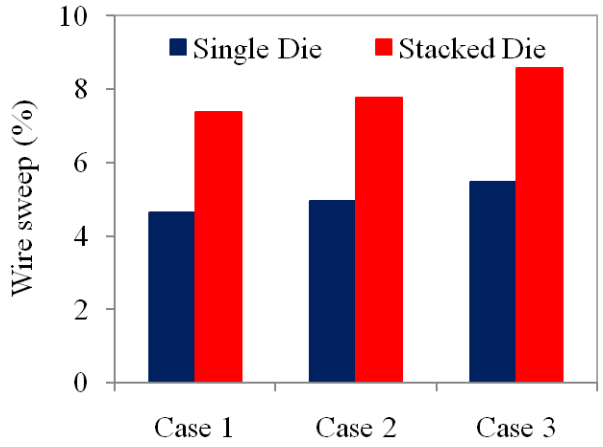


(a) Wire 2.

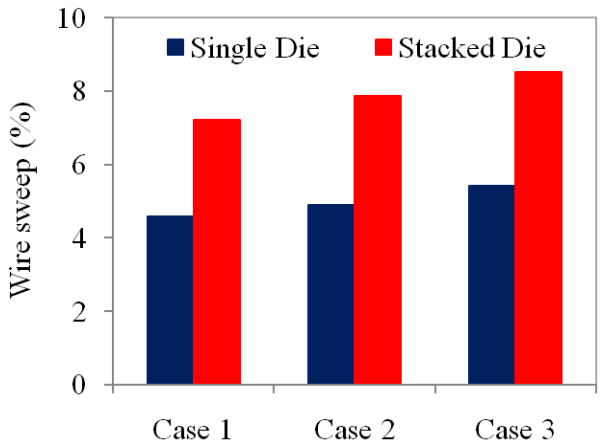


(b) Wire 6.

Figure 4.51 Deformations of wires 2 and 6 of scale-up eight-wire PBGA with corner inlet for all case: (a) Wire 2 and (b) Wire 6.

### 4.5.2 Stress Analysis (Shear Stress)

The FSI modelling technique is capable to handle the prediction and simulation of complicated geometry in the structural analysis. In the actual experiment and in the industry, the stress of the structures during FSI is difficult to determine and costly, especially for miniaturised IC packaging. Therefore, this technique is essential for the continuous improvement and the investigation of microelectronic reliability.

Figure 4.52a - 4.57 illustrate the phenomenon of wire deformation, which predicted by ABAQUS. Detailed view of stress distribution of wires 2 and 6, at maximum displacement is shown in Figure 4.52a, 4.52b, 4.53a and 4.53b that demonstrates the highest stress around un-deformed fixed boundary, especially near to the wire bonds for single and stacked die respectively. According to the simulation, stress distribution varied according to the fluid force. At 2.0 s, maximum stress was concentrated at the joint between the die and the bumps (bending region). This means the sweep displacement of wire is dominated by the bending moment instead of the twisting moment (Kung, 2006a). For clarity, only the two bond regions are shown where the stress was concentrated for the higher deformation of wires (2 and 6). The consolidated data of maximum Von-Mises stress in wire 2 and wire 6 for the three cases is given in Figure 4.54. It is clearly shown that wires 2 and 6were subjected to maximum stress, owing to the influence of higher pressure force. It is noting that the stress increased significantly with the increased in the inlet pressure.

Figure 4.55 and Figure 4.56 shows the shear stress of the structures during the filling process for single and stacked die. The fluid flow into the cavity subjected force upon the structure and induced stress in x and z direction such as shown in Figure 3.22 of Chapter 3. The maximum of shear stress distribution was concentrated at the twisting region. The consolidated data of maximum shear stress in wire 2 and wire 6 for the three cases is given in Figure 4.57. Comparison of von Mises and Shear stress of Wire 2 and Wire 6 of scale-up eight-wire PBGA with corner inlet is shown in Appendix H.

In the actual IC packaging, improper process control could lead the unintended occurrences on the wire such as overstress, serious deformation, and its may causing failure or short circuit in the packaging. High shear stress can cause the reduction of reliability; the wire may degrade or fail, due to the overstress. Therefore, the FSI phenomenon during encapsulation for actual-size of PBGA, and 3D packaging and integration should be considered in the process.

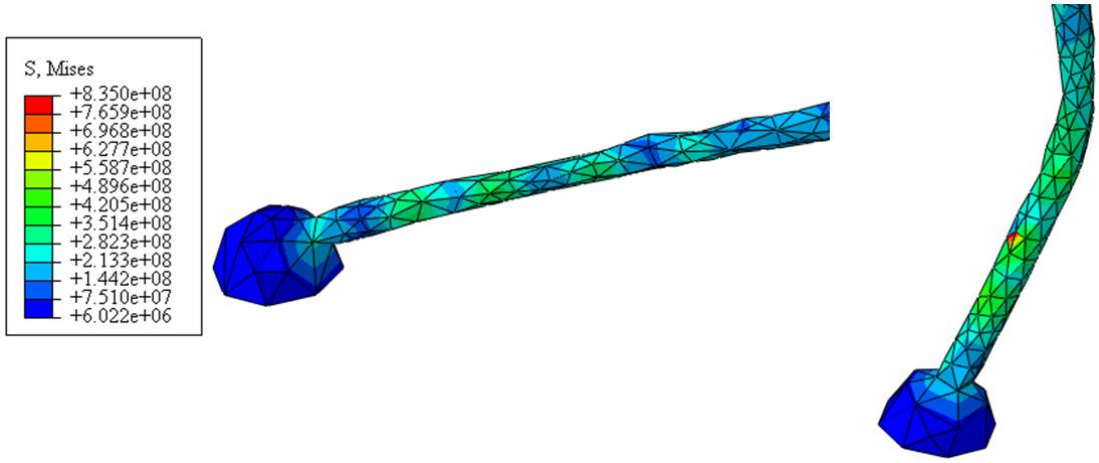


(a) Case 1.

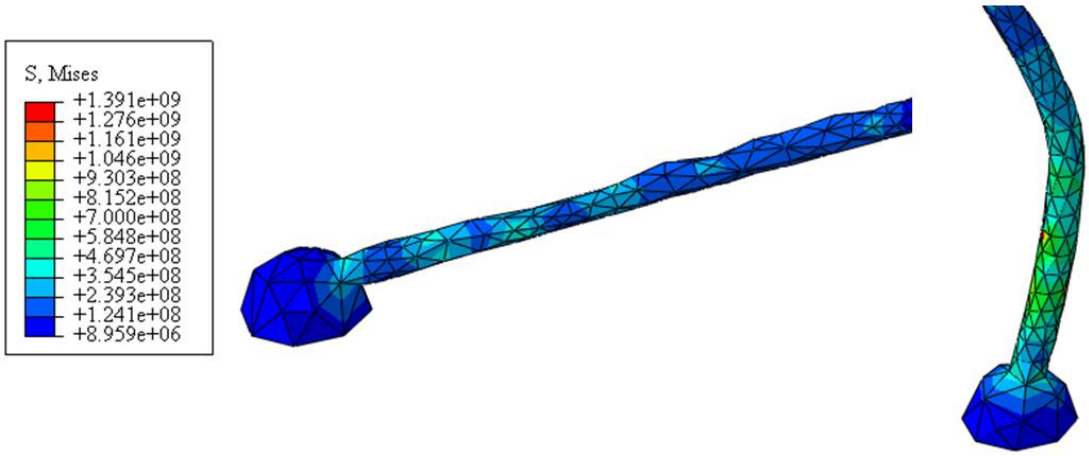


(b) Case 2.

Figure 4.52a Detailed view of maximum von Mises stress distribution for single die of scale-up eight-wire PBGA with corner inlet for all cases for wire 6: (a) Case 1 and (b) Case 2.

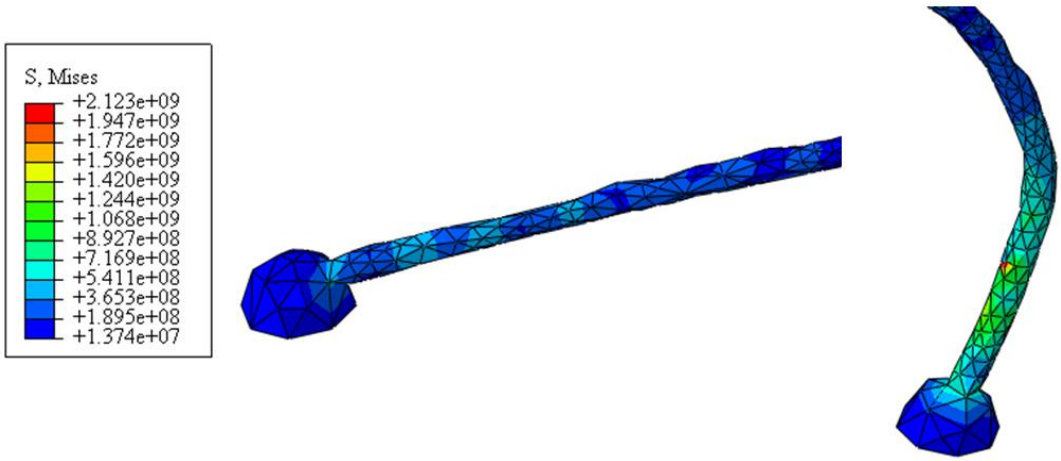


(c) Case 3.

Figure 4.52b Detailed view of maximum von Mises stress distribution for single die of scale-up eight-wire PBGA with corner inlet for all cases for wire 6: (c) Case 3 (continued).

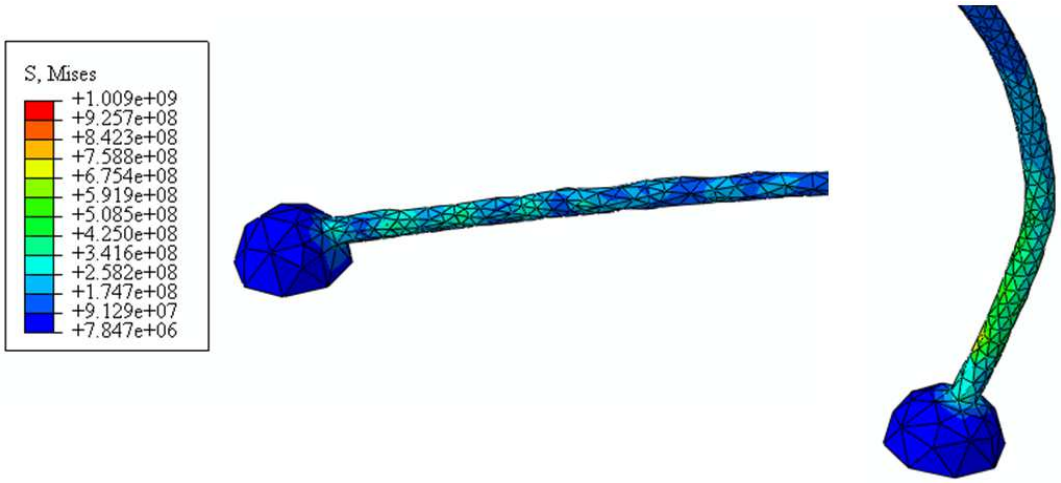


(a) Case 1.

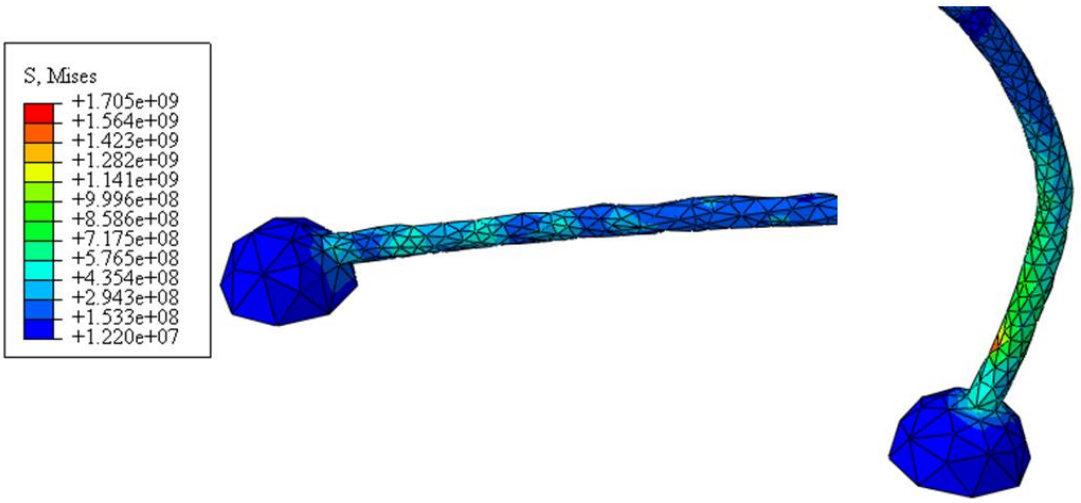


(b) Case 2.

Figure 4.53a Detailed view of maximum von Mises stress distribution for stacked die of scale-up eight-wire PBGA with corner inlet for all cases for wire 6: (a) Case 1 and (b) Case 2.

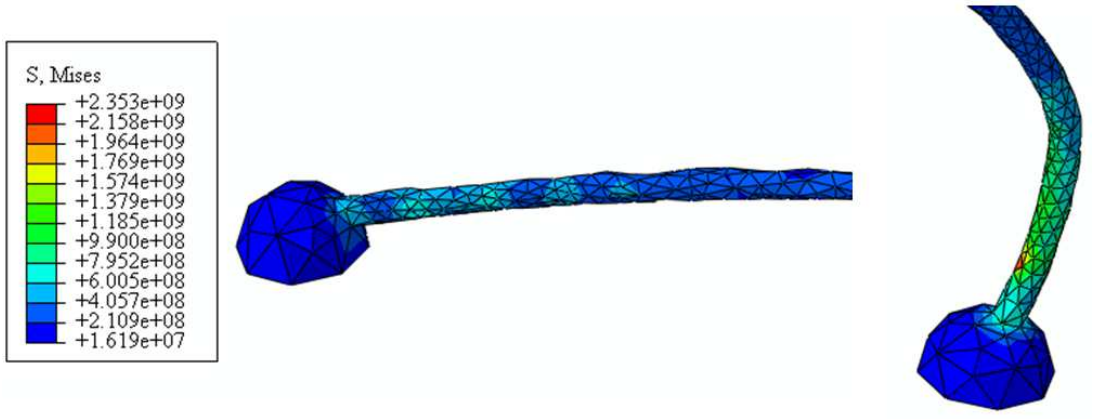


(c) Case 3.

Figure 4.53b Detailed view of maximum von Mises stress distribution for stacked die of scale-up eight-wire PBGA with corner inlet for all cases for wire 6: (c) Case 3 (continued).

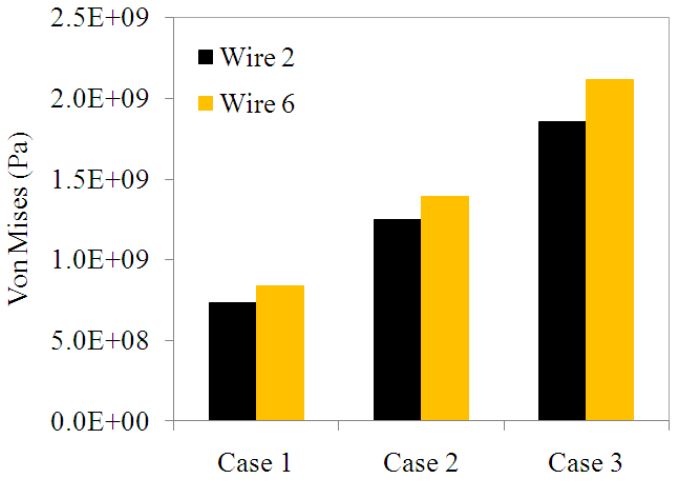


(a) Single die.

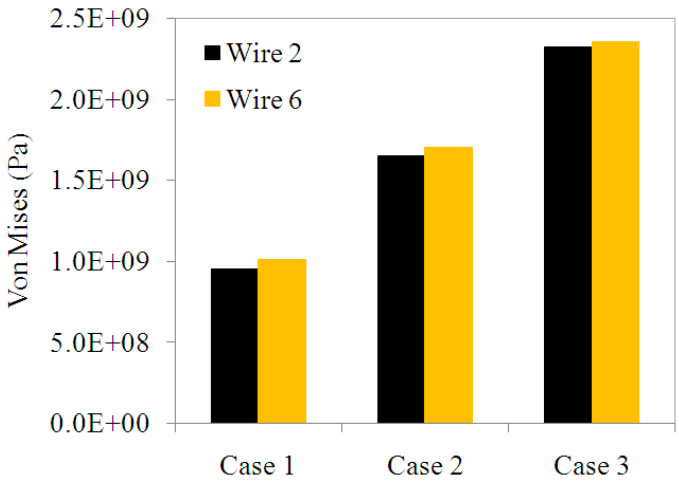


(b) Stacked Die.

Figure 4.54 Maximum von Mises for all cases of scale-up eight-wire PBGA with corner inlet: (a) Single die and (b) Stacked die.

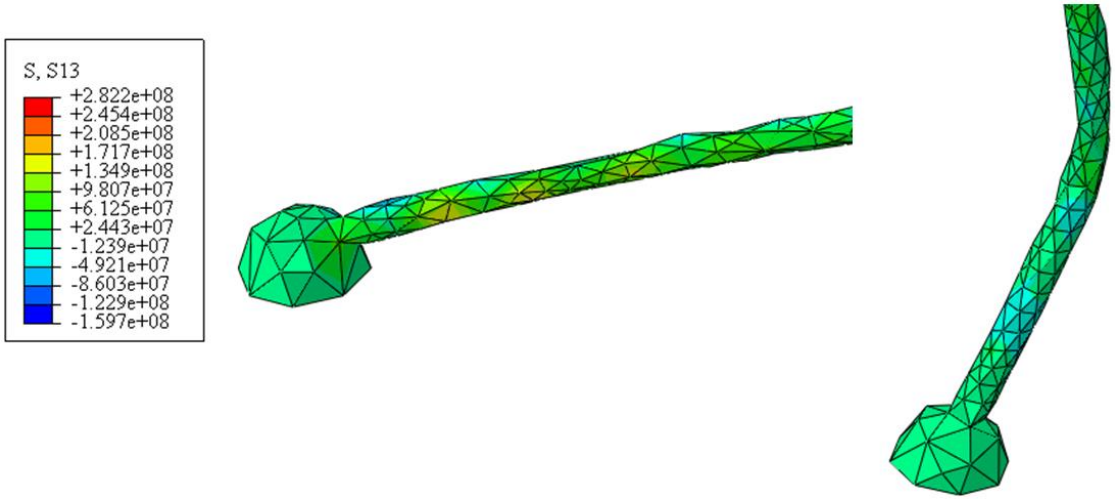


(a) Case 1.

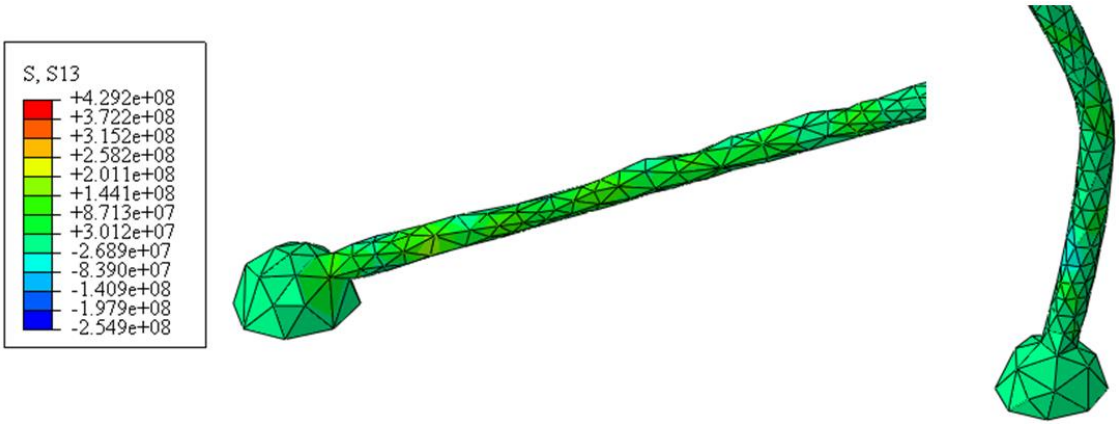


(b) Case 2.

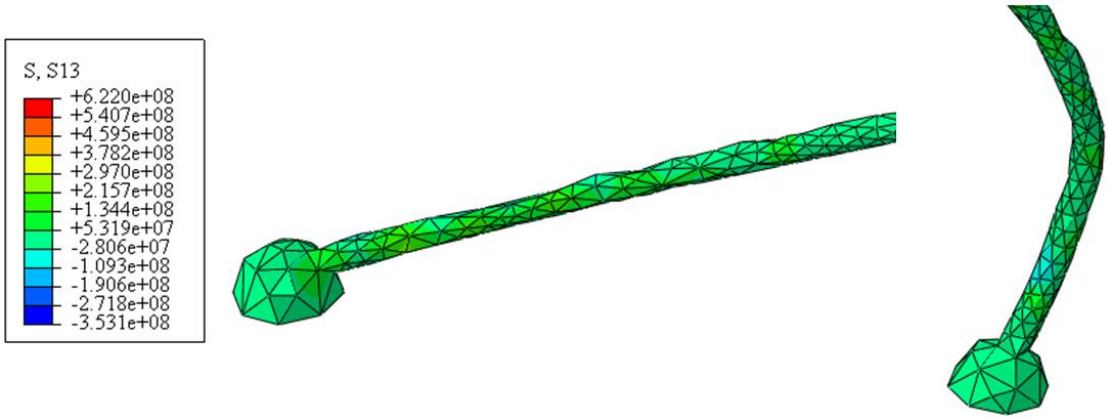


(c) Case 3.

Figure 4.55 Detailed views of maximum shear stress distributions for single die of scale-up eight-wire PBGA with corner inlet for all cases for wire 6: (a) Case 1, (b) Case 2 and (c) Case 3.

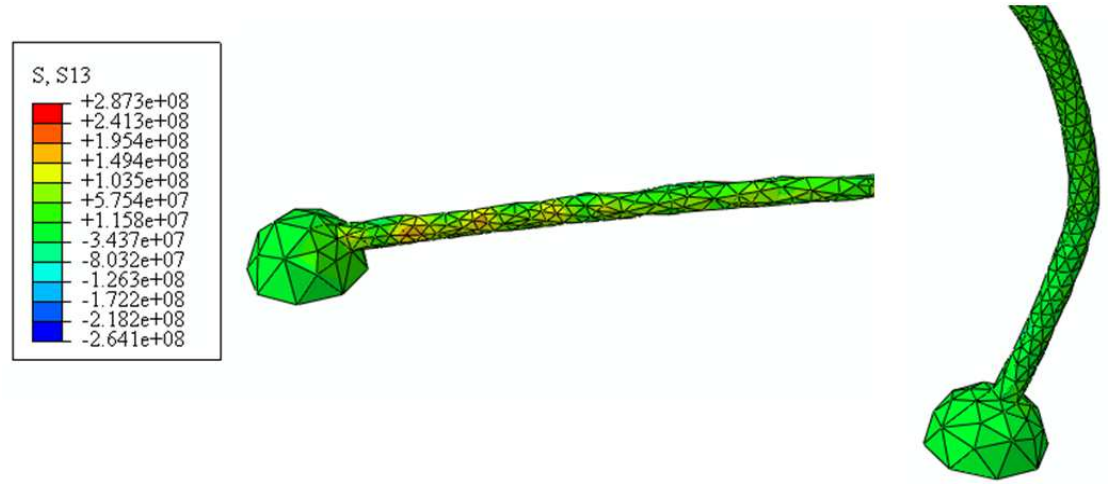


(a) Case 1.


(b) Case 2.

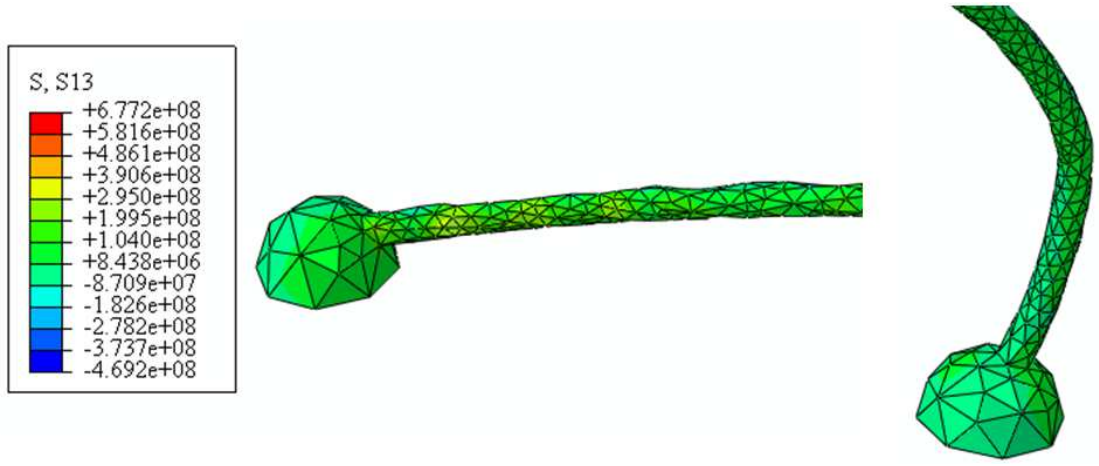


(c) Case 3.

Figure 4.56 Detailed views of maximum shear stress distributions for stacked die of scale-up eight-wire PBGA with corner inlet for all cases for wire 6: (a) Case 1, (b) Case 2 and (c) Case 3.

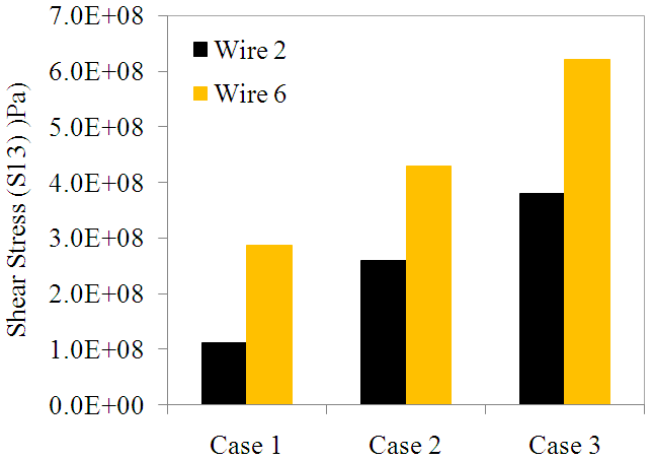


(a) Single die.

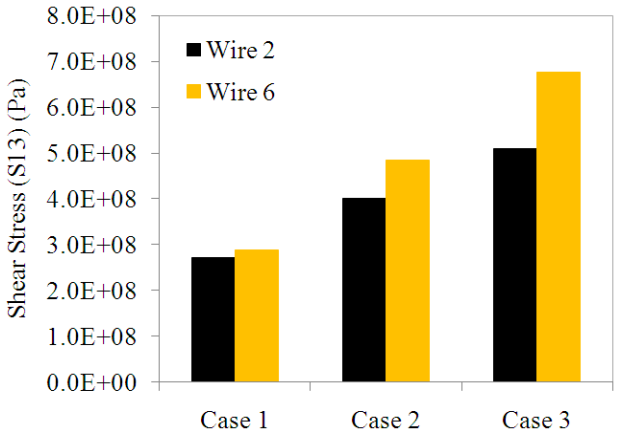


(b) Stacked Die.

Figure 4.57 Maximum shear stress for all cases of scale-up eight-wire PBGA with corner inlet: (a) Single die and (b) Stacked die.

## 4.6 Effects of Die Heights and Inlet Arrangement on Wire Sweep Behaviour

### 4.6.1 Effects of Die Heights on Wire Sweep behaviour

To investigate the die height effect on wire sweep behaviour, two die heights, i.e. 1.1 mm and 2.2 mm were used to analyze the wire sweep values, which were compared with that from the FSI simulation and the experiment. Besides, to make the wire sweep of different die height comparable, the wire loop heights were considered as a constant (1.5 mm) for these designs. Figure 3.15 indicates the two die height designs. Wire sweep results from a scale-up eight-wire PBGA with centre and corner inlet gate for Case 3 are illustrated in Figure 4.58. As shown in Figure 4.58, the trends of wire sweep distribution with different die heights are similar. However, higher die height brings about bigger wire sweep (Han et al., 2011b).

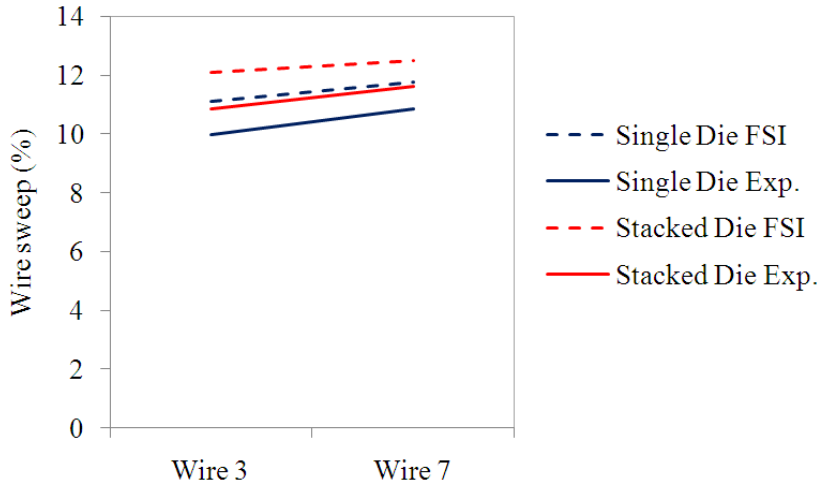


(a) Centre inlet of Wire 3 and Wire 7.

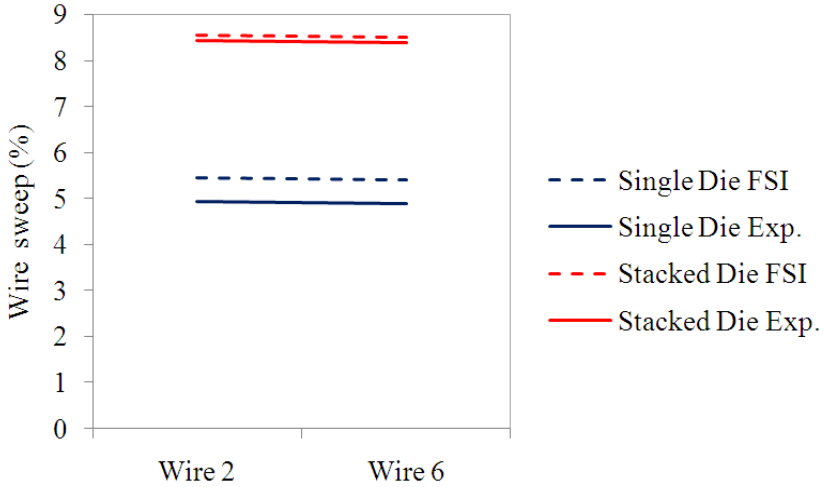


(d) Corner inlet of Wire 2 and Wire 6.

Figure 4.58 Comparison of wire sweep of single and stacked die of a scale-up eight-wire PBGA for Case 3: (a) Centre inlet of Wire 3and Wire 7 and (b) Corner inlet of Wire 2 and Wire 6.

### 4.6.2 Effects of Inlet Arrangements on Wire Sweep Behaviour

#### 4.6.2.1 PBGA Package with Centre Inlet

The wire bond profiles at several stages of filled fluid percentage volume are shown in Figure 4.5 and Figure 4.6. It can be seen that the wire bonds were deflected in the direction of the mould front. The greatest wire sweep occurs in the middle portion of the die because these wire bonds being orthogonal to the melt-front generally are subjected to higher flow-induced forces.

#### 4.6.2.2 PBGA Package with Corner Inlet

The wire bond profiles at several stages of filled fluid percentage volume are shown in Figure 4.10 and Figure 4.11. It can be observed that inlet gate position has a significant effect on wire sweep. The shifting of the inlet gate from the centre to the corner changes the flow pattern in the cavity and the pattern of wire bond deformation. In this case, the melt front meets at the corner opposite the gate. Even though the wire bonds in the region where the melt fronts meet may be deflected in directions opposite to each other, the risk of wire bond shorting may be lower than that with a centre inlet gate because the space between wire bonds at the corner inlet of the package is normally larger.

## 4.7 Wire Sweep Considering Rheology Effect of Actual Size PBGA Encapsulation Process

Different EMC material properties show the different flow behaviours during the encapsulation process. The characteristic of EMC material properties in electronic packaging gives significant effect to the package during encapsulation such as void formation and warpage on silicon die. EMC material properties with highest viscosity may require the proper setting in processing parameter to reduce the void formation and filling time. Thus, the EMC characteristic may cause the unpredicted flow front profile in the encapsulation process. Three types of moulding compound with different material properties have been utilized in the actual size PBGA encapsulation process, which is available in the literatures. The EMC fluid behaves according to non-uniform flow profiles and viscosity variation during filling process. The behaviour of moulding compound is also influenced by the filler content. The filler content in the EMC gives the important effect to the warpage trend, and it is dominant in the compound properties (Yong, 2006). Besides, the type and percentage of filler content also affect the thermal conductivity, thermal expansion coefficient and dielectric constants (Kim et al., 1999). The Al-N (Aluminium Nitride) filler improved the thermal conductivity until 7-8 times compared with crystalline silica at 70 % of EMC volume.

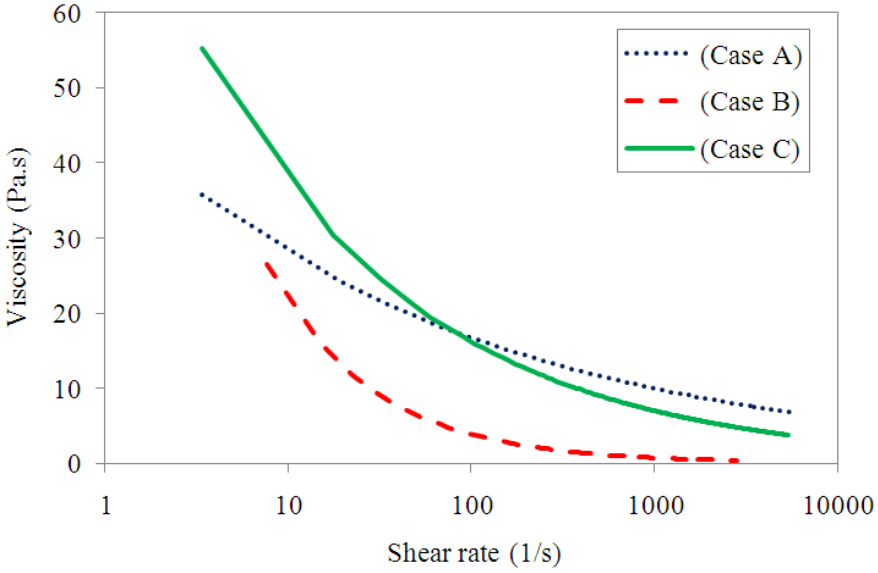

Figure 4.59 Viscosity versus shear rate.

Figure 4.59 illustrates the viscosity variation versus shear rate for three different EMC material properties that were used in the present study. The curves show an exponential relation of viscosity variation where the viscosity reduces with the shear rate. EMC material properties used in Case B shows the higher viscosity variation, followed by Case A and Case C. The variations of viscosity-shear rate in Figure 4.59 were obtained from the FLUENT simulation results. The FLUENT software calculated the variation of the viscosity shear-rate for EMC material properties during the encapsulation process depending on the material properties. The capability of the FLUENT in handling this problem was reported by Khor et al. (2010c) in their experimental and simulation of polymer rheology during injection moulding process. Hence, the realistic predictions could be achieved by using FLUENT software. In the polymer fluid processing, viscosity is normally independent of pressure, but liquids under extreme pressure often experience an increase in viscosity (Liang, 2001). Since liquids are normally incompressible, an increase in pressure does not really bring the molecules significantly closer together.

### 4.7.1 Analysis of Pressure Effect in Packaging

Pressure distribution during the mould filling process is also important in electronic packaging, especially for the wire bonding and lead frame. Dissimilarity of the pressures may give the undesirable effect to the wire such as serious deformation, failure or fracture; hence, reduce the package reliability. Point position of measured pressure is shown in Figure 4.60. Thus, the pressure distributions during the PBGA encapsulation process are observed in the present study. Pressure distribution of all cases at Point 1, 2, 3 and 4 are shown in Figure 4.61a and 4.61b and pressure behaviour of each point of Case C is shown in Figure 4.62. From Figure 4.61, the similarity of the pressure trends of Case B and Case C may be due to the viscosity behaviour that mainly influenced by the complex rheological of the EMCs. This is evidently from the Figure 4.59, where they show the almost similar trend of the viscosity-shear rate although with different values compared to the EMC of Case A. As illustrated in Figure 4.62, the maximum pressure at Point 1 is due to the impact of continuous flow from the inlet gate. The pressure gradually reduces with flow front advancement as evident from the

pressures at the symmetric locations of Point 2 and Point 4, and the lower pressure at the location Point 3, which near to the outlet vent.

Pressure distributions contour for Case A, Case B and Case C are shown in Figure 4.63. The contour colours represent the pressure drop around package during the filling process; higher pressures are observed near the inlet gates and lower pressures around the outlet vent.

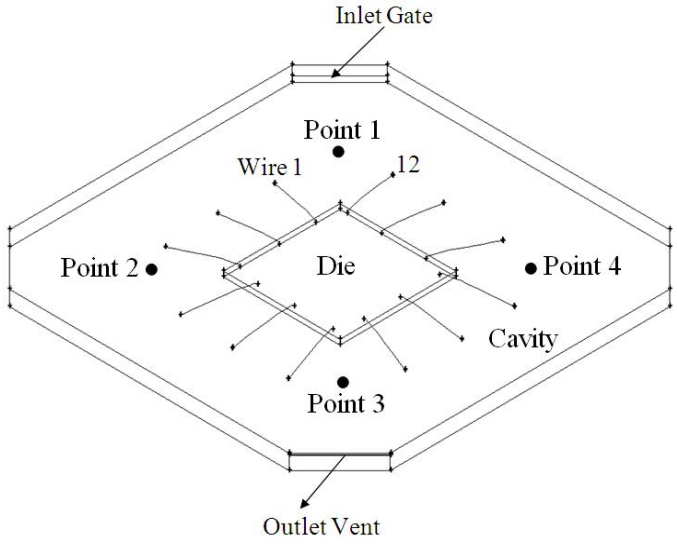


Figure 4.60 Point position of measured pressure of actual size PBGA.

The pressure at all locations shows the similar pressure distribution contour for all cases of filling process. From the results, the relationship between pressure and types of EMC are obvious, Case A with maximum viscosity (as illustrates in Figure 4.59) the higher pressure distributions. Besides, the pressure around outlet vents is found lower compare to pressure nearer to inlet gates. From the simulation analysis, filling process of Case A shows the highest pressure with comparing to Case B, and Case C. This phenomenon is caused by the flow interaction from the different parameter of EMC properties.

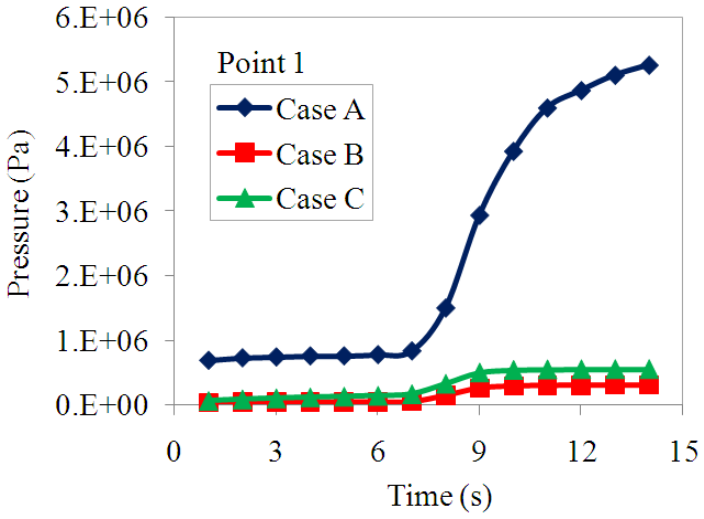


(a) Point 1.

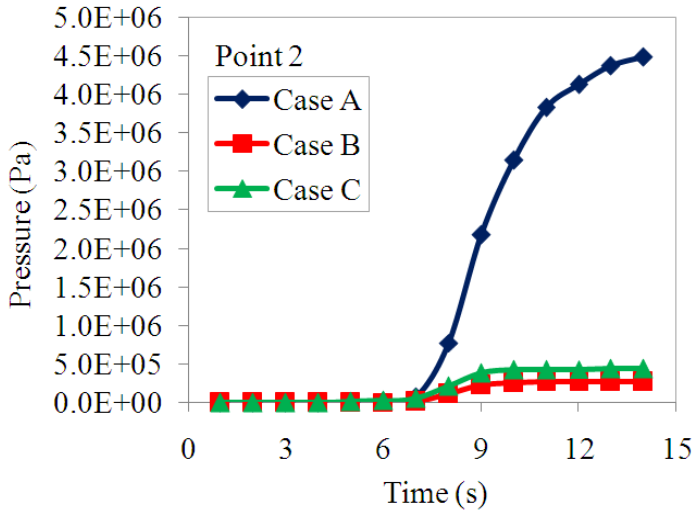


(b) Point 2.

Figure 4.61a Pressure distributions of all Cases of actual size PBGA: (a) Point 1 and (b) Point 2.

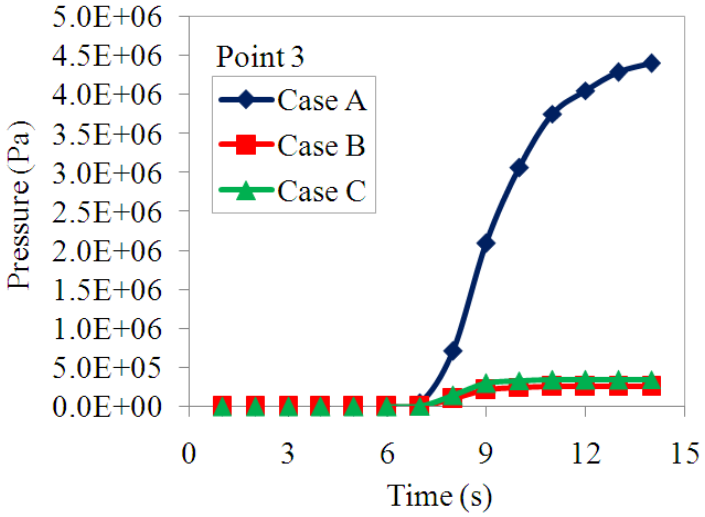


(c) Point 3.

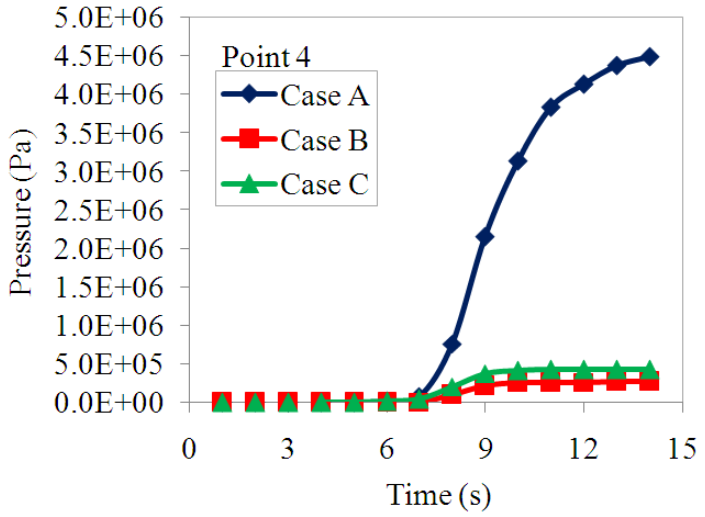


(d) Point 4.

Figure 4.61b Pressure distributions of all Cases of actual size PBGA: (c) Point 3 and (d) Point 4 (continued).

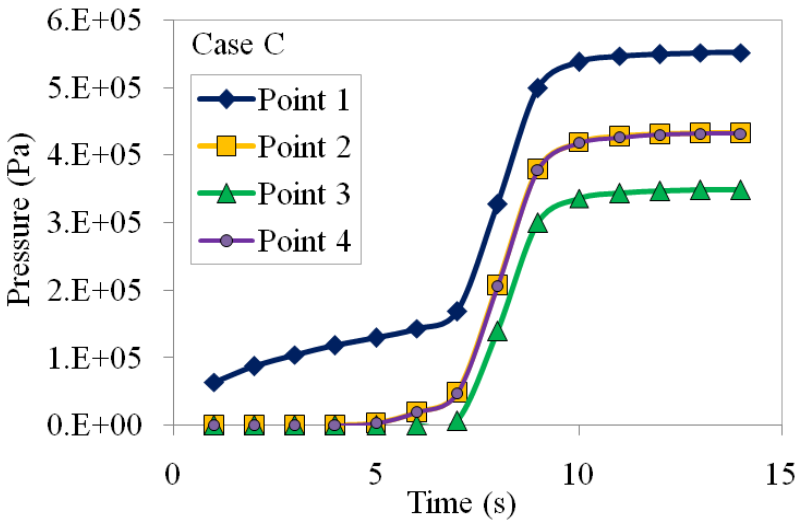


Figure 4.62 Pressure behaviour of each point of Case C of actual size PBGA.

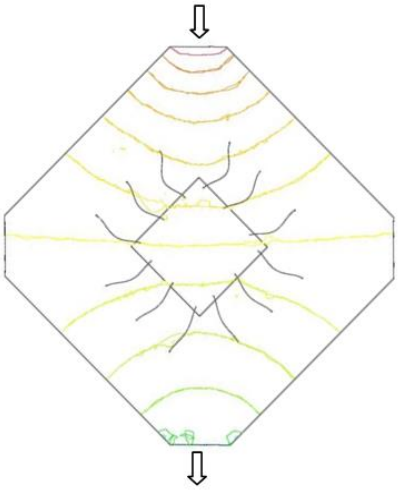

(a) Case A.

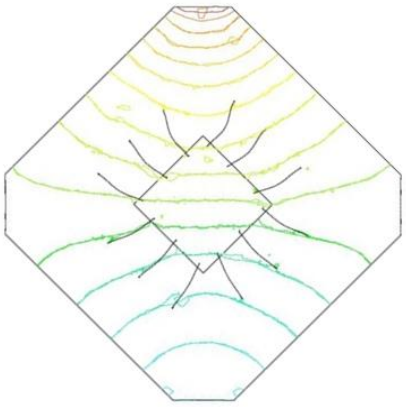

(b) Case B.

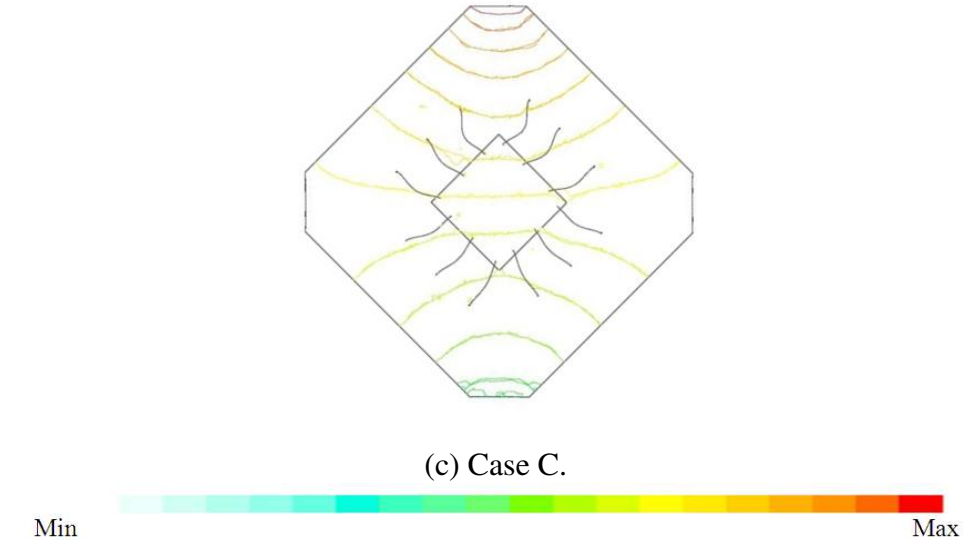


Figure 4.63 Pressure profiles for different parameter of material properties of actual size PBGA: (a) Case A, (b) Case B and (c) Case C.

### 4.7.2 Void Occurrence

The possibility of air trap or incomplete filling in the package is observed in the present case. Three cases of different properties of EMC are used in the analysis. Figure 4.64a and 4.64b shows the possibility of the air trap or incomplete filling at 14 s of the package for all cases. The circles show in Figure 4.64a and 4.64b is the location of the high possibility of void formation that causes by air trap or incomplete filling during the process. Case B (Figure 4.64b) is found to have the lowest air trap volume during filling process. This is clearly presented in Figure 4.65, which shown fewer and smaller air trap regions for Case B. Decreasing of viscosity may be the need for Case A, Case Band Case C to reduce the possibility of the air trap in the package. Comparison of EMC filling volume for the three cases with different parameters is presented in Figure 4.66. The results are obtained from simulation analysis show the Case B and Case C have higher and faster filling of the EMC volume compared to Case A. These filling phenomena are obviously shown in Figure 4.59 where the EMC with lowest viscosity (Case C) and the changes of the viscosity in Case B have significantly affected the EMC filling during the encapsulation process.

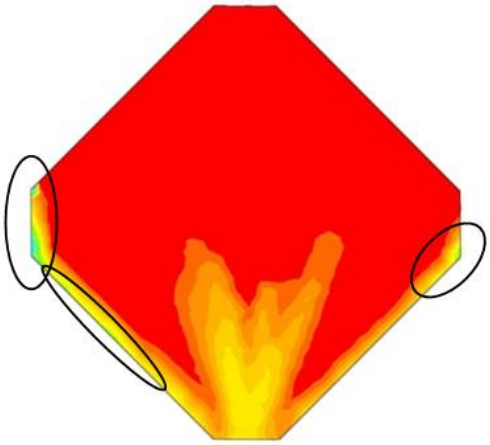

(a) Case A.

Figure 4.64a Comparison position posibility of void at 14 s of actual size PBGA: (a) Case A.

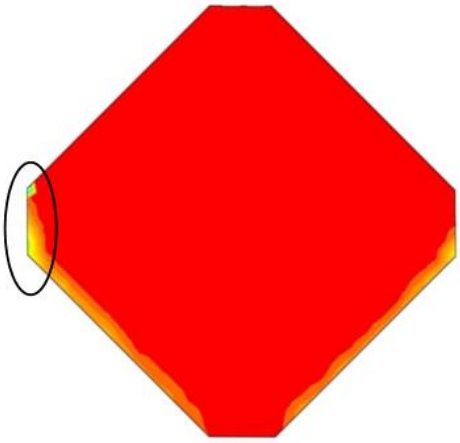

(b) Case B.

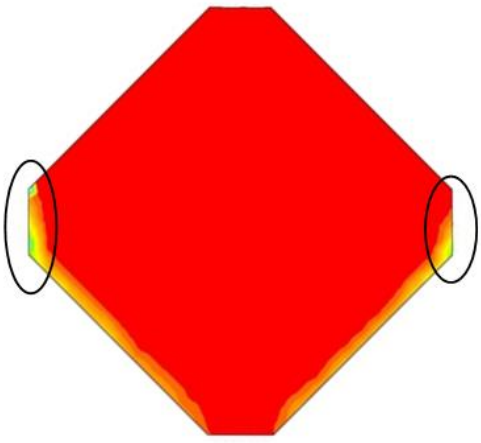

(c) Case C.

Figure 4.64b Comparison position posibility of void at 14 s of actual size PBGA: (b) Case B and (c) Case C (continued).

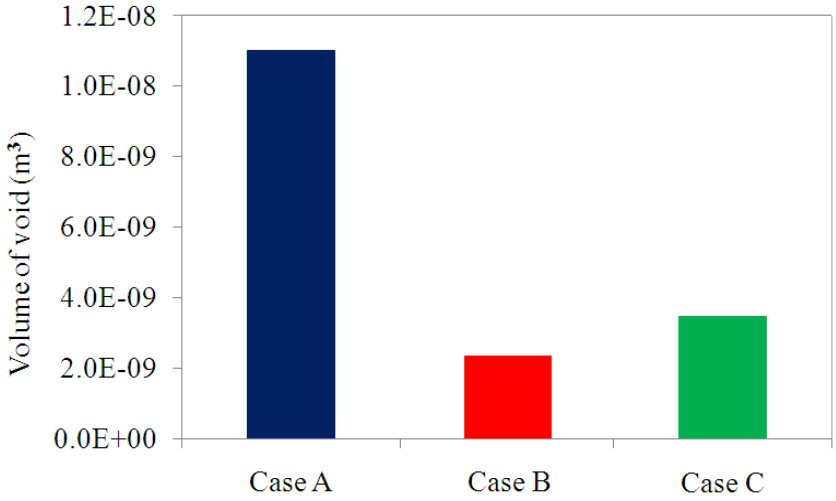


Figure 4.65 Volume of air trap (void) for all cases of actual size PBGA.

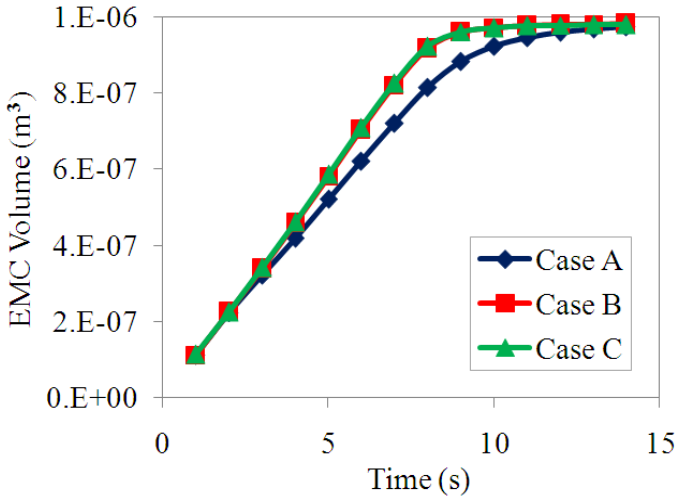


Figure 4.66 EMC volume of each Case of actual size PBGA.

### 4.7.3 Melt Front Profile

The comparison of simulation results between all Cases at 3, 7 and 11 s is shown in Figure 4.67. The predicted flow front shows different profiles for three cases. At the initial stage (1 s), the simulation flow-front profile is similar in all cases. The EMC flowed into the cavity without any obstacles before it reached the die or gold wires. So the EMC expanded ahead synchronously, and the melt front during this time tended to have a smooth curve shape. This may be attributed to the lower flow resistance around the inlet gate as the encapsulant is allowed to enter freely through the inlet gate. However, at 3s of filling time, the simulation displays different between Case A, Case B and Case C. In this state, the EMC encapsulant has already covered more than half of the silicon die and the flow front of Case A shows a non-uniform profile around the silicon die region compared to the uniform profiles for Case B and Case C. The effect of the gold wires and the die is obviously shown in the flow front profiles. The EMC in this region was retarded. At 7 s of filling time, the flow front on the top of the die was concave, while the flow front around was convex. At 11 s, the EMC completely flowed over the area of the die and the gold wires, and filled the whole cavity. Case B and Case

C show a faster flow compared to Case A, which is observed at 11 s of filling time during the simulation.

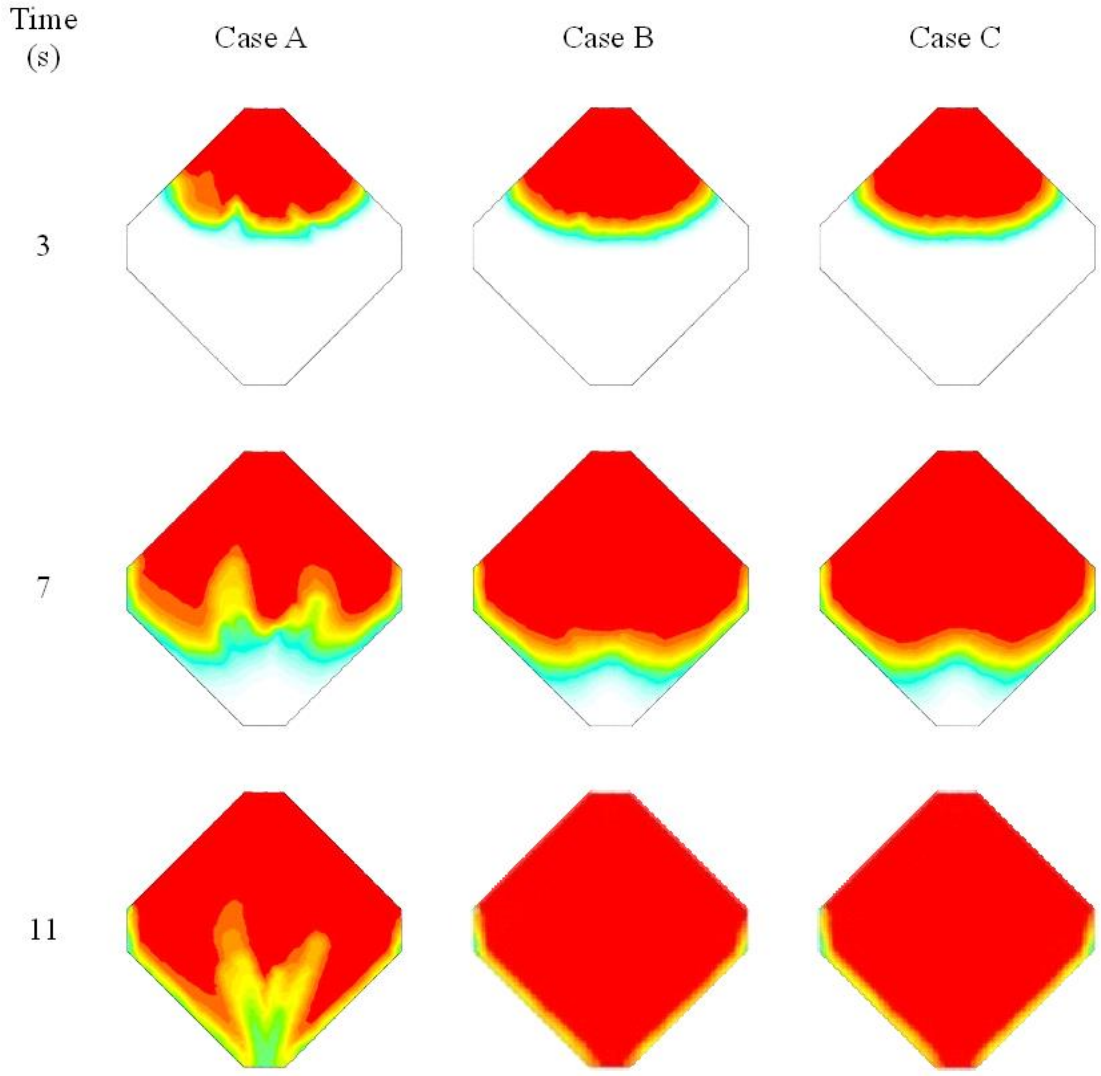


Figure 4.67 Simulation comparisons between different EMC parameters of actual size PBGA.

### 4.7.4 Conversion of the Compound

Degree of conversion within the mould cavity had been explained by Khor et al., (2010a). The top view of conversion distribution of the packages is presented in Figure 4.68a and 4.68b for different cases of material properties. It is observed that the conversion level is quite low at the cavity inlet gate but higher around the package region. The predicted conversion of the mould compound at 14 s is 8.06e-01, 8.02e-01 and 7.75e-01 for Case A, Case B and Case C, respectively. This phenomenon is reasonable with the viscosity variation that is shown in Figure 4.59. This is predictable because the combination of the Castro−Macosko viscosity model and the Kamal curing kinetics model has taken into account two important factors, i.e. the dependence

viscosity on the shear rate and the dependence of conversion level (which also affects the viscosity of the moulding compound) on the temperature.

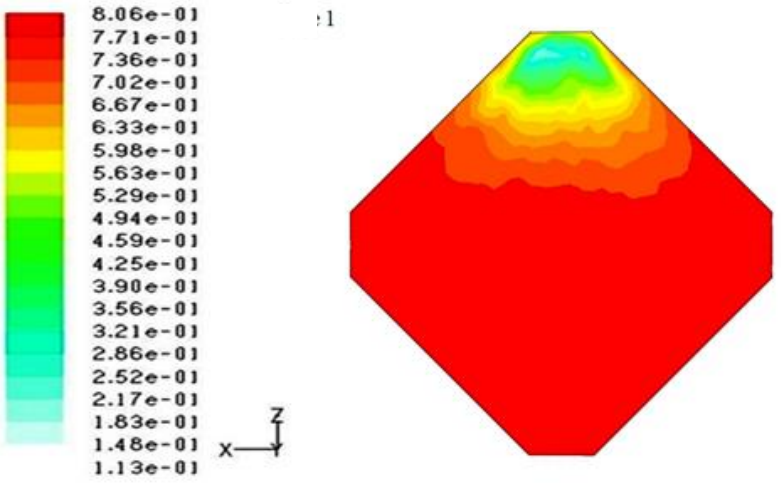


(a) Case A.

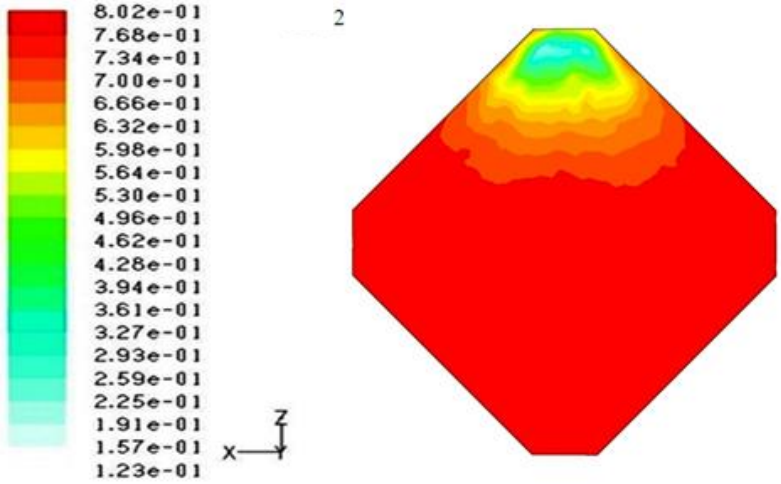


(b) Case B.

Figure 4.68a Predicted conversion of the mould compound at top of the package for different parameter of material properties at 14 s of actual size PBGA: (a) Case A and (b) Case B.

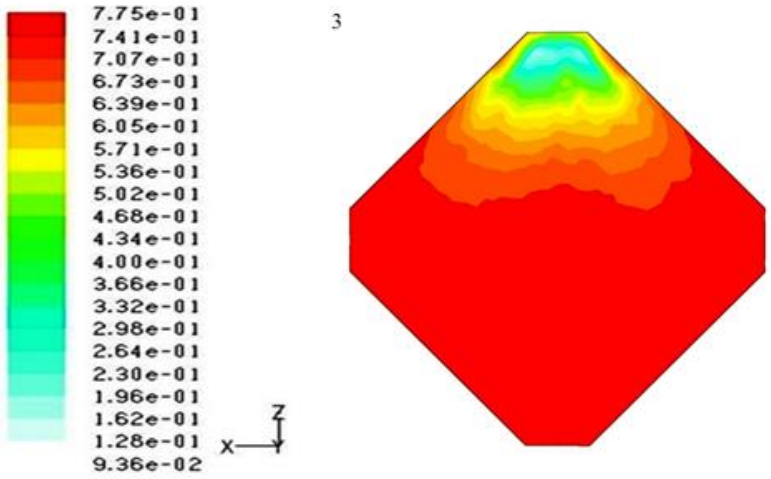


(c) Case C.

Figure 4.68b Predicted conversion of the mould compound at top of the package for different parameter of material properties at 14 s of actual size PBGA: (c) Case C (continued).

### 4.7.5 Wire Sweep Analysis

Figure 4.69 illustrates the melt-front advancement for the PBGA package obtained from FLUENT, and the phenomenon of wire deformation predicted by ABAQUS. At the initial filling stage as shown in Figure 4.69 (2 s), two wire deformations are observed. However, the wire deformation occurs when EMC fills and covers the die and the wires in the package, or the wire sweep occurs when EMC interacts with the solid surface of the wire, as observed in Figure 4.69 (4 to 14 s). Figure 4.70 shows the percentage of maximum wire sweep of each wire, and Figure 4.71 describes the percentage of wire sweep in Case C at 6, 10 and 12 s. In the present study, the effect of viscosity on pressure is found to directly influence the wire displacement and drag force that act on the wire structure, during the filling process. Thus, wires that experience a high viscosity flow or high pressure distribution are expected to deform more compared to those at a low viscosity or pressure, as is clear from the increase of wire sweep at wires 1 and 12, which are closer to Point 1.

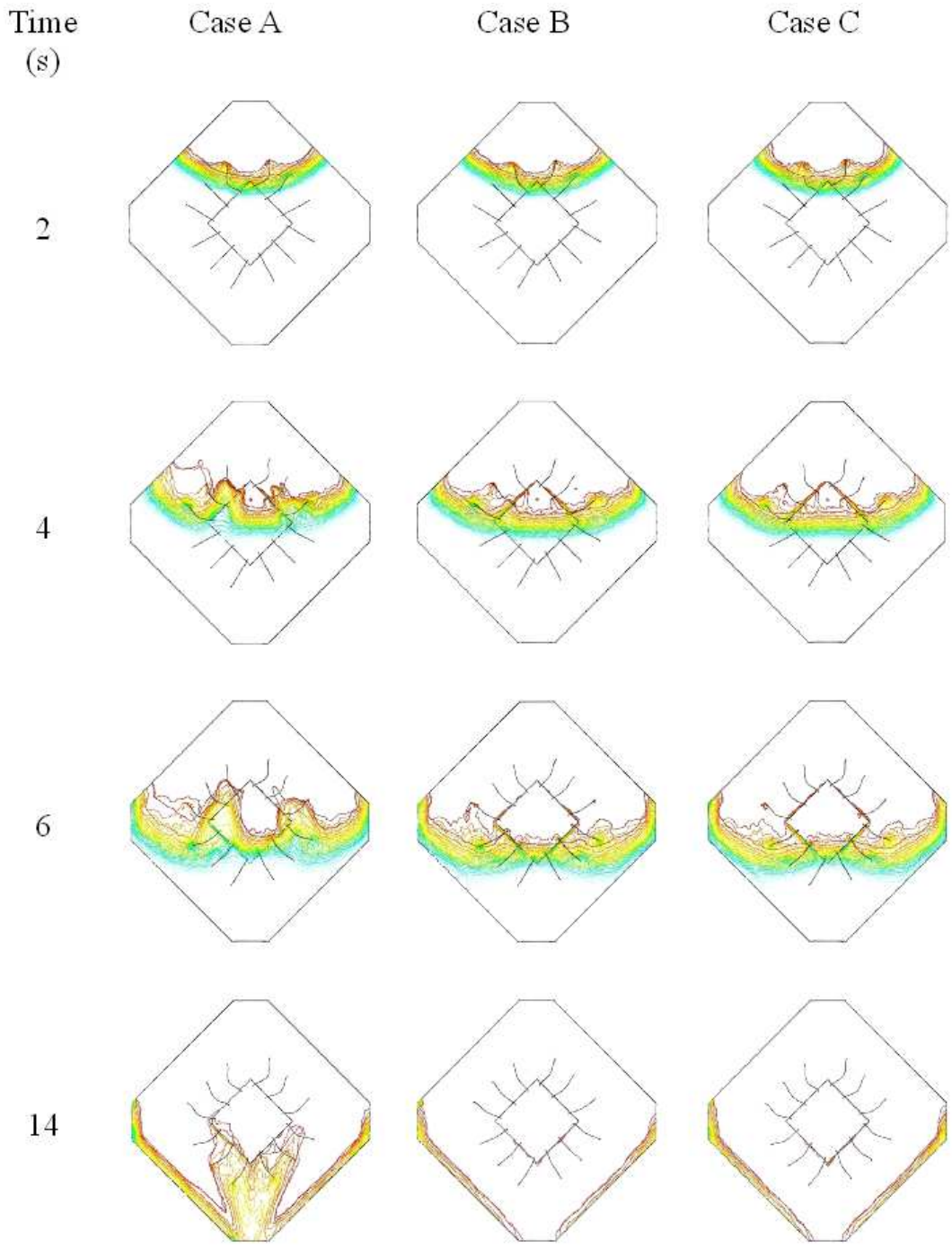


Figure 4.69 Behaviour of wire sweep of actual size PBGA of Case A, Case B and Case C at 2 s, 4 s, 6 s and 14 s.

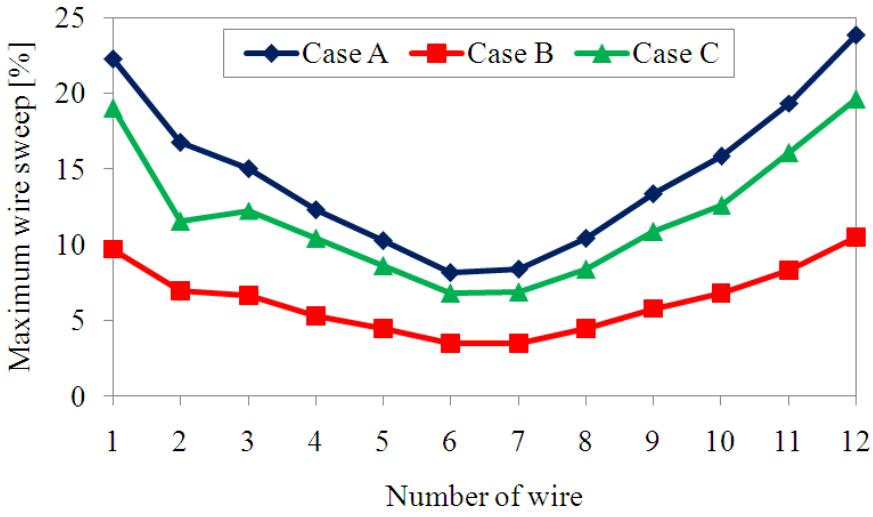


Figure 4.70 Percentage maximum wire sweep of each wire of actual size PBGA.

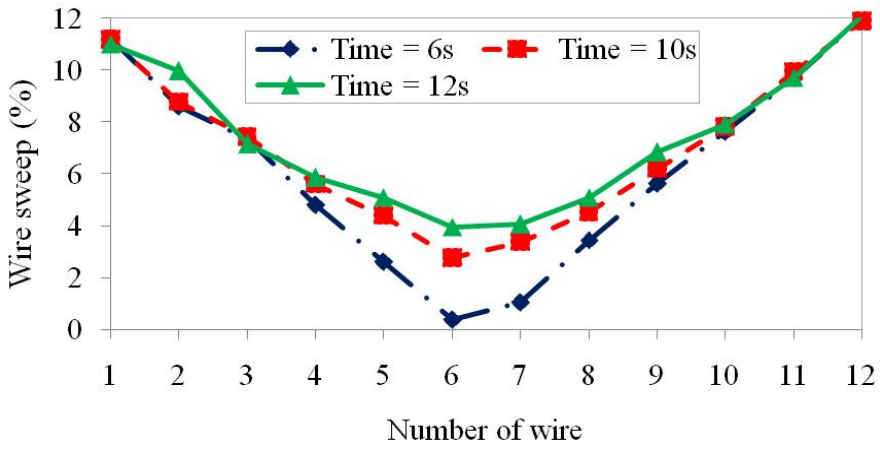


Figure 4.71 Percentage wire sweep of Case C at 6 s, 10 s and 12 s of actual size PBGA.

## 4.8 Optimisation Using RSM on Actual Size PBGA Encapsulation Process

### 4.8.1 Result of the Central Composite Design

In this numerical analysis, a total of 20 CCD batch runs were conducted (Table 4.6). The targets of the study are to minimize the wire sweep ($Y_1$), filled time ($Y_2$), and void in package ($Y_3$) during the actual size PBGA encapsulation process. The wire deformation on the structures will cause unintended defects to the package reliability, especially for high-density of wire applications. Void formation in the package might induce delamination (Tay and Lin, 1999) on the interface of the actual size PBGA. Proper control of filling time can reduce production cycle time and cost.

Table 4.7 Results of the central composite design

| Run | Factor (codec) | | | Response (*Y*) | | | | | |
|---|---|---|---|---|---|---|---|---|---|
| | | | | Simulation | | | Model Prediction | | |
| | *A* | *B* | *C* | *1* | *2* | *3* | *1* | *2* | *3* |
| 1 | 0 | 0 | 1 | 0.71874 | 4 | 0.09955 | 0.7065 | 4.1125 | 0.28031 |
| 2 | -1 | 0 | 0 | 0.64396 | 10.5 | 0.80213 | 0.57339 | 10.7625 | 1.48013 |
| 3 | 0 | 0 | 0 | 0.87091 | 7.5 | 0.22754 | 0.86492 | 7.7125 | 0.26589 |
| 4 | 1 | 0 | 0 | 1.11645 | 5 | 0.08949 | 1.15645 | 4.6625 | -0.9483 |
| 5 | 0 | 0 | -1 | 0.94459 | 11.5 | 8.73617 | 1.02334 | 11.3125 | 7.41965 |
| 6 | 1 | 1 | -1 | 0.42154 | 6.5 | 7.83664 | 0.48823 | 6.6375 | 7.5028 |
| 7 | 0 | 0 | 0 | 0.87091 | 7.5 | 0.22754 | 0.86492 | 7.7125 | 0.26589 |
| 8 | 0 | 0 | 0 | 0.87091 | 7.5 | 0.22754 | 0.86492 | 7.7125 | 0.26589 |
| 9 | 0 | 0 | 0 | 0.87091 | 7.5 | 0.22754 | 0.86492 | 7.7125 | 0.26589 |
| 10 | 0 | -1 | 0 | 1.78421 | 7.25 | 0.23322 | 1.66608 | 7.7125 | -0.4299 |
| 11 | -1 | -1 | 1 | 0.96508 | 6 | 0.78257 | 0.93666 | 5.5375 | 1.40034 |
| 12 | 0 | 1 | 0 | 0.3527 | 7.5 | 0.16884 | 0.31776 | 7.7125 | 0.96169 |
| 13 | -1 | 1 | -1 | 0.23983 | 16.5 | 10.1431 | 0.16786 | 15.9875 | 10.7712 |
| 14 | -1 | 1 | 1 | 0.21518 | 5.75 | 0.34034 | 0.33226 | 5.5375 | -0.7968 |
| 15 | 0 | 0 | 0 | 0.87091 | 7.5 | 0.22754 | 0.86492 | 7.7125 | 0.26589 |
| 16 | 1 | -1 | 1 | 1.67217 | 3 | 0.15591 | 1.7824 | 2.6875 | -0.1882 |
| 17 | 1 | -1 | -1 | 2.65929 | 7 | 1.10144 | 2.58048 | 6.6375 | 2.52249 |
| 18 | 1 | 1 | 1 | 0.35954 | 2.75 | 0.02316 | 0.28268 | 2.6875 | 0.7059 |
| 19 | 0 | 0 | 0 | 0.87091 | 7.5 | 0.22754 | 0.86492 | 7.7125 | 0.26589 |
| 20 | -1 | -1 | -1 | 1.24965 | 16 | 9.28092 | 1.36478 | 15.9875 | 8.88213 |

*A*, *B*, and *C* = inlet pressure, diameter of wire, vent height.
1, 2 and 3 = wire sweep, filling time and void.

In the actual size PBGA encapsulation process, the stress and deformation of wire imposed on the structure are resulted from the fluid–structure interaction. Thus, wire sweep ($Y_1$) was evaluated during the encapsulation process. However, package filling time ($Y_2$) and void in the package ($Y_3$) were estimated at the final of the process. From the CCD batch runs, the maximum wire deformation is 2.65 mm, when high inlet pressure (5 MPa) is applied to 0.03 mm of diameter of wire, and 0.40 vent height. Therefore, this situation should be avoided in the PBGA encapsulation. Moreover, the lowest void formation is found on run 18, whereas the middle inlet pressure, wire diameter and vent height applied. This condition may be attributed to the large pressure, which gives lower resistance to the EMC to freely flow through. The fastest filling time (3 s) for run 16 is achieved at the highest inlet pressure (*A*) with 0.04 mm for factors *B*, and 0.22 mm for factor *C*.

### 4.8.2 Regression Model Equation and Analysis of Variance (ANOVA)

The regression models for responses, maximum wire sweep ($Y_1$) filled time ($Y_2$) and void in package ($Y_3$), and were selected based on the highest-order polynomials, the significant additional terms and the absence of aliased models through the software. The

best fitting was the quadratic model (Eqs. (4.1)– (4.3)) for all significant model terms (values of ''Prob > F'' less than 0.05) as suggested by the software.

Based on the sequential model sum of squares, the models for wire sweep and filling time percentages reduce were selected based on the highest order polynomials where the additional terms were significant and the models were not aliased. The models were coded as $Y_1$, $Y_2$ and $Y_3$ for wire sweep, filling time and void respectively.

The quadratic model for wire sweep, filling time and void terms, $Y_1$, $Y_2$ and $Y_3$ were selected as suggested by the software and are shown in Eqs. (4.1), (4.2) and (4.3). The independent variables in the models were inlet pressure, wire diameter and vent height and were coded as $A$, $B$, and $C$, respectively. The final empirical models used to generate coded factors for each variable are as follows:

$$Y_1 = 0.8649215 + 0.2915288A - 0.6741609B - 0.1584183C + 0.1269982B^2 - 0.2238325AB - 0.09248875AC + 0.14813BC \quad (4.1)$$

$$Y_2 = 7.7125 - 3.05A - 3.6C + 1.625AC \quad (4.2)$$

$$Y_3 = 0.265893 - 1.21424A + 0.6958B - 3.56967C + 3.584086C^2 + 0.772815AB + 1.192763AC - 1.02154BC \quad (4.3)$$

The quality of the model was evaluated based on the coefficient of determination in addition to the ANOVA statistical analysis. The ANOVA results for the quadratic model for wire sweep, filling time and void percentage reduce are shown in Table 4.6 − 4.8.

Tables 4.7 – 4.9 show the ANOVA results for the models ($Y_1$–$Y_3$). In the ANOVA analysis, the quality of the model was evaluated according to the coefficient of determination ($R^2$). The information from the ANOVA analysis showed the $R^2$ for every empirical equation (Eqs. (4.1) – (4.3)) were 0.98, 0.99, and 0.96 for responses $Y_1$ to $Y_3$; meanwhile, the standard deviations of each model were 0.08, 0.31, and 0.88. The $R^2$ values of all models were considerably high. Thus, the percentages of total variability of each empirical model were 98% ($Y_1$), 99% ($Y_2$), and 96% ($Y_3$), respectively.

Table 4.8 ANOVA of quadratic model for maximum wire sweep ($Y_1$) with operating parameters (Inlet pressure ($A$), Wire diameter ($B$), and Vent height ($C$))

| Source | Sum of Squares | DF | Mean Square | F Value | Prob> F |
|---|---|---|---|---|---|
| Model ($Y_1$) | 6.371207 | 7 | 0.91017 | 121.371 | < 0.0001 |
| $A$ | 0.84989 | 1 | 0.84989 | 113.333 | < 0.0001 |
| $B$ | 4.544929 | 1 | 4.54493 | 606.065 | < 0.0001 |
| $C$ | 0.250964 | 1 | 0.25096 | 33.4659 | < 0.0001 |
| $B2$ | 0.080643 | 1 | 0.08064 | 10.7537 | 0.0066 |
| $AB$ | 0.400808 | 1 | 0.40081 | 53.4477 | < 0.0001 |
| $AC$ | 0.068433 | 1 | 0.06843 | 9.12557 | 0.0106 |
| $BC$ | 0.17554 | 1 | 0.17554 | 23.4082 | 0.0004 |
| Residual | 0.089989 | 12 | 0.0075 | | |
| Lack of Fit | 0.089989 | 7 | 0.01286 | | |
| Pure Error | 0 | 5 | 0 | | |

| | | | |
|---|---|---|---|
| Std. Dev. | 0.086597 | R-Squared | 0.98607 |
| Mean | 0.928421 | Adj R-Squared | 0.97795 |
| C.V. | 9.327366 | Pred R-Squared | 0.80463 |
| PRESS | 1.262305 | Adeq Precision | 44.0509 |

Sample ANOVA calculations for maximum wire sweep ($Y_1$) are presented in Appendix I.

Table 4.9 ANOVA of quadratic model for filling time ($Y_2$) with operating parameters (Inlet pressure (*A*), Wire diameter (*B*), and Vent height (*C*))

| Source | Sum of Squares | DF | Mean Square | F Value | Prob> F |
|---|---|---|---|---|---|
| Model ($Y_2$) | 243.75 | 3 | 81.25 | 847.251 | < 0.0001 |
| *A* | 93.025 | 1 | 93.025 | 970.037 | < 0.0001 |
| *C* | 129.6 | 1 | 129.6 | 1351.43 | < 0.0001 |
| *AC* | 21.125 | 1 | 21.125 | 220.285 | < 0.0001 |
| Residual | 1.534375 | 16 | 0.0959 | | |
| Lack of Fit | 1.534375 | 11 | 0.13949 | | |
| Pure Error | 0 | 5 | 0 | | |
| Std. Dev. | 0.309675 | | R-Squared | 0.99374 | |
| Mean | 7.7125 | | Adj R-Squared | 0.99257 | |
| C.V. | 4.015231 | | Pred R-Squared | 0.98823 | |
| PRESS | 2.887262 | | Adeq Precision | 96.0353 | |

Table 4.10 ANOVA of quadratic model for void in package ($Y_3$) with operating parameters (Inlet pressure (*A*), Wire diameter (*B*), and Vent height (*C*))

| Source | Sum of Squares | DF | Mean Square | F Value | Prob> F |
|---|---|---|---|---|---|
| Model ($Y_3$) | 235.7469 | 7 | 33.6781 | 43.346 | < 0.0001 |
| *A* | 14.74382 | 1 | 14.7438 | 18.9763 | 0.0009 |
| *B* | 4.841383 | 1 | 4.84138 | 6.23119 | 0.0281 |
| *C* | 127.4256 | 1 | 127.426 | 164.005 | < 0.0001 |
| *C2* | 64.22837 | 1 | 64.2284 | 82.6663 | < 0.0001 |
| *AB* | 4.77794 | 1 | 4.77794 | 6.14953 | 0.0290 |
| *AC* | 11.38147 | 1 | 11.3815 | 14.6487 | 0.0024 |
| *BC* | 8.348394 | 1 | 8.34839 | 10.745 | 0.0066 |
| Residual | 9.323517 | 12 | 0.77696 | | |
| Lack of Fit | 9.323517 | 7 | 1.33193 | | |
| Pure Error | 0 | 5 | 0 | | |
| Std. Dev. | 0.881453 | | R-Squared | 0.96196 | |
| Mean | 2.057936 | | Adj R-Squared | 0.93976 | |
| C.V. | 42.83191 | | Pred R-Squared | 0.57362 | |
| PRESS | 104.4925 | | Adeq Precision | 21.0223 | |

### 4.8.3 Effect of Factors on Wire Sweep, Filling Time and Void

The sensitivity of each factor was identified through the perturbation plots as presented in Figure 4.72a and 7.72b for (a) wire sweep, (b) filling time and (c) void. Wire sweep was mostly influenced by inlet pressure and wire diameter as compared to the outlet vent height (Figure 4.72a). Inlet pressure and vent height appeared to be the most influential factor for filling time and void (Figure 4.72b). However, the vent height had shown a dominant effect to percentage of void in the encapsulation process (Figure 4.72 (c)).

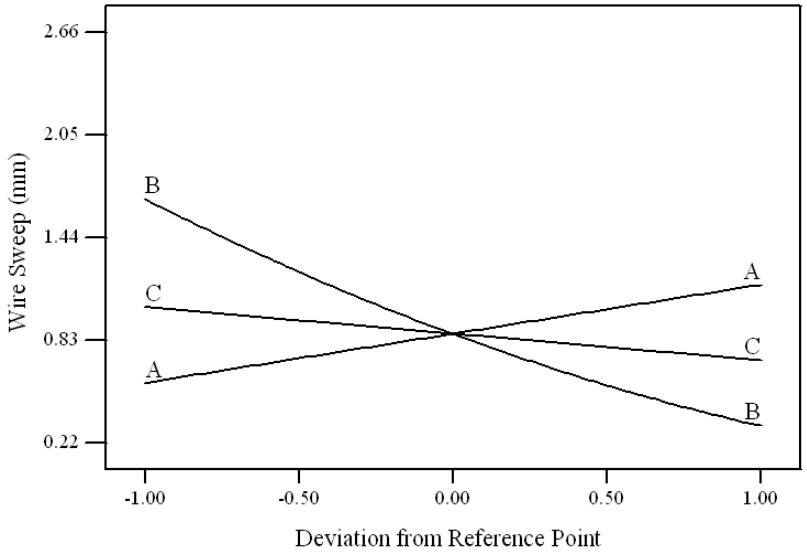


(a) Wire sweep

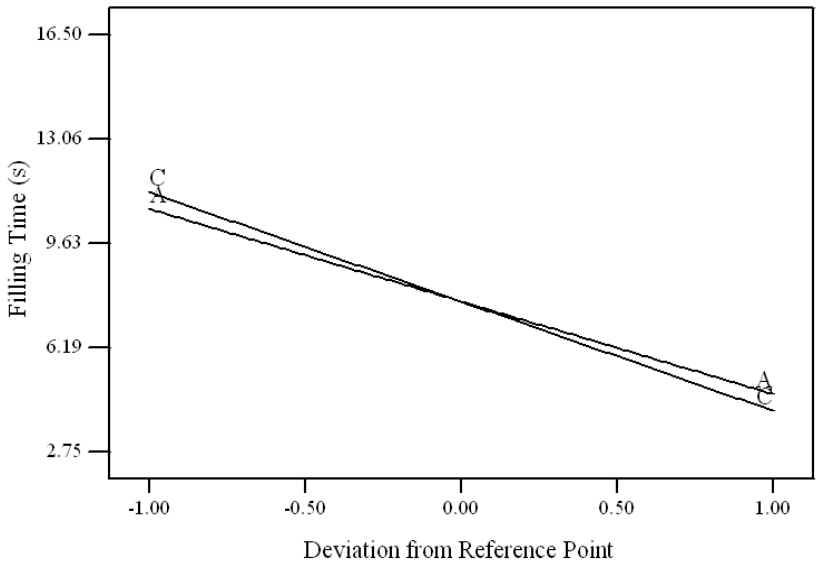


(b) Filling time

Figure 4.72a Perturbation plot for: (a) Wire sweep and (b) Filling time. Coded values for each factor are referring to the actual values listed in Table 3.2. (Note: *A* = inlet pressure, *B* = wire diameter, and *C* = vent height)

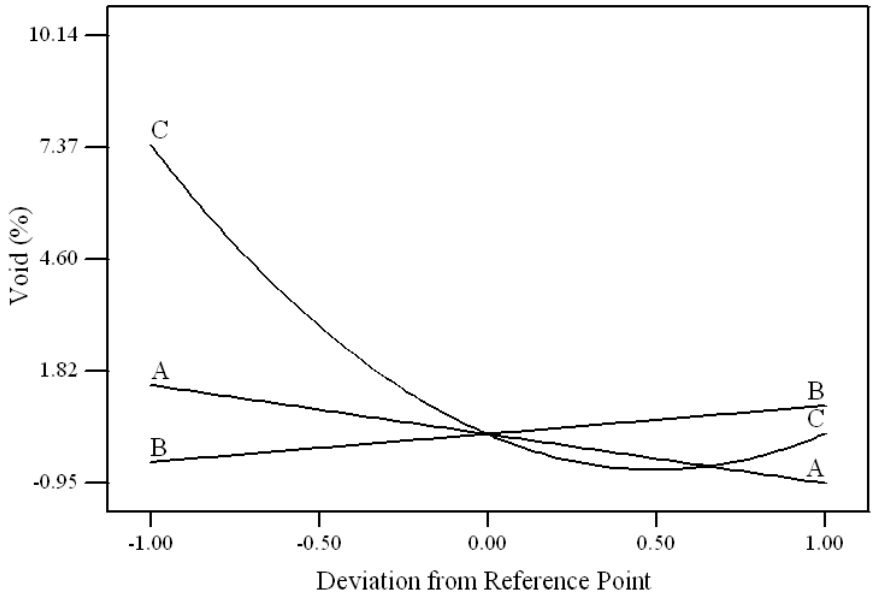


(c) Void

Figure 4.72b Perturbation plot for: (c) Void. Coded values for each factor are referring to the actual values listed in Table 3.2. (Note: $A$ = inlet pressure, $B$ = wire diameter, and $C$ = vent height) (Continued).

The factors exhibited crucial effects on the particular responses in the PBGA encapsulation process are as mentioned above. Inlet pressure ($A$) showed a significant effect to the wire sweep, percentage of void formation and filling time. This situation may be ascribed to the EMC flow in the feeding process, whereas at high pressure, faster flow front shortens the filling time and reduces the void formation (Khor et al., 2012b). The void formation can be minimized through high pressure and low transfer speed (Liu et al, 2004a). From the perturbation graphs (Figure 4.72 (b) and (c)), the design of the vent height ($C$) crucially affected the filling time and void formation. The increased in wire diameter reduced the wire sweep and the increased vent height reduced the filling time. This may provide a challenge to the package designer when using a small wire diameter with the vent height arrangement in the moulded PBGA package. Alternatively, this problem can be overcome by increasing the number of wires in the package; meanwhile, the application of high density (number) of wires had reduced the wire sweep (Jong, 2005).

Moreover, vent height ($C$) mainly affected to the filling time and void formation as illustrated in Figure 4.72(b) and (c). Small wire diameter experienced high wire deformation in the encapsulation process. The wire experienced an interaction with continuous EMC flow and the unstable flow front induced unstable forces acted on the wires. As mentioned in sub Section 4.6.2, void formation would induce the delamination (Tay and Lin, 1999) problem in the actual size PBGA package.

Other factors such as inlet design (Lee et al., 2008a), vent arrangement (Chai and Zohar, 1999; Lee et al., 2008b) may influence the void formation in the IC encapsulation.

Figure 4.73a and 7.73b depicts the 3D surface response and contour plots of the quadratic model, which was plotted using Design Expert software to study the interactive relationship between each factor and responses. In the 3D surface response,

the selection of two variables and a constant variable was determined according to the level of sensitivity towards the responses that depended on the perturbation plots in Figures 4.72.

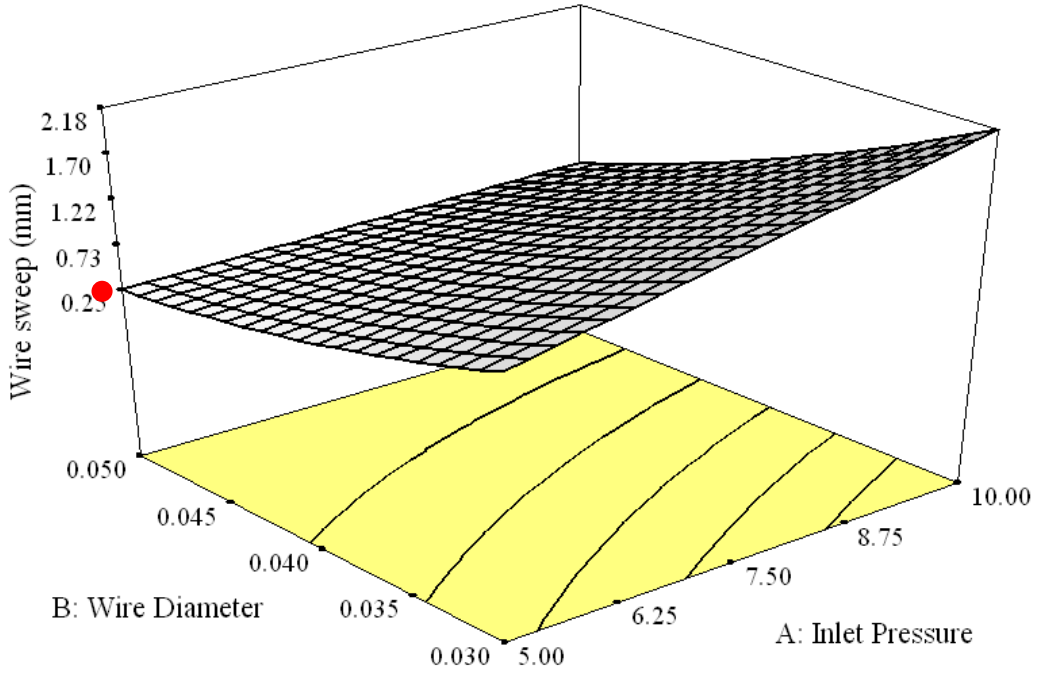


(a) Wire sweep.

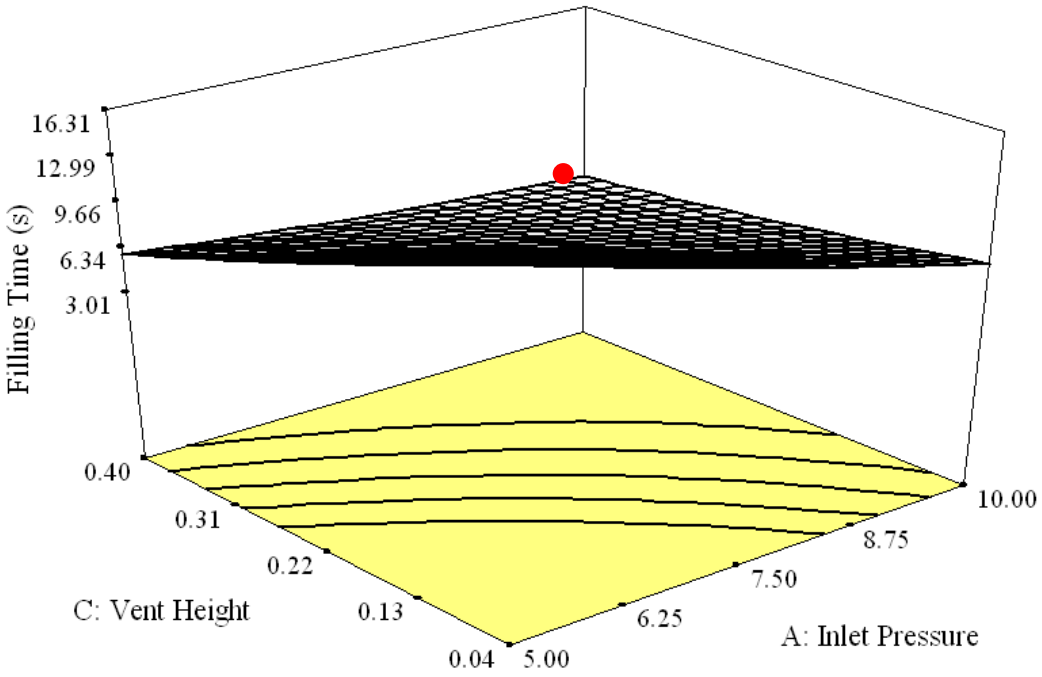


(b) Filling time.

Figure 4.73a 3D response surfaces for: (a) Wire sweep and (b) Filling time.

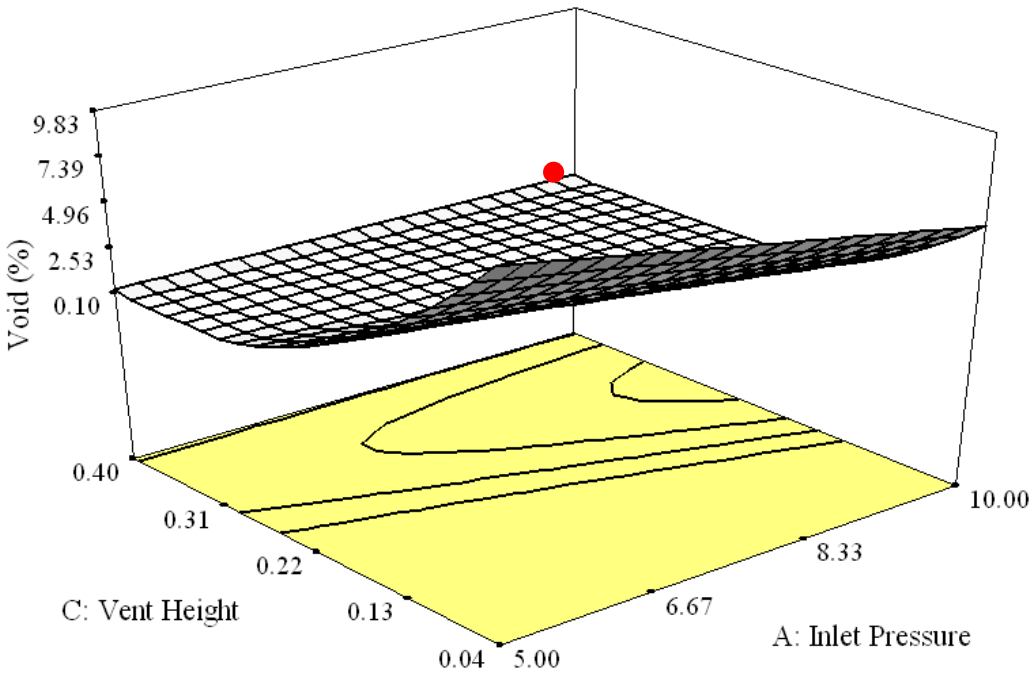


(c) Void.

Figure 4.73b 3D response surfaces for: (c) Void (continued).

The minimum wire sweep ($Y_1$) was identified at 0.05 mm wire diameter and 5 MPa inlet pressure (red dot). Similarly, two variables were also selected for plotting 3D surface response for responses $Y_2$ and $Y_3$. Inlet pressure and vent height were selected to vary with filling time and void formation due to their significance as shown in Figure 4.72(b) and (c). The shortest filling time was found at 0.4 mm of vent height and 10 MPa of inlet pressure. However, the lower void formation was achieved also at 0.4 mm of vent height and 10 MPa of inlet pressure. The minimum value of the responses ($Y_1$–$Y_3$) varied with two of the most influential factors is summarized in Table 4.10.

Table 4.11 Minimum value of the responses varied with two of the most influential factor

| Response | $Y_1$ (mm) | $Y_2$ (s) | $Y_3$(%) |
|---|---|---|---|
| 2 of the most influence factors | $A$ | $A$ | $A$ |
| | $B$ | $C$ | $C$ |
| Minimum Value | 0.25 | 4.46 | 2.52 |

### 4.8.4 Optimisation of Simulation Conditions

The solution for the optimized factors in order to minimize the responses as suggested by Design Expert software was examined through the FSI simulation at $A$ = 5.57 MPa, $B$ = 0.05 mm and $C$ = 0.36 mm. The comparison results between model response and simulation are listed in Table 4.11. The discrepancy in results varied within the range of 0.20 – 11.88 %, which demonstrates that reasonable prediction can be achieved using the empirical model. The interactive relationship and optimum value of each factor were successfully determined using the response surface methodology.

The percentage of wire sweep for all wires of simulation optimization result is shown in Figure 4.74. The isometric view in detail for all wire sweeps is shown in Appendix J. It can be found that the maximum wire sweep is at wire nos. 3 and 11 with wire sweep index about 8 % and 7.5 % respectively. The trend of the wire sweep of each position was similar with previous work by Su et al. (2003) and Wu et al. (1998).

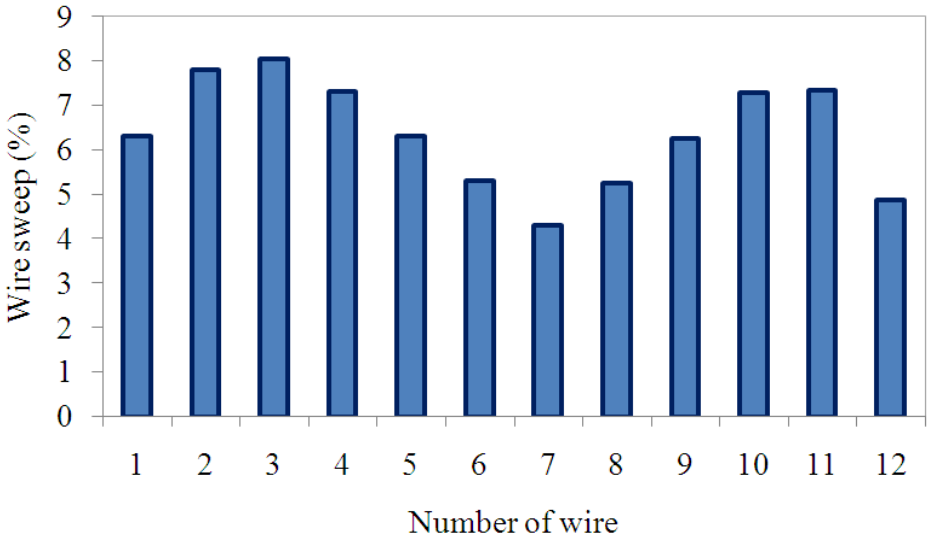


Figure 4.74 Percentage of wire sweep for all wires of simulation optimization result.

The Von Mises and Shear Stress formation for all wires of simulation optimisation result are shown in Figure 4.75 and 4.76 respectively.

Table 4.12 Validation of model response and simulation for factor a) inlet pressure (5.57 MPa), b) wire diameter (0.05 mm) and c) vent height (0.36 mm).

| | Response ($Y$) | | |
|---|---|---|---|
| | Wire sweep (mm) | Filling time (s) | Void (%) |
| Model Response | 0.86 | 7.71 | 0.27 |
| Simulation | 0.98 | 7.70 | 0.24 |
| Error (%) | 11.88 | 0.20 | 11.81 |
| Standard deviation | 0.08 | 0.01 | 0.02 |

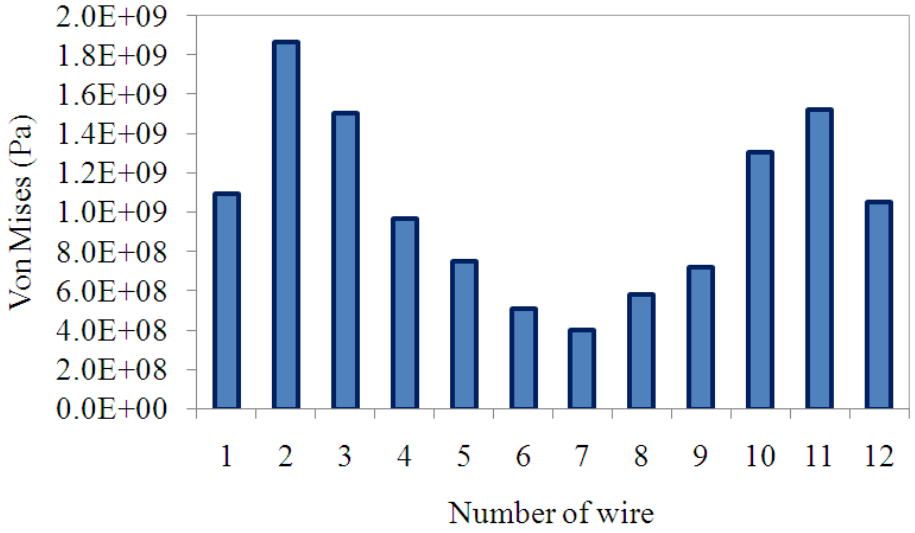


Figure 4.75 Von Mises for all wires of simulation optimization result.

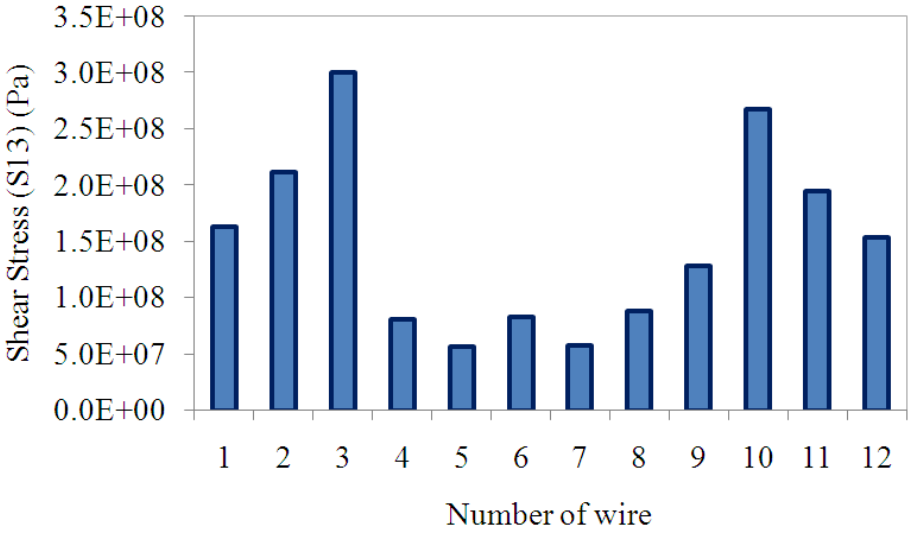


Figure 4.76 Shear Stress for all wires of simulation optimization result.

Whereas the detailed view of maximum von Mises stress and Shear stress distribution for wire 4 of simulation optimization result are shown in Figure 4.77 and 4.78 respectively, that demonstrates the highest stress around un-deformed fixed boundary, especially near to the wire bonds (isometric view of von Mises and Shear Stress in detail is shown in Appendix K). According to the simulation, stress distribution varied according to the fluid force. At 6.0 s, maximum stress was concentrated at the joint between the die and the bumps or bending region (red circle). This means the sweep displacement of wire is dominated by the bending moment instead of the twisting moment (Kung et al., 2006a).

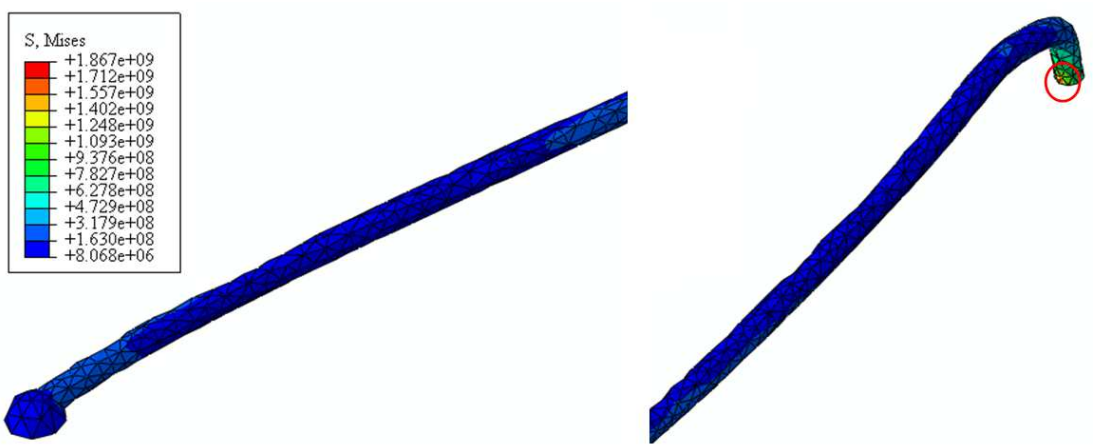


Figure 4.77 Detailed view of maximum von Mises stress distribution for Wire 4 of simulation optimization result.

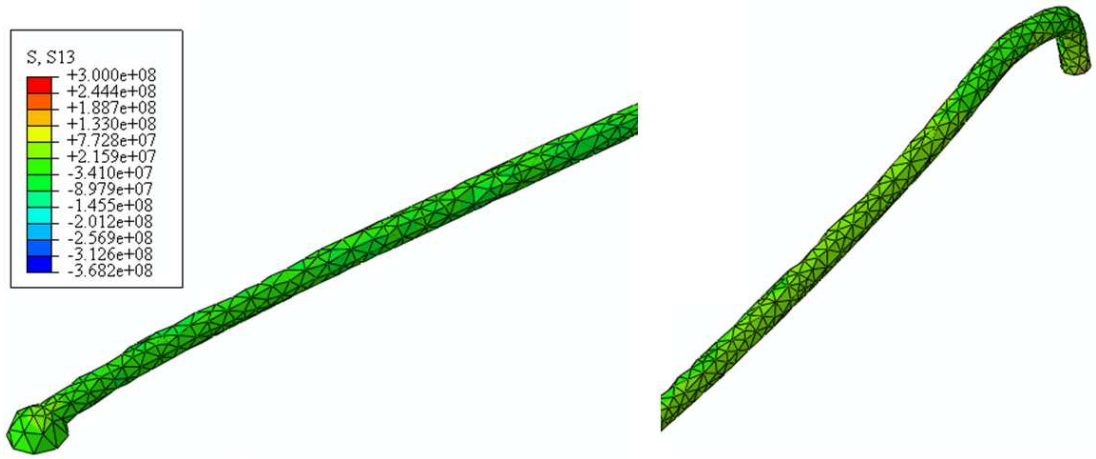


Figure 4.78 Detailed view of maximum Shear stress (S13) distribution for Wire 4 of simulation optimization result.

## 4.9 Summary

This chapter has explained the results from the research work in the encapsulation process of both the scale-up and the actual size PBGA. This study started with the grid independent test for all cavity designs. Grid independence test is performed to obtain the optimum mesh size. Five different mesh sizes were tested, and the corresponding filling percentage were calculated for a scale-up single die with four-wire in a PBGA package, a scale-up single and stacked die with eight-wire in a PBGA package and also finally an actual size PBGA.

The experimental and model validation of fluid flow and wire deformation for scaled-up four and eight-wire PBGA and actual size PBGA encapsulation process were obtained for the validation of simulation.

Several parameters for the observation of wire sweep behaviour of scaled up and actual size PBGA such as stacking die, inlet and outlet arrangement and inlet pressure were studied. The wire sweep profiles and pressure distribution were analyzed and presented. The flow front of test fluid and EMC and wire sweep phenomenon could be simultaneously visualised through the FSI simulation and experiment.

The physical and process parameters of the PBGA package in the encapsulation process were optimized through RSM. The influence of three factors (i.e., inlet pressures ($A$), wire diameter ($B$), and vent height ($C$)) were modelled and optimized to minimise wire sweep ($Y_1$), filling time ($Y_2$), and void formation ($Y_3$).

## REFERENCES


**Books:**

Ardebiri,H., Pecht, M. (2009)Encapsulation Technologies for Electronic Applications.Linacre House, Jordan Hill, Burlington, USA, Elsevier.

Montgomery, D.C.,(2009) Design and Analysis of Experiments, seventh ed. John Wiley&Sons, New York.

**Journal:**

Abdullah, I., Ahmad, I., Talib,M. Z. M., Bachok,N. N., Mokhtar, U., Said A.E.(2008a), Warpage and Wire Sweep Analysis of QFN Molded Array Strip Using Modeling and Experimental Methods.Solid State and Technology, 16(2), p. 153-163.

Abdullah, M. K., Abdullah, M. Z., Kamaruddin, S., Ariff, Z. M. (2007a) Study of Flow Visualization in Stacked-chip Scale Packages (S-CSP).International Communications in Heat and Mass Transfer. 34, p. 820-828.

Abdullah, M. K., Abdullah, M. Z., Mujeebu, M. A., Kamaruddin, S., Ariff, Z. M.(2008b)Study on the Effect of Stack Thickness during Encapsulation of Stacked-chip Scale Packages (S-CSP).Journal of International Microelectronics and Electronics Packaging 5(2),p. 62-67.

Abdullah,M. K., Abdullah,M. Z., Mujeebu,M. A., Kamaruddin, S. (2009) A Study on the Effect of Epoxy Molding Compound (EMC) Rheology during Encapsulation of Stacked-chip Scale Packages (S-CSP).Journal of Reinforced Plastics and Composites. 28(20), p. 2527-2538.

Abdullah, M. K.,Abdullah, M. Z., Mujeebu, M. A., Ariff, Z. M., Ahmad, K. A. (2010) Three-Dimensional Modeling to Study the Effect of Die-stacked Shape on Mould Filling during Encapsulation on Microelectronic Chips. IEEE Transactions on Advanced Packaging.33(2), p. 438-446.

Abdullah, S., Aziz, Z.A., Ahmad, I. I., Abdullah, M.F.(2008c) Low Looping Challenges in The QFN Wire Bonding Process. Solid State Science and Technology, 16(2), p. 25-32.

Adlan, M.N.B., Palaniandy, P., Aziz, H.A. (2011) Optimization of Coagulation and Dissolved Air Flotation (DAF) Treatment of Semi-aerobic Landfill Leachate Using Response Surface Methodology (RSM).Journal of Desalination. 277, p. 74-82.

Brand,J.M., Ruggero,S.A., Shah,A.J. (2008) Wire Sweep Reduction via Direct Cavity Injection during Encapsulation of Stacked Chip-scale Packages.Journal of Electronics Packaging. 130, p. 011011-(1-6).

Chai, H. and Zohar, Y. (1999) Wire Sweep Due to Transfer Molding in A 160L QFP Package under Steady-State Condition. ASME Journal of Electronic Packaging. 121, p. 137-142.

Chang, R. Y., Yang, W. H., Hwang, S. J., Su, F. (2004) Three Dimensional Modeling of Mold Filling in Microelectronics Encapsulation Process. IEEE Transactions on component and Packaging Technologies. 27(1), p. 200-209.

Gokce A.and Advani, S. G. (2004)Simultaneous Gate and Vent Location Optimization in Liquid Composite Molding Processes, Composites Part A. 35,p. 1419-1432.

Han,S.J., Huh,Y.J. (2000) A Study of Wire Sweep During Encapsulation of Semiconductor Chips.Journal of the Microelectronics and Packaging Society. 7(4), p. 17-22.

Han, S., Wang, K.K. (1995a) A Study on Wire Sweep in Encapsulation of Semiconductor Chips Using Simulated Experiments. Journal of Electronics Packaging.Transaction of the ASME, 117, p.178-184.

Han, S., Wang, K.K. (1995b) Effects of Fillers on Wire Sweep inSemiconductor Chip Encapsulation. IEEE Transaction on Components, Packaging, and Manufacturing Technology-Part B, 18(4), p. 744-750.

Hassan, H., Regnier, N., Pujos, C., Defaye, G. (2008) Effect of viscous dissipation on the temperature of the polymer during injection molding filling, Polymer Engineering and Science 48,p. 1199–1206.

Ishiko,M, Usui,M, Ohuchi,T, Shirai,M. (2006) Design Concept for Wire Bonding Reliability Improvement by Optimizing Position in Power Devices.Microelectronics Journal. 37, p. 262-268.

Jong,W.R., Chen,Y.R., Kuo,T.H. (2005) Wire Density in CAE Analysis of High Pin Count IC Packages: Simulation and verification.International Communications in Heat and Mass Transfer. 32, p. 1350-1359.

Khor, C.Y., Abdullah, M.K., Abdullah, M.Z., Mujeebu, M.A., Ramdan, D., Majid, M.F.M.A., Ariff,Z.M.. (2010a) Effect of Vertical Stacking Dies on Flow Behavior of Epoxy Molding Compound during Encapsulation of Stacked-chip Scale Packages.Heat Mass Transfer. 46, p. 1315-1325.

Khor,C.Y., Mujeebu,M.A., Abdullah,M.Z., Che Ani,F. (2010b) Finite Volume Based CFD Simulation of Pressurized Flip-chip Underfill Encapsulation Process.Journal of Microelectronics Reliability.50, p. 98-105.

Khor, C.Y., Ariff, Z.M., Che Ani, F., Mujeebu, M.A., Abdullah, M.K., Abdullah, M.Z., Joseph,M.A..(2010c) Three-dimensional Numerical and Experimental Investigations on Polymer Rheology in Meso-scale Injection Molding.International Communicationin Heat and Mass Transfer. 37, p. 131-139.

Khor, C.Y., Abdullah, M.Z., Abdullah, M.K., Mujeebu, M.A., Ramdan, D, Majid, M.F.M.A., Ariff, Z.M., Abdul Rahman, M.R. (2011) Numerical Analysis on The Effects of Different Inlet Gates and Gap Heights in TQFP Encapsulation Process.International Journal of Heat and Mass Transfer.54, p. 1861-1870.

Khor, C.Y., Abdullah, M.Z., Tan, H.J.T., Leong, W.C., Ramdan, D. (2012a) Investigation of the Fluid/Structure Interaction Phenomenon in IC Packaging.Microelectronics Reliability. 52(1), p. 241-252.

Khor, C.Y., Abdullah, M.Z. (2012a) Optimization of IC Encapsulation Considering Fluid/Structure Interaction Using Response Surface Methodology. Simulation Modelling Practice and Theory, 29, p. 109-122.

Khor, C.Y., Abdullah, M.Z. (2012b)Modeling and Analysis of the Effect of Stacking Chips withTSVS in 3D IC Package Encapsulation Process.Maejo International Journal Science Technology.2012, 6(02), 159-185.

Kim,W., Bae,J.W., Choi,I.D., Kim,Y.S. (1999) Thermally Conductive EMC (Epoxy Molding Compound)for Microelectronic Encapsulation.Polymer Engineering and Science. 39(4), p. 756-766.

Kung,H.K., Lee,J.N., Wang,C.Y. (2006a) The Wire Sweep Analysis Based on the Evaluation of the Bending and Twisting Moments for Semiconductor Packaging.Microelectronic Engineering. 83, p. 1931-1939.

Kung, H.K., Huang, B.W.(2006b) High-temperature Wire Sweep Characteristics of Semiconductor Package for Variable Loop-height WireBonding Technology.Microelectronic Engineering, 83, p. 197-205.

Kung,H.K., Sun,Y.P., Lee,J.N., Chen,H.S. (2008) A Method to Determine the Sweep Resistance of Wire Bonds for Microelectronic Packaging.Microelectronic Engineering. 85, p. 1902-1909.

Kung, H.K., Chen, H.S., Lu, M.C. (2012) TheWire Sag Problem in Wire Bonding Technology for Semiconductor Packaging. Microelectronics Reliability, http://dx.doi.org/10.1016/j.microrel.2012.08.017.

Lee, T.K., Han, S., Ko, Y. S., Kim, J.H. (2008a) Some Case Studies on Air Venting Analysis of Semiconductor Packages Using MOLFLOW. IEEE 10th Electronics Packaging Technology Conference. p. 444-449.

Liang,J.Z. (2001) Pressure Effect of Viscosity for Polymer Fluids in Die Flow.Polymer. 42, p. 3709-3712.

Lim, S. T., Lee, W. I. (2000) An Analysis of the Three-dimensional Resin Transfer Mold Filling Process. Composites Science and Technology. 60, p. 961-975.

Liu,D.S., Chao,Y.C., Wang,C.H.(2004a) Study of Wire Bonding Looping Formation in the Electronic Packaging Process Using the Three-dimensional Finite Element Method.Finite Elements in Analysis and Design. 40, p. 263-286.

Liu, S.L., Chen, G., Yong, M.S. (2004b) EMC Characterization and Process Study for Electronics Packaging.Thin Solid Films. 462-463, p. 454-458.

Mulgaonker, S. and Berg, H.M. (1996) Thermal Sensitivity Analysis for the 119 PBGA-A Framework for Rapid Prototyping.IEEETransactions on Components, Packaging, andManufacturing Technology-Part A, 19(1), March 1996, p. 66-74.

Nguyen,L., Quentin,C., Lee,W., Bayyuk,S., Bidstrup-Allen,S.A., Wang,S.T.(2000) Computational Modeling and Validation of the Encapsulation of Plastic Packages by Transfer Molding.Journal of Electronics Packaging. 122, p. 138-146.

Onodera, M., Meguro, K., Tanaka, J., Shinma, Y., Taya, K., and Kasai, J., 2007, Low-cost Vacuum Molding Process for BGA Using a Large Area Substrate,IEEE Transactions on Advanced Packaging, 30(4), November 2007, pp. 674-680.

Pei,C.C., Hwang,S.J. (2005a) Prediction of Wire Sweep during the Encapsulation of IC Packaging with Wire Density Effect.ASME Journal of Electronic Packaging. 127, p. 335-339.

Pei,C.C., Hwang,S.J. (2005b) Three-dimensional Paddle Shift Modeling for IC Packaging. Transactions of the ASME, 127, p. 324-334.

Reddy, A.M.K., Han, R., Gupta, M. (1998) Numerical and Experimental Investigation of Microchip Encapsulation.Journal of Reinforced Plastics and Composites. 17(1), p. 70-93.

Sato, M. Yokoi, H. (2000) Visualization Analysis of Melt Flow in IC Packaging Process along Thickness Direction. IEEE Transaction on Advanced Packaging. 23(4), p. 729-737.

Schreiber,A., Metsch,T., Kersken,H.P. (2005) A Problem Solving Environment for Multidisciplinary Couple Simulations in Computational Grids.Future Generation Computer System. 21, p. 942-952.

Schueller, R.D.,Plepys, A.P. (1996) Design of a Low Cost Wire BondTape Ball Grid Array Package. Circuit World, 22(3), p. 10-15.

Shojaei, A., Ghaffarian, S. R., Karimian, S. M. H. (2002) Numerical Simulation of Three-Dimensional Mold Filling Process in Resin Transfer Molding Using Quasi-steady State and Partial Saturation Formulations. Composites Science and Technology. 62, p. 861-879.

Su, J., Hwang, S.J., Su, F., Chen, S.K.(2003) An Efficient Solution for Wire Sweep Analysis in IC Packaging.ASME Journal of Electronic Packaging. 125, p. 139-143.

Tay, A.A.O., Lin, T.Y. (1999) Influence of Temperature, Humidity and Effect Location on Delamination in Plastic Packages. IEEE Transaction on Component Packaging Manufacturing Technology. Part A 22(4), p. 512-518.

Teng,S.Y., Hwang,S.J. (2008) Simulation and Experiments of Three Dimensional Paddle-shift for IC Packaging.Microelectronics Engineering. 28, p. 115-125.

Wang,H, Zhou,H, Zhang,Y, Li D. (2010) Stabilized Filling Simulation of Microchip Encapsulation Process.Microelectronics Engineering. 87, p. 2602-2609.

Wu, J.H., Tay, A.A.O., Yeo,K. S., Lim, T.B. (1998)A Three-dimensional Modeling of WireSweep Incorporating Resin Cure. IEEE Transactions on Components, Packaging, and Manufacturing Technology—Part B, 21(1), February 1998, p. 65-71.

Yang,H.Q., Mazumder,S., Lowry,S., Krishnan,A., Przekwas,A., Nguyen, L. (2001) Time Accurate, 3-D Computation of Wire Sweep during Plastic Encapsulation of Electronic Components.Journal of Pressure Vessel Technology.123, p.501-509.

Yang,S.Y., Jiang,S.C., Lu,W.S. (2000) Ribbed Package Geometry for Reducing Thermal Warpage and Wire Sweep during PBGA Encapsulation.IEEE Transactions on Components and Packaging Technologies. 23(4), p. 700-706.

Yao,F., Njoman,B., Chua,K.H., Lin, T.Y. (2005) New Encapsulation Development for Fine Pitch IC Devices.Microelectronics Reliability. 45, p. 1222-1229.

Yao,Y.F., Lin,T.Y., Chua,K.H. (2003) Improving the Deflection of Wire Bonds in Stacked Chip Scale Package (CSP).Microelectronics Reliability.43(12), p. 2039-2045.

Yigit, S., Schafer, M., Heck, M. (2008) Grid Movement Techniques and Their Influence on Laminar Fluid/Structure Interaction Computations.Journal of Fluids and structures. 24, p. 819-832.

Yong, T.P., Yoo, K.W., Joon, K.H., Kwang, Y.B. (2006) Warpage Analysis of FBGA (Fine Ball Grid Array) Package by the Altered EMC (Epoxy Molding Compound) Filler Contents, Key Engineering Material. 306-308, p.625-630.

Yoshihara, T., Yuki, M., Hayashida, T., Ohno,Y. (1999a) Factor Governing Wire Sweep in Plastic IC Encapsulation.Electronics Communication Japan.82(7), p. 59-67.

Yoshihara, T., Ohno, Y., Kusuhara, A., Fujita, H., Maeda, M. (1999b) Effects of Molding Compound on Wire Sweep in PlasticEncapsulated IC Packages. Electronics and Communications in Japan, Part 2, 82(11), p. 28-34.

Zhang, K. and Pecht, M., (2000) Effectiveness of Conformal Coatings on a PBGASubjected to Unbiased High Humidity, High Temperature Tests, MicroelectronicsInternational, vol. 17, no. 3, p. 16-20.

**Proceedings/Sumposium/Conference:**

Abdullah, I., Chiang, N.C., Mokhtar, U., Said, A., Talib, M.Z.M., Ahmad, I. (2007b) Warpage and Wire Sweep Analysis of QFN Molded Strip Using Experimental and Modeling Methods. In: Proceedings IEEE 9th Electronics Packaging Technology Conference, 10-12 Dec. 2007, p. 494-498.

Abdullah, S., Aziz, Z. A., Ahmad, I., Jalar, A., Abdullah, M.F. (2008d) Wire Sweep Issue in a Newly Developed Quad Flat No-lead(QFN) Semiconductor Package. In Proceedings: 7th WSEAS International Conference on Microelectronics,

Nanoelectronics, Optoelectronics (MINO '08), Istanbul, Turkey, May 27-30, 2008, p. 40-44.

Bailey, J., Sett, S., Benko, R.J. (2006) A Fluid/Structure Interaction Analysis of the VernaFlo Flow Control Device, 2006 ABAQUS Users' Conference, p. 53-62.

Brunner, J., Qin, I.W., Chylak, B. (2004) Advanced Wire Bond Looping Technology for Emerging Packages. In:Proceedings IEEE International Electronics Manufacturing Technology Symposium, July 14-16, 2004, p. 85-90.

Chen, J.Y., Teng, S.Y., Hwang, S.J., Lee, H.H., Huang,D.Y., Lin, Y.J., Stoke Chen, Shen, G.S., Lily Wu (2007a) Prediction of Flow Induced Lead Deflection of Leadframe Assemblies in Plastic Encapsulation during Molding. In Proceedings: IEEE, 8th ICEP International Conference on Electronic Packaging Technology,14-17 Aug. 2007,p. 1-5.

Chou, Y.Y., Chiu, H.S., Yang, W.H. (2009) Three-dimensional CAE of Wire Sweep and Paddle Shift in Microchip Encapsulation. In Proceedings: IEEE 4thInternational Microsystems, Packaging, Assembly and Circuits Technology Conference, IMPAC 2009, 21-23 Oct. 2009, p.35-38.

Chylak, B., Levine, L., Babinetz, S., Kwon, O.D.(2006) Advanced Ultra-low-loop Wire Bonds. SEMICON China 2006, SEMI 2006.

Cohn, C.,Richman,R.M., Saxena,L.S., Shih, M.T. (1995) High I/O Plastic Ball Grid Array PackagesAT&T Microelectronics Experience. In Proceedings: IEEE Electronic Components and Technology Conference, 1995. Proceedings., 45th,21-24 May 1995, p. 10-20.

Ganesh, V.P. Sivakumar, M. (2002) Process Development for Ultra Low Loop Reverse Wire Bonding on Copper Bond Pad Metallization.In Proceedings: Electronics Packaging Technology Conference, 2002. 4th, 10-12 Dec. 2002, 356-360.

Gatzhammer,B., Mehl,M., Neckel,T. (2010) A Coupling Environment for Portioned Multiphysics Simulations Applied to Fluid/Structure Interaction Scenarios.In Proceedings: Computer Science I, p.681-689.

Han, J., Chen, H., Xue, K., Wong, F., Leung, K., Shiu, I., Wu, J. (2011a) Wire Sweep Study for SOT Package Array Matrix Molding with Simulation and Experimental Analysis. In Proceeding: IEEE International Conference on Electronic Packaging Technology & High Density Packaging, 8-11 Aug. 2011, p. 601-606.

Han, J., Chen, H., Wong, F., Leung, K., Shiu, I., Wu, J. (2011b) Effects of Package and Mold Cavity Structures on the Wire Sweep Behavior duringPackage Array Transfer Molding. In Proceeding: IEEE International Conference on 13th Electronics Packaging Technology Conference, 7-9 Dec. 2011,p. 667-673.

JoppichW., Urschner M.K., the MpCCI team (2006), MpCCI—a tool for thesimulation of coupledapplications, CONCURRENCY AND COMPUTATION: PRACTICE AND EXPERIENCE*Concurrency Computat.: Pract. Exper.*2006; **18**:183–192

Kapoor,R, Kuan,L.B., Hao,L. (2004) Package Design Optimization and Materials Selection for Stacked Die BGA Package.In Proceedings: IEEE/CPMT/SEMI 2004 29thInternational Electronics Manufacturing Technology Symposium,San Jose, CA USA, July 14-16, 2004, p. 113-118.

Kung, H.K., Huang, C.H., Chanyshev, A.I. (2006c)On the Study of Loop Profiles in Improving the Sweep Stiffness of Wire Bond. In Proceedings: IEEE 8th Electronics Packaging Technology Conference, 2006, EPTC, 6-8 Dec. 2006, p. 472-477.

Lee,M.W., Khim,J.Y., Yoo,M., Chung,J.Y., Lee,C.H. (2006) Rheological Characterization and Full 3D Mold Flow Simulation in Multi-die Stack CSP of Chip Array Packaging.In Proceedings: IEEE,56thElectronics Components Technology Conference, San Diego, CA, p. 1029-1037.

Lee, M.W., Jung, W.K., Sohn, E.S., Lee, J.Y., Hwang, C.H., Lee, C.H. (2008a) A Study on the Rheological Characterization and Flow Modeling of Molded Underfill (MUF) for Optimized Void Elimination Design. In Proceedings: Electronic Components and Technology Conference 27-30 May, Lake Buena Vista, FL, p. 382-388.

Lee, T.K., Han, S., Ko, Y.S., Kim, J.H. (2008b) Some Case Studies on Air Venting Analysis of Semiconductor Packages using Moldflow™.In Proceedings: IEEE 10th Electronics Packaging Technology Conference. 9-12 Dec. 2008, p. 444-449.

Liu, J.M., Yao, J.Z., Wei, G., Lu, Y.S. (2007a) Wire Sweep Improvement Study for Fine Pitch Device. In Proceedings: IEEE 2007 9th Electronics Packaging Technology Conference, 10-12 Dec. 2007, p.61-65.

Liu, J.M., Lu, Y.S., Pang, X.S. (2007b) FFT (Flow Free Thin) Mold Study for 44 μm Fine Pitch Device Application, In Proceeding: CS MANTECH Conference, 14-17 May 2007, p. 25-28.

Lu, X., Xu, L., Lai, H., Du, X., Liu, J., Cheng, Z. (2009) Studies on Microstructure of Epoxy Molding Compound (EMC)-Leadframe Interfaceafter Environmental Aging.In Proceedings: IEEE 2009 International Conference on Electronic Packaging Technology & High Density Packaging (ICEPT-HDP), 10-13 Aug. 2009,p. 1051-1053.

Muniandy, K., Ruzaini, I., Wei, S.K. (2006) Top-gate Molding Process Deveopment of Cavity Down TBGA for High Density Wire Bonding and Low K Dielectric Wafer Technology Application. In Proceedings: International Electronic Manufacturing Technology, IEMT, Putrajaya, Malaysia, p. 390-395.

Nguyen, L.T. and Lim, F.J.(1990) Wire Sweep during Molding of Integrated Circuits. In Proceedings: IEEE Conference, 40th Electronic Components and Technology Conference, 1990, 20-23 May 1990, p. 777-785.

Nguyen, L., Jackson, J., Teo, C.H., Chillara, S., Asanasavest, C., Ho, D., Rauhut, H (1997) Wire Sweep Control with Mold Compound Formulations.In: Proceedings., 47thElectronic Components and Technology Conference. 18-21 May 1997, p. 60-71.

Nguyen, L.T., Quentin, C.G., Lee, W.W. (1999) Flow Modeling and Visualization of the Transfer Molding of Plastic Ball Grid Array Packages.In: IEEE 1999 Proceedings. 49thElectronic Components and Technology Conference, p. 177-184.

Qin, H.B., Li, X.P., Zhang, X.P. (2012) Solder Volume Effects on Fatigue Life of BGA Structure Cu/Sn-3.0Ag-0.5Cu/Cu Interconnects. In Proceedings: EMAP 2012, The 14th International Conference on Electronic Materials and Packaging, December 2012, Citygate, Lantau Island, Hong Kong, p. 360-366.

Schueller, R.D., Aeschliman, D., Han, C.T. (1997) Performance and Reliability of a Cavity DownTape BGA Package. In: IEEE EPTC ConferenceProceedings of the 1997 1stElectronic Packaging Technology Conference,8-10 Oct 1997, p. 151-162.

Shu, W.K. (1996) PBGA Wire Bonding Development. In: IEEE Proceedings., 46thElectronic Components and Technology Conference, 28-31 May 1996, p. 219-225.

Sze, H.M.W., Papageorge, M. (1998) Encapsulation Selection, Characterization and Reliability for Fine Pitch BGA (fpBGA$^{TM}$), ASAT, LTD, Hongkong, p.1-7.

Wintergerste, T. (2002) Computational of Fluid-Structure Interaction in a Static Mixer Using MpCCI. In Proceedings: ASME Pressure Vessels and Piping Conference (PVP2002) 5-9August, 2002, Vancouver, BC, Canada, p. 57-65.

Yang,W.H., Hsu,D.C., Yang,V, Chang,R.Y., Su,F, Huang,S.J. (2004) Three Dimensional CAE of Wire-sweep in Microchip Encapsulation.In Proceedings: Soc.PlasticsEngineering, Technical Conference-ANTEC, Conference Proceeding, Brookfield, IL, 2, p.1679-1683.

Tay,A.A.O., Lee, W.H. (2002) Transient Three Dimensional Simulation of Mold Filling and Wire Sweep in an Over Mold BGA Package.In Proceedings:IEEE 2002, 52$^{nd}$ Electronics Component Technology Conference, San Diego, CA, 2002, p. 897-904.

**Thesis:**

Chen,Y.R. (1990) Mold Flow Simulation and Wire Sweep in IC Encapsulation, M.S. Thesis, Mech. Eng., Christian Univ. of Chun Yuan, Taiwan.

Pei, C.C. (2004) Wire Sweep and Paddle Shift Modeling of IC Packages During Encapsulation Process, M.S. Thesis, Mech. Eng., National Cheng Kung Univ., Tainan, Taiwan.

**Others:**

MpCCI 3.1.0-1 Documentation Part I Overview, Fraunhofer Institute for Algorithms and Scientific Computing SCIA, Germany, January 2009.

Mawer A. (1996) Plastic Ball Grid Array (PBGA). Motorola Semiconductor Technical Data.Motorola Fast Sram, P. 1-27.

Michael, S., Halger, L., Markus, H. (2005) Implicit Partitioned FSI Coupling. Resumepoerle 1er Colloqkie du GDR Interaction Fluid-Structure, 26-27 Sept 2005.

National Semiconductor Corporation (2000),Semiconductor Packaging Assembly Technology. www.national.com.

Plastic Ball Grid Array (PBGA), Application Report, Texas Instruments, Submit Documentation Feedback. SSZA002–August 2009, p. 1-17.

Prior, B. Low Cost, Small Form Factor Packaging.BiTS Workshop 2010 Archive, Comprise the Proceedings of the 2010 BiTS Workshop, p. 1-8.

Wolf, K. (2007) MpCCI the General Code Coupling Interface. Dynamore GmbH, LS-Dyna Anwenderforum. p. 1-8.

**Internet Source:**

Fraunhofer Institute for Algorithms and Scientific Computing SCIA.(2009, Jan.).MpCCI 3.1.0-1 Documentation Part I Overview, SanktAugustin, Germany [Online]. Available: http://www.scai.fraunhofer.de/mpcci

Thirifay,F., Geuzaine,P. (2008)Numerical simulations of fluid-structure interaction problem using MpCCI [Online].Available: http://mecanique.in2p3.fr/JU-samtech/ proceedings/03_16_CENAERO_Delanaye/ 03_16_CENAERO_Delanaye.pdf.

**Dadan Ramdan** was born in Bandung, Indonesia. He received the B.S degree in physics from the Pandjadjaran University of Bandung, and the M.Sc. and M.Eng. degrees from the Bandung Institute of Technology, Bandung, and the Toyohashi University of Technology, Toyohashi, Japan, respectively. He received the Ph.D. degree with Universiti Sains Malaysia, Penang, Malaysia. Until now, He as a Lecturer of mechanical engineering and Electrical Engineering with the Engineering Faculty, Medan Area University, Medan, Indonesia. His current research interests include electronic instrumentation, control systems engineering, and Computational Fluid Dynamics of electronic packaging and casting. His Proffesor in Compuer Programming and Control System Engineering.

**Dadan Ramdan:**

# Applied Computational Fluid Dynamics in Electronics Packaging

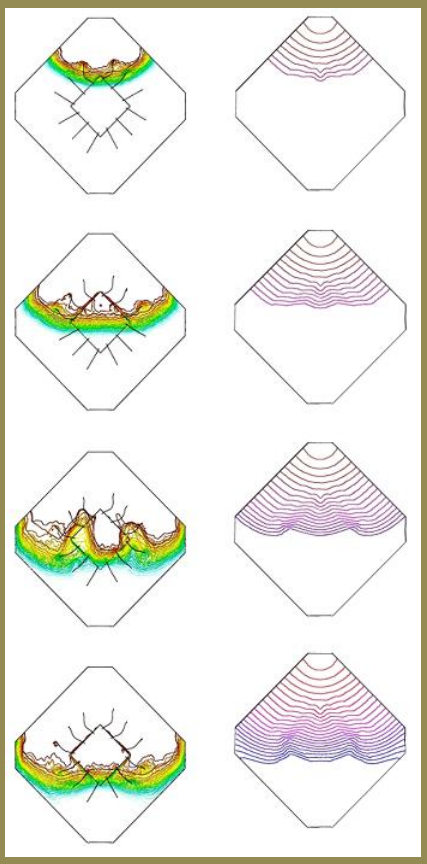

ISBN: 978 - 602 – 1577 - 11-0

medan area university press